UNIVERSITY OF TECHNOLOGY, SYDNEY

MECHANICAL AND STRUCTURAL PROPERTIES OF POLYVINYL ALCOHOL FIBRE REINFORCED CONCRETE (PVA-FRC)

AMIN NOUSHINI

MASTER OF ENGINEERING

2013

Mechanical and Structural Properties of Polyvinyl Alcohol Fibre Reinforced Concrete (PVA-FRC)

by

Amin Noushini

A thesis submitted for the fulfilment of the requirements for the degree of

Master of Engineering

School of Civil and Environmental Engineering
Faculty of Engineering and Information Technology
University of Technology Sydney

2013

CERTIFICATE OF AUTHORSHIP/ORIGINALITY

I certify that the work in this thesis has not previously been submitted for a degree nor has it been submitted as part of requirements for a degree except as fully acknowledged within the text.

I also certify that the thesis has been written by me. Any help that I have received in my research work and the preparation of the thesis itself has been acknowledged. In addition, I certify that all information sources and literature used are indicated in the thesis.

Production Note:
Signature removed prior to publication.

Amin Noushini

Sydney, August 2013

ACKNOWLAGEMENTS

This thesis would not have been completed without the guidance, advice and support of a number of individuals whose contribution I would gratefully like to acknowledge. I would specially like to express my gratitude to my supervisors, *Professor Bijan Samali* and *Dr Kirk Vessalas*. Herein, I would like to express my deepest gratitude to Professor Samali, who has been my principal supervisor for this research, not only because of his invaluable guidance and expert advice throughout the research but also on account of his strong support like a kind father during the last two years. The author would also very much like to record his appreciation to Dr Vessalas for his valuable advice and constant support from the commencement of this project to the end, much more than just a co-supervisor.

I would also like to convey my thanks to University of Technology Sydney (UTS) Civil Engineering Laboratories staff, specially the laboratories manager *Mr Rami Haddad*, senior project engineer *Mr Peter Brown* and technical officer *Mr David Dicker* who kindly helped me in project experimental stages.

Furthermore, I am obliged to many of my colleagues and friends who assisted me during my studies. Special thanks must go to my dear friends and co-researchers, *Mr Rami Haddad*, *Ms Nassim Ghosni* and *Ms Negin Sharifi* for their unfailing assistance and support in this research work.

The support from the Centre for Built Infrastructure Research (CBIR) and assistance of academics and researchers in the School of Civil and Environmental Engineering at UTS, particularly *Dr Hamid Valipour* and *Dr Nima Khorsandnia* is highly acknowledged.

Lastly, I would like to extend my love and gratitude to my dearest parents for their support and encouragement. I want to sincerely thank them from the bottom of my heart and acknowledge that without them none of this could have happened and I was not able to achieve most of the things I have in my life.

Hereby, I would like to dedicate this thesis to my parents for being such great supports in my life.

LIST OF PUBLICATIONS BASED ON THIS THESIS

Journal Articles

1. Noushini, A., Samali, B., Vessalas, K. 2013, 'Effect of Polyvinyl Alcohol (PVA) Fibre on Dynamic and Material Properties of Fibre Reinforced Concrete', *Construction and Building Materials*, vol. 49, pp. 374-383
2. Noushini, A., Vessalas, K. and Samali, B. 2014, 'Rheological Properties and Compressive Strength Behaviour of Polyvinyl Alcohol Fibre-Reinforced Concrete', *Australian Journal of Structural Engineering (AJSE)*, vol. 15, no. 1
3. Noushini, A., Vessalas, K., Samali, B., Arabian, G., 'Drying Shrinkage Behaviour of Fibre Reinforced Concrete Incorporating Polyvinyl Alcohol (PVA) Fibres and Fly ash', *Magazine of concrete research* – under review
4. Noushini, A., Vessalas, K., Samali, B., 'Static Mechanical Properties of Polyvinyl Alcohol Fibre Reinforced Concrete (PVA-FRC)', *Magazine of concrete research* – under review
5. Noushini, A., Samali, B., Vessalas, K., 'Ductility and Damping Characteristics of Polyvinyl Alcohol Fibre Reinforced Concrete Beam Elements', *composite structures* – under review

Conference Papers

1. Noushini, A., Vessalas, K., Ghosni, N., Samali, B. 2013, 'Effect of Polyvinyl Alcohol Fibre and Fly Ash on Flexural Tensile Properties of Concrete', *Proceeding of the 22nd Australasian Conference on the Mechanics of Structures and Materials (ACMSM 22),* Sydney, Australia, pp. 1165-1170
2. Noushini, A., Samali, B., Vessalas, K. 2013, 'Flexural Toughness and Ductility Characteristics of Polyvinyl Alcohol Fibre Reinforced Concrete (PVA-FRC)', *VIII International Conference on Fracture Mechanics of Concrete and Concrete Structures (FraMCoS-8),* Toledo, Spain, pp. 1110-1121

3. Noushini, A., Samali, B., Vessalas, K. 2013, 'Effect of Polyvinyl Alcohol Fibre on Dynamic Properties of Concrete Containing Fly Ash', *Composite Construction VII (CCVII)*, Palm Cove, Queensland, Australia

4. Noushini, A., Samali, B., Vessalas, K. 2013, 'Damping Properties of Polyvinyl Alcohol Fibre Reinforced Concrete', *The Thirteenth East Asia-Pacific Conference on Structural Engineering and Construction (EASEC-13)*, Sapporo, Japan

5. Noushini, A., Samali, B., Vessalas, K. 2013, 'Influence of Polyvinyl Alcohol Fibre Addition on Fresh And Hardened Properties of Concrete', *The Thirteenth East Asia-Pacific Conference on Structural Engineering and Construction (EASEC-13)*, Sapporo, Japan

6. Noushini, A., Vessalas, K., Samali, B. 2013, 'Flexural and Tensile Characteristics of Polyvinyl Alcohol Fibre Reinforced Concrete (PVA-FRC)', *The Thirteenth East Asia-Pacific Conference on Structural Engineering and Construction (EASEC-13)*, Sapporo, Japan

ABSTRACT

Concrete is a brittle material that has low tensile strength and low strain capacity. In fact, many deteriorations and failures in the concrete structures are due to the brittle nature of this material (Hamoush et al. 2010). These disadvantages may be avoided by adding short discontinuous fibres to plain concrete which has been a major motivation for many research works in recent years (Wu & Sun 2003).

Fibres are added into a brittle-matrix composite to help improve three major aspects; toughness, ductility and strength (tensile) (Arisoy 2002). Fibres tend to increase toughness of the composite material by bridging the cracks and provide energy absorption mechanism related to de-bonding and fibre pull-out. Furthermore, they can increase the ductility of the composite by allowing multiple cracking. They may also help increase the strength by transferring load and stresses across the cracks.

Advancement of fibre reinforced concretes (FRCs) started in the 1970s. By that time, only glass fibre and steel fibre were investigated (Perumalsamy & Surendra 1992). Synthetic fibres have become more attractive in recent years as reinforcements for cementitious materials. This is due to the fact that they can provide inexpensive reinforcement for concrete and if the fibres are further optimized, greater improvements can be gained without increasing the reinforcement costs (Li et al. 1991; Wang et al. 1989). Moreover, unlike the steel fibre which is highly corrosive in nature, there is no corrosion concern regarding synthetic fibres in concrete.

During the past 20 years (since early 1990s), polyvinyl alcohol (PVA) fibre has been introduced in the production of cementitious composites (Li 1998; Redon et al. 2001; Shen et al. 2008; Sun & Wu 2008). PVA fibres act greatly in a cement based matrix with no coarse aggregates due to their surface formation and high strength (Li et al. 2001). The resulting composite, which exhibits a pseudo ductile behaviour, is called engineered cementitious composites (ECC).

Although many research works have been performed to date on the properties of PVA fibre reinforced ECC, there has not been much investigation on the mechanical and structural characteristics of PVA fibre reinforced concrete. Accordingly, the objective of this study is to experimentally observe the effects of adding PVA fibres to the conventional concrete to assess its mechanical and structural properties.

To achieve this aim, a comprehensive set of experiments were carried out to investigate the effect of PVA micro fibre addition on mechanical and structural properties of conventional concrete. Therefore, concrete mixes containing PVA fibres of varying lengths (6 and 12 mm) in different fibre volume fractions ranging from 0.125% - 1% were prepared and tested for their fresh and hardened properties. The optimum fibre contents in terms of FRC performance were then selected to cast several concrete beams. These beams have later been tested for 4-point monotonic and 3-point cyclic flexure, to assess their structural properties. Hammer test was also conducted to evaluate the dynamic characteristics of conventional and FRC specimens as well as concrete beams.

TABLE OF CONTENTS

LIST OF TABLES

LIST OF FIGURES

NOTATIONS

The symbols used in this thesis, including their definitions, are listed below.

A_s	cross-sectional area of reinforcement
A_{sc}	cross-sectional area of compressive reinforcement
A_{st}	cross-sectional area of longitudinal tensile reinforcement
b	width of a rectangular cross-section
c	distance from the extreme compression fibre to the neutral axis
d	effective depth (the distance from the extreme fibre to the centroid of the tensile steels)
d'	distance from the extreme compressive fibre to the centroid of the compression steels
d_f	diameter of fibre
E_c	static modulus of elasticity of concrete
E_f	modulus of elasticity of fibre
E_s	modulus of elasticity of steel reinforcement
f_c	compressive strength of concrete – stress in concrete
f'_c	characteristic compressive (cylinder) strength of concrete
f_{ct}	uniaxial tensile strength of concrete
$f_{ct.sp}$	indirect (splitting) tensile strength of concrete
$f_{ct.f}$	flexural strength (modulus of rupture) of concrete
f_s	stress in tension reinforcement
f_y	specified yield strength of steel reinforcement
f_{sy}	yield strength of steel reinforcement
f_{su}	ultimate strength of steel reinforcement
F_u	ultimate (maximum) load applied

h overall height of a rectangular cross-section

I_g second moment of area of the uncracked cross-section

I_{cr} second moment of area of the cracked cross-section

L_f length of fibre

M_{cr} cracking moment

M_y yield moment

n modular ratio (E_s/E_c)

V_f fibre volume fraction

ε_{cu} strain at peak stress (compression) of concrete

ε_{cc} concrete strain in compression

ε_{ts} steel strain in tension

ε_s strain in tension reinforcement

ε_{sy} yield strain of steel reinforcement

ε_{su} uniform strain at maximum stress, corresponding to the onset of necking

ρ_s longitudinal tension reinforcement ratio (A_{st}/bd)

ρ'_s longitudinal compression reinforcement ratio (A_{sc}/bd)

ξ damping ratio (percentage of critical damping)

δ logarithmic decrement

δ_y yield displacement of reinforced concrete beam

δ_u ultimate displacement of reinforced concrete beam

μ ductility factor

$\varnothing_{cr}$ curvature corresponding to the cracking moment (M_{cr})

$\varnothing_y$ curvature corresponding to the yield moment (M_y)

Chapter 1

Introduction

1.1 Overview

1.2 Research objectives and plan

1.3 Thesis layout

1.4 Terminologies

1 INTRODUCTION

1.1 Overview

Concrete is known as a brittle-like material that has high compressive strength and low tensile strength and strain capacity, thus, shows no post peak behaviour. In fact, many deteriorations and catastrophic failures without noticeable warning in a concrete structure are due to the brittle nature of this material (Hamoush et al. 2010).

An approach introduced to improve the post peak behaviour and ductile performance of concrete is using fibres as intrinsic reinforcement. Use of randomly distributed short fibres to improve the physical properties of concrete or other brittle materials is an old concept. Straw reinforced mud bricks were used in the Middle East as long as 10,000 years ago. At 1400 BC the sun-baked bricks reinforced with straw were used to build the 57 m high hill of Aqar Quf near Baghdad (Hannant 2003). Sundried adobe bricks (a mixture of sand, clay and straw) were also used for a long period in the Americas by the indigenous inhabitants, particularly in the American Southwest and in parts of South America (Mindess 2007a).

The modern usage of fibres in construction industry goes back to about 100 years ago (1900s) and creation of asbestos cement. However, the first serious theoretical studies of fibre in concrete were developed in the early 1960s by Romualdi, Batson, and Mandel when they published their research (Romualdi & Batson 1963; Romualdi & Mandel 1964; Zollo 1997). It initially brought fibre reinforced concrete (FRC) into attention of academic and industry research scientists around the world as a viable solution for improving post peak behaviour and ductility of concrete. Advancement of FRCs then continued in the 1970s when mostly glass fibre and steel fibre were investigated (Perumalsamy & Surendra 1992). In the middle 1980s many new fibre types and fibre geometries have been introduced which significantly altered FRC production techniques and influenced FRC strength and toughness (crack control) performance measures (Zollo 1997).

According to the terminology adopted by the American Concrete Institute (ACI) Committee 544, Fibre Reinforced Concrete, there are four categories of FRC based on fibre material type. These are SFRC, for steel fibre FRC; GFRC, for glass fibre FRC;

SNFRC, for synthetic fibre FRC including carbon fibres; and NFRC, for natural fibre FRC.

From amongst the many types of synthetic fibres used in SNFRCs and cementitious composites, polyvinyl alcohol (PVA) fibre is a relatively new inclusion. PVA fibre is known to be stable and durable in the alkali environment present in the concrete matrix (Garcia et al. 1997). These fibres are characterised by their high tensile strength (0.9 – 1.6 GPa), high elastic modulus (23 – 40 GPa) and hydrophilic surface which creates a strong chemical bond with the cementitious material (Redon et al. 2004). The high tensile strength of PVA fibres is attributed to sustaining the first crack stress and resisting pull out force due to the strong bond present between the fibre and cementitious matrix. On the contrary, the low lateral resistance of the fibres may also lead to fibre rupture before being pulled out of the matrix (Atsuhisa et.al, 2006). PVA fibres elongate and transfer the load to different parts of the matrix and as a result the load applied is distributed more evenly between the loading surfaces.

1.2 Research objectives and plan

Although a considerable amount of research has been done to date on the concept of using PVA fibre in cementitious composites, limited studies is performed on structural properties of PVA fibre reinforced concrete (PVA-FRC). Most of previous works on PVA fibre has focused on PVA engineered cementitious composites (ECC).

This research work shall therefore aim to advance the knowledge of using PVA-FRC in structural applications. The main objective of this study is to investigate how the mechanical, structural and damping characteristics of concrete are affected by addition of a certain amount of PVA fibres into the concrete. Accordingly, after a broad literature review on application of fibres in concrete, PVA fibres of two geometric lengths (6 and 12 mm) were selected to be investigated in order to evaluate their effect on fresh and hardened properties of concrete and concrete beam elements.

Experimental investigations are categorised into two stages. Stage one can be referred to as “Material Testing” which mainly focuses on the properties of PVA fibre reinforced concretes (PVA-FRCs) in fresh and hardened state. In this phase, FRCs with 6 and 12 mm fibres and volume fractions ranging from 0.125% - 1% are investigated to find out the optimum fibre content with regards to concrete workability and also mechanical

properties i.e. compressive strength, tensile strength, flexural strength, modulus of elasticity and damping ratio.

Selected mix designs of previous investigations (material testing), are studied in stage two which is categorised as “Structural Testing”. In this section, structural properties and behaviour of PVA-FRC beams were assessed under the action of both monotonic and cyclic loads. Herein, flexural capacities, damping properties and ductility of different FRC beams are compared with conventional reinforced concrete (RC) beams.

Finally, the concrete beams are modelled using finite element (FE) software. FE analysed results are them compared to the experimental results to show how computer modelling can be a reliable tool in analysing PVA-FRC beams.

Furthermore, to help with concrete sustainability and use of more environmentally friendly materials, 30% of the Portland cement in all mixes in this project is replaced with Fly ash, which is also the perspective of the ” Green Building Council Australia” ('*Green Building Council Australia*').

1.3 Thesis layout

This thesis is divided into 6 chapters. Chapter 1 provides an introduction to the problem in addition to some background information regarding fibre reinforced concrete and its applications. The objectives of the research following some of the terminologies and concepts used in the thesis are clearly defined in this chapter.

Chapter 2 presents a comprehensive review on the concept of FRC as well as review of previous studies on PVA fibre in concrete and cementitious composites. A review of previous investigations on RC beams reinforced with fibres is also covered within this chapter.

Chapter 3 discusses the materials used in this study and the methodology followed in experimental studies of this research. In addition, the experimental program and testing methods are described further in details.

In Chapter 4, results obtained for the fresh properties (e.g. slump, compacting factor, air content and mass per unit volume) and hardened properties (e.g. compressive, tensile and flexural strength, modulus of elasticity and damping properties) of conventional and fibre reinforced concrete samples and structural testing results (4-point monotonic and 3-point cyclic flexural tests on concrete beams) are discussed in details.

Chapter 5 is dedicated to the finite element modelling and analysis of the concrete beams which have previously been tested. For this purpose, ATENA FE software that is mainly designed for concrete structures is used. The results of FE analysis are compared with that of experimental studies (from Chapter 4) to evaluate the validation of FE modelling in the case of FRC beams.

Finally, summary and conclusions as well as future works are presented in Chapter 6 and references to literature referred in this study and appendices are then presented at the end of the thesis to support the results of this research as supplementary materials.

1.4 Terminologies

The following concepts and terminologies are widely used in this thesis;

1.4.1 *Fibre reinforced cementitious composite:*

Fibre reinforced cementitious composite is a material made from hydraulic cement and discrete, discontinues fibres (but containing no coarse aggregate).

1.4.2 *Fibre reinforced concrete (FRC):*

FRC is a material made from hydraulic cement and aggregates of various sizes incorporating discrete, discontinues fibres.

1.4.3 *Ductility:*

Ductility is usually defined as ratio of the post yield deformation to yield deformation.

1.4.4 *Strain softening:*

Strain softening is the process in which the stress in the material is actually decreasing with an increase in strain.

1.4.5 *Strain hardening:*

Strain hardening is the process in which the post-peak (after limit of proportionality) stress in material is increasing with increase in strain.

1.4.6 *Fibre equivalent diameter:*

The equivalent diameter of a non-circular and prismatic in cross-section fibre is the diameter of the circle having the same area as that of the average cross-sectional area of an actual fibre (Zollo 1997).

1.4.7 *Fibre aspect ratio:*

The fibre aspect ratio is a measure of the slenderness of individual fibres which can be calculated as fibre length divided by the equivalent fibre diameter. Fibres for FRC can have an aspect ratio varying from approximately 40 to 1000 but typically less than 300. This parameter is also a measure of fibre stiffness and will affect mixing and placing procedures (Zollo 1997).

Chapter 2

Literature Review

2 LITERATURE REVIEW

2.1 Preface

In this chapter, the concept of fibre reinforced concrete and the function of fibres in a cement based matrix are comprehensively explained. Different categories of fibres and their effect on mechanical, structural and dynamic (damping) properties of concrete and cementitious composite are broadly investigated. Furthermore, PVA fibre characteristics are introduced and the effect of this fibre on mechanical properties of concrete and cementitious composite is described in details.

2.2 Fibre Reinforced Concrete (FRC)

The mechanical behaviour of a structure is greatly influenced by the constituent materials used. Based on their tensile load-deformation (displacement) response, most engineering materials can be categorized in three groups; brittle, quasi-brittle, and ductile (with or without strain-hardening) as shown in Figure 1.

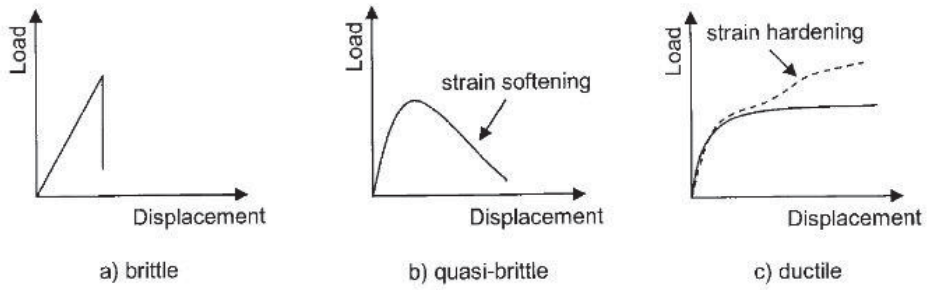

Figure 1. Three type of failure modes observed in materials (Frances Cyr 2003)

Brittle failure can be observed in hardened cement paste material. This type of failure, as illustrated in Figure 2 is characterized by a linear load-deflection curve followed by a sudden drop in load at first cracking with an ultimate tensile strain in the order of 0.01 % (Li 1998). Quasi-brittle (brittle-like) failure can be observed in concrete and most fibre reinforced cementitious composites which is characterized by a linear stress-strain curve followed by a softening tail after first cracking. The quality of softening part depends on the matrix components. This softening mostly occurs due to bridging action of aggregates, cement ligaments, and/or fibres. As graphically shown in Figure 2,

conventional concrete, avoiding fibre, demonstrates limited strain softening behaviour after peak load, however, a proper softening with an acceptable ductility can be observed in the case of FRC depending on fibre type and volume fraction. Ductile Strain-hardening materials (Figure 1- c), on the other hand, are capable of maintaining increasing levels of loading after first crack happens while undergoing large deformation (Li 1998). This behaviour can only be achieved by means of special matrix composition, suitable fibre type and mostly high fibre volume fraction.

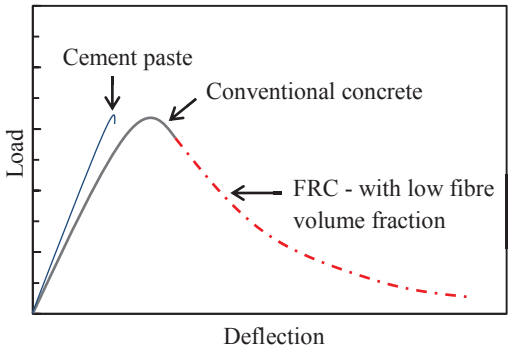

Figure 2. Schematic failure modes for cement, concrete and low fibre volume fraction FRC

Accordingly, it can be stated that fibres are added into a brittle-matrix composite to help improve three major aspects, namely; toughness, ductility and strength (tensile) (Arisoy 2002). Fibres tend to increase toughness of the composite material by bridging the cracks and providing energy absorption mechanism related to de-bonding and fibre pull-out. Furthermore, they can increase the ductility of the composite by allowing multiple cracking. They may also help increase the strength by transferring load and stresses across the cracks.

FRCs can be subdivided into three different classes, with regards to structural application. This characterisation is based on the fibre volume fraction, which ranges from low to high and intended functions of the reinforcing fibres. Fibre content may be considered low if ranging from 0.1 to 1.0%, moderate if ranging between 1 to 3% and high if in the range 3 to 12%, based on the volume fraction of total concrete produced. It is investigated that the fibre contents below the 0.1% volume fraction statistically have no significant effect on the characteristics of the hardened concrete (Midwest-Research-Institute 1994).

Fibres in low volume fraction do not serve any structural function and are often used for plastic shrinkage crack control. Moderate fibre volume fraction FRCs, are versatile

materials which can be found in both cast-in-place and pre-cast structural members. These types of FRCs are characterized by their improved modulus of rupture (MOR), fracture toughness, fatigue resistance, impact load resistance and other desirable mechanical properties (Balaguru & Shah 1992; Bentur & Mindess 1990). Fibres in such FRCs are often considered as secondary reinforcement used in combination with main reinforcing steel. Many successful investigations have been reported for partial replacement of shear steel reinforcement (Batson et al. 1972; Li et al. 1992) and for crack width control (Stang & Aarre 1992; Stang et al. 1995). In recent years, new techniques have been successfully introduced in order to place large amounts of fibres into bulk structures such as beams, columns and joints. High fibre volume FRCs have demonstrated excellent strength properties, fracture toughness, and sometimes even appear to exhibit strain-hardening behaviour. Due to the significant improvement in mechanical properties, these materials often share primary importance with the main reinforcements in a given structural member. Despite their high performance, when higher fibre volume fractions are used, wider applications of FRC might be hampered by special processing requirements. This concern often restricts the use of this material to precast members. Other important related concerns are the high cost and weight associated with high fibre volume fractions. These materials are usually restricted to steel fibre type.

Fibre amount and concentration affects the choice of FRC production technology. A summary of the basic fibre types, their ranges of commercial application, including the low, moderate, and high regimes, and the associated production technologies are presented in Figure 3. It is worth noticing that lower ranges of fibre additions are commonly more appropriate to be used in batch mix preparation utilizing conventional mixing equipment and traditional placement techniques (drop placement). When higher percentages are utilized, more complicated or special mixing and placing techniques should be explored.

Current concrete mixing and placing technologies include: batch mixing and placing, pneumatic placement, slip forming (moving-form extrusion), extrusion (through a stationary die), slurry infiltration, and sheet production with or without vacuum or pressure forming. By the means of specific production techniques, almost any fibre geometry and a wide range of fibre amount can be mixed and placed.

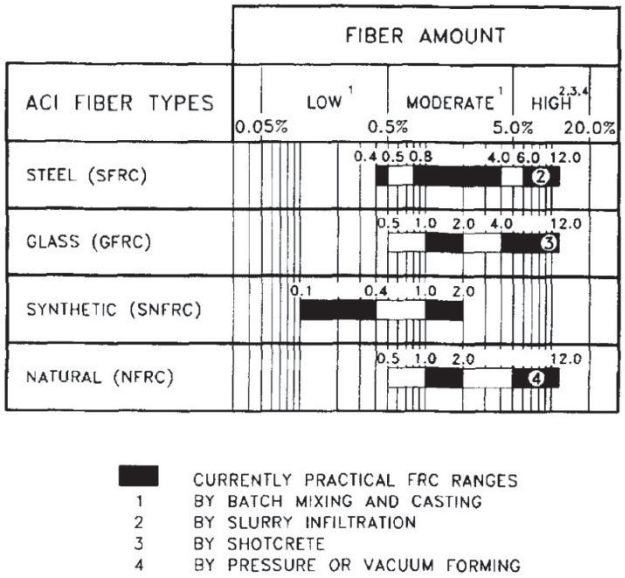

Figure 3. Fibre types and amount used by volume percent of matrix (Zollo 1997)

However, it is now well-known that composite properties depend on three groups of constituent properties; the fibre, matrix and interface properties (Li 1998). Fibre/matrix interaction plays an important role on controlling the material engineering properties and energy absorption capacities. Several types of fibre/matrix interactions include; interface debonding, frictional sliding, and inclined angle effects associated with random fibre orientations also exist, which lead to energy absorption in the fibre bridging zone of an FRC (Brandt 1986). Although the amount of energy associated with each mechanism for a single fibre may not be considerably high, the large number of fibres bridging over an extended length can dramatically help with improving the toughness of the composite (Li & Maalej 1996).

Figure 4, illustrates the mechanism by which fibres act to absorb energy and control crack growth. From left to right along the crack, the mechanism can be categorised as; fibre rupture, fibre pull-out, fibre bridging by tension through the fibre, and debonding at the fibre/matrix interface, respectively.

Where bridging zone ends, fibres tend to being pulled out of the matrix which is typical of steel and polymer fibre reinforced concrete. For composites incorporating brittle fibres such as carbon, the end of the bridging zone is associated with the rupturing of fibres. Fibre debonding involves the failure and breakdown of the material in the interfacial transition zone (ITZ) due to interfacial shear created from the pulling out mechanism of a fibre bridging a crack (Li & Maalej 1996).

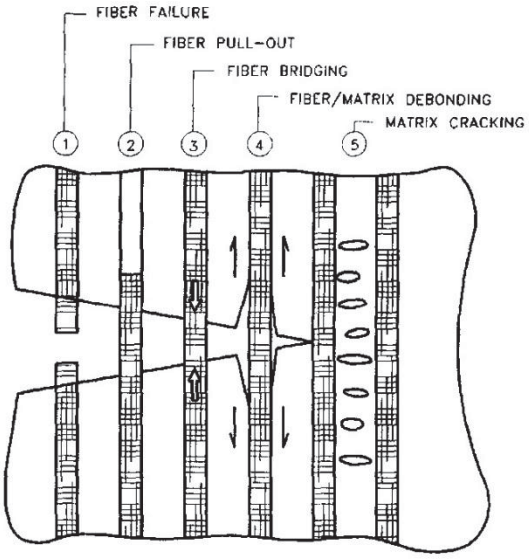

Figure 4. Energy-absorbing fibre/matrix mechanisms (Anderson 2005)

Commonly, fibre pull-out rather than rupture provides a larger ductility to the fibre reinforced composites (Cooper & Kelly 1970; Li et al. 1997; Lin & Li 1997). It is most desired to have composites showing strain-hardening behaviour which can be achieved through multiple cracking of reinforced matrix (Naaman & Reinhardt 1996).

Figure 5 and Figure 6 show some scanning electron microscope (SEM) images of fibre rupture and fibre pull-out. Figure 5 demonstrates the structure of a fibre in a cementitious matrix before fibre is pulled-out and the remained groove just after the fibre pull-out.

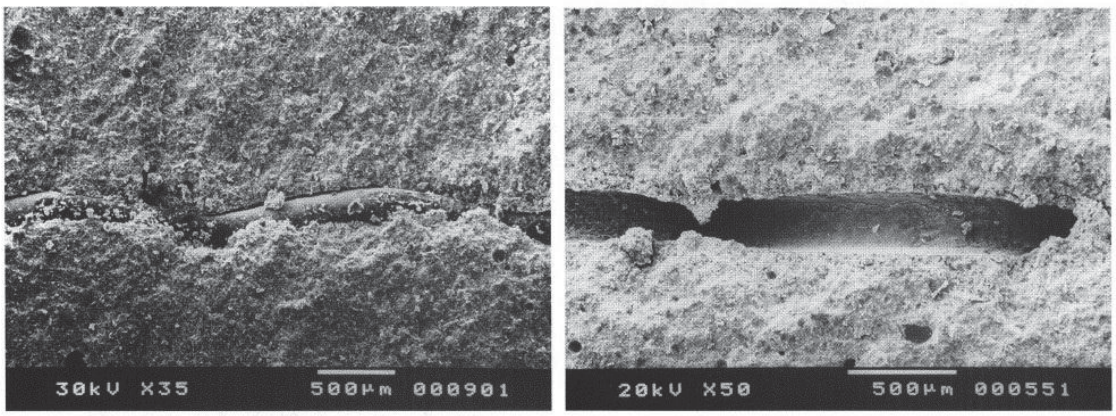

(a) (b)

Figure 5. The structure of fibre in matrix: (a) fibre prior to pull-out and (b) the groove after fibre pull-out (Bentur et al. 1997)

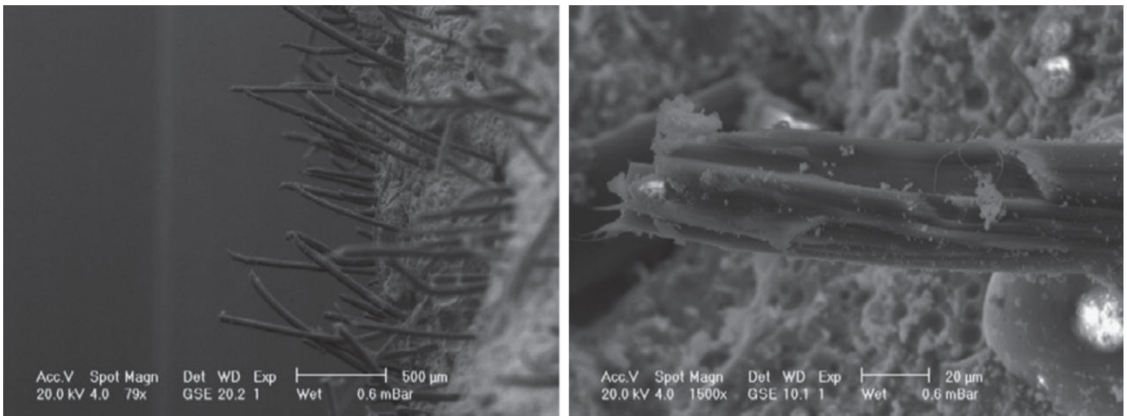

(a) (b)

Figure 6. Fibre pull-out (a) and fibre rupture (b) (Mechtcherine et al. 2011)

Depending on the physical nature of the fibre/matrix interface, different types of debonding mechanism can be observed which can be whether strength or fracture controlled. In a composite, fibres can be expected to have different embedment lengths. When crack opening is small, most of the fibres are anticipated to undergo de-bonding which results in an ascending stress-strain relationship (strain hardening). However, when the matrix of a typical FRC cracks under uniaxial tension, this behaviour might not be possible to be observed since the load would have exceeded the maximum bridging stress when the matrix cracks. This will result in a sudden load drop with a large crack opening and descending stress-strain relationship. The strain hardening can only be captured in the case of pseudo strain hardening FRCs. This is possible since in such a composite, the material can continue to carry higher load after matrix first crack. This stress-strain relationship can be obtained by tracking the load-crack opening on one of the multiple cracks in a uniaxial tension test (Li & Maalej 1996).

The above mentioned mechanisms are effective, although in insignificantly small amounts, even for a single fibre. The reason is that, these mechanisms do not depend on fibre spacing and fibre amount within the matrix and only relies on the fibre/matrix interaction. However, it is the cumulative effect of large numbers of fibres located in the constrained topography of the brittle FRC composite which has been shown to be significant.

Primary benefit of fibre reinforced concrete (FRC) arises from the fibre-bridging effect across matrix cracks. As soon as a crack forms or extends in the matrix, the modulus within the crack is effectively zero and crack opening is only resisted by the transfer of

stress through the fibre. This is the case if adequate bond or anchorage of the fibre is provided and there is sufficient opportunity for the fibres to participate in the process, i.e. an adequate concentration of fibre. It should also be taken into account that mixing and placement processes ensure that the fibre will not adversely affect composite fracture toughness by becoming matrix-disruptive. For instance, if coarse and stiff fibre is employed, the mix design should be modified with regards to the size of aggregate used to minimize this effect.

As shown in Figure 7, Two typical type of tensile stress-strain curves are available depending on fibre/matrix interaction and also fibre content. In cases where fibre volume fraction is very low or the fibre are so well bonded that majority of them break at concrete cracking, the stress-strain behaviour of the matrix is similar to curve A. Whereas in presence of higher fibre volume fractions which are mostly pull-out rather than break, the resulting behaviour is comparable to curve B. However, depending on the type of fibre used in the composite, the shape of this curve may vary (Hannant 2003).

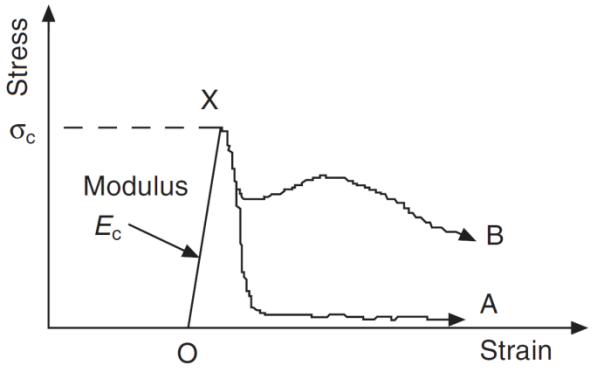

Figure 7. Typical stress-strain curves for fibre reinforced concrete (Hannant 2003)

More modern usage of fibres in construction industry goes back to about 100 years ago and creation of asbestos cement. Cellulose fibres were also used for at least 50 years. Furthermore, steel, glass, carbon and polymeric fibres such as polypropylene, polyethylene, and nylon fibres have been used for the past 3 decades to reinforce cementitious materials (Hannant 2003; Mindess 2007b). These types of fibres vary considerably in properties, effectiveness and cost. Some common fibres and their typical properties are listed in Table 1.

Table 1. Typical properties of concrete versus common used fibres in concrete and cementitious composites (Bentur & Mindess 2007; Hannant 2003)

Material	Modulus of elasticity [GPa]	Tensile strength [MPa]	Failure strain [%]
Concrete	20-45	1-7	0.1-0.2
Asbestos fibre	164-196	200-3500	2.0-3.0
Cellulose fibre	10-50	300-1000	20
Steel fibre	200	700-2000	0.5-5.0
Glass fibre	70-80	600-4000	2.0-3.6
Carbon fibre	30-390	600-4000	0.5-2.4
Polypropylene fibre	3.5-10	450-760	15-25
PVA fibre	23-40	900-1600	7.0-8.0

Since the early theoretical studies of FRC in the 1960s dealt primarily with the behaviour of steel fibre reinforced concrete (SFRC) it has become the most commonly-used fibre in concrete. Although steel fibres are still widely used, however, it is being overtaken by synthetic fibres (Bentur & Mindess 2007). One possible reason is that, unlike the steel fibre which is considerably prone to corrosion when present in close proximity to the surface of concrete, synthetic fibres are generally inert and have noncorrosive nature (Ong et al. 1999).

Synthetic fibres have become more popular in recent years as secondary reinforcement in cementitious materials. This is due to the fact that they can provide effective and relatively inexpensive reinforcement for concrete compared to conventional fibres such as asbestos, steel and glass.

Synthetic fibre types that have been utilized in cementitious matrices so far are namely; polyethylene (PE), polypropylene (PP), acrylics (PAN), polyviny1 alcohol (PVA), polyamides (PA), aramid, polyester (PES) and carbon. The properties of synthetic fibres may vary broadly, especially in term of modulus of elasticity. This characteristic plays an important role when fibres are used for producing composites (Zheng & Feldman 1995).

A synthetic fibre can be pronounced as a flexible, macroscopically homogeneous body, with a high aspect ratio and a small cross-section manufactured from naturally occurring macromolecules and synthetic polymers. The chemical, physical and mechanical properties of a synthetic fibre highly depends on the arrangement of the polymer chains in three-dimensional space. By improving the intermolecular chain organization that can generally be described as highly oriented and crystalline, we are able to enhance the characteristics of this type of fibres. All fibres have one specific structural feature in common which is a preferential orientation of their elemental units with respect to the

fibre axis. In the case of synthetic fibres, the preferential orientation is achieved through mechanical drawing operations, during which the filament is extended, instantaneously after extrusion, to several times compared to its initial length. Drawing plays two major roles, one of which is orientating structural elements with respect to the fibre axis in order to bring these elements into optimal stress-bearing positions and the other is of allowing the development of three-dimensional structural regularity. Macromolecular compounds used for making fibres are similar to those used as plastics, but for fibres, processing must produce an essentially infinite length to diameter ratio (Zheng & Feldman 1995).

In order to increase the strength of cementitious composites, fibres must have a modulus of elasticity greater than that of the matrix. Since the modulus of elasticity of cementitious composite is ranging from about 15 to 45 GPa, this condition is difficult to meet with most of synthetic fibres. Therefore, to overcome this challenge, attempts have been made to develop fibres with a very high modulus of elasticity. However, both theoretical and applied research have specified that, even by employing low modulus fibres, considerable improvements can be obtained with respect to the strain capacity, toughness, impact resistance and crack control of the FRC. In many applications, the improvement of these properties are much more significant than a slight increase in tensile (flexural) strength (Bentur & Mindess 2007).

In some applications, the low tensile strength of concrete can be enhanced by adding small diameter fibres which can be synthetic fibres. Majority of current FRC applications involve the use of fibres with approximately 1% volume fraction. Fibres are commonly considered not to affect the tensile strength of the matrix and only contribute after the initiation of the cracks by bridging the cracks (Zheng & Feldman 1995).

It is generally accepted that the inclusion of any type of randomly distributed short fibre at practical fibre volume fractions do not significantly change the first cracking load in hardened concrete (Hannant 2003). Incorporation of polymeric fibres in concrete are recognised to be most effective in controlling and mitigating susceptibility to plastic shrinkage cracking. In the role of intrinsic reinforcement, these fibres contribute to improving the ductile and damping behaviour of the concrete.

The main benefit of fibre addition relates to the post-cracking state of hardened concrete. It is worth considering an understanding of the word 'reinforcement'. If any load bearing capacity greater than zero is described as reinforcement, then all types of fibres at any volume addition will reinforce hardened concrete. However, if we consider 'reinforcement' to mean carrying a load in excess of the load required to crack the concrete, then less than about 0.4% volume fraction of fibres will not generally enhance the concrete capacities. Actually, two or three times this fibre volume is needed to increase the load capacity of concrete in uniaxial tension (Hannant 2003).

It has been observed that fibres in concrete enhance resistance to cracking due to external load and improve energy absorption capacity or toughness of conventional concrete (Alhozaimy et al. 1996; Gopalaratnam et al. 1991). Furthermore, the crack resistance is improved and delayed with increase in fibre content (Mobasher et al. 1990; Sivakuram & Sathanam 2007). Fibres can also improve the tensile strength, ductility, impact resistance, dynamic ability and durability of the concrete (Gencturk 2011; Kou & Poon 2010; Xu et al. 2010).

Previous research has demonstrated that reinforcing concrete with micro fibres does not contribute to the first crack stress as well as the maximum stress and its corresponding strain (Bayasi & Zeng 1993; Soroushian & Bayasi 1991). Authors of past research studies indicate that fibres assist with increasing concrete's volumetric strain capacity after cracking by bridging cracks and, thereby, changing the post peak behaviour of FRC.

Previous field and laboratory research (Padron & Zollo 1990) at 0.1% of synthetic fibre and 0.5% of steel fibre, reveal that the influence of fibre addition to the concrete is more in the nature of energy absorption and crack control rather than in increasing the load bearing capacity. Even though the fibre volume percentage is relatively low, since the fibres are uniformly distributed throughout the concrete mass and present in large numbers, they are affecting crack propagation in both concrete early ages as well as long term.

2.3 Polyvinyl Alcohol Fibre (PVA)

Poly(viny1 alcohol) is adopted from poly(viny1 acetate) which is readily hydrolysed by treating an alcoholic solution with aqueous acid or alkali (Feldman 1989) , leading to the structure shown in Figure 8. PVA contains hydroxyl groups (OH) which have the potential to form hydrogen bond between molecules resulting in a remarkable change in surface bond strength between PVA fibers and the matrix (Xu et al. 2010).

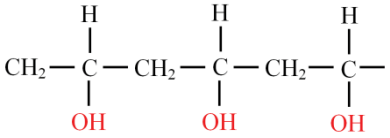

Figure 8. PVA fibre structure

PVA is a white powder with specific gravity ranging from 1.2 – 1.3 (1200-1300 kg/m^3) (Toutanji et al.). This powder is then formed and extruded to become PVA fibers which are commercially produced. Table 2 shows the most common types of PVA fibre commercially available in the market. PVA fibres mostly have aspect ratios (L_f/d_f) of 45 to 250 and different cut length varying from 6 to 30 mm to make fibres suitable for different applications. Depending on fibre geometry (length and diameter), the tensile strength and elastic (Young's) modulus of PVA fibre differ. It varies from 1600 to 800 MPa in the case of tensile strength and 40 to 23 GPa with respect to the elastic modulus with increase in fibre length and diameter. PVA fibres are also available in both resin bundled (oil coated) and virgin (non-coated) type.

Table 2. Common types PVA fibre available in the market

Length [mm]	Diameter [mm]	Tensile strength [MPa]	Modulus of elasticity [GPa]	Manufacturer
6	0.024	1600	39	Nycon Corp. - USA
6	0.027	1600	39	Kuraray Co., LTD - Japan
8	0.038	1600	40	Nycon Corp. - USA
8	0.038	1400	30	Nycon Corp. - USA
8	0.04	1600	40	Kuraray Co., LTD - Japan
8	0.04	1300	30	Kuraray Co., LTD - Japan
13	0.1	1200	25	Nycon Corp. - USA
18	0.2	1000	29	Kuraray Co., LTD - Japan
19	0.2	1000	29	Nycon Corp. - USA
30	0.66	900	23	Kuraray Co., LTD - Japan
30	0.66	800	23	Nycon Corp. - USA

PVA fibre has a rough surface. This property significantly improves the mechanical interlocking related adhesion capacity of this fibre in a matrix (Felekoğlu et al. 2009).

Generally, the surface structure of a fibre is very effective on its performance. The highly hydrophobic and smooth surfaces usually reduce the composite performance (Li & Stang 1997). To illustrate the surface roughness differences between fibres, SEM images captured at the same magnification of PVA fibre versus Polypropylene (PP) fibre, which has a very smooth surface structure, are presented in Figure 9.

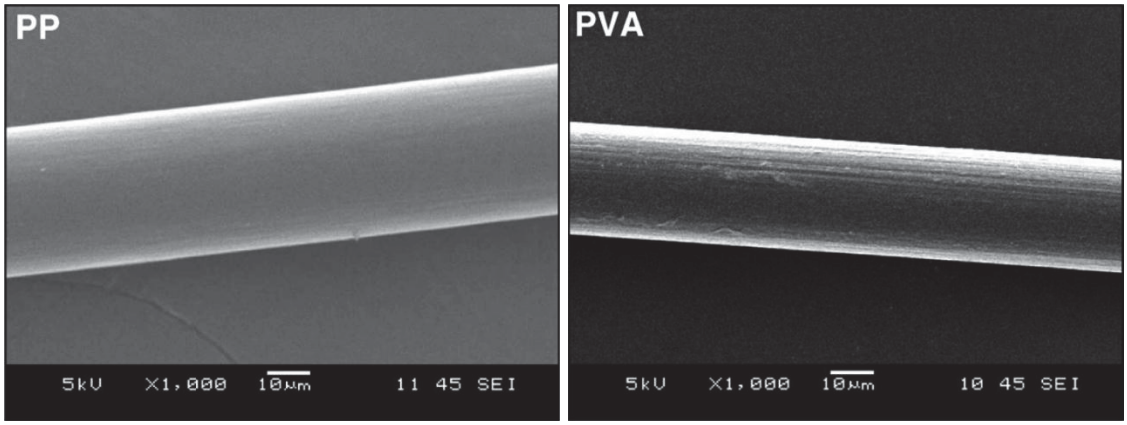

Figure 9. Scanning electron microscope (SEM) images of Polypropylene (PP) and PVA fibres (Felekoğlu et al. 2009)

2.4 Mechanical properties of PVA-FRC

The pioneering works (Hannant 1980; Krenchel & Shah 1986; Zensveld 1975) on synthetic fibre reinforced concrete and cementitious composites, emphasized the need to overcome disadvantages due to the low modulus of elasticity and poor bonding properties of synthetic fibres within the matrix. The latter is particularly a problem in reference to many of the synthetic fibres due to their chemical composition and their surface properties (Bentur & Mindess 2007).

PVA fibre serves several advantages when used in concrete or cementitious composites. It has high aspect ratio, high ultimate tensile strength, relatively high modulus of elasticity, good chemical compatibility with Portland cement, good affinity with water and no health risks. Since PVA fibres are mostly stiffer than the concrete matrix and also provide a good interfacial bond with the cement matrix, they generally have a positive effect on the bending strength and other mechanical properties of their composites. The high tensile strength of PVA fibres contributes to sustaining the first crack stress and resisting pull out force due to the strong bond present between the fibre and the cementitious matrix. In contrast, the low lateral resistance of the fibres may also lead to premature fibre rupture before being pulled out of the matrix (Atsuhisa et.al, 2006). PVA fibres elongate and transfer the load to different parts of the matrix and as a result the load applied is distributed more evenly between the loading surfaces.

The good interfacial bond between PVA fibre and matrix is attributed to non-circular cross-section of the fibres, and hydrogen bonds between the fibres and the cement matrix (Zheng & Feldman 1995). However, this very strong chemical bonding of PVA fibres with cementitious materials, which is due to the presence of the hydroxyl group in PVA molecular chains, brings up a challenge. This high chemical bonding leads to tendency of fibre to rupture and limits the multiple cracking effect which results in a lower tensile strain capacity and strain hardening profiles of the resulting composite (Redon et al. 2001). Felekoğlu and colleagues (Felekoğlu et al. 2009) reported that, in a concrete sample containing PVA fibres subjected to flexural loading, after the maximum load, PVA fibres were ruptured, beginning from the bottom of crack plane. By using scanning electron microscope (SEM) images, they have stated that hardly any elongated or slipped fibres were observed on fracture surface of the sample and fibres were mostly ruptured.

Figure 10 shows the surface of PVA fibre after failure. As seen, PVA fibres severely delaminate at the previous embedded ending after the extraction. This is due to the strong interfacial bond between fibre and matrix. Since failure always occurs in the weakest point through which load is transferred between the matrix and fibre, in this case the failure is shifted to the fibres in proximity of the interface, as the fibre–matrix bond strength is greater than the fibre shear strength (Di Maggio et al. 1997). For this reason, PVA fibres usually rupture without elongation (they preserve their initial diameters) or fibre surface gets extremely damaged if slippage rarely happens (Felekoğlu et al. 2009).

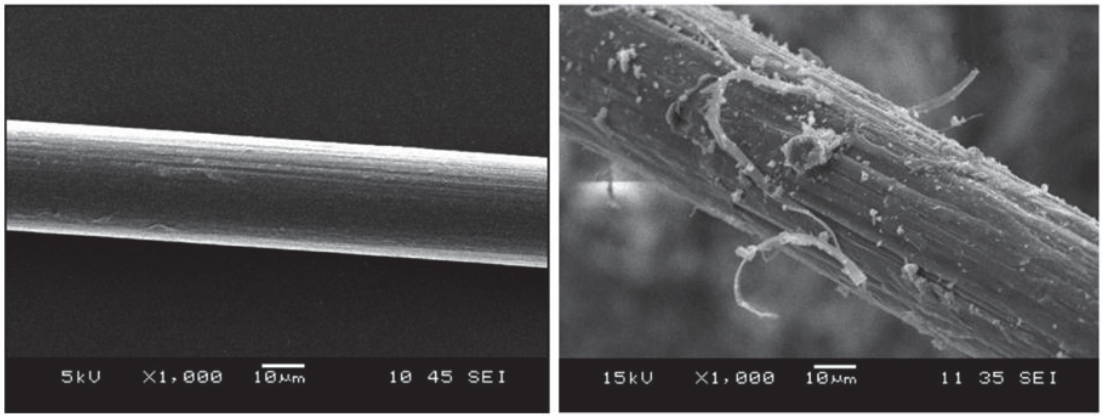

(a) (b)

Figure 10. Scanning electron microscope (SEM) images of PVA fibres surface; (a) original fibre (b) after failure (Felekoğlu et al. 2009)

Reducing the chemical bond between PVA fibre and matrix, enhances the complementary energy (Li et al. 1997) by minimizing premature fibre breaking during the fibre/matrix interface debonding process, prior to fibre slippage. Decreasing the interfacial frictional bond strength within a certain limit at the beginning of fibre slippage process can also facilitate fibre pull-out which results in even further energy absorption (Redon et al. 2001). In order to reduce the frictional bond, an oiling agent may be applied to the surface of PVA fibres. An oiling agent makes PVA fibres more hydrophobic and allow them to slip-out more easily and minimize the rupture in composite (Redon et al. 2001). This way, fibre slipping from the matrix and slip-hardening response during fibre pull-out might be obtained. This increase in displacement capacity results in formation of a higher area under the load–displacement

curve and enhances the composite toughness (Felekoğlu et al. 2009; Li et al. 2002; Redon et al. 2001).

Up to now, many research works have been carried out to investigate the effect of PVA fibre on different aspects of engineering cementitious composites (ECCs) such as; material properties (Kong et al. 2003; Li & Wang 2006), structural performance under cyclic loading (Fischer & Li 2007), nanoscale chemical and microstructural mechanical properties (Li & Stang 1997; Li & Wang 2006; Sakulich & Li 2011), fatigue performance (Zhang & Li 2002), durability (Şahmaran & Li 2007, 2008, 2009), water permeability (Lepech & Li 2009), autogenous and drying shrinkage (Şahmaran et al. 2009), cyclic freeze–thaw resistance (Şahmaran et al. 2012) and impact resistance (Yang & Li 2012).

ECC is a mortar-based composite reinforced with specially selected short random fibres invented in the early 1990's. ECC is a class of ultra-ductile fibre reinforced cementitious composites. Unlike conventional concrete, ECC has a strain capacity in the range of 3 - 7 % which is hundred times more than that of concrete. In terms of matrix component, it is very similar to normal concrete, except it does not include coarse aggregate (Li 2003).

PVA-ECC shows a strain hardening behaviour with average strain at peak stress of approximately 5 - 6 % (Li et al. 2002). A successful strain-hardening performance in PVA-ECC has been reported using PVA fibres of 12.7 mm length and 0.048 mm diameter (Kong et al. 2003). PVA fibre is likely to rupture rather than being pulled out in a cementitious matrix, as a result of the strong chemical bonding with cement due to the presence of the hydroxyl group in its molecular chains (Li et al. 2001). Therefore, the surface of the PVA fibres is coated with a proprietary hydrophobic oiling agent of 1.2% by mass. This treatment helps with increasing the interfacial properties between fibre and matrix for ECC strain-hardening performance (Şahmaran et al. 2012).

In a previous study (Şahmaran et al. 2012) on PVA-ECC, it has been reported that (Table 3) the compressive strength of ECC is improved by adding PVA fibres to the mix. In addition, an acceptable freeze–thaw resistance (according to ASTM C666, Procedure A) has also been recorded.

Table 3. Compressive strength of ECC with and without PVA fibres (Şahmaran et al. 2012)

Mix ID	Ingredients [kg/m^3]					Compressive Strength [MPa]	
	PC	FA	Sand	Water	PVA	14-day	28-day
ECC-without fibre	558	669	446	356	-	36.1	60.3
ECC-with fibre	558	669	446	356	26	39.2	62.5

According to isotropic mechanical properties of PVA-ECC which results in a ductile material with high energy absorption capacity (toughness) and high tensile and flexural strength leading to a significant impact on structural response, Li (Li 1998) states that PVA-ECC has the potential to be used in applications such as seismic retrofits, joints, structures subjected to dynamic and impact loads (e.g. pavements, bridge decks) and concrete covers for durability.

Betterman and colleagues (Betterman et al. 1995) studied the tensile properties of PVA fibre reinforced mortar. In their investigation, specimens reinforced with varying volume fractions (V_f = 1%, 2% and 4%) of different-sized (L_f = 4, 7 and 12 mm) fibres were tested in direct tension. The diameter of fibres varied (d_f = 0.012, 0.024 and 0.041 mm) so that each fibre length had an approximate aspect ratio of 300. The experimental results indicate that the first peak stress increases with increasing fibre volume fraction as well as a decrease in fibre diameter for a constant fibre aspect ratio. On the other hand, the toughness increases with an increase in fibre volume fraction as well as an increase in fibre diameter.

PVA fibre has also been used in self-compacting micro-concrete composite. In a study carried out by Felekoğlu et al. (Felekoğlu et al. 2009), 1% by volume of 8 mm length PVA fibres with diameter of 0.030 mm (aspect ratio = 267) were added to a micro-concrete composite containing; Portland cement, fly ash and limestone powder as micro-aggregate. Results conclude that the flexural strength and toughness of micro-concrete significantly improves by incorporation of PVA fibres. The rate of improvement in flexural strength is in the range of 100%.

PVA has also been used in high performance lightweight concrete. Arisoy and Wu (Arisoy & Wu 2008) investigated the effect of adding 1.5% volume fraction of PVA fibre (L_f = 15 mm, d_f = 0.037, E_f = 40 GPa) on a lightweight concrete matrix containing; Portland cement, fly ash, silica fume, lightweight aggregates, regular sand, air entraining agents and superplastisizer. Results of the experiments showed that

lightweight concrete exhibits higher flexural strength, ductility and also strain hardening behaviour by adding 1.5% volume fraction of PVA fibre.

Limited research has also been carried out to date to investigate the effect of adding PVA fibre to a concrete matrix. Researchers (Bangi & Horiguchi 2012) have reported that the use of PVA fibres in concrete affect the fresh properties of concrete demonstrating a decrease in the workability of the mix. Comparing 6mm length PVA fibre in two different diameters, 16 and 40 μm, Bangi and Horiguchi observed that the air content remained constant at 1.7% for both mixes whereas slump decreased significantly from 209 to 49 mm with an increase in fibre diameter (Bangi & Horiguchi 2012). Fibres with smaller diameter showed 115% higher compressive strength than other fibre sizes and both PVA concrete mixes demonstrated lower air content (AC) and compressive strength compared to control concrete. These results are also supported by Li and Yang (Li 2008; Yang 2008).

Furthermore, from past experimental research carried out on PVA fibre reinforced mortar incorporating 30% styrene butadiene polymer-latex (Debs et al. 2006), it has been reported that the compressive strength and indirect tensile strength increased from 35 MPa to 45 MPa and 4.0 MPa to 4.6 MPa for mixes containing a fibre volume fraction of 2%, 3% and 4%,, respectively.

In a recently completed research (Li et al. 2012), using 6 mm length PVA fibre in a concrete matrix with a mix proportion shown in Table 4, it has been reported that although the concrete compressive strength was not considerably affected by adding PVA fibre, the crack resistance and flexural properties of concrete and, to some degree, its toughness increased.

Table 4. Mix proportions and concrete samples compressive strength (Li et al. 2012)

Mix ID	Ingredients [kg/m^3]					28-day Compressive Strength [MPa]
	PC	Sand[1]	Gravel[2]	Water	PVA[3]	
Plain concrete	432	587	1190	200	-	39.3
PVA-FRC	432	587	1190	200	1.5	39.2

[1] Fineness modulus = 2.13, silt content = 1.5%
[2] limestone gravel with continuous distribution size of 5–25 mm
[3] L_f = 6 mm, d_f = 0.015 mm, tensile strength = 1200 MPa, E_f = 35 GPa

In an investigation (Ong et al. 1999) on PVA-FRC slabs subjected to low velocity projectile impact, it has been concluded that slabs reinforced with 12 mm length PVA fibres of three different fibre volume fraction (0.5%, 1% and 2%) exhibited higher

fracture energy values compared to the conventional concrete (Table 5). A comparison of failure pattern of PVA-FRC slabs showed that as the fibre content increased, the number of cracks and the size of the failure zone decreased. It was also observed that fibres have been failed due to pull-out at the fracture zone.

Table 5. Mix proportion and slabs fracture energy values (Ong et al. 1999)

Mix ID	Mix proportions (by weight)			W/C	V_f [3]	Fracture energy
	PC	Sand[1]	Gravel[2]		[%]	[N.m]
Plain concrete	1	1.3	2.1	0.4	-	154.40
PVA-FRC-1	1	1.3	2.1	0.4	0.5	283.20
PVA-FRC-2	1	1.3	2.1	0.4	1.0	321.95
PVA-FRC-3	1	1.3	2.1	0.4	2.0	391.34

[1] Natural sand
[2] Crushed granite aggregate with maximum nominal size of 10 mm
[3] PVA fibre; L_f = 12 mm, d_f = 0.2 mm, tensile strength = 900 MPa, E_f = 29 GPa

In a study carried out by Bangi and Horiguchi (Bangi & Horiguchi 2012), it was generally observed that addition of synthetic fibres reduced the workability of concrete which may have been caused by intertwining of the fibres during mixing which results in a lower slump. Furthermore, as shown in Table 6, a reduction in compressive strength and an increase in tensile strength have been recorded. It is also noticeable that with the same fibre length (6 mm), PVA fibres of greater diameter (0.040 mm) reduce the concrete workability and compressive strength more than that of smaller diameter (0.016 mm) fibres.

Table 6. Mix proportions and mechanical properties (Bangi & Horiguchi 2012)

Mix ID	Ingredients [kg/m^3]			W/C	V_f	Slump	AC	$f_{c,28}$	$f_{ct,28}$
	PC	Sand	Gravel[1]		[%]	[MPa]	[%]	[MPa]	[MPa]
Plain concrete	567	795	771	0.3	-	198	1.8	89.70	5.31
PVA- 6(16)	567	795	771	0.3	0.1[2]	209	1.7	79.23	5.56
PVA- 6(40)	567	795	771	0.3	0.1[3]	49	1.7	69.14	5.60

[1] Crushed stone with maximum nominal size of 13 mm
[2] PVA fibre; L_f = 6 mm, d_f = 0.016 mm
[3] PVA fibre; L_f = 6 mm, d_f = 0.040 mm
* Note: A polycarboxylate ether based superplasticiser was used at a dosage of 0.9% of cement content to achieve desired workability.

An investigation (Sun et al. 2001) on shrinkage and water permeation of concrete (matrix ingredients; PC, silica fume, river sand, crushed diabase stone with continuous grading of 5 – 15 mm and W/C = 0.32) containing different types of fibres, including PVA fibre of 8 mm length, 0.015 mm diameter with tensile strength of 1200 MPa and Young's modulus of 26-28 GPa, showed that a hybrid of PVA and steel fibre significantly reduce the shrinkage of concrete. It was also observed that when the

volume fraction of fibre was kept constant, the effect of fibre on drying shrinkage depended on the elastic modulus of fibre besides its size and volume fraction. Fibres with higher elastic modulus in a relatively high volume fraction (1.5%) are the most effective to reduce the concrete shrinkage strains.

It is reported by Flores-Johnson and Li (Flores-Johnson & Li 2012) that the compressive strength, tensile strength and integrity of foamed concrete was considerably increased by reinforcing matrix with 3% volume fraction of 8 mm length PVA fibres (d_f = 0.04 mm, tensile strength = 1600 MPa, E_f = 40 GPa). It is notable that foam concrete is an ideal core material for composite sandwich structures. This material is a type of cellular solid composed of cement mortar matrix and air-void of minimum 20% in volume which is manufactured by incorporating air-voids into the cement matrix using preformed foam.

In a study (Corinaldesi & Moriconi 2011) performed on self-compacting concrete (SCC) reinforced with PVA fibres (L_f = 12 mm, d_f = 0.2, tensile strength = 1000 MPa, E_f = 30 GPa), has revealed that compressive strength at 28 days of SCC increases by adding PVA fibre to the mix. On the other hand, results show that the flexural strength of the concrete decreased with inclusion of PVA fibres. It has also been reported that the modulus of elasticity of concrete seems not to be noticeably affected by fibre additions, although a very small reduction is observed for PVA-SCC. In the case of concrete drying shrinkage, PVA-SCC showed higher drying shrinkage values compared to the reference concrete at the first 3 weeks of age, however, after 21 days of age the reverse is true. PVA-SCC showed 25% lower drying shrinkage at 180 days of age.

2.5 Structural properties of FRC beams

Low tensile strength and brittleness are the main weak points of concrete as a structural material. The addition of fibres may significantly enhance the mechanical properties of concrete such as ductility and residual load bearing capacity (toughness) (Radtke et al. 2012). Ductility is characterized as a dominant safety feature of a structure since it demonstrates the ability of a structural element to withstand inelastic deformation prior to failure without significant loss in resistance. Ductility, acts prevailingly in delaying local failure of statically indeterminate structures by permitting redistribution of stresses from one critical section to another (Jeong 1994).

Adding fibres into a conventional concrete matrix, significantly improves the post-peak behaviour by providing an enhanced residual strength which is also defined as toughness. At the structural level, FRC toughness allows smaller crack opening which results in a higher durability. This property is particularly significant at serviceability limit state. Furthermore, by using FRC, it may be possible to reduce (or even totally remove) the shear reinforcement (Meda et al. 2012).

When a reinforced concrete is subjected to bending load, it is susceptible to cracks initiating from tensile stresses. Stress redistribution after initiation of cracks, creates stress concentrations where the cracks meet the reinforcing steel bars resulting in the plastic deformation of the bars. Addition of fibre to the concrete mix, may suspend the steel bar yielding by bridging the cracks and restricting the crack development which results in higher load bearing capacities. Furthermore, fibres may also act as secondary reinforcement in the plastic region of RC beams and contributes to transferring the load through the cracks which leads to an increase in tensile ductility.

Literature offers some specific information and research outcomes on the evaluation of FRC reinforced beams. The best test methodology to evaluate the post-cracking and toughness properties of FRC is the beam bending test. Design codes recommend one of two bending test configurations: the three-point or the four-point bending test (Bencardino et al. 2012).

On the utilisations of different types of fibres in concrete to measure the structural behaviour, findings are summarised in the following paragraphs;

The effect of steel, glass and polypropylene fibre have been reported in an earlier investigation (Fanella & Naaman 1985) to improve the post peak behaviour of concrete.

By increasing fibre content, ductility and toughness (energy absorption) are also increased.

It has been noted that, use of steel fibre in concrete can be very beneficial in improving the mechanical behaviour of the mix. These fibres have been investigated extensively during the past few decades. For instance, Craig (Craig 1987) studied that adding 2% fibre by volume of the mix is very beneficial to improve behaviour of the reinforced concrete beams. This study shows that by adding mentioned amount of fibre into the mix, increase in ductility, ultimate strength and especially the compressive strength and stiffness can be observed. Soroushian and Bayasi (Soroushian & Bayasi 1991) investigated that using steel fibres in the mix can effectively improve the impact strength and toughness. Investigating the use of fibre in FRC, it is reported that using steel fibre in concrete can enhance the bond between the steel reinforcement and concrete paste (Hota & Naaman 1997).

In a study (Meda et al. 2012) carried out on full-scale RC beams reinforced with steel fibres subjected to 4-point bending test, it has been established that, fibres can modify the collapse mode of RC beams and shift the failure from concrete crushing to steel rupture and higher ductility is observed for FRC beams. Moreover, fibres greatly enhance the behaviour of FRC beams at service conditions through increasing the cracked-stage stiffness and as a result limiting the crack openings and deformations.

Bentur and mindess (Bentur & Mindess 1983) also report that the addition of steel fibres to conventional RC beams improves strength (ultimate load), rigidity and ductility under static loading. Furthermore, the addition of fibres is associated with a decrease in the width of the cracks and an increase in their quantity. In addition, the length of the cracks was much greater in the conventionally reinforced concrete which has almost extended to the top of the beam; however, the cracks in the fibre concrete did not usually extend beyond half the depth of the beam. The addition of fibres to conventionally reinforced concrete changes the cracking pattern on loading; the number of cracks increases and their width and length decreases. These observations are also supported by Purkiss and Blagojević (Purkiss & Blagojević 1993).

Rinaldi and colleagues (Rinaldi et al. 2006) have investigated the effect of adding 1% volume fraction of steel fibres (L_f = 30 mm, d_f = 0.6 mm) to a concrete beam (f_c = 25 MPa) reinforced with steel bars (f_{sy} = 460 MPa, f_{su} = 550 MPa) with geometry as shown

in Figure 11. Results obtained confirmed that the addition of fibre to the RC beams improves the ductility by 166%.

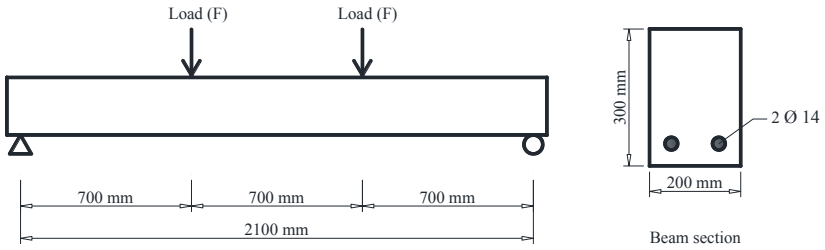

Figure 11. Schematic beam and reinforced section geometry (Rinaldi et al. 2006)

Swamy and Al-Ta'an (Swamy & Al-Ta'an 1981) studied the influence of fibres on the deformational behaviour and ultimate strength in flexure of reinforced concrete beams with 20 mm maximum size of aggregates and containing steel bar reinforcement with specified minimum yield strengths of 460 and 617 N/mm^2, respectively. Their experimental work consisted of flexural test (3-point bending test over a span of 2250 mm) on 130 × 203 × 2500 mm RC beams with steel ratio ranging from 0.99% to 1.78% containing 0.5% and 1% steel fibres (L_f = 50 mm, d_f = 0.5 mm). Test results indicated that FRC beams demonstrated much higher inelastic deformations and ductility at failure. The ultimate strength of the beams only showed a slight improvement whereas the post cracking behaviour has improved noticeably. As fibres arrest advancing cracks, the post cracking stiffness at all stage of loading up to failure increases; therefore, narrower crack widths and substantially less deformation can be observed.

A study (Soliman & Osman 2012) conducted on glass fibre reinforced RC beams under 4-point bending test, indicated that the failure mode of test samples become more ductile by the means of discrete glass fibres. Furthermore, an increase in the crack numbers and decrease in their width were also reported.

The addition of synthetic fibres to RC beams has rarely been investigated previously. Mindess and colleagues (Mindess et al. 1986) reported that the addition of polypropylene fibres to RC beams had only a small effect on toughness in static loading, whereas it exerts a much bigger influence on ductility during impact. Ramadevi and Venkatesh (Ramadevi & Venkatesh Babu 2012) have also reported that brittleness in concrete is reduced and an adequate ductility is ensured by the addition of synthetic hybrid fibres to the conventional RC beams.

In a study (Shimizu et al. 2004) on ECC beam reinforced with conventional steel bars and PVA fibres (Table 7) it has been observed that maximum strength of concrete beam increases by addition of fibre to the mix. Crack numbers were also increased and crack widths decreased – multiple cracking.

Table 7. PVA-ECC reinforced beam specifications and test results

Sample ID	Matrix properties				Beam specifications		Test results	
	V_f [1] [%]	$f_{c,28}$ [MPa]	ε_{cu} [%]	E_c [2] [GPa]	Section [3] b×d [mm^2]	Span Ratio [4]	Fist crack load [kN]	Maximum load [kN]
ECC	0.0	39.0	0.23	26.2	180×280	1.5	43.6	116.4
PVA-ECC	1.0	37.3	0.35	17.8	180×280	1.5	26.7	123.9

[1] PVA fibre; L_f = 12 mm, d_f = 0.04 mm, tensile strength = 1600 MPa, E_f = 40 GPa
[2] 1/3 secant modulus
[3] Section has 8Ø13 as beam longitudinal reinforcement.
[4] Shear span / beam depth
* Note: Steel bar properties; f_{sy} = 719.7 MPa, ε_{sy} = 3779, E_s = 190.5 GPa

In another study (Li & Xu 2009), the bending behaviour of RC beams with composite sections of conventional concrete on top and PVA-ECC at the bottom was investigated. Beams had a 80×120 mm rectangular cross section, 2000 mm span and longitudinal reinforcement ratio of 1.18%. The PVA fibre used was 12 mm in length and 0.039 mm in diameter with a tensile strength and modulus of elasticity of 1620 MPa and 42.8 GPa, respectively. The results of 4-point bending test showed that compared with the reference concrete beams (full section made of conventional concrete), introduction of PVA-ECC layer at the bottom of the beam significantly improved the load bearing capacity and ductility as well as controlling the beam deformations.

2.6 Damping characteristics of FRC and FRC beams

In places such as New Zealand or Australia, earthquakes or wind loads, respectively, pose high risks to buildings and more specifically tall buildings. Vibrations in a structure which are caused by these dynamic loads highly depend on the amplitude and frequency content of the excitation source. There is no doubt that dynamic properties of concrete materials are of great significance, particularly in vibration control and noise mitigation.

Damping is defined as a process whereby vibrational energy is dissipated over a period of time (Smith 1988). To avoid resonance of a specific structure at typical modes, whether at material level or member and structural level, damping is helpful in reducing vibration and resonance (Amick & Monteiro 2005; Zheng et al. 2008).

Two main sources of damping are categorised as intrinsic damping which is basically provided by the structure and the material damping. The other damping is the supplementary damping created utilizing additional devices attached to the structure such as tuned mass dampers, sloshing dampers, viscous dampers, and friction devices. Concrete buildings are generally known to have damping ratios between 1% and 3% of critical damping depending on the amplitude of motion. If it is possible to increase this percentage to say 5% or more, dampers can be eliminated or reduced in some of the structures and save lots of energy and money. It is also investigated that by increasing the damping ratio of concrete to 10 or 15% the structure gains the capacity to dissipate the vibrating energy without needing any additional dampers (Jinping et al. 2008; Ou 2002).

Damping ratio is the main parameter representing the property of materials in vibration reduction (Zheng et al. 2008). Due to the number of variables that affect damping in a system, the most realistic way of determining damping of a material or structure is through laboratory or field investigations. From amongst several methods for measuring and calculating the damping properties of materials and structures, logarithmic decrement method and hysteresis loop method are the most popular ones for concrete.

Logarithmic decrement (δ) which simply provides a measure of the rate of decay of oscillation is used to find the damping ratio (ξ) of an underdamped system based on the assumption of viscous damping. The logarithmic decrement is defined as the natural

logarithm of the ratio of any two successive positive amplitude peaks as shown in Equation (1) (Chopra 1995) and graphically illustrated in Figure 12.

$$\delta = \frac{1}{m} \ln \frac{U_n}{U_{n+m}} = \frac{2\pi\xi}{\sqrt{1-\xi^2}} \tag{1}$$

where U_n is the amplitude of nth peak, U_{n+m} is the amplitude of a peak after m cycles and m is the number of cycles between the two successive positive peaks.

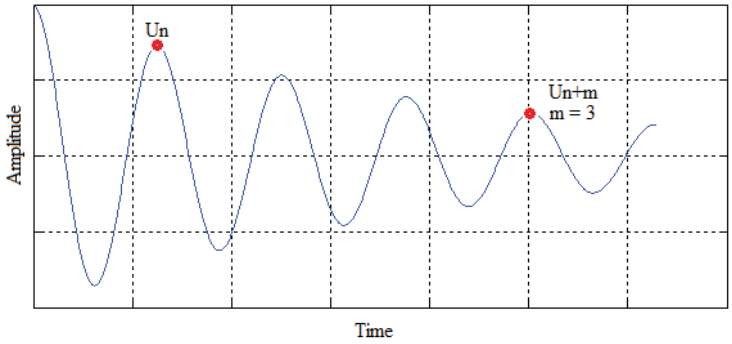

Figure 12. Schematic amplitude-time curve for the determination of logarithmic decrement

Since damping ratio is generally small in the case of concrete (<20%) (Menefy 2007), Equation (1) can be further simplified to give a direct relationship between δ and ξ as follows;

$$\delta \approx 2\pi\xi \tag{2}$$

Thus, damping ratio (ξ) can be calculated as;

$$\xi = \frac{1}{2\pi m} \ln \frac{U_n}{U_{n+m}} \tag{3}$$

The other method of measuring the damping property is hysteresis loop method. When vibration happens, hysteresis damping is generated by the internal friction within the body of the material (Menefy 2007). The damping measured by means of this method, is proportional to the amplitude of the deformed elastic body but independent of the frequency of vibration (Smith 1988). When cyclic loading is applied, the load-deflection curve gives an indication of the energy loss per cycle. The loop formed by the load-deflection curve is called a hysteresis loop (Figure 13) and the area enclosed within this loop represents the energy loss per cycle as shown in Equation (4);

$$E_D = \int f_D du = 2\pi\xi \frac{\omega}{\omega_n} k {u_0}^2 \quad (4)$$

where ω is the excitation frequency, ω_n is the natural frequency and k is the equivalent stiffness. As shown in Equation (4), the energy dissipated is proportional to the square of the amplitude of motion (u_0) and it is not a constant value for any given amount of damping and amplitude since the energy dissipated increases linearly with excitation frequency (Chopra 1995).

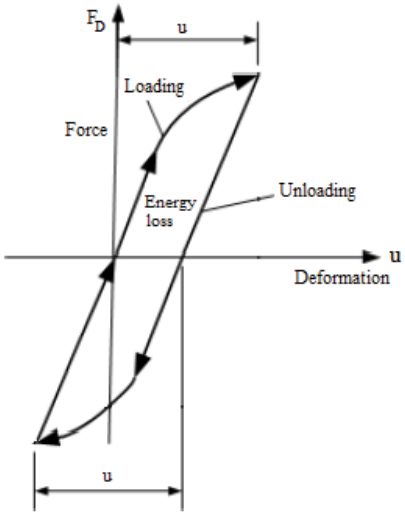

Figure 13. the hysteresis loop (Tedesco et al. 1999)

From the hysteresis loop and energy dissipated in each cycle, the damping ratio can be calculated as (Chopra 1995);

$$\xi = \frac{1}{2\pi} \frac{E_D}{E_{S0}} \quad (5)$$

where E_{S0} is the strain energy and can be calculated as;

$$E_{S0} = \frac{k\, {u_0}^2}{2} \quad (6)$$

Both the energy dissipated in each cycle of dynamic loading (E_D) and strain energy (E_{S0}) are shown in Figure 14.

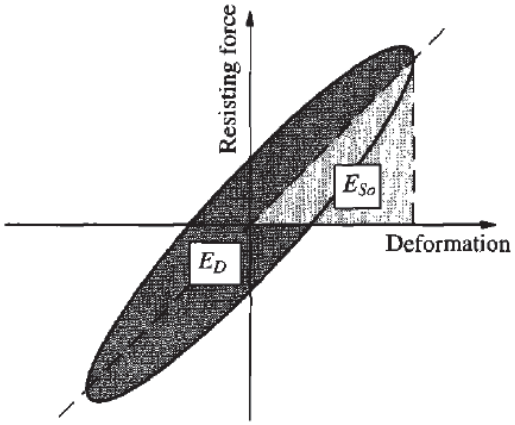

Figure 14. Definition of energy loss E_D in a cycle of harmonic vibration and maximum strain energy E_{S0} (Chopra 1995)

The first serious study on the damping behaviour of concrete was performed in 1940 by Thomson (Thomson 1940). In this investigation, it has been reported that the mechanical properties of concrete i.e. compressive strength and modulus of elasticity can be predicted through dynamic methods and damping measurements. Following the mentioned study, many research works have been carried out to explore the effect of various parameters (such as concrete composition, curing condition, moisture content, temperature, compressive strength and modulus of elasticity) on damping properties of concrete and concrete elements.

It has been stated (Cole 1966; Cole & Spooner 1965; Jordan 1980; Kesler & Y.Higuchi 1954; Swamy & Rigby 1971; Swamy 1970) that the moisture content of the specimen is the primary factor effecting concrete damping capacity, as the moisture in the pore structure contributes to the viscous component of damping. It was observed that concrete damping ratio is increasing with increase in moisture content.

The effect of ageing on damping property is also investigated. It has been stated by many researchers (Amick & Monteiro 2006; Cole & Spooner 1965; Swamy & Rigby 1971; Yan et al. 2000a) that concrete damping property decreases by ageing.

Moreover, it has been reported that compressive strength has no significant effect on damping properties of concrete (Cole & Spooner 1965) and damping ratio is more dependent on the interfacial relations of the microstructure within the concrete matrix (Jones 1957).

Micro cracking is also of importance in determining the damping properties (Swamy 1970). The degree to which micro cracking is allowed to propagate, has a major

influence on the damping capacity (Jordan 1980) as friction between interfaces of the internal structure contributes significantly to the Coulomb damping component (Menefy 2007). Researchers have revealed that the damping ratio of a crack free concrete is around 0.32% - 0.64%, while this value for a cracked concrete is around 1.3% - 2.1% (Yan et al. 2000a).

The effect of frequency on damping properties of concrete has also been studied by Jones (Jones 1957). The results of which stated that negligible differences exists when comparing the damping characteristics of concrete beams under the three main modes of vibration, which are longitudinal, flexural and torsional.

As a concrete specimen is excited dynamically, each element of the matrix absorbs a portion of the dynamic energy. The synthetic fibre itself, due to its viscoelastic energy dissipation character as a polymeric material, is able to absorb the energy inside itself (Sun et al. 1985). However, although fibres in synthetic FRC are viscoelastic and have damping ratios higher than concrete, the FRC composite is not a good viscoelastic material since it is usually accompanied by a low volume fraction of fibres. In such cases, adequate damping may not necessarily be produced due to the hysteresis energy loss in matrix because of the strain cycling in the vicinities of fibre ends, nor from synthetic fibres (Yan et al. 2000a). It can take place due to fibre/matrix debonding which may occur under certain strain and stress conditions surrounding the fibres. This may cause energy loss under alternating loading. Concrete is considered a brittle material which contains micro cracks that may open and close during dynamic loading under flexure. Theses cracks may cause the matrix to rub on the fibre surface and results in energy loss during vibration (Yan et al. 2000a, 2000b) and accordingly higher damping ratio can be achieved for FRCs (Fu & Chung 1996; Nelson & Hancock 1979).

The effect of steel fibre addition on dynamic properties of SFRC showed that the damping property of wet-cured FRC is almost 50% higher than that of plain concrete and dynamic modulus of elasticity remained approximately constant. The logarithmic decrement was reduced substantially by age and drying for both FRC and plain concrete (Swamy & Mangat 1974).

Giner and colleagues (Giner et al. 2012) have recently investigated the effect of discontinuous random fibre addition on dynamic properties of concrete. The fibres used in their study are carbon fibre (L_f = 3.5 mm, d_f = 0.0072 mm, tensile strength = 3800

MPa, E_f = 242 GPa) and steel fibre (L_f = 35 mm, d_f = 0.55 mm, tensile strength = 1200 MPa) with volume fraction ranging from 0.5% to 1%. To evaluate the fundamental frequencies of longitudinal, transverse and torsional modes of vibration for different concretes, prismatic specimens of 100 × 100 × 400 mm were tested following the specifications of the standard test method in ASTM C 215 as shown in Figure 15. The experimental values of resonant frequencies shows similar pattern in the three modes of vibration for different concrete samples. From the results of this investigation as shown in Table 8, it can be observed that under dynamic loads of low magnitude and high frequency, when cracks have not yet been developed, the addition of carbon fibre increases the damping ratio of concrete. However, under the same conditions, it is reduced by the addition of steel fibre. This fact makes carbon fibre more effective than steel fibre for reducing and controlling vibrations in structure.

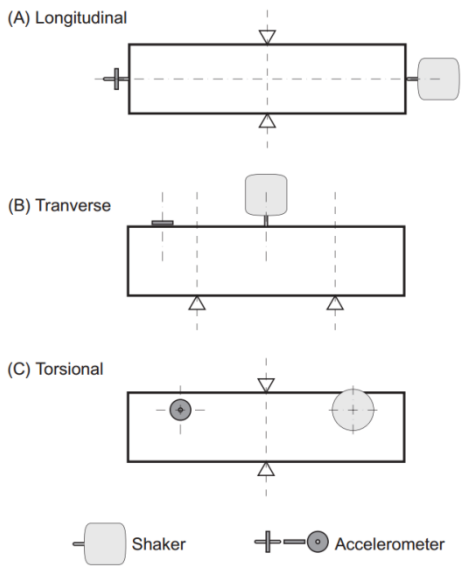

Figure 15. Experimental tests to obtain dynamic characteristics (longitudinal, transverse and torsional resonant frequency) of the concrete specimens (Giner et al. 2012)

Table 8. 28-day properties of plain and fibre reinforced concretes (Giner et al. 2012)

Type	$f_{c,28}$ [MPa]	Static modulus of elasticity [GPa]	Dynamic modulus of elasticity [GPa]	Dynamic modulus of rigidity [GPa]	Dynamic poisson's ratio	Damping ratio [%]
Reference	48.51	35.26	40.85	16.29	0.28	0.63
0.5% Carbon fibre	47.85	36.16	42.51	16.52	0.29	0.67
0.5% Steel fibre	46.80	33.73	41.43	16.13	0.26	0.63
1.0% Steel fibre	46.44	35.46	40.52	15.58	0.30	0.58

In another study (Bai et al. 2009) on glass fibre reinforced concrete (GFRC) using glass fibres of different length (5 – 25 mm) in different volume fractions ranging from 1 –

5%, it was observed that the damping ratio of GFRC is increased by using longer fibres up to a certain length (L_f = 20 mm). Thereafter, using longer fibre decreases the damping values. Furthermore, the damping ratio is increased as more glass fibres are used in GFRC.

Yan et al. (Yan et al. 2000a) investigated the dynamic properties of synthetic-FRC using polyolefin fibres of different geometric lengths (25 – 50 mm) and diameters (0.15 – 0.6 mm). The results of this study state that fibres significantly improve the damping ratio of concrete. In another research carried out by Yan and colleagues (Yan et al. 2000b), it has been concluded that in order to gain higher damping, fibres with a diameter less than 0.6 mm should be used. However, low aspect ratio fibres with a diameter greater than 0.6 mm may also be a prospective candidate to be used in concrete to enhance damping.

The relationship between damping ratio and other characteristics of a concrete matrix have been studied in some previous research works, for example, as the damping ratio changes, the flexural stiffness and ductility change as well (Arivalagan & Kandasamy 2009; Yan et al. 2000a). Accordingly, damping ratio can be used as an indication of changes in concrete characteristics. The benefit of damping test is that, it is generally a non-destructive test and the structure, element or specimen remains undamaged after the test.

First investigations into the dynamic behaviour of the reinforced concrete beams go back to 1950s (Penzien & Hansen 1954). The ongoing research has clarified some uncertain areas but further investigations in some aspects are still needed. Bellow, some findings in literature regarding the damping characteristics of the reinforced concrete beam elements is presented:

- Cracking is investigated to be the main reason for changes in frequency and damping of concrete elements in addition to moisture content (Askegaard & Langsoe 1986). Uncracked concrete has low damping characteristics and by starting the cracks, damping increases dramatically (Askegaard & Langsoe 1986; Chowdhury 1999; Penzien 1964; Wang et al. 1998).
- Concrete composition, age and curing which affect the material damping as outlined earlier, also contribute to the damping properties of structural elements (James & Lutes 1964).

- With the same concrete characteristics, increase in reinforcement leads to decrease in damping ratio (Carneiro et al. 2006).

2.7 Concluding Remarks:

According to previous studies on FRC, it can be concluded that fibre reinforcement is an effective way of improving the strength, ductility, and toughness of brittle materials. To achieve the best FRC function, fibres are supposed to have a relatively higher modulus of elasticity, higher tensile strength (at least 200% - 300%) and significantly higher elongation in tension compared to that of plain concrete and also in addition, having proper bond characteristics with cement matrix (Naaman et al. 2001).

PVA fibre was observed to have significant effect on improving the ductility and toughness of engineered cementitious composite (ECC) and it has great potential to be used in concrete as an intrinsic reinforcement due to its unique characteristics such as high tensile strength, high modulus of elasticity and proper bond with cement matrix.

Most of previous theoretical and experimental studies on FRC beams are limited to steel fibre reinforced RC beams. The result of those studies show that addition of fibres to the mix contributes effectively to preserve the structural stability and integrity as well as improving ductile behaviour of a concrete beam (Alsayed 1993; Bencardino et al. 2012; Lim et al. 1987; Patton & Whittaker 1990; Swamy & Al-Ta'an 1981).

Fibres generally, and synthetic fibres specifically, are reported to enhance the dynamic properties of concrete by increasing the damping ratio of plain concrete (Yan et al. 2000a). Furthermore, it has been reported that damping ratio can be used as an indication of changing concrete mechanical characteristics i.e. flexural strength and ductility (Arivalagan & Kandasamy 2009).

Chapter 3

Materials and Experimental Methodology

3 MATERIALS AND EXPERIMENTAL METHODOLOGY

3.1 Preface

In this chapter, the materials used and the methodology followed in order to carry out the experimental program are firstly presented and explained in details. Thereafter, the mix designs, material proportioning and mixing sequences are defined. The fabrication of test specimens and curing methods are then discussed. Finally, the different material and structural testing methods, testing ages and related standards are described in details and instrumentation and equipment utilised are presented.

3.2 Project materials

Several series of concrete mixes have been prepared using materials with specific properties as explained below;

3.2.1 *Shrinkage limited cement*

Portland cement (PC) is a hydraulic cement that is manufactured as homogeneous product by grinding together Portland cement clinker and calcium sulfate. The PC used in this study is shrinkage limited cement complying with Australian Standard; AS 3972, Type SL. Shrinkage limited cement is a special purpose PC manufactured from specially prepared Portland cement clinker and gypsum. It often contains up to 5% by mass of minerals addition in accordance with AS 3972. This cement is designed to be used in applications where there is a desire to minimise concrete drying shrinkage. Table 9 provides some characteristics of cement used in this project compared with the relevant specified requirements of AS 3972 for type SL cement.

Table 9. Typical properties of shrinkage limited cement versus AS 3972 requirements

Property		AS 3972 requirements	Typical properties of project cement
Setting time	(min.)	45 min	1.5 – 3 h
	(max.)	10 h	2.5 – 4 h
Soundness	(max.)	5%	<3%
Drying shrinkage	28-day (max.)	750 μstrain	550 μstrain
Compressive strength	7-day (min.)	35 MPa	42 – 50 MPa
	28-day (min.)	45 MPa	57 – 64 MPa

3.2.2 *Fly ash (FA)*

Fly ash, a by-product of coal combustion, is the solid material extracted from the flue gases of a boiler fired with pulverized coal (Standard 2010). In current project cement is partially replaced with 30% FA. The FA used in this study is a low-calcium type with loss of ignition (LOI) value of 1.65%. The fineness of FA by 45 μm sieve was determined to be 94% passing (tested in accordance with AS 3583.1-1998) which is categorized as fine grade FA. According to AS 3583.1, it has been mentioned that fine grade FA should have LOI value less than 4%. However, previous investigations (Feng & Krark 2001; Vandenberghe et al. 2010) has recommended FA to be used with the LOI value of less than 3%, since beyond this point due to higher portions of un-burnt carbon in FA structure, more water is required for the mix. The oxide compositions of binders (SL type cement and fly ash) are listed in Table 10.

Table 10. Oxide compositions of binders by x-ray fluorescence method

	SiO_2	Al_2O_3	Fe_2O_3	CaO	MgO	Na_2O	K_2O	TiO_2	MnO	P_2O_5	SO_3
PC [wt. %]	20.16	4.62	4.56	65.35	1.06	-	0.44	0.28	0.60	0.07	2.55
FA [wt. %]	65.13	23.75	3.38	1.92	0.49	0.48	1.46	0.92	0.07	0.25	0.07

From the literature (Malhotra 1990; Meyer 2009; Siddique 2004) it has been proven that, FA addition to the mix increases the long term strength and durability of concrete by prolonging the hydration process.

The main two products of cement hydration are calcium silicate hydrate (C–S–H) with 50 – 70% and calcium hydroxide (CH) with 20 – 25%. From these two components, C–S–H is the strength building binder for concrete where CH has no contribution to strength development and has no strength-forming properties. CH is also a potential site of weakness for certain forms of chemical degradation and leads to efflorescence and poor chemical resistance. Since FA is a pozzolanic material with aluminosilicate structure, it can react with CH to form additional C–S–H binder which is deposited in pore spaces. This leads to a general densification of the cement matrix, which contributes to increased strength, reduced permeability, and increased long-term durability (Fraay et al. 1989).

It has also been reported that FA improves the rheological properties and workability of concrete due to its spherically shaped particles and fineness (Neville 1991).

3.2.3 *Fine and Coarse aggregates*

A maximum nominal size of 20 mm aggregate is used in all mixes. All aggregates used in this project are sourced from Dunmore, Australia, which includes 50/50 blended fine/coarse manufactured sand and 10 mm and 20 mm crushed latite gravel. The grading of all aggregates as shown in Table 11 properly complies with the Australian Standard; AS 2758.1 specifications and limits. It should also be mentioned that, all fine and coarse aggregates are prepared to saturated surface dry (SSD) condition prior to batching.

Table 11. Sieve analysis

Sieve aperture	Fine aggregate		Coarse aggregate			
			10 mm (nominal size)		20 mm (nominal size)	
	Limits[1] [%]	Passing [%]	Limits [%]	Passing [%]	Limits [%]	Passing [%]
26.5 mm	-	-	-	-	100	100
19.0 mm	-	-	-	-	85 to 100	95
13.2 mm	-	-	100	100	-	51
9.5 mm	100	100	85 to 100	87	0 to 20	14
6.7 mm	-	100	-	49	-	6
4.75 mm	90 to 100	98	0 to 20	11	0 to 5	4
2.36 mm	60 to 100	81	0 to 5	3	-	3
1.18 mm	30 to 100	65	0 to 2	2	0 to 2	2
600 µm	15 to 80	55	-	-	-	-
300 µm	5 to 40	38	-	-	-	-
150 µm	0 to 25	8	-	-	-	-
75 µm	0 to 20	4	-	-	-	-
Absorption [%]		1.2%		1.8%		1.6%

[1] Limits define in accordance with AS 2785.1(1998)

3.2.4 *Polyvinyl alcohol fibre (PVA)*

PVA fibres of two different geometries, 6 and 12 mm, sourced from China as shown in Figure 16 are used in this study. Table 12 shows properties of PVA fibres as provided by the manufacturer. Both 6 and 12 mm fibres have the same diameter, thus the aspect ratio of the longer fibre ($L_f/d_f = 857$) is twice as the shorter one ($L_f/d_f = 428$).

Table 12. Properties of PVA fibres (provided by the manufacturer)

Type	Density [g/cm^3]	Length (L_f) [mm]	Diameter (d_f) [mm]	Tensile strength [MPa]	Young's Modulus (E_f) [GPa]	Elongation [%]
W2-6	1.29	6	0.014	1500	41.7	7
W2-12	1.29	12	0.014	1500	41.7	7

(a) (b)

Figure 16. Fibres used in this study (a) 6 mm fibres (b) 12 mm fibres

3.2.5 *High range water reducing admixture (HWR)*

In order to improve the workability a polycarboxylic-ether based high range water reducing admixture (HWR) under commercial brand of Glenium 51 from BASF chemical company is used. Glenium 51 is an innovative admixture based on modified polycarboxylic ether (PCE) polymers. It greatly enhances the rheological properties of concrete by initiating an electrostatic dispersion mechanism which stabilises the cement particles ability to separate and disperse due to electrical repulsion. The typical properties of Glenium 51 are tabulated in Table 13.

Table 13. Typical properties of Glenium 51 (provided by the manufacturer, BASF chemical company)

Appearance	Brown liquid
Specific Gravity at 20°C	1.095 ± 0.02 g/cm^3
pH value	7.0 ± 1
Alkali content [%]	Less than or equal to 5.0
Chloride content [%]	Less than or equal to 0.10

3.2.6 *Water*

Drinkable grade tap water is used for all mixes after conditioning to room temperature (23 ± 2 °C).

3.2.7 *Steel reinforcement (rebar)*

In order to reinforce the concrete beam elements of this study, different types of steel reinforcements are utilised as shown in Table 14. The stress-strain relationship of longitudinal steel bars derived from tensile test performed in accordance with AS 1391(2007) are demonstrated in Figure 17 to Figure 19. Proof strength at 0.2% strain is also determined to identify the yield strength of steel reinforcements.

Table 14. Properties of steel reinforcement

Diameter [mm]	Type	Designation grade[1]	Uniform strain[1]	Ductility class[1]	f_{sy} [MPa]	f_{su} [MPa]	Function
10	Plain	R250N	0.05	N	250 [2]	-	Stirrup
10	Deformed	D250N	0.05	N	370	465	Longitudinal
12	Deformed	D250N	0.05	N	290	470	Longitudinal
12	Deformed	D500N	0.05	N	590	670	Longitudinal

[1] In accordance with AS 3600 (2009), table 3.2.1
[2] Characteristic yield strength

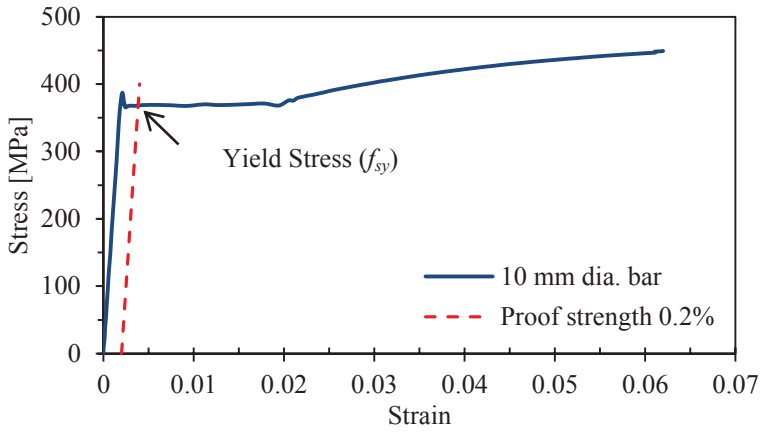

Figure 17. Stress-strain curve for 10 mm diameter reinforcement

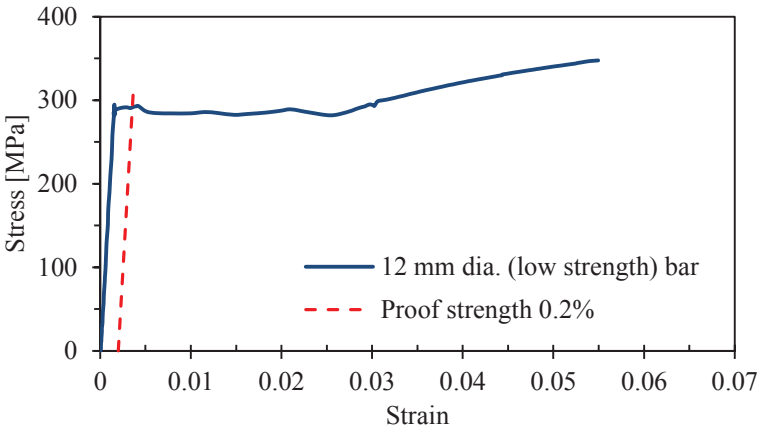

Figure 18. Stress-strain curve for 12 mm diameter low strength reinforcement

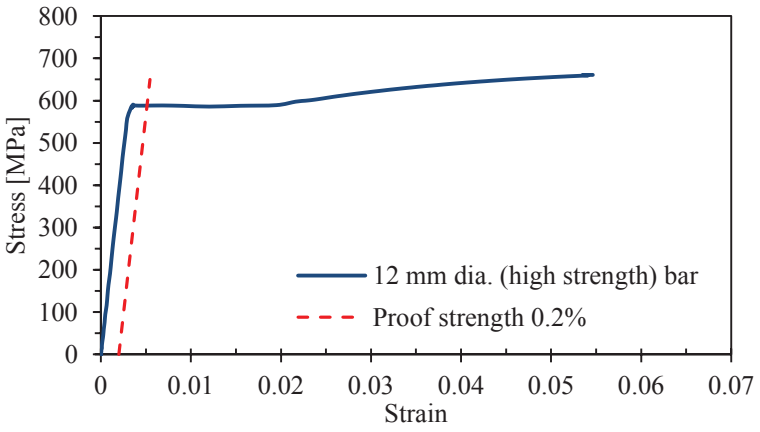

Figure 19. Stress-strain curve for 12 mm diameter high strength reinforcement

3.3 Experimental program

The experimental program of this study is mainly divided into two parts;

Part 1, which is 'material testing', is allocated to material testing of conventional concrete and PVA-FRCs. In this section, fresh and hardened properties of materials are investigated by conducting different mechanical and dynamic tests. To evaluate the properties of freshly mixed concrete, slump, compacting factor, air content (AC) and mass per unit volume (MPV) tests were carried out. The first two tests, determine the rheological properties of concrete where AC test measures the air void percentages within the mix. Compressive, indirect tensile ('Brazil' or splitting test), modulus of rupture (MOR), modulus of elasticity (MOE), residual flexural strength (fracture test) and impact resonance tests are also carried out to assess the mechanical and damping properties of hardened concrete.

In Part 2, which is categorized as 'structural testing', properties and behaviour of PVA-FRC beams are investigated under the action of both monotonic and cyclic loads. Herein, flexural capacities, damping properties and ductility of different FRC beams are compared with that of conventional reinforced concrete (RC) beam elements. Four-point static flexural tests were conducted on 150 × 200 × 1900 mm beams reinforced with top and bottom steel bars to evaluate the flexural capacity and ductility of PVA-FRC beams. Furthermore, hammer test is also carried out on the concrete beam before, during and after each flexural test to capture the damping characteristics of reinforced concrete beams. In order to study the dynamic behaviour of PVA-FRC beams, 3-point cyclic tests were conducted on RC beams of the same geometry and property from which the hysteresis diagrams are produced. The damping ratio of concrete beams is also calculated from the hysteresis loops and the results are compared with conventional concrete.

Accordingly, a systematic mixing and testing program started. At the first step, a total of nine different batches of concrete including PVA-FRC and control with details as explained in Table 15 were prepared and tested for fresh properties and compressive strength. From the results of this set of experiments, four PVA-FRC mixes plus the control were selected for further investigations on the material characteristics. Finally, from the latter mixes, two PVA-FRCs and control mix designs were chosen to prepare 10 concrete beams reinforced with low and high strength steel bars (5 beams for 4-point

flexural tests and 5 beams for 3-point cyclic tests).

Parallel to all above investigations, another mix design avoiding PVA fibres and FA, with 100% PC as cementitious material was also prepared and tested in order to study the effect of replacing 30% PC with FA.

Table 15. Mix designations

Mix reference	Binders		Fibre	
	PC [%]	FA [%]	V_f [%]	L_f [mm]
Control	70	30	0	-
6PVA-0.125%	70	30	0.125	6
6PVA-0.25%	70	30	0.250	6
6PVA-0.375%	70	30	0.375	6
6PVA-0.50%	70	30	0.500	6
12PVA-0.125%	70	30	0.125	12
12PVA-0.25%	70	30	0.250	12
12PVA-0.375%	70	30	0.375	12
12PVA-0.50%	70	30	0.500	12
Conventional	100	0	0	-

3.4 Mix proportioning and sequences

Mix designs were adopted to obtain a characteristic compressive strength (f'_c) of 50 MPa to conform to AS 3600 requirements as structural concrete (ranging from 20 MPa to 100 MPa).

Mix proportioning of the raw material ingredients, as listed in Table 16, was carried out by mass. The fibre volume fractions employed were up to a threshold limit of 0.5%; this limit is derived from the results of several preliminary trial mixes indicating that the incorporation of higher volume fraction results in a loss of cohesiveness of concrete. In order to obtain a desired slump of 80 ± 20 mm, HWR dosage was varied.

Table 16. Mix proportions

Materials	PC	FA	Sand	Coarse aggregate		HWR	PVA fibre	
				10 mm	20 mm		6 mm	12 mm
	[kg/m^3]	[kg/m^3]	[kg/m^3]	[kg/m^3]	[kg/m^3]	[Lit/m^3]	[kg/m^3]	[kg/m^3]
Control	301	129	635	390	700	1.215	-	-
6PVA-0.125%	301	129	635	390	700	1.876	1.613	-
6PVA-0.25%	301	129	635	390	700	1.774	3.225	-
6PVA-0.375%	301	129	635	390	700	2.143	4.838	-
6PVA-0.50%	301	129	635	390	700	2.143	6.450	-
12PVA-0.125%	301	129	635	390	700	2.338	-	1.613
12PVA-0.25%	301	129	635	390	700	2.468	-	3.225
12PVA-0.375%	301	129	635	390	700	2.597	-	4.838
12PVA-0.50%	301	129	635	390	700	3.506	-	6.450
Conventional	430	-	635	390	700	0.923	-	-

* W/C (Water /Cementitious materials) ratio maintained at a constant rate of 0.35 for all mixes.

For the control concrete, mixing was performed in accordance with AS 1012.2 as shown in Figure 20; however, for FRC mixes, due to the presence of the hydrophilic fibres, the standard mixing regime suggested in Australian Standard for conventional concrete, was modified. Fine aggregates were firstly mixed with PVA fibres in a vertical pan mixer until fibres observed to be dispersed uniformly. Coarse aggregates were then added and further mixed for 3 minutes. Thereafter, cement, fly ash and water were introduced and mixed for a further 3 minutes. In order to adjust the slump, HWR was added within the first minute of adding cementitious material. Following 3 minutes of mixing, a rest period of 2 minutes was applied followed by a further 3 minutes of mixing to achieve a homogeneous mix. The rest of the procedure is the same as what is mentioned in AS 1012.2 (1994).

Modifying the standard mixing sequences, in order to achieve a more uniform mix, has also previously been investigated by different researchers. For instance, Manolis et al.

(Manolis et al. 1997) have suggested a 3 to 5 minutes of mixing after fibre addition to achieve a proper fibre dispersion.

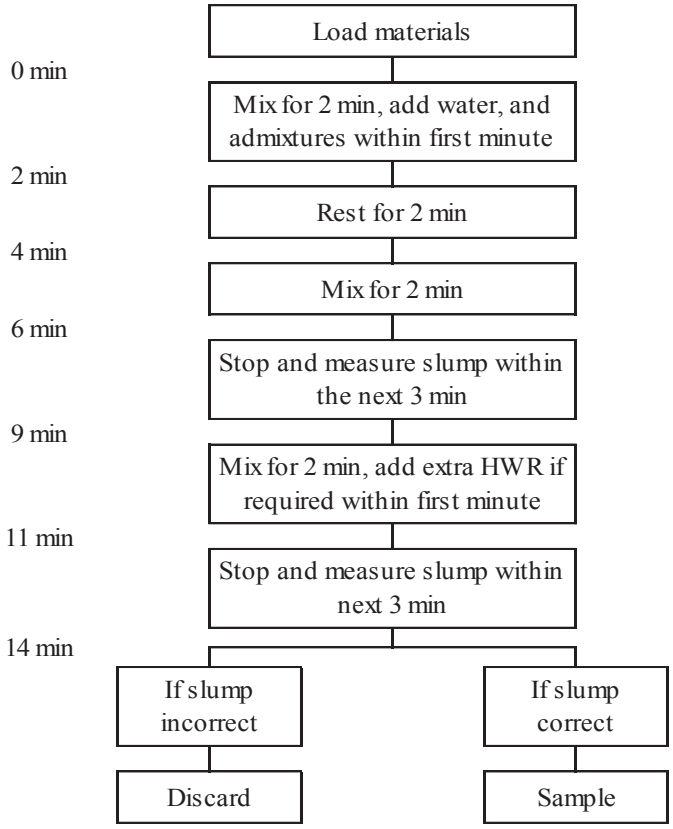

Figure 20. Mixing procedure (AS1012.2-1994)

3.5 Fabrication of test specimens and curing

After carrying out all fresh property tests, the fresh mix was placed into moulds according to pre-arranged testing schedule with specifications as below;

Compressive test	Steel cylindrical mould (100 × 200 mm)
Indirect tensile test	Steel cylindrical mould (100 × 200 mm)
MOR test	Plexiglass prismatic mould (100 × 100 × 350 mm)
MOE test	Steel cylindrical mould (150 × 300 mm)
Fracture test	Steel prismatic mould (150 × 150 × 550 mm)
Impact resonance test	Plexiglass prismatic mould (75 × 100 × 350 mm)
RC beam tests	Steel prismatic mould (150 × 200 × 1900 mm)

To achieve a proper consolidation and also to minimise the amount of the entrapped air arising within the mix, an external vibrator was used for all above mentioned specimens except for the latter one. Figure 21 shows a sample of material testing specimen preparation.

Figure 21. Preparation of material testing specimens

In order to prepare the RC beams, fabricated steel cages were placed into the steel moulds using plastic bar chairs and wheel spacers to provide a uniform concrete cover in all directions of the concrete beam (see Figure 22). Thereafter, concrete was cast and compacted by the means of an internal (poker) vibrator. Finally, the concrete surface was levelled using a concrete trowel.

Figure 22. Preparation of concrete beams

Moulds were covered with plastic sheets to retain moisture. At 24 h for cylindrical specimens and 48 h for prismatic samples, specimens were demoulded and placed in lime-saturated water at a temperature of 20 ± 2 °C until the test date. RC beam samples were wet-cured in moulds for 7 days and after that demoulded and air cured until the test dates.

Preparing and curing of all concrete samples for material testing complied with AS 1012.8, method of making and curing concrete, except for the residual flexural strength test (fracture test) and the impact resonance test which followed the European EN standard and American ASTM standard, respectively.

3.6 Description of test methods

For each concrete batch, fresh properties (slump, compacting factor, AC and MPV) are assessed complying with designated Australian Standards as further discussed in the following. Moreover, In order to evaluate the material characteristics (mechanical and dynamic) of concrete samples, compressive strength, indirect tensile strength, modulus of rupture (MOR) or flexural strength, static chord modulus of elasticity (MOE), residual flexural strength and dynamic characteristics (dynamic modulus of elasticity (DMOE) and damping ratio) are also investigated through specific standard testing methods at different ages. Concrete beams were also tested for 4-point static flexural and 3-point cycling tests in order to capture the structural properties of PVA-FRCs.

Herein, the details of all above mentioned tests are further discussed as follows;

3.6.1 *Slump test*

Slump test is an empirical method that measures the workability of fresh concrete. More specifically, it measures the consistency and variations in uniformity of the concrete in a specific batch. The slump test is prescribed by AS 1012.3.1 (1998). The apparatus used for this test is a hollow frustum of a cone with specifications shown in Figure 24.

The slumped concrete may take one of the three forms; true slump, shear slump and collapse slump as shown in Figure 23. If concrete is slumping evenly all rounds, it is called true slump which is of use in the tests. If instead of true slump, one half of the cone slides down an inclined plane, a shear slump is said to have taken place. In this case the test should be repeated and if the shear slump persists, this is an indication of lack of cohesion in the mix. It may undergo segregation and bleeding and thus is not desirable. A collapse slump generally means that the mix is too wet or there is a high workability level, for which the slump test is not appropriate. The concrete slump values may vary in the range between zero (no slump-very low workability) to collapse.

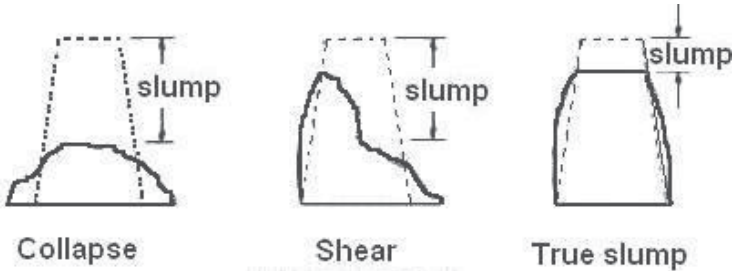

Figure 23. Different profiles of concrete slump

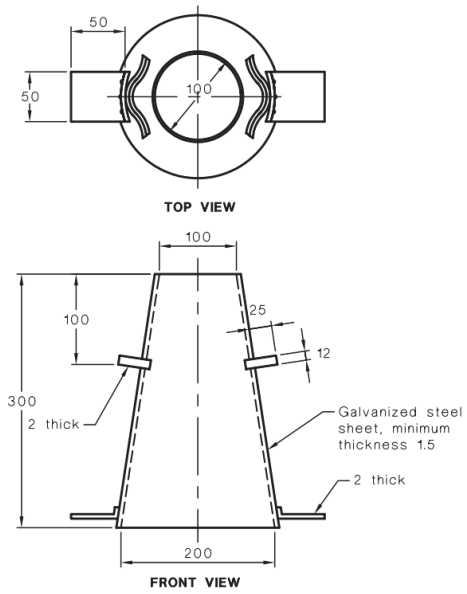

Figure 24. Typical mould for slump test (AS 1012.3.1-1998)

3.6.2 *Compacting factor test*

Compacting factor or the degree of compaction, is measured by the density ratio, i.e. the ratio of the density achieved in the test (partially compacted concrete) to the density of the same concrete fully compacted. The test, known as the compacting factor test, is described in AS 1012.3.2 (1998). The concrete compacting factor value may vary in a range between 0.78 (very low workability) to 0.95 which presents a high level of workability (Neville 1991). Figure 25 demonstrates the standard apparatus for the test in accordance with AS 1012.3.2 (1998).

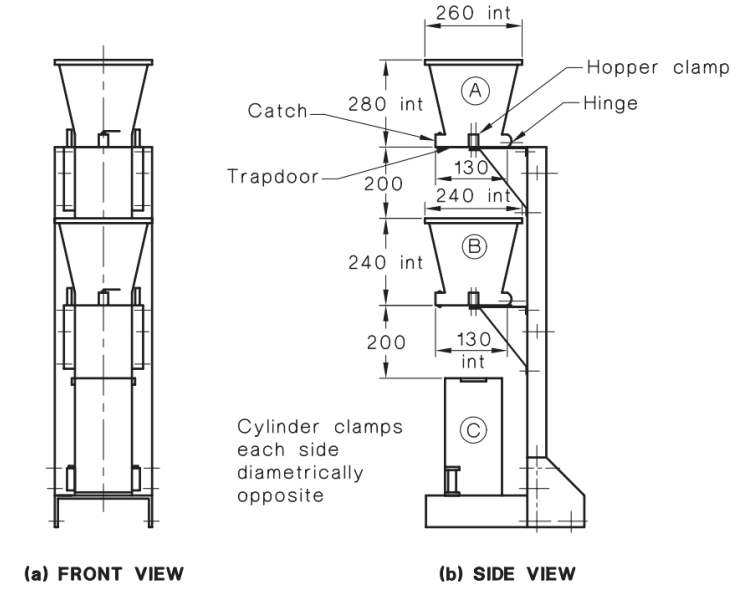

Figure 25. Standard compacting factor test apparatus (AS 1012.3.2-1998)

3.6.3 *Air content (AC) test*

The AC test is a method to determine the air content of freshly mixed concrete. There are few methods to evaluate the AC of concrete from which the test method described in AS 1012.4.2 (1999) is more popular since there is no need for calculations. The reading shown on the pressure gauge, which is calibrated to record the reduction in a predetermined test pressure applied to the concrete, is directly related to the air content of the concrete. In this test method, the observations of the air pressure reduction in a chamber above the concrete, determines the concrete AC when it is exposed to the air pressure.

Figure 26 shows a typical test apparatus in accordance with AS 1012.4.2 (1999).

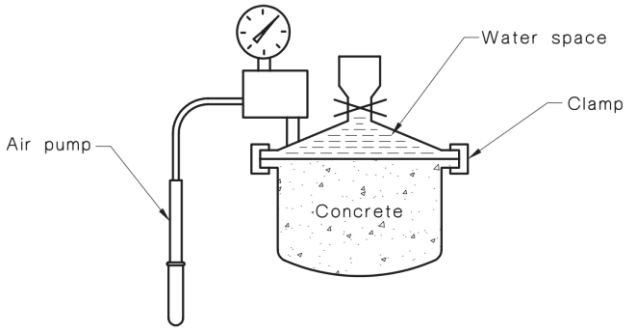

Figure 26. typical apparatus for measuring air content by drop in gauge pressure (AS 1012.4.2-1999)

3.6.4 *Mass per unit volume (MPV) test*

This test sets out the method for determining the mass per unit volume of freshly mixed concrete that is in the plastic state. AS 1012.5 (1999), describes the standard test method of measuring the concrete MPV. In this test method, the MPV of concrete, expressed in kilograms per cubic metre, is calculated by dividing the mass of fully compacted concrete in the measure by the capacity (volume) of the measure. The standard states that for testing concrete with aggregates of nominal size not exceeding 40 mm, the capacity of the measure should not be less than 5 litres. The measure shall be calibrated at a known temperature by determining the mass in kilograms of water required to precisely fill it and the capacity of the measure shall be obtained by dividing the mass of water by the unit mass of water at calibration temperature.

3.6.5 *Compressive test*

The most common of all tests on hardened concrete is the compressive strength test. This is partly because it is an easy test to perform. Moreover, many of desirable characteristics of concrete are qualitatively related to its compressive strength. However, the main reason for compressive test popularity is the intrinsic importance of the compressive strength in concrete structural design (Neville 1991). In Australian Standard, method of testing concrete, only cylindrical specimens which are prepared in accordance with AS 1012.8 are accepted to be tested to determine the concrete compressive strength.

Therefore, all compressive tests are performed on cylindrical specimens of 100 mm diameter with 200 mm length following AS 1012.9 (1999) procedural requirements. Prior to the test, concrete samples were properly capped complying with the latter mentioned standard. For each concrete type, compressive strength test is performed at 7, 28 and 56 days of age and for each age, 3 cylindrical samples were tested. The tests were conducted under a load rate control condition in an 1800 kN universal testing machine with load rate equivalent to 20 ± 2 MPa compressive stress per minute. The compressive strength of the specimens is calculated by dividing the maximum force applied to the specimen by the cross sectional area. This area is calculated from the average of the two measured diameters.

The behaviour of concrete under compressive load has also been assessed by mounting 60 mm length strain gauges at the surface of specimens as shown in Figure 27.

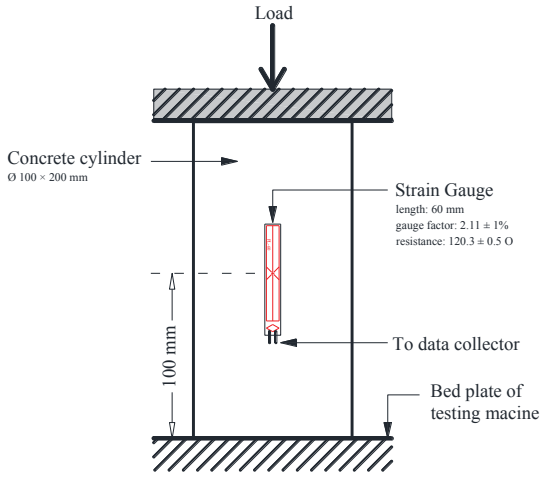

Figure 27. Schematic of compressive strength test with strain gauge

Strain gauges were employed to monitor the longitudinal deformations of test specimens under compressive load and from the results of which the stress-stress relationship of different concrete were studied.

3.6.6 *Indirect tensile test*

The indirect tensile test ('Brazil' or splitting test) is a simple and indirect way of determining the tensile strength of concrete which gives more uniform results than other tension tests. The strength measured in the splitting test is believed to be close to the direct tensile strength of concrete and approximately, 5 to 12 percent higher (Neville 1991).

In this study, the indirect tensile test is conducted in accordance with AS 1012.10 (2000) on cylindrical specimens of 100 mm diameter by 200 mm length. The concrete cylinder is placed, with its axis horizontal, between the plates of testing machine as shown in Figure 28, and is loaded until the failure takes place by indirect tension in the form of splitting along the vertical diameter. For each concrete type, indirect tensile test is performed at 7, 28 and 56 days of age and for each age, 3 cylindrical samples are tested. The test is conducted under a load rate control condition in an 1800 kN universal testing machine with load rate equivalent to 1.5 ± 0.15 MPa indirect tensile stress per minute. The indirect tensile strength of the specimen can be calculated using below equation;

$$f_{ct.sp} = \frac{2000\,P}{\pi LD} \tag{7}$$

where $f_{ct.sp}$ is the indirect tensile strength in MPa, P is the maximum applied force in kN, L is the length of specimen in mm and D is the diameter in mm.

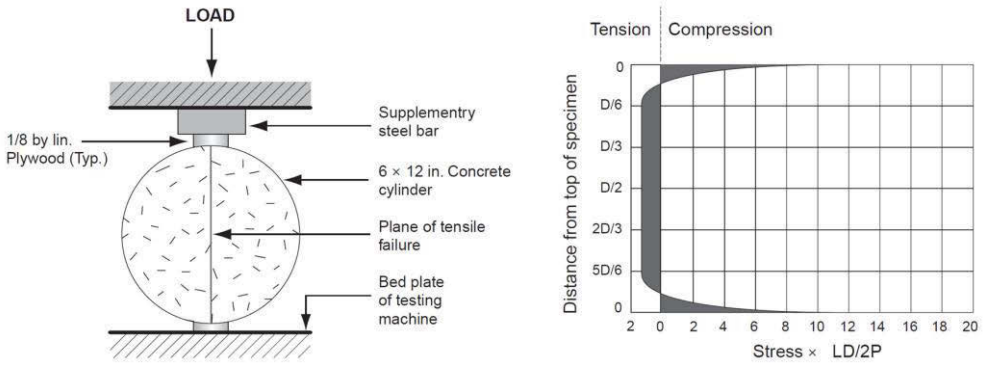

Figure 28. Splitting tensile test; (left) typical arrangement of the test (right) stress distribution across the loaded diameter of a cylinder compressed between two plates (Mehta & Monteiro 2005).

3.6.7 *Modulus of rupture (MOR) test*

In MOR test an unreinforced concrete prism is subjected to 4-point flexural load until failure. The theoretical maximum tensile stress in the bottom fibre of the test specimen is known as the modulus of rupture which can be calculated on the basis of ordinary elastic theory (Equation (8)).

Herein, the MOR is obtained from four-point bending tests on 100 × 100 × 350 mm prisms at a loading rate of 1 ± 0.1 MPa/min until fracture, following AS 1012.11 (2000). Four-point loading was applied and mid-span deflection of the flexural specimens is measured by means of a linear variable differential transformer (LVDT) at the centre of each specimen. The flexural stress is calculated as;

$$f_{ct.f} = \frac{PL1000}{BD^2} \tag{8}$$

where $f_{ct.f}$ is the modulus of rupture in MPa, P is the maximum applied force in kN, L is span length in mm, B is the average width of the specimen at the section of failure in mm and D is the average depth of specimen at the failure section in mm.

Figure 29 shows the typical arrangement of 4-point bending test to evaluate the modulus of rupture of concrete samples. The compressive and tensile stress distribution across the depth of the concrete beam under flexure is also demonstrated within the same figure.

Previous investigations (Raphael 1984) show that the correct value of concrete tensile strength is about 0.75% of the theoretical modulus of rupture. A reason for this phenomenon is that there is a gradual increase in strain with an increase in stress above about one-half of the tensile strength. Consequently, the shape of the actual stress block under loads adjacent to failure is parabolic and not triangular (Neville 1991).

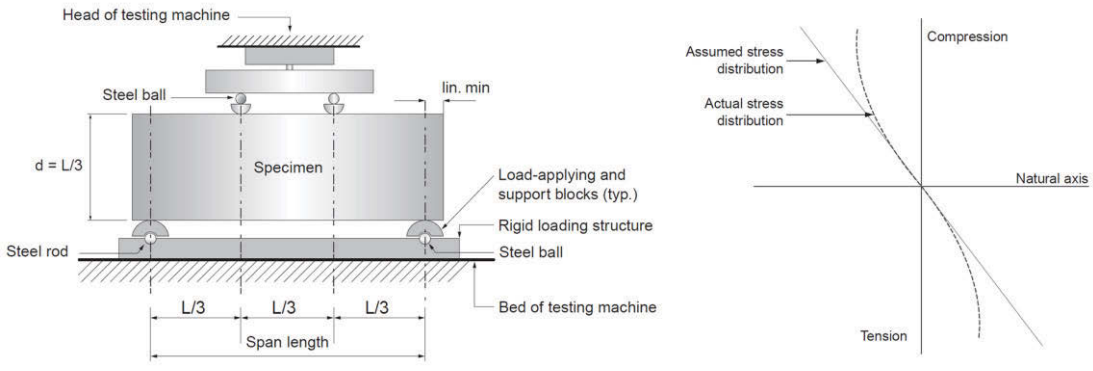

Figure 29. Modulus of rupture test; (left) typical arrangement of the test (right) stress distribution across the depth of a concrete beam under flexure (Mehta & Monteiro 2005)

3.6.8 *Modulus of elasticity (MOE) test*

Static chord MOE is defined as gradient of the chord drawn between two specific points on the stress-strain curve. AS 1012.17 explains that these two points should be taken as follows;

Point 1 50 micro-strains and stress corresponding to this strain

Point 2 stress equivalent to "test load" and its corresponding strain

where the test load is equivalent to 40 percent of the average compressive strength, tested in accordance with AS 1012.9 immediately prior to the static chord MOE test.

Herein, the MOE test is performed on 150 × 300 mm cylindrical specimens in accordance with AS 1012.17 (1997). For each concrete type, MOE test is performed at 7, 28 and 56 days of age and for each age, 2 cylindrical samples were tested. Since the MOE test is a non-destructive test, the specimens can further be used for different ages. Test is conducted under a load rate control condition in an 1800 kN universal testing machine with load rate equivalent to 15 ± 2 MPa per minute. The MOE of the concrete sample can be calculated as follows;

$$E_c = \frac{(G_2 - G_1)}{(\varepsilon_2 - 0.00005)} \tag{9}$$

where E_c is the concrete modulus of elasticity in MPa, G_2 is the test load (as described above), divided by the cross-sectional area of the specimen in MPa, G_1 is the applied load at a strain of 50×10^{-6} divided by the cross-sectional area of the specimen in MPa and ε_2 is strain corresponding to deformation at test load (strain = deformation divided by the gauge length) in 10^{-6} m/m.

In order to measure of the longitudinal strain, a compressometer as shown in Figure 30 was used.

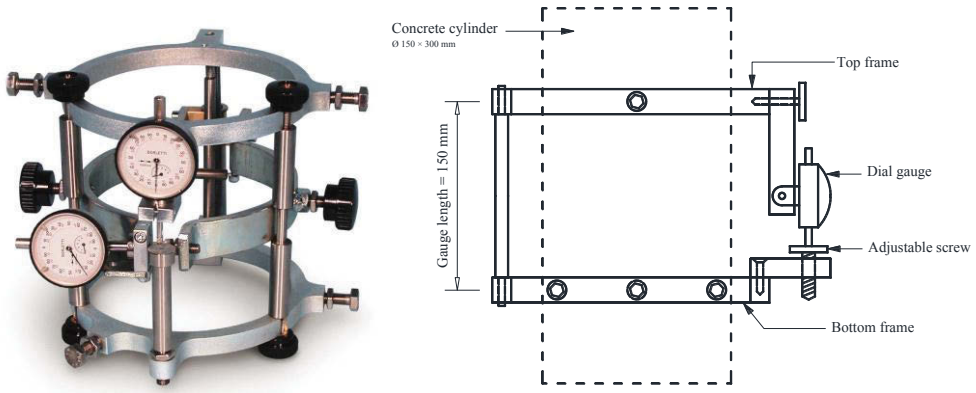

Figure 30. Typical compressometer arrangement for measurement of longitudinal strain

3.6.9 *Residual flexural strength test*

This test method is performed in order to evaluate the residual flexural tensile strength of FRC samples. Due to lack of proper test method in Australian Standard, the European Standard (EN 14651:2005+A1:2007) is used to specify a method of measuring the residual flexural tensile strength and limit of proportionality (LOP) of concrete.

The specimens used for the test are 150 × 150 × 550 mm prisms prepared in accordance with specifications of the above mentioned standard. After 25 days of curing, a middle notch was sawn using a rotating diamond blade wet saw. This age was selected for notching the samples due to the criteria mentioned by the standard to let the specimens be cured for a minimum of 3 days after sawing. The specimens were rotated 90° around their longitudinal axis and then sawn through the width at mid-span as shown in Figure 31. The width of the notch is less than 5 mm and the depth is approximately 25 mm and the distance h_{sp}, as shown graphically in Figure 31, is 125 ± 1 mm. Test specimens were then returned to curing tanks for further curing until 28 days and removed from water 3 h before testing.

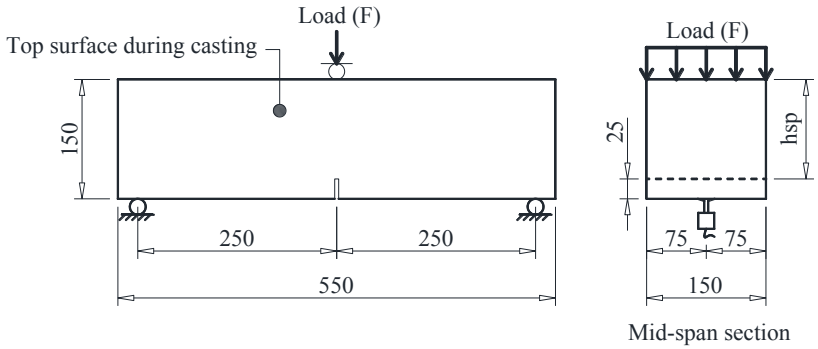

Figure 31. Typical arrangement of 3-point bending test over notched sample with measuring CMOD (EN 14651:2005)

Three-point bending test on notched concrete prisms with the typical arrangement shown in Figure 31 is used to determine the limit of proportionality (LOP) and residual flexural tensile strength of specimens. A 500 kN universal testing machine, capable of measuring loads to an accuracy of 0.1 kN, with a controlled load rate applied to produce a constant rate of crack mouth opening displacement (CMOD) was used. A clip gauge (extensometer) with an accuracy of 0.01 mm was also used to measure CMOD. For CMOD values less than 0.1 mm, the load rate was adjusted so that CMOD could increase at a constant rate of 0.05 mm per minute. When CMOD = 0.1 mm, the machine

was adjusted to increase CMOD at a constant rate of 0.3 mm per minute. The values of load and corresponding CMOD were recorded at a rate of 5 Hz during the test.

3.6.10 *Impact resonance test*

The dynamic properties of concrete material such as natural frequency, dynamic modulus of elasticity and damping ratio can be calculated from the fundamental resonant frequencies of concrete prisms measured through impact resonance test. Since there is no relevant testing method in Australian Standard, the test method recommended in American Standard, ASTM C 215 (08), is used in this study.

The impact resonance test is used to determine the resonant frequency of 75 × 100 × 400 mm prisms by applying a small load impulse and measuring the resulting acceleration through the specimen for different modes of vibration. To excite the various modes of vibration, a small metal hammer (impactor) is used to manually apply a small load impulse to the specimen. The accelerometer attached to the specimen, is used to transform the resulting vibrations into electrical signals. The miniature accelerometer is assumed to have no influence on the resonant frequencies of the beam. Soft rubber supports were also used to permit the specimen to vibrate freely in each mode of vibration. The schematic of test apparatus and specification of impactor (hammer) and accelerometer are shown in Figure 32 and Table 17, respectively. A computer based data acquisition system is used to record hammer force and acceleration response signals during the tests. Data were recorded by the means of a data acquisition card (model: NI PCI-6133). In order to interface with the data acquisition card, a software called 'LABVIEW' was also utilised.

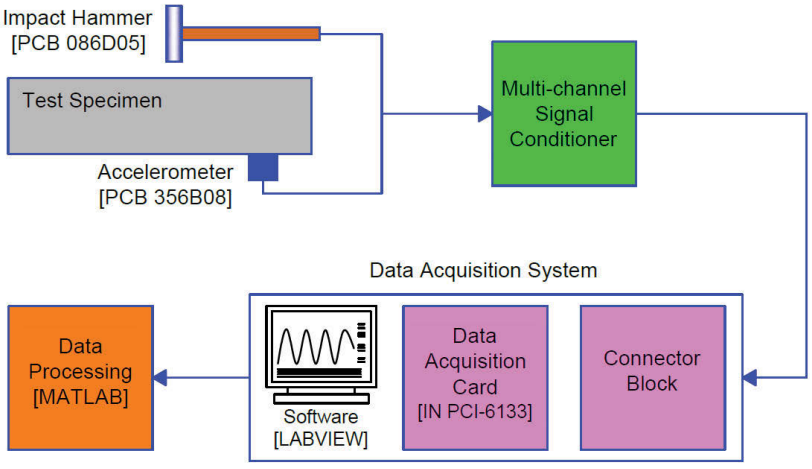

Figure 32. Schematic of apparatus for impact resonance test

Table 17. Impactor and accelerometer specifications

Impactor (hammer)	
Model	PCB 086D05
Sensitivity (±15%)	0.23 mV/N
Measurement range	± 22,240 N pk
Resonant frequency	≥ 22 kHz
Non-linearity	≤ 1%
Accelerometer	
Model	PCB 356B08
Sensitivity (±10%)	10 mV/(m/s^2)
Measurement range	± 490 m/s^2 pk
Frequency range (±5%)	0.5 – 5000 Hz
Frequency range (±10%)	0.3 – 6500 Hz
Resonant frequency	≥ 20 kHz
Broadband resolution	0.001 m/s^2 rms
Non-linearity	≤ 1%
Transverse Sensitivity	≤ 5%
Weight	20 gm

The fundamental frequencies for the three different modes of vibration; transverse, longitudinal and torsional can be obtained by choosing a proper location for the impact point and the accelerometer as demonstrated in Figure 33.

For each concrete type, impact resonance test was carried out at 14 and 28 days of age. For each age, 3 specimens of the same concrete were tested and since the test is non-destructive, the same specimens were used for the next testing age. Each sample is tested for transverse and longitudinal modes of vibration by changing the position of impact and accelerometer. To provide more accurate results, at least 5 strikes were applied on each sample for each mode of vibration and the average is taken from the successive results.

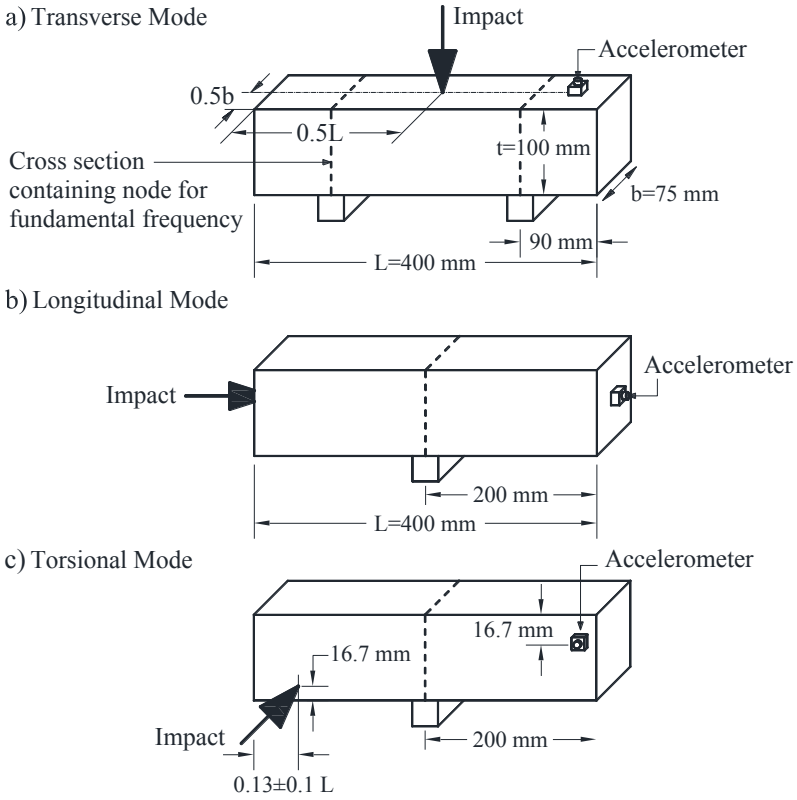

Figure 33. Typical impact resonance test set-up (locations of impact and accelerometer) for different modes of vibration (ASTM C 215 – 08)

From the test results, the fundamental (natural) frequencies are measured and acceleration-time history graphs are prepared. Acceleration-time history is used in order to calculate the damping ratio, following logarithmic decrement method described previously in section 2.6.

The dynamic modulus of elasticity (DMOE) can be calculated from the fundamental transverse and longitudinal frequencies, using the below mentioned equations;

$$DMOE_{transverve} = CMn^2 \tag{10}$$

where M is the mass of specimen in kg, n is the fundamental transverse frequency in Hz, C is equal to "$0.9464 \times (L^3T/bt^3)$" in m^{-1}, L is the length of specimen in m, t and b are dimensions of cross-section in m (t being in the direction in which load is driven) and T is a correction factor that depends on the ratio of the radius of gyration (K) to the length of the specimen (L) and on Poisson's ratio. In this case T = 1.39 which is calculated from Table 1 "values of correction factor" of ASTM C 215-08.

$$DMOE_{longitudinal} = DM(n')^2 \tag{11}$$

where n' is the fundamental longitudinal frequency in Hz and D is equal to "4 × (L/bt)" in m^{-1}.

3.6.11 *4-point static flexural test*

This test was performed after a minimum of 56 days of curing age (7 days of wet curing and then air cured until the test day) to make sure that sufficient strength is gained due to the pozzolanic reaction of FA which mostly decreases the concrete strength development rate. This procedure was also recommended in previous investigations (Felekoğlu et al. 2009)

The RC beams used for this test are designed in accordance with AS 3600 (2009). All specimens were 1.9 m long with a span of 1.8 m and a depth of 200 mm (effective depth (d) = 159 mm). A concrete cover of 25 mm was also applied for all beams. Figure 34 shows the beam geometry and the reinforcement details.

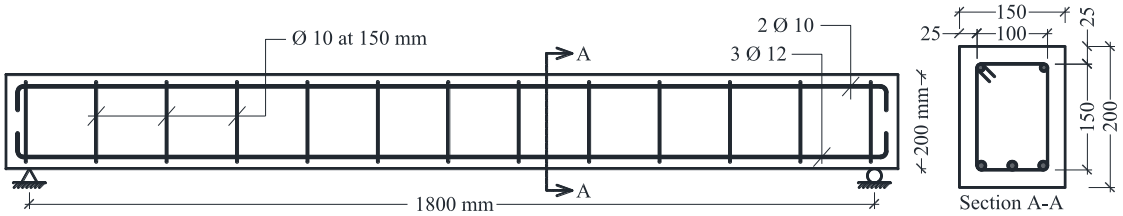

Figure 34. Schematic of RC beam

In order to investigate the fibre contribution to flexural behaviour of RC beams, two different types (A and B) of steel reinforcement arrangements as shown in Table 18 were utilised. All beams of series A (made with steel arrangement of type A) and series B (made with steel arrangement of type B) were provided with 10 mm diameter stirrups (Ø10) with a constant spacing of 150 mm (centre-to-centre) over the whole of their length in order to avoid shear failure and have a reinforcement ratio (ρ_s) of 1.42%.

Table 18. Steel reinforcement arrangements

	Tension steel reinforcement			Compression steel reinforcement		
	Diameter [mm]	No.	f_{sy} (nominal) [MPa]	Diameter [mm]	No.	f_{sy} (nominal) [MPa]
Type A	12	3	250	10	2	250
Type B	12	3	500	10	2	250

Besides recording values of the applied load, the following measurements were also taken;

(1) Deflection: This was determined using LVDTs mounted along the beam axis in middle section and one-fourth spans.

(2) Strain: Values of strain were measured at various locations of the beam using several strain gauges with specifications as shown in Table 19, to monitor the behaviour of the specimen during the test. Strain gauges attached to steel bars (imbedded in concrete) can capture the stress-strain behaviour of rebars during the test, where, concrete strain gauges mounted on the beam face, can measure the strain changes on top (compression zone), bottom (tension zone) and middle (neutral axis) of the mid span section. The steel strain gauges were attached on bottom reinforcements at the centre and one-third span. Figure 35 illustrates the LVDTs together with concrete and steel strain gauge arrangement on the RC beam.

(3) Cracking: For all the test specimens the crack propagation has been monitored and noted visually.

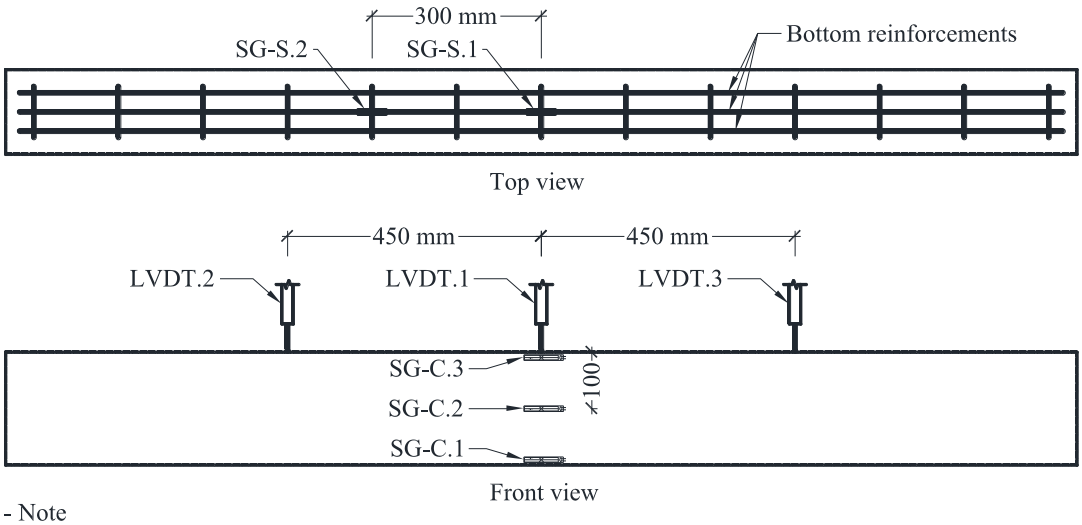

- Note
LVDT: Linear Variable Differential Transformer
SG-C: Strain gauge mounted on concrete surface
SG-S: Strain gauge mounted on steel rebar

Figure 35. LVDTs and strain gauge arrangement on concrete beam

Figure 36 shows a sample steel strain gauge mounting procedure. As illustrated, from the most left-hand side, the location of strain gauges were first measured and marked upon fabricated steel cage. This area was then grinded by means of a hand grinder to prepare a flat surface for strain gauge to be mounted. Thereafter, the strain gauge was glued on using a specific instant glue. Finally, the strain gauge was covered with silicon glue in order to be protected from any damage during the casting procedure.

Figure 36. Strain gauge mounting procedure on tensile steel reinforcement

Table 19. Steel and concrete strain gauge specifications

Steel strain gauges	
Gauge length	5 mm
Gauge factor	2.11 ± 1 %
Gauge resistance	119.8 ± 0.5 Ω
Concrete strain gauges	
Gauge length	60 mm
Gauge factor	2.11 ± 1 %
Gauge resistance	120.3 ± 0.5 Ω

An impact resonant frequency test (hammer test) is also conducted, for transvers and longitudinal modes of vibration, to assess the dynamic properties of the RC beams before, after and during the test when the first crack occurs. The beam is subjected to an impulsive load produced by two different hammers to excite its higher transverse and longitudinal frequencies. For the transverse mode, the impacts are applied at mid span and third span using hammer A and for longitudinal mode, end face of the beam was impacted by hammer B. The beam response to these impulsive loads is captured by the means of 6 accelerometers mounted at different places on the beam as illustrated in Figure 37. The points to attach the accelerometers are; the one-fourth spans and mid span on top surface along the centreline of the beam, on one side at centre and at two face ends of the beam on top. Similar to the impact resonance test arrangement for small prismatic samples (section 3.6.10, Figure 32), a computer based data acquisition system is used to record hammer force and acceleration response signals during the tests and the data processing software (MATLAB) was used to produce the fast Fourier transform (FFT) spectra of vibration signals.

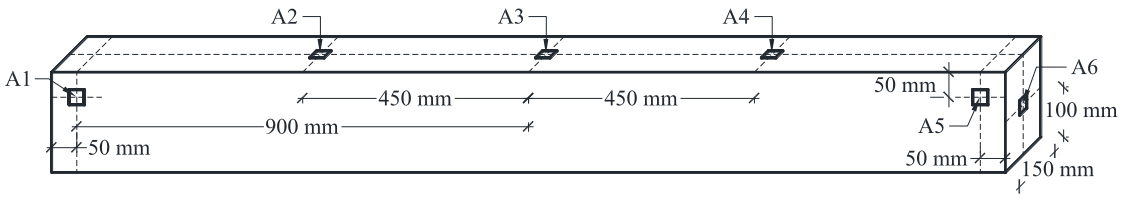

Figure 37. Accelerometers arrangement on RC beam

Figure 38 shows hammers and one sample accelerometer used in this test while their specifications are tabulated in Table 20. The most important data captured, which is the focus of this study, is corresponding to the mid span. To minimise errors and noise affecting the results, 5 hits were carried out for every strike location.

Table 20. Hammers and accelerometers specifications

	Hammer A	Hammer B
Model	PCB 086D20	PCB 086D05
Sensitivity (±15%)	0.23 mV/N	0.23 mV/N
Measurement range	± 22,240 N pk	± 22,240 N pk
Resonant frequency	≥ 12 kHz	≥ 22 kHz
Non-linearity	≤ 1%	≤ 1%
Accelerometers		
Model	PCB 352C34	
Sensitivity (±10%)	10.2 mV/(m/s^2)	
Measurement range	± 490 m/s^2 pk	
Frequency range (±5%)	0.5 – 10000 Hz	
Frequency range (±10%)	0.3 – 15000 Hz	
Resonant frequency	≥ 50 kHz	
Broadband resolution	0.0015 m/s^2 rms	
Non-linearity	≤ 1%	
Transverse Sensitivity	≤ 5%	
Weight	5.8 gm	

Figure 38. Hammers and accelerometer; left: hammer A, middle: hammer B, right: accelerometer

The test set-up is arranged in a way to ensure the simply supported beam condition is satisfied. Thus, the supports allow the beam to rotate freely and minimise the friction which may produce some bending moment at the end of the beam (at the supports location). The supports are also designed in such a way that the vertical displacement at both supports is removed but horizontal displacement at one end can take place (see Figure 39). The specimens are loaded at one-third span by the means of two hydraulic jacks. The schematic of 4-point static flexural test set-up is illustrated in Figure 42. As shown in Figure 40, the left-hand side support is designed to satisfy the pin support condition. The pin support can resist both horizontal and vertical forces but not moment. It allows the beam to rotate, but not to translate in any direction. The right-hand side support is a roller type support which is free to rotate as well as translate horizontally (see Figure 41).

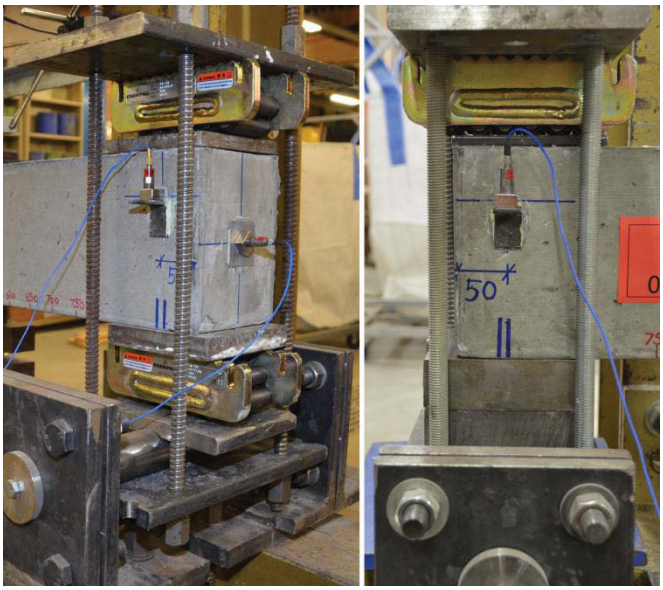

Figure 39. Beam supports

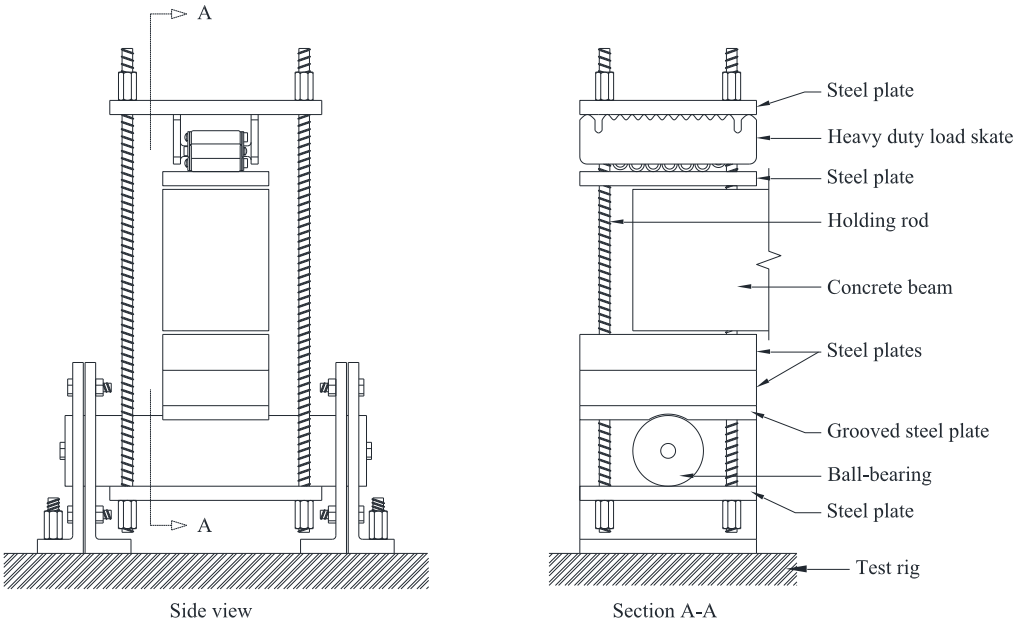

Figure 40. Support A (pinned support) details

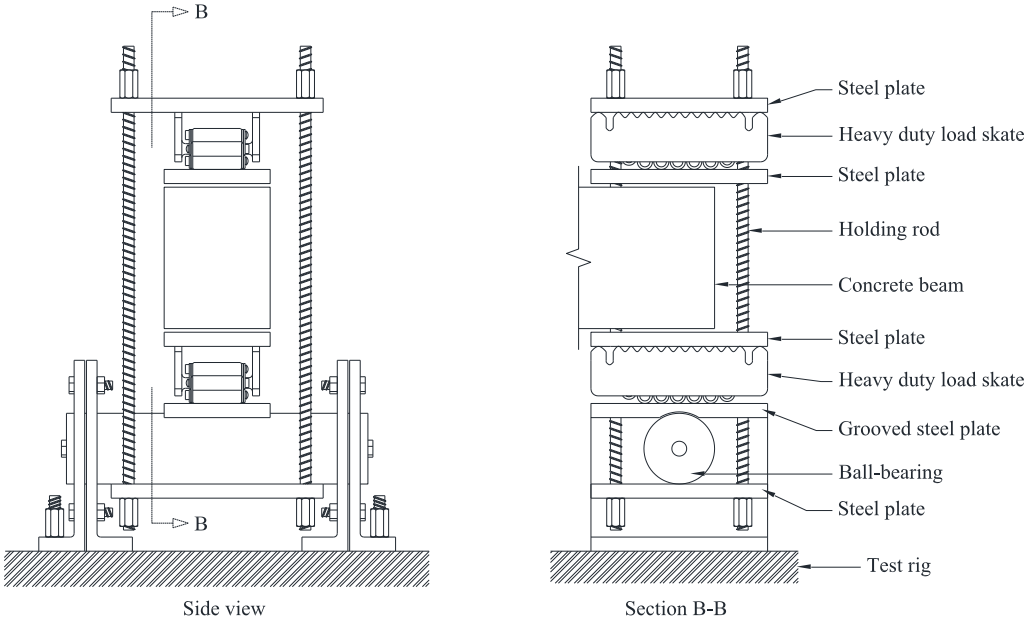

Figure 41. Support B (roller support) details

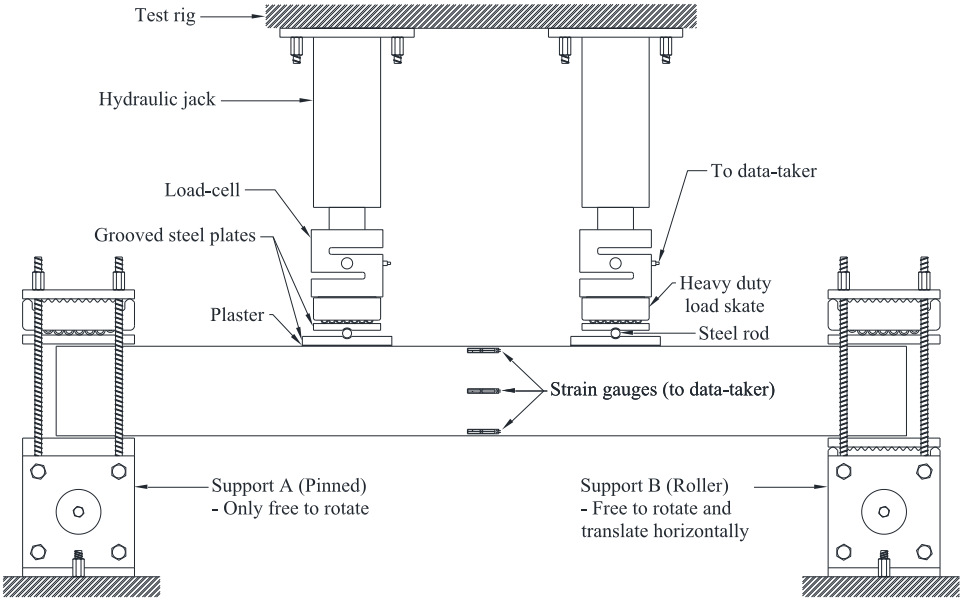

Figure 42. Schematic of 4-point static flexural test set-up

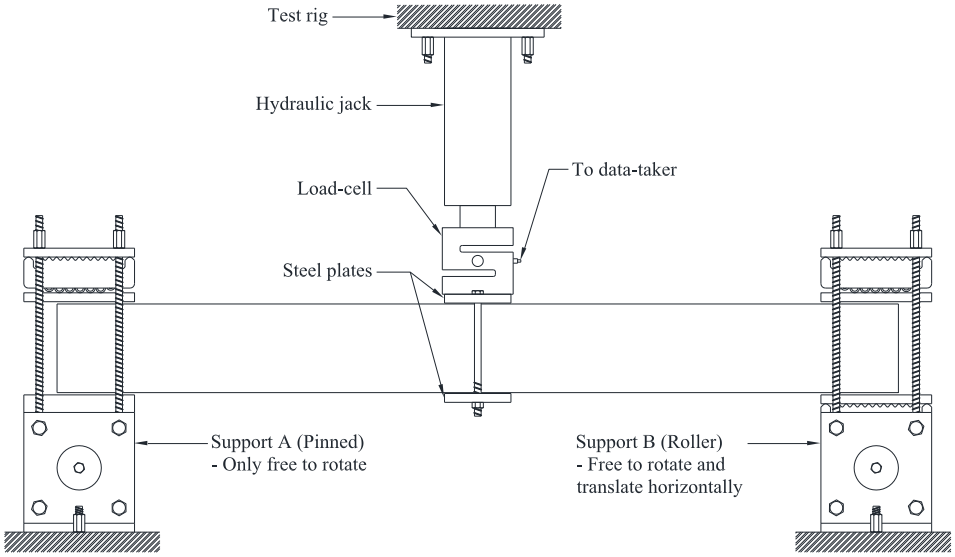

Figure 43. Schematic of 3-point cyclic test set-up

3.6.12 *3-point cyclic test*

Similar to 4-point flexural test, this test is also conducted after a minimum of 56 days of age. The test specimens represent a simply supported beam designed in accordance with AS 3600 (2009) with specifications mentioned in section 3.6.11 (Figure 34 and Table 18). The 3-point cyclic test set-up shown in Figure 43, is similar to that for 4-point bending test except for the loading part which is a concentrated load at the centre. The specimens were subjected to a quasi-static load controlled system. Two sets of loading regimes with increasing load magnitude were defined as shown in Figure 44 and Figure 45.

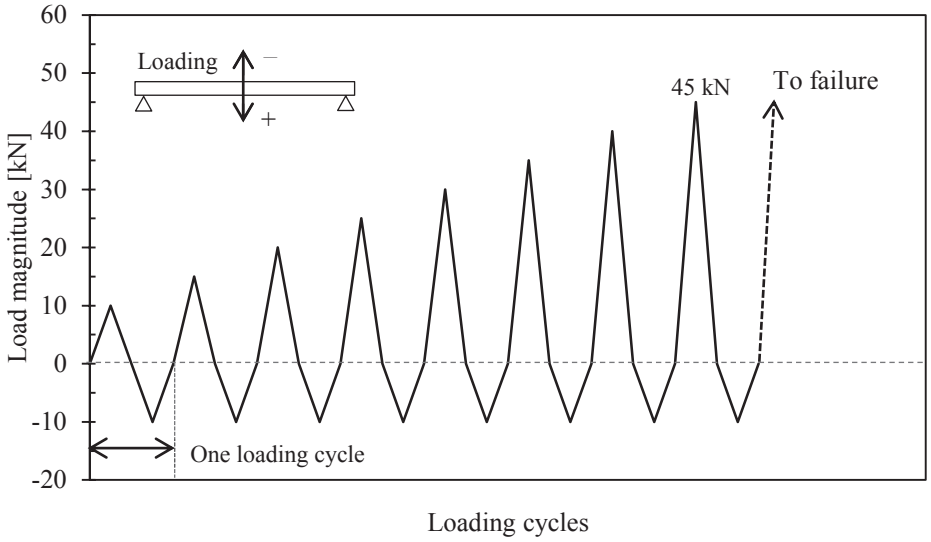

Figure 44. Loading regime A imposed to the specimens of series A

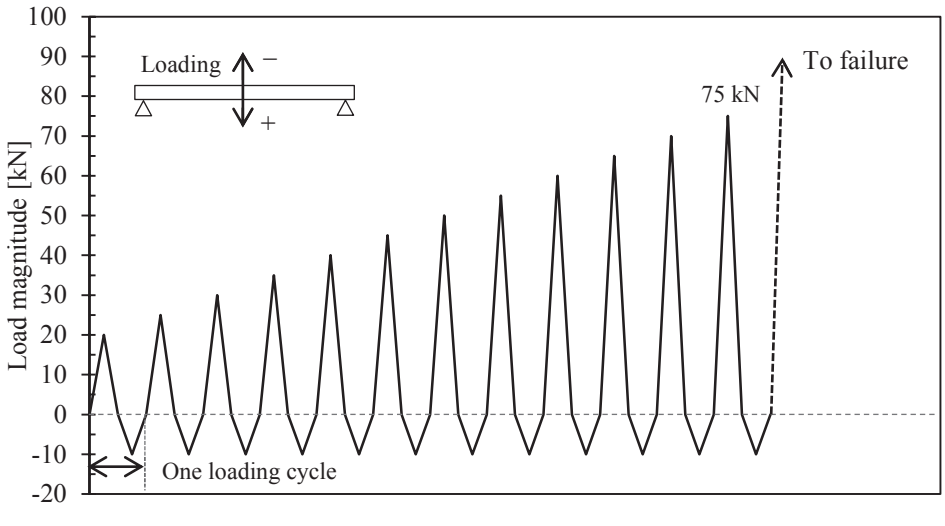

Figure 45. Loading regime B imposed to the specimens of series B

Loading regime A was applied to specimens of series A, having low strength (f_{sy} = 250 MPa) longitudinal tensile reinforcement where loading regime B has been used for specimens of series B which are made of high strength (f_{sy} = 500 MPa) tensile reinforcements.

In cyclic tests, besides recording values of the applied load, the beam deflection was also determined using LVDTs mounted along the beam axis in middle section and one-third spans. Furthermore, the strain gauges attached to bottom steel bars (imbedded in concrete) at the centre and one-third span captured the stress-strain behaviour of rebars during the tests. For all the test specimens crack propagation was monitored and noted visually.

From data collected over cyclic loading, the load-deflection curves can be prepared which give an indication of the energy loss per cycle. The loop formed by the load-deflection curve is called a hysteresis loop and the area enclosed within this loop represents the energy loss per cycle. From the hysteresis loop and energy dissipated in each cycle, the damping ratio can be calculated as previously explained in section 2.6.

3.7 Concluding remarks

The materials used in this study are; shrinkage limited Portland cement, fly ash, fine and coarse aggregates, PVA fibres of two different lengths (6 and 12 mm), high range water reducing admixture, water and steels bars of two different strength grades (f_{sy} = 250 and 500 MPa). The experimental program of the project is mainly divided into two parts; material and structural testings. At the first step, 10 different concrete mixes, including PVA fibres of different volume fractions ranging from 0.0 to 0.5% were prepared and tested in order to investigate the effect of PVA fibre addition on fresh and hardened properties of conventional concrete. For each concrete batch, fresh property tests (slump, compacting factor, AC and MPV) were conducted complying with designated Australian Standards. To evaluate the material characteristics of hardened concrete samples, compressive strength, indirect tensile strength, modulus of rupture (MOR) or flexural strength, static chord modulus of elasticity (MOE), residual flexural strength and impact resonant tests were carried out at different ages. From the results of this stage, two FRC and control concrete mixes were selected to be used to fabricate 10 reinforced concrete beams. These beams were then tested under 4-point static flexure and 3-point cyclic loads.

Chapter 4

Test Results and Discussion

4 TEST RESULTS AND DISCUSSION

4.1 Preface

As mentioned earlier in section 3.3, several pilot mixes including control and eight FRCs with fibre contents ranging from 0.0% to 0.50%, have been tested for their fresh properties and compressive strength. According to the results of this investigation which are discussed in this chapter, four FRC mixes as listed below, were selected for further studies;

1) 6PVA-0.25%
2) 12PVA-0.25%
3) 6PVA-0.50%
4) 12PVA-0.50%

The first 2 mixes, including 0.25% volume fraction of 6 and 12 mm fibres, were selected due to their high compressive strength amongst all other mixes. The latter two mixes having fibre content of 0.50% were chosen, since literature (Fu & Lauke 1996) states that longer fibre may have higher potential to act better in terms of tensile and flexural strength. Therefore, the mechanical and dynamic properties of these mixes were thoroughly investigated.

Among these four mixes, mix number 1 (6PVA-0.25%) almost showed the best behaviour in the case of hardened concrete properties. Mix number 4 (12PVA-0.50%) also demonstrated the most ductile failure pattern compared to all other concrete mixes. Thus, these two mixes were selected to be tested for their structural properties. Accordingly, 10 reinforced concrete beams were made out of these two mix designs including control. All beams had the same geometric properties and the only difference was in the concrete type and longitudinal tensile reinforcement strength. Six beams were prepared with low strength (f_{sy} = 250 MPa) steel bars as their longitudinal tensile reinforcement, while the other four had high strength (f_{sy} = 500 MPa) reinforcement. The objective of using steel reinforcement of two strength levels was to investigate the FRC function with different types of steel bars.

The summary of the systematic experimental procedure, thoroughly explained in this section, is listed in Table 21. If a test is performed for a specific mix design, the tick mark (✓) is printed, otherwise the cross mark (×) is shown.

In this chapter, the results of different tests are broadly discussed. Comparisons are also made between FRCs and control, when needed, to evaluate the effect of PVA fibre addition to the concrete.

Table 21. Summary of testing procedure

Mix reference	Fresh property tests				Material tests						Structural tests[1]			
											Series A		Series B	
	Slump test	Compacting factor test	AC test	MPV test	Compressive test	Indirect tensile test	MOR test	MOE test	Residual flexural test	Impact resonance test	4-point flexural test	3-point cyclic test	4-point flexural test	3-point cyclic test
Control	✓	✓	✓	✓	✓	✓	✓	✓	✓	✓	✓	✓	✓	✓
6PVA-0.125%	✓	✓	✓	✓	✓	×	×	×	×	×	×	×	×	×
6PVA-0.25%	✓	✓	✓	✓	✓	✓	✓	✓	×	✓	✓	✓	×	×
6PVA-0.375%	✓	✓	✓	✓	✓	×	×	×	×	×	×	×	×	×
6PVA-0.50%	✓	✓	✓	✓	✓	✓	✓	✓	✓	✓	×	×	×	×
12PVA-0.125%	✓	✓	✓	✓	✓	×	×	×	×	×	×	×	×	×
12PVA-0.25%	✓	✓	✓	✓	✓	✓	✓	✓	×	✓	×	×	×	×
12PVA-0.375%	✓	✓	✓	✓	✓	×	×	×	×	×	×	×	×	×
12PVA-0.50%	✓	✓	✓	✓	✓	✓	✓	✓	✓	✓	✓	✓	✓	✓
Conventional	✓	✓	✓	✓	✓	✓	✓	✓	✓	✓	×	×	×	×

[1] Series A has low strength longitudinal tensile reinforcement where series B has high strength reinforcements.

4.2 Fresh properties

Slump, compacting factor, air content and mass per unit volume of different mixes were measured in order to evaluate the effect of PVA fibre addition on properties of freshly mixed concrete. Herein, the results of all above mentioned tests as summarized in Table 22 are further discussed in details.

Table 22. Fresh properties of control and FRCs

Mix reference	HWR/C [%]	Slump[1] [mm]	Compacting factor	Air Content[1] [%]	Mass per unit volume[1] [kg/m^3]
Control	0.33	75	0.85	1.0	2450
6PVA-0.125%	0.47	75	0.84	1.2	2430
6PVA-0.25%	0.54	65	0.82	1.4	2410
6PVA-0.375%	0.59	65	0.85	1.2	2370
6PVA-0.50%	0.65	70	0.89	1.4	2340
12PVA-0.125%	0.45	70	0.82	1.4	2420
12PVA-0.25%	0.54	60	0.84	1.2	2390
12PVA-0.375%	0.62	60	0.81	1.0	2370
12PVA-0.50%	0.88	60	0.84	1.4	2300
Conventional	0.25	60	0.86	0.8	2510

[1] Slump, Air content and Mass per unit volume are calculated to the nearest 5 mm, 0.2% and 10 kg/m^3, respectively, in accordance with AS1012.3.1, AS1012.4.2 and AS1012.5

4.2.1 *Slump*

Comparing FRCs slump versus control confirms the fact that, fibre addition to the mix decreases the concrete slump. In the case of control concrete, introducing 0.33% HWR proportional to the cementitious materials resulted in the desired slump (80 ± 20 mm). However, Experiments show that higher amounts of HWR needs to be added to FRCs to achieve the target slump. For most FRCs, even with higher dosage of HWR, lower slump is recorded compared to the control concrete. It can also be observed that, slump has a decreasing trend with increasing fibre addition. Furthermore, 12 mm fibre with a bigger aspect ratio shows lower slump in the same fibre volume fraction and higher amounts of HWR is required (these trends can be observed in Figure 46). This observation has previously been proven by other researchers (Hamoush et al. 2010; Han et al. 2009; Hannant et al. 1978; Swamy 1974) that increasing the fibre volume fraction and aspect ratio leads to decrease in concrete workability.

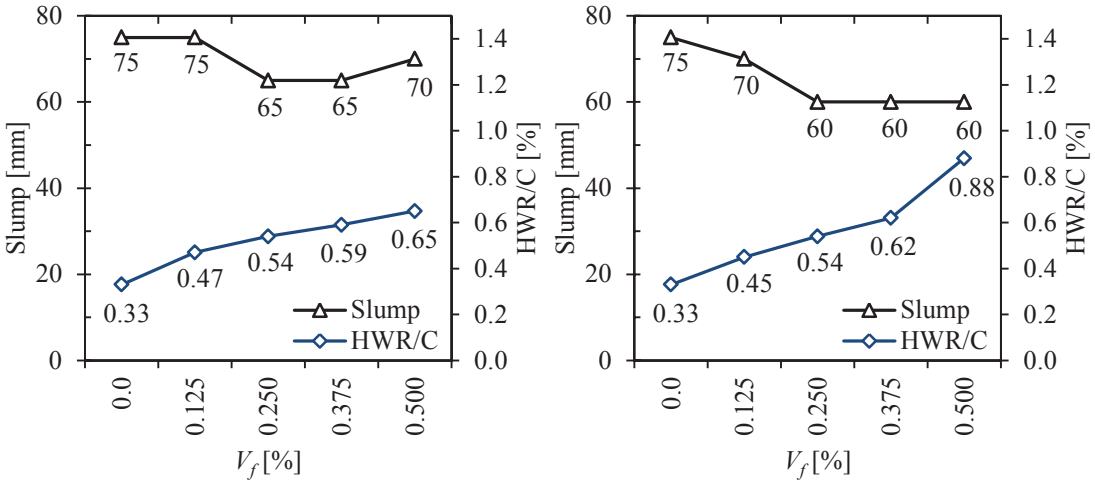

Figure 46. Slump versus HWR/C for FRCs compared to control; FRCs with 6 mm fibres (left) FRCs with 12 mm fibres (right)

A comparison of the slump of control with conventional concrete (devoid of FA) shows that adding Fly ash increases the concrete workability which is complying with previous investigations (Álvarez et al. 1988; Bai et al. 2003). This may be due to the ball-bearing effect of spherical fly ash particles that improves concrete workability (Manz 1999).

4.2.2 *Compacting factor*

Compacting factor, another parameter describing the concrete mix consistency, shows that the low additions of PVA fibres are insignificant in contributing to the concrete self-compaction characteristics although a small decrease in the compaction factor has been recorded for some FRCs compared to the control concrete. As previously mentioned by Neville (Neville 1991), in the case of concrete with low workability, the compacting factor test is very sensitive and variations in rheological properties of concrete are reflected in large changes in the compacting factor as shown in Table 23.

Table 23. Description of workability and compacting factor (Neville 1991)

Description of workability	Compacting factor	Corresponding slump
Very low	0.78	0 – 25 mm
Low	0.85	25 – 50 mm
Medium	0.92	50 – 100 mm
High	0.95	100 – 175 mm

However, in this case as shown in Figure 47, observing approximately the same compacting factor explains that the workability of FRCs are very similar to that of control concrete.

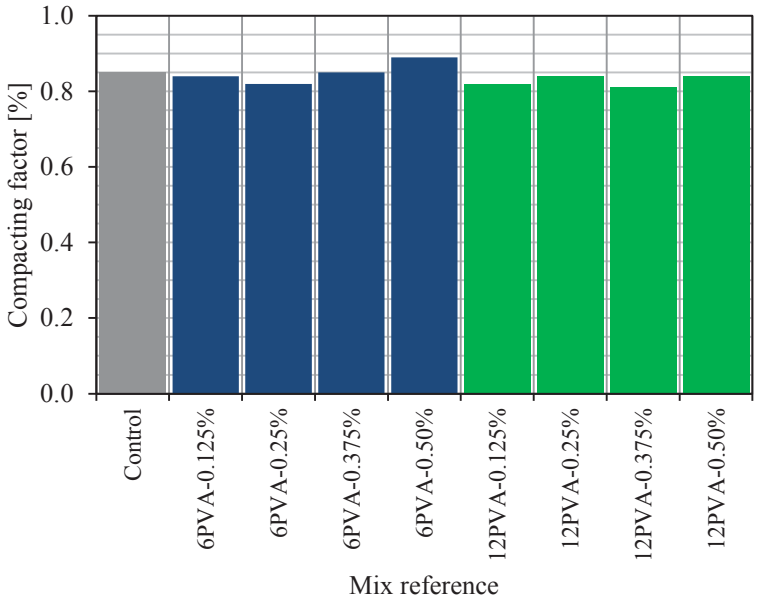

Figure 47. Compacting factor of FRCs and control concrete

4.2.3 *Air content*

Comparing the air content (AC) of FRCs and control versus HWR/C, shown in Figure 48, illustrates that the AC of FRCs is slightly higher than that of control, although this enhancement is very small in magnitude (from 1.0% to 1.4%). Such observations were previously mentioned in literature (Heo et al. 2012), it was expected that by adding fibres to the mix and also increasing the HWR amount, a higher air content would result.

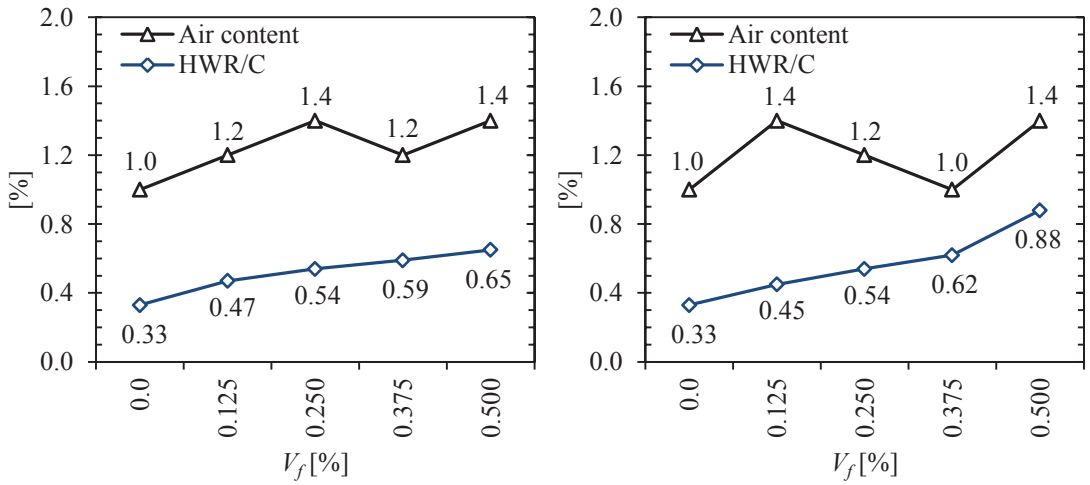

Figure 48. Air content versus HWR/C for FRCs and control; FRCs with 6 mm fibres (left) FRCs with 12 mm fibres (right)

4.2.4 *Mass per unit volume*

Mass per unit volume of FRCs versus control is presented in Figure 49. The MPV of concrete is observed to decrease with increasing fibres addition. This is due to the lower mass per unit volume of the fibres. Results show that by increasing the amount of fibre in the mix, the density decreases from 2450 kg/m^3 for control to 2300 kg/m^3 for 12PVA-0.50%. The decrease noted in the MPV is highly dependent on the volume and amount of fibres for the matrix as well as the length and number of fibres. It is also understandable that for the same fibre volume fraction, 12 mm fibres affect the MPV more than 6 mm fibres, which may be attributed to the higher aspect ratio of longer fibres.

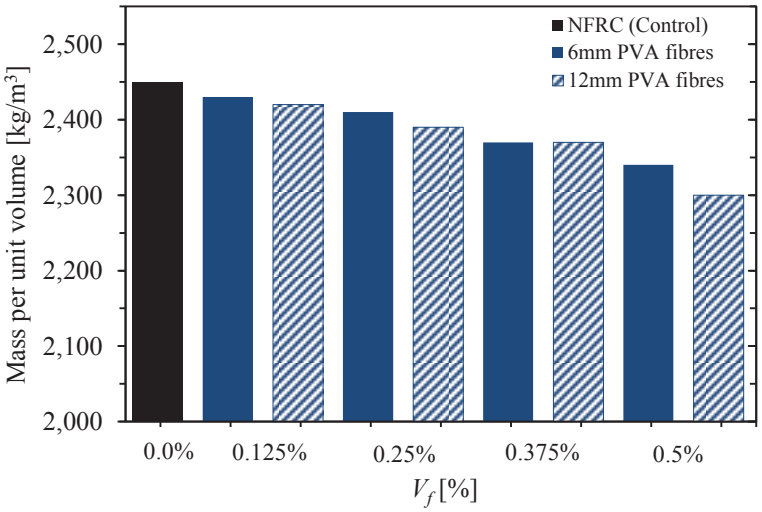

Figure 49. Mass per unit volume of FRCs versus control

4.3 Material Properties

4.3.1 *Compressive strength*

The compressive strength of control and FRCs with different fibre volume fractions ranging from 0.0% to 0.5% at 7, 28 and 56 days of age are presented in Table 24 and Figure 50. Standard deviations calculated for compressive strengths of each concrete set, show the level of variation from average strength reported out of 3 specimens tested for each age. A low standard deviation indicates that the individual compressive strength of test specimens tend to be very close to the average strength of that group which is associated with a higher level of confidence in statistical average strength reported.

Table 24. Compressive strength of control and FRCs at 7, 28 and 56 days

Mix reference	7 day strength - $f_{c,7}$		28 day strength - $f_{c,28}$		56 day strength - $f_{c,56}$	
	Average Strength[1] [MPa ± SD[2]]	Strength effectiveness [%]	Average Strength [MPa ± SD]	Strength effectiveness [%]	Average Strength [MPa ± SD]	Strength effectiveness [%]
Control	46.0 ± 1.7	N/A	60.0 ± 3.2	N/A	72.5 ± 3.0	N/A
6PVA-0.125%	45.0 ± 0.5	-2.1	65.0 ± 4.6	+8.3	79.0 ± 2.1	+9.0
6PVA-0.25%	48.0 ± 4.1	+4.3	67.0 ± 3.2	+11.7	82.5 ± 4.2	+13.8
6PVA-0.375%	43.0 ± 1.8	-6.5	62.0 ± 2.3	+3.3	73.5 ± 2.6	+1.4
6PVA-0.50%	40.5 ± 3.5	-12.0	61.5 ± 2.5	+2.5	70.0 ± 3.8	-3.4
12PVA-0.125%	41.5 ± 1.0	-9.7	63.0 ± 1.8	+5.0	70.5 ± 2.8	-2.8
12PVA-0.25%	43.5 ± 3.6	-5.4	64.5 ± 3.2	+7.5	73.0 ± 2.9	+0.7
12PVA-0.375%	41.0 ± 2.6	-10.9	60.0 ± 1.7	0.00	67.5 ± 1.5	-6.9
12PVA-0.50%	39.5 ± 2.4	-14.1	58.5 ± 2.8	-2.5	64.0 ± 4.2	-11.7
Conventional	61.5 ± 1.4	N/A	73.5 ± 1.2	N/A	76.5 ± 4.5	N/A

[1] Average compressive strength of the test specimens calculated to the nearest 0.5 MPa in accordance with AS 1012.9
[2] SD: Standard deviation

Strength effectiveness (S.E) which can be defined as the percentage of increase or decrease in FRCs strength compared to the control mix at the same age is also calculated;

$$S.E = \frac{FRC\ strength - Control\ strength}{Control\ strength} \times 100\% \qquad (12)$$

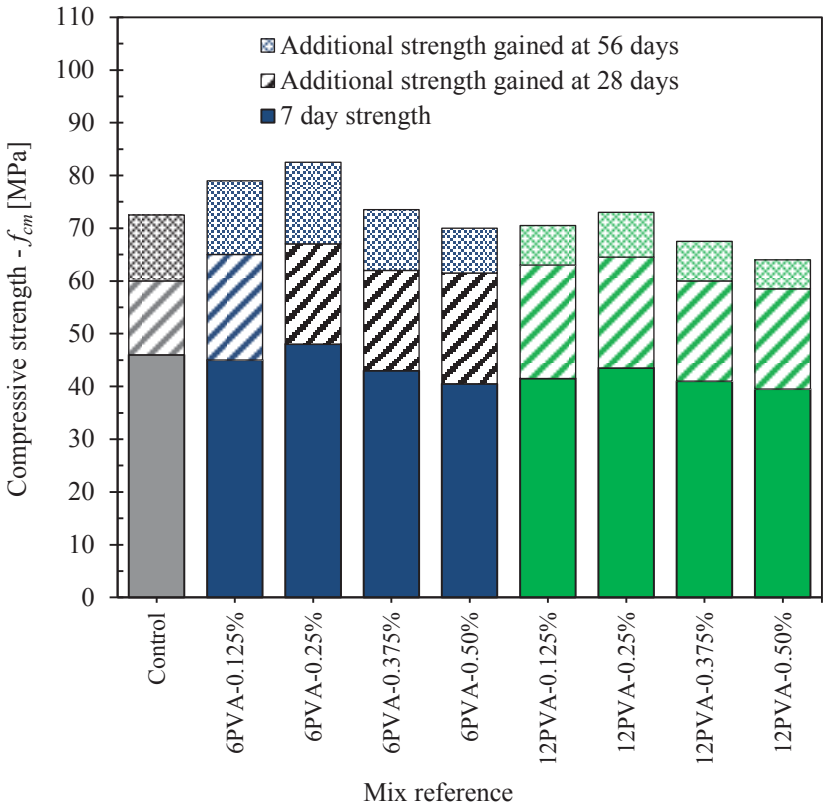

Figure 50. Compressive strength development from 7 to 28 and 56 days of FRCs versus control

The values of FRCs compressive strength at 7, 28 and 56 days are normalised with respect to the control compressive strength at the same age and plotted against fibre volume fraction in Figure 51 to Figure 53. Results show that fibres are not always beneficial to compressive strength, especially when the fibre content increases beyond a certain level. As also previously stated by Li (Li 1992), the compressive strength may first rise, then drop, with increasing fibre volume fraction. Results indicate that when fibres are added to cement composite, two opposing processes of strength improvement and degradation is observed. When fibres are present, strength improvement can be an indication of increase in resistance to micro crack sliding and extension, whereas strength degradation can be a resultant of increase in either pore or micro crack density. The pores may be related to insufficient compaction and the additional micro cracks may be related to touching fibres, (unbonded) fibre end cracks, poor fibre/matrix bonding, or poor adhesion between filaments within fibre bundles (Li 1992).

By viewing the results, it can be noted that FRCs with lower fibre additions have higher compressive strength compared to the control. In addition, with the same fibre volume fraction, shorter fibres are noted to enhance compressive strength more so than longer fibres. Furthermore, the optimum fibre volume fraction was found to be 0.25% across

all ages with a 14% increase in 56 day compressive strength noted compared to the control.

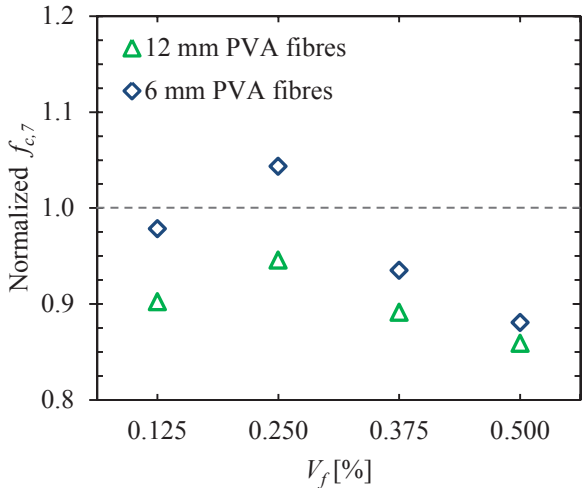

Figure 51. Normalized 7-day compressive strength of FRCs with respect to control concrete

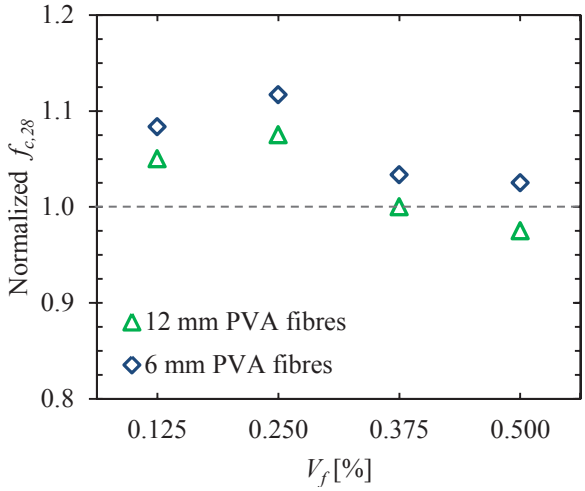

Figure 52. Normalized 28-day compressive strength of FRCs with respect to control concrete

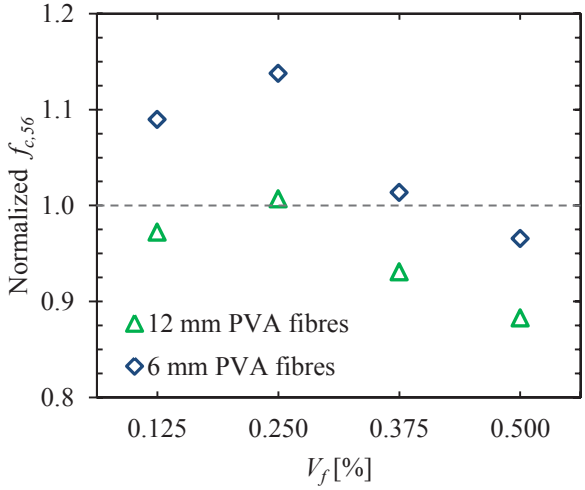

Figure 53. Normalized 56-day compressive strength of FRCs with respect to control concrete

Figure 54 shows the compressive strength of all concretes versus age. The slope of the curves in each region (0 – 7 days, 7 – 28 days and 28 – 56 days) shows the rate of strength gained within that period. The slope of the curve between 7 and 28 days for all FRCs is considerably higher than that of control which means that both 6 and 12 mm fibres assist with compressive strength development within this time frame. In other words, the lower 7 day and higher 28 day compressive strengths of FRCs compared to the control, indicates that the introduction of PVA fibres affects strength gain by decreasing the value at early ages (by 7 days) and accelerating the strength improvement from 7 to 28 days. For instance, the concrete including 0.25% of 6 mm fibres can achieve the 28-day strength of control concrete at approximately 20 days. This noted increase in strength is likely due to the enhanced bond strength achieved between the cementitious material and fibres as a function of increasing age.

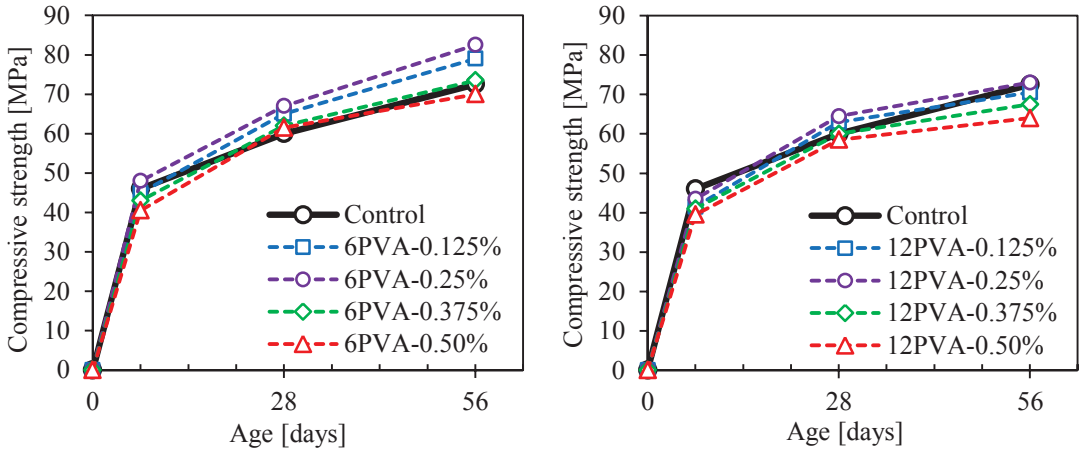

Figure 54. Compressive strength development of FRCs versus control by ageing; FRCs with 6 mm fibres (left) FRCs with 12 mm fibres (right)

The slope of the third part of the curve from 28 to 56 days illustrates that 6 mm fibres in low percentages (< 0.25%) contribute to the strength gain of concrete from 28 to 56 days; however, higher additions of 6 mm fibre and all additions of 12 mm fibre affect the strength gain in this period with lower 56 day strength compared to the expected values. Here again the concrete having 0.25% of 6 mm fibres can reach the control 56-day strength at 38 days of age.

If the 56-day strength of control and FRCs are assumed to be their ultimate strength, then the ratio of compressive strength at 7 and 28 days to the ultimate strength, which is called ‘relative strength’, can be calculated using Equation (13). The resulting values are presented in Table 25.

$$Relative\ strength_{x-56} = \frac{f_{c,x}}{f_{c,56}} \times 100\% \quad (13)$$

where x is the specific curing age which can be either 7 or 28 days.

Table 25. Relative compressive strengths for control and FRCs

Mix reference	Relative strength$_{7\text{-}56}$ [%]	Relative strength$_{28\text{-}56}$ [%]
Control	63.4	82.8
6PVA-0.125%	57.0	82.3
6PVA-0.25%	58.2	81.2
6PVA-0.375%	58.5	84.3
6PVA-0.50%	57.9	87.9
12PVA-0.125%	58.9	89.4
12PVA-0.25%	59.6	88.4
12PVA-0.375%	60.7	88.9
12PVA-0.50%	61.7	91.4

Literature (Ramamurty & Narayanan 2000; Şahin et al. 2003) states that, for plain concrete, compressive strength decreases with reduction in mass per unit volume. However, as shown in Figure 55, nearly all PVA-FRCs have higher compressive strength than control although their MPV is lower which deviates from accepted theory. Possible reasons for this noted increase in strength include the tendency of PVA fibres to provide a strong chemical bond with the cementitious matrix originating from a hydroxyl group present in the molecular chain of the fibre. In essence, this means that PVA-FRC can achieve marginally higher or same compressive strength with 5% less density.

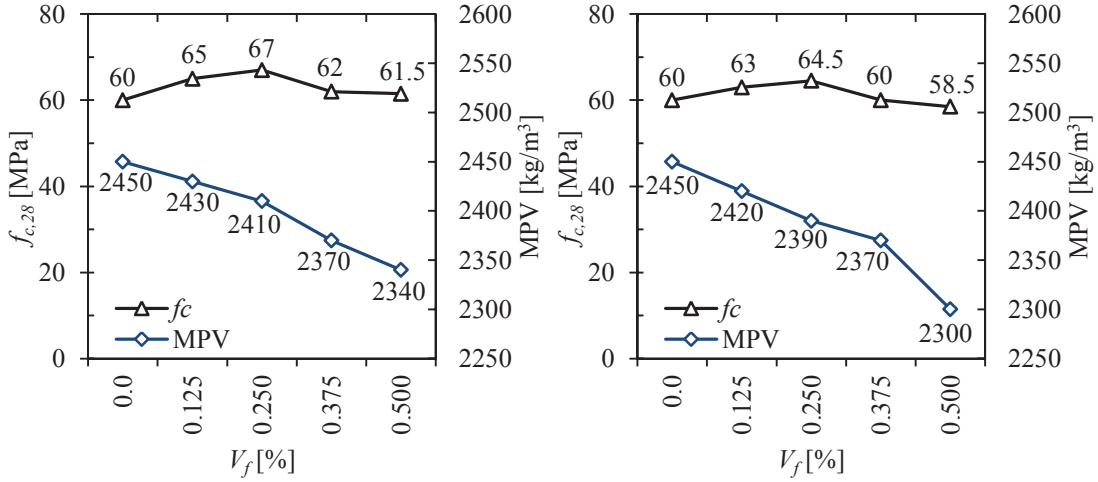

Figure 55. 28 day compressive strength versus Mass per unit volume of FRCs and control; FRCs with 6 mm fibres (left) FRCs with 12 mm fibres (right)

As concrete contains voids of various size and shape in the matrix, and micro cracks at the interfacial transition zones (ITZ), it represents a very complex failure mode under different types of stress application. When concrete is loaded under uniaxial tension, less energy is required for the crack initiation and growth in the concrete matrix (Mehta & Monteiro 2005). The brittle-like behaviour of concrete in tension results from rapid propagation and inter-linkage of pre-existing cracks at ITZ and newly formed cracks in the matrix. Since concrete has much load bearing capacity in compression, much more energy is needed to create new cracks or extend pre-existing cracks in the matrix and accordingly, concrete compression failure is less brittle compared to failure under tension. In low or medium strength concrete, theory states that when a uniaxial compression load is applied, no cracks commence in the matrix up to about 50 precent of failure stress (Mehta & Monteiro 2005). Meanwhile, in the locality of coarse aggregate, a stable system of shear-bond cracks already exists. Cracking will initiate in the matrix at higher stress levels and their size and quantity increase as the stress level is amplified. These cracks will eventually join the pre-existing cracks in the ITZ (shear-bond cracks) and initiate a failure surface approximately at 20° to 30° angled from the direction of the load (Mehta & Monteiro 2005).

Qualitative observations during the compressive strength test indicate that the failure modes for FRCs and control are significantly different. Figure 56 shows a sample of the compressive failure modes experienced for different cylindrical specimens. For control concrete (Figure 56, item 1), failure mode was seen to be quite brittle and the specimens failed in an almost explosive-like manner. Specimens at later ages failed with a more pronounced explosive-like failure compared to those of early ages. Whereas, for FRCs, more ductile behaviour was observed and depending on the fibre volume fraction, specimens were noted to destruct with many cracks on the surface. (Figure 56, item 2 = 6PVA-0.125%, item 3 = 12PVA-0.25%, item 4 = 6PVA-0.50%, item 5 = 12PVA-0.50%)

The integrity of FRC specimens was found to improve due to the restriction of PVA fibres. It has been previously stated that fibres assist avoiding a sudden and brittle concrete crushing owing to their ability of enhancing concrete toughness in compression (Meda et al. 2012). For specimens with higher fibre additions, i.e. 0.50%, an obvious unloading process was observed once the load reached the critical stress and the failure mode thereafter was seen to be almost ductile. Consequently, the incorporation of fibres

greatly improves the compressive failure properties of concrete specimens, which has also previously reported by Zheng et al. (Zheng et al. 2012). It has also been reported that (Lam et al. 1998) by using FA, the post-peak compressive behaviour of concrete increases and the strain value at maximum stress improves.

Figure 56. Compression failure modes of FRCs and control at 28 days

Previous research (De Nicolo et al. 1994) indicated that the strain at peak stress in uniaxial compression for conventional concrete is 0.002. However, mix composition, curing conditions, shape and size of specimen, loading rate, age of loading, and test techniques used, all have a bearing on the resulting strain at compressive strength (Tasdemir et al. 1998).

Herein, the strain corresponding to ultimate stress for two selected fibre volume fractions compared to the control concrete are given in Table 26. Strain at peak load was observed to decrease with a decrease in compressive strength for conventional concrete (NFRC), which follows the same trend observed by Tasdemir et al. (Tasdemir et al. 1998), that is, the strain at ultimate stress increases as the compressive strength increases. However, for FRCs strain at peak stress increases although the compressive strength decreases. This possibly can be due to the fibres presence in the matrix contributing to the interfacial transition zone (ITZ) between the matrix and aggregates in concrete. Past studies have demonstrated that ITZ plays an important role in the resultant shape of the stress-strain curve under uniaxial compression (Tasdemir et al. 1998).

Table 26. Stress and strain at ultimate stress in compression at 28 days for FRCs versus control

Mix Reference	V_f [%]	$f_{c,28}$ [MPa]	Strain at peak stress (ε_{cu})
Control	0.00	57.5	0.0025
6PVA-0.25%	0.25	67.0	0.0026
6PVA-0.50%	0.50	61.5	0.0034
12PVA-0.25%	0.25	64.5	0.0026
12PVA-0.50%	0.50	58.5	0.0035

4.3.2 *Indirect tensile strength*

The indirect tensile (splitting tensile) strength of control and FRCs with 0.25% and 0.5% fibre volume fractions at 7, 28 and 56 days of age are presented in Table 27. As indicated, the splitting tensile strength of plain concrete is significantly enhanced by introducing PVA fibres to the mix. The $f_{ct.sp,28}$ values of all FRCs are higher than that of control concrete, ranging from 11% for 12PVA-0.50% to 32.5% for 6PVA-0.25%. Figure 57 shows the normalised indirect tensile strength of FRCs at 7, 28 and 56 days with respect to the control concrete.

Table 27. Indirect (splitting) tensile strength of control and FRCs at 7, 28 and 56 days

Mix reference	7 day - $f_{ct.sp,7}$		28 day - $f_{ct.sp,28}$		56 day - $f_{ct.sp,56}$	
	Average strength[1] [MPa]	Standard deviation [MPa]	Average strength [MPa]	Standard deviation [MPa]	Average strength [MPa]	Standard deviation [MPa]
Control	3.0	0.3	3.7	0.5	4.3	0.2
6PVA-0.25%	3.9	0.2	4.9	0.2	5.7	0.3
6PVA-0.50%	3.1	0.1	4.2	0.3	4.6	0.1
12PVA-0.25%	4.0	0.3	4.7	0.2	5.5	0.1
12PVA-0.50%	3.0	0.2	4.1	0.4	4.3	0.4
Conventional	3.7	0.2	4.3	0.3	4.6	0.2

[1] Average splitting tensile strength of the test specimens calculated to the nearest 0.1 MPa in accordance with AS 1012.10

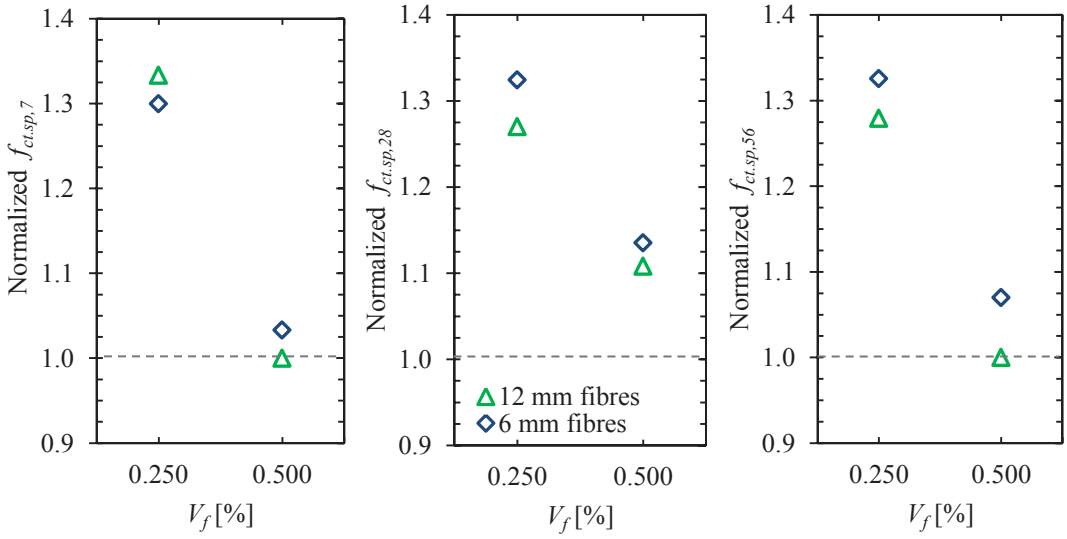

Figure 57. Normalized indirect tensile strength of FRCs at 7, 28 and 56 days with respect to control

4.3.3 *Modulus of rupture (flexural strength)*

The flexural strength or modulus of rupture test of control and FRCs with 0.25% and 0.5% fibre volume fractions were conducted at 7, 28 and 56 days of age (Figure 58) and the results are presented in Table 28.

Figure 58. Modulus of rupture test

Table 28. Flexural strength of control and FRCs at 7, 28 and 56 days

Mix reference	7 day - $f_{ct,f,7}$		28 day - $f_{ct,f,28}$		56 day - $f_{ct,f,56}$	
	Average strength[1] [MPa]	Standard deviation [MPa]	Average strength [MPa]	Standard deviation [MPa]	Average strength [MPa]	Standard deviation [MPa]
Control	4.4	0.3	5.6	0.2	7.1	0.2
6PVA-0.25%	4.8	0.1	6.8	0.2	8.3	0.4
6PVA-0.50%	4.1	0.2	6.3	0.1	7.2	0.1
12PVA-0.25%	4.7	0.1	6.7	0.2	7.6	0.5
12PVA-0.50%	4.1	0.3	6.2	0.5	6.6	0.1
Conventional	6.0	0.1	6.9	0.5	7.5	0.1

[1] Average flexural strength (MOR) of the test specimens calculated to the nearest 0.1 MPa in accordance with AS 1012.11

Figure 59 is showing the normalised modulus of rupture of FRCs at 7, 28 and 56 days with respect to the control concrete.

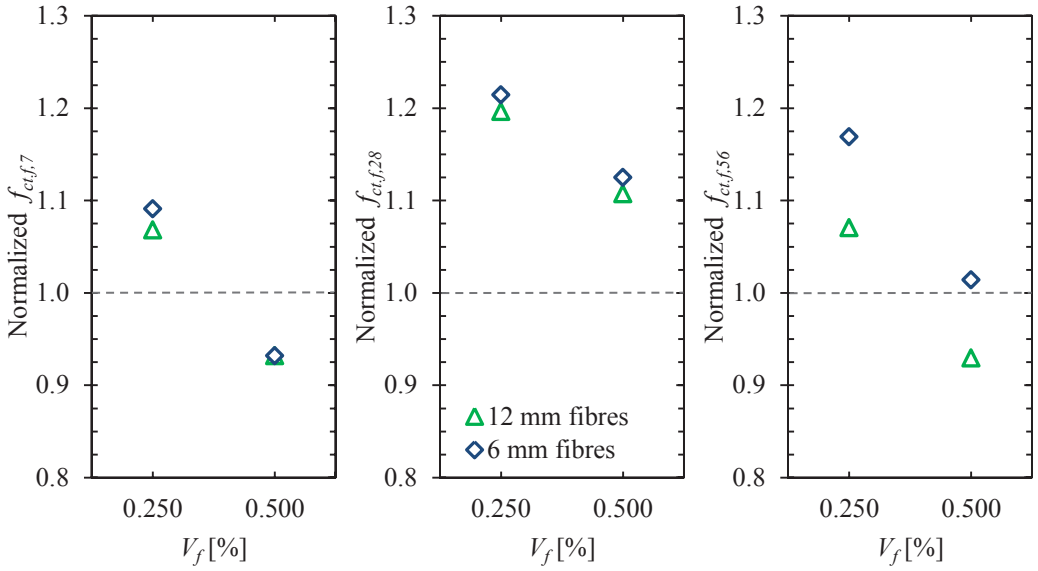

Figure 59. Normalized modulus of rupture of FRCs at 7, 28 and 56 days with respect to control concrete

Similar to splitting tensile strength, results of flexural strength at 28 days ($f_{ct,f,28}$) of FRCs versus control show considerable improvement ranging from 11% up to 21.5%. Moreover, in terms of flexural strength, optimum fibre content goes to 0.25% volume fraction. At this optimum value, fibres provide a proper bridging effect which leads to strength improvement, however, higher fibre content had reverse effects. This can be caused by non-uniform fibre distribution and improper orientation due to large number of fibres in the mix. Fibres which are not parallel to the cracks, can contribute to the stress bridging process by preventing a proper fibre orientation. Furthermore, as it is inferred from the results, shorter fibres demonstrate a better effect on improving the flexural strength. Higher aspect ratio of the fibres can be responsible for this effect. It is assumed that these fibres may bend and not stay straight in the matrix. Therefore, their total length cannot contribute to load bearing process and stress control mechanism.

As stated in the literature (Jastrzebski 1977; Low & Beaudoin 1994) the flexural toughness and ductility can be determined from the flexural load-deflection curves. The flexural toughness is calculated as the area under the entire load-deflection curve and ductility is determined from deflection in post-peak region.

As shown in Figure 60, the sum of all finite area increments over the entire region under ABC curve, known as the work done leading to fracture, represents total flexural toughness. The flexural toughness can be mathematically calculated from Equation (14).

$$T = \sum \left(\frac{P_i + P_j}{2}\right) \times \left(X_j - X_i\right) \tag{14}$$

where P_i and P_j represent two different applied loads for a finite increment and (X_j - X_i) is the change of deflection within the finite increment.

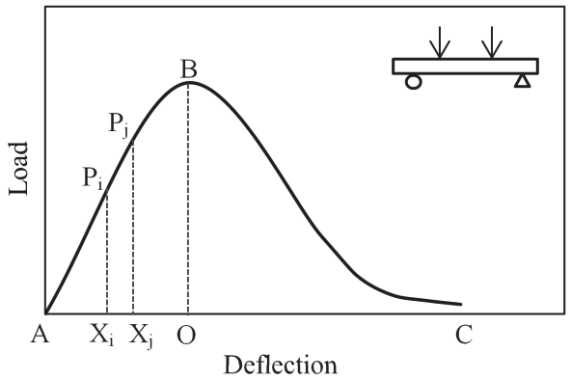

Figure 60. Schematic of a typical load-deflection curve in flexure (Low & Beaudoin 1994)

As shown in Figure 60, the total ABC area can be divided into two regions. The deflection prior to the peak (AO) in ABO region is more related to rigidity, strength and micro-cracking process of the composite, where the post-peak deflection (OC) is a measure of ductility. The region ABO which is limited to initial point of the curve (A) and the peak load (B) is the area in which elastic and some inelastic deformations occur due to strain hardening.

Figure 61 and Figure 62 illustrate the Load-mid span deflection of test specimens in flexure, at 28 days of age. It can be observed that, fracture and total failure in the plain concrete occur suddenly just after exceeding the maximum load with a straight drop in the load-deflection curve. However, the load-deflection curves of FRCs vary significantly. FRCs show considerably larger deflections at the ultimate state as well as higher loads compared to the control concrete. This will result in a bigger area under the load-deflection curves (ABC) which can be an indication of increasing toughness. Consequently, it can be stated that the flexural toughness of concrete enhances by introducing PVA fibres to the mix and it will be further increased if more fibres are added.

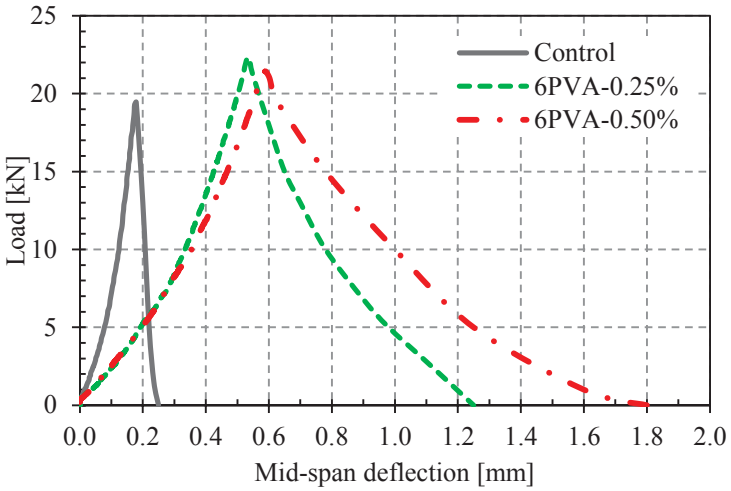

Figure 61. Load-mid span deflection curves in 28-day MOR test of control and FRCs with 6 mm fibres

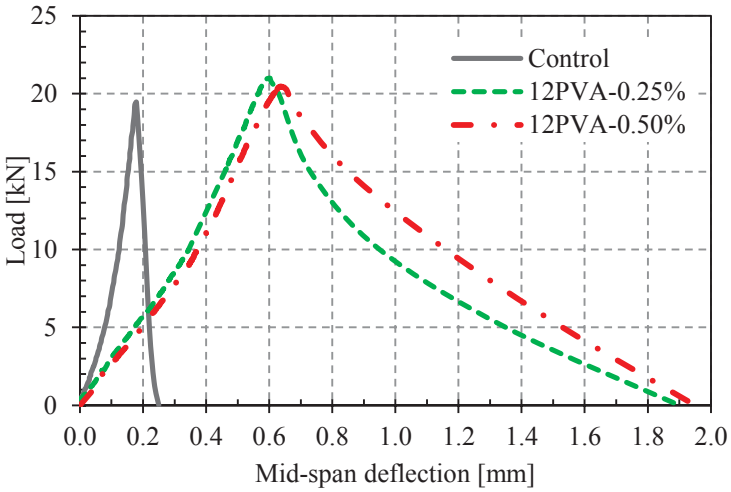

Figure 62. Load-mid span deflection curves in 28-day MOR test of control and FRCs with 12 mm fibres

As a well-known fact, the slope of the load-deflection curve in flexure represents the flexural stiffness. As can be observed from Figure 61 and Figure 62, the FRCs flexural stiffness is lower than the control concrete although they have higher load bearing capacities. This behaviour which is a result of fibre bridging in concrete matrix, although may bring up few concerns regarding the serviceability characteristics by imposing larger deflections within serviceability state, is a proper behaviour for concrete in seismic applications. This kind of behaviour provides large deflections before failure and dissipates more energy compared to the conventional concrete in a critical situation such as earthquake.

Figure 63 shows the normalized peak load deflection of FRCs of both fibre lengths. As illustrated, this deflection is improved by more than three times when fibres are added to the control concrete. However, for fibre content more than 0.25% no significant

improvement in peak load deflection is observed and only a slight increase was recorded.

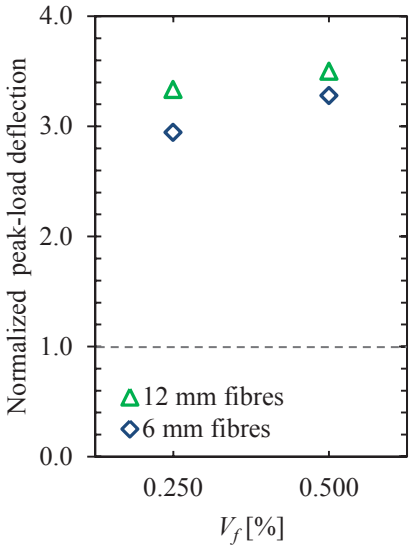

Figure 63. Normalized peak-load deflection of FRCs in 28-day MOR test with respect to control concrete

4.3.4 *Modulus of elasticity*

Static Chord modulus of elasticity of FRCs and control at 7, 28 and 56 days are compared in Table 29 and Figure 64. From the results, it can be noted that modulus of elasticity of concrete mixtures increase with age. It is also observed that PVA fibres in low volume fractions used in this study (0.25% and 0.50%) do not significantly affect the modulus of elasticity although some fluctuations are observed. These variations are more noticeable at early ages (7 and 28 days) while at 56 days most FRCs have very similar values to that of control. These observations were also previously reported by researchers that fibres of different types with various modulus of elasticity do not significantly affect the values of static elastic modulus of concretes, due to the low fibre content (Corinaldesi & Moriconi 2011; Hannant 2003). However, it is anticipated that within the FRCs, adding more fibres leads to a decrease in concrete modulus of elasticity and in a same fibre content longer fibres have lower MOE.

Table 29. Elastic modulus of control and FRCs at 7, 28 and 56 days

Mix reference	$E_{c,7}$[1] [GPa]	$E_{c,28}$ [GPa]	$E_{c,56}$ [GPa]
Control	37.7	39.3	41.4
6PVA-0.25%	39.0	40.1	41.9
6PVA-0.50%	33.3	38.8	40.0
12PVA-0.25%	35.0	39.2	40.3
12PVA-0.50%	32.1	33.2	38.7
Conventional	38.2	40.3	44.6

[1] Elastic modulus of the test specimens calculated to the nearest 0.1 GPa in accordance with AS 1012.17

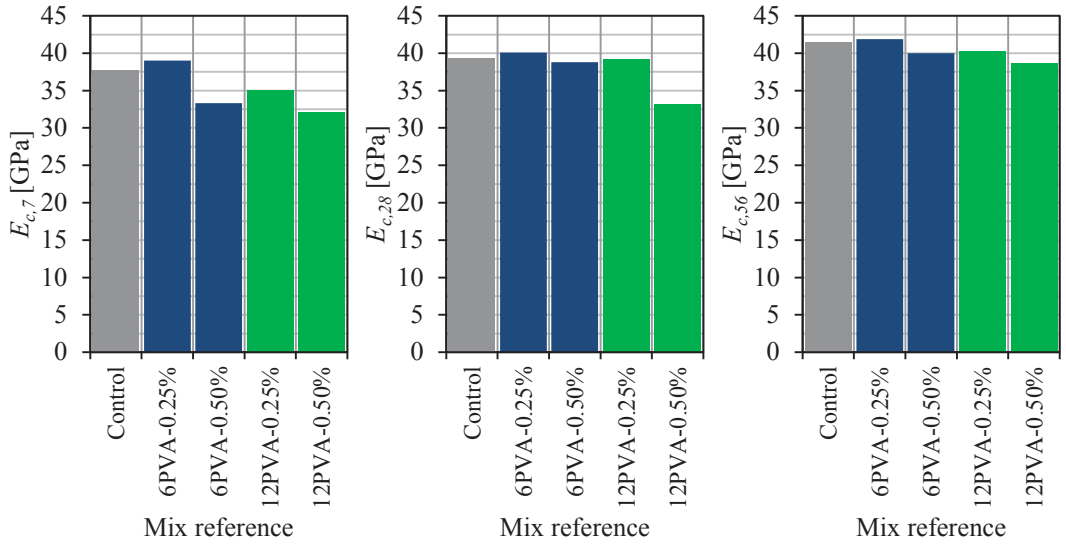

Figure 64. Elastic modulus of control and FRCs at 7, 28 and 56 days

Previous investigations on conventional concrete (Bouzoubaâ et al. 2001; Gencel et al. 2012; Siddique 2004) show that the concrete modulus of elasticity has a relationship with the compressive strength and air content as seen in Figure 65 to Figure 67. It has been stated that the concrete MOE has a direct relationship with compressive strength and an in-direct relationship with AC. Actually there is a combined effect of these two properties on concrete MOE. Herein, the trend of MOE, compressive strength and AC variations follow the previous observations showing that an increase in concrete AC and decrease in compressive strength, leads to the elastic modulus of concrete's decrease.

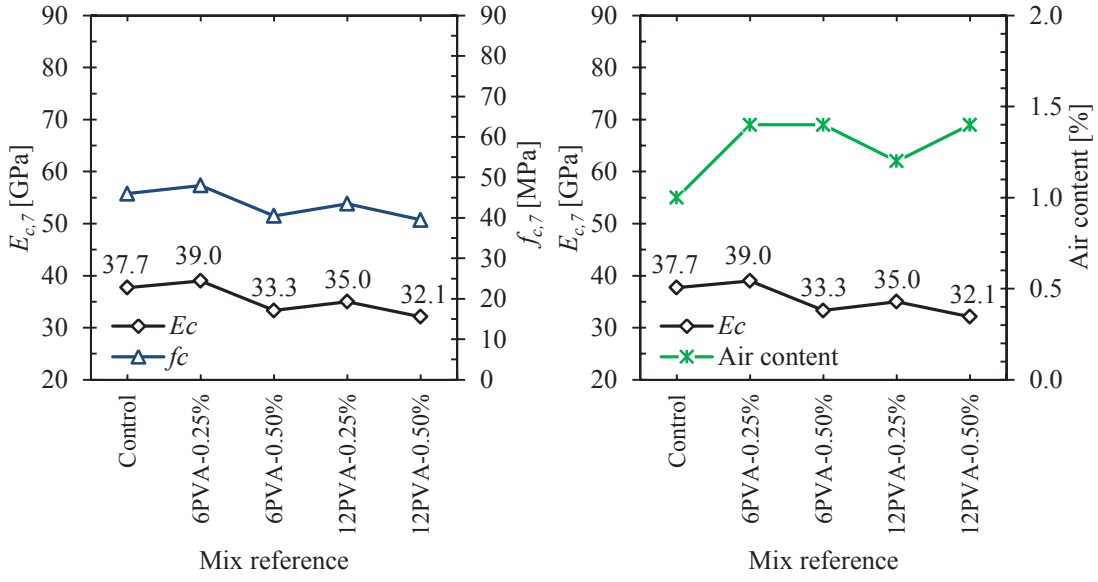

Figure 65. 7-day MOE versus 7-day compressive strength and air content

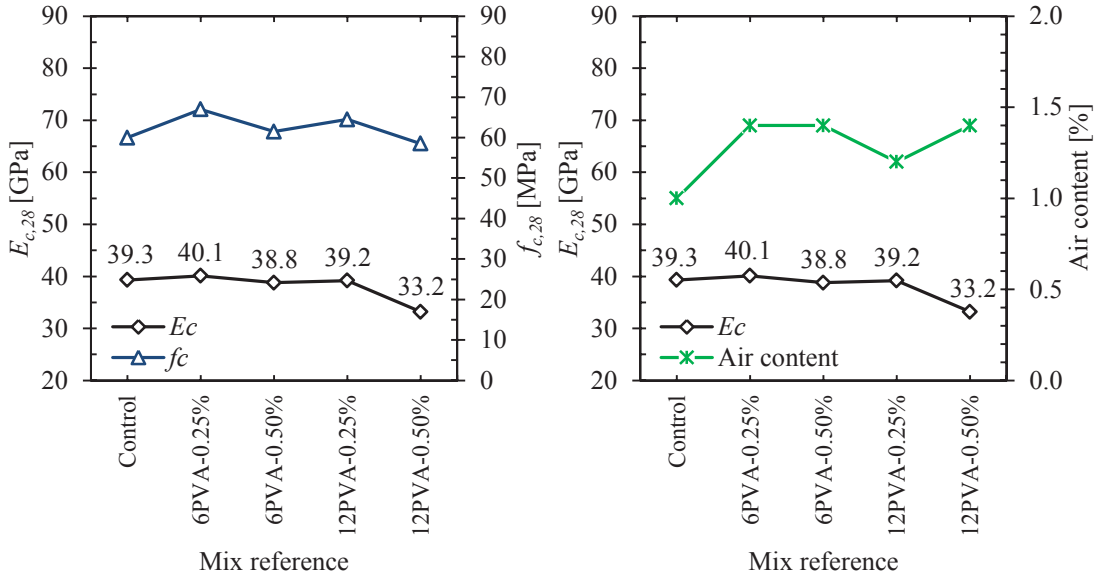

Figure 66. 28-day MOE versus 28-day compressive strength and air content

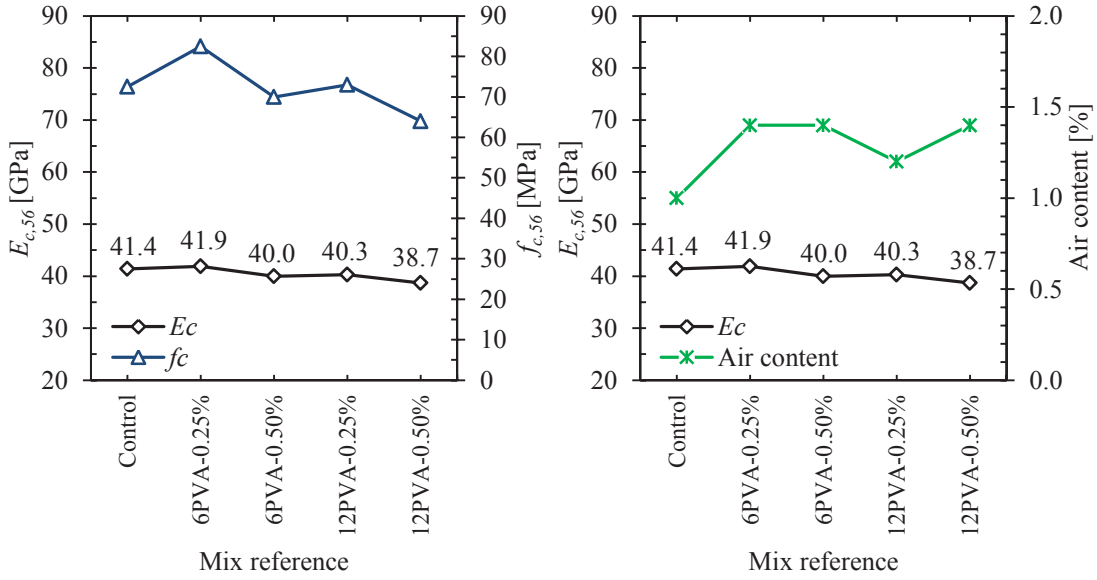

Figure 67. 56-day MOE versus 56-day compressive strength and air content

4.3.5 *Residual flexural tensile strength*

Ductile behaviour of concrete under loading conditions is of attention and interest. Ductile behaviour is defined as the ability of the concrete matrix to absorb energy, maintaining load bearing capacity. It is important to have a concrete matrix where tensile strain increases, when the first crack occurs and beyond. In concrete, improving the post peak response is a requirement as concrete does not have to exhibit sufficient post peak behaviour. To evaluate the concrete post peak properties, different types of tests are presented in standards world wide, where flexural tests are of great attention.

The reason flexural test is well known is that it simulates the real condition in a more practical and simpler way than that of other tests such as the tension test (Gopalaratnam & Gettu 1995). Furthermore, the notched beam test using crack mouth opening displacement (CMOD) has proven to be a good test to evaluate the post peak behaviour and toughness of fibre reinforced concrete (FRC) (Gopalaratnam & Gettu 1995).

Pantazopoulouet et al. studied that, fibres contribute to tensile resistance due to the post peak ductile behaviour before failure but the addition of fibre prevents particle movement in the matrix which lowers the Poison‘s ratio regardless of the fibre type used (Pantazopoulou & Zanganeh 2001). Addition of synthetic fibres does not affect the pre peak behaviour (Meddah & Bencheikh 2009), whereas in the post peak response the reverse is true. The post peak behaviour of concrete and its elastic behaviour has been investigated in past studies and the results suggest that although fibre addition does not greatly increase the flexural strength it generally improves concrete toughness (Buratti et al. 2011). Moreover, synthetic fibres have been reported to improve the post peak response of concrete aiding to reduce the rate of strength loss from the peak value (Pantazopoulou & Zanganeh 2001). Other investigations performed on long synthetic and steel fibres (e.g. more than 30 mm in length) reported that fibres significantly improve the post peak behaviour and residual flexural strength of plain concrete (Buratti et al. 2011).

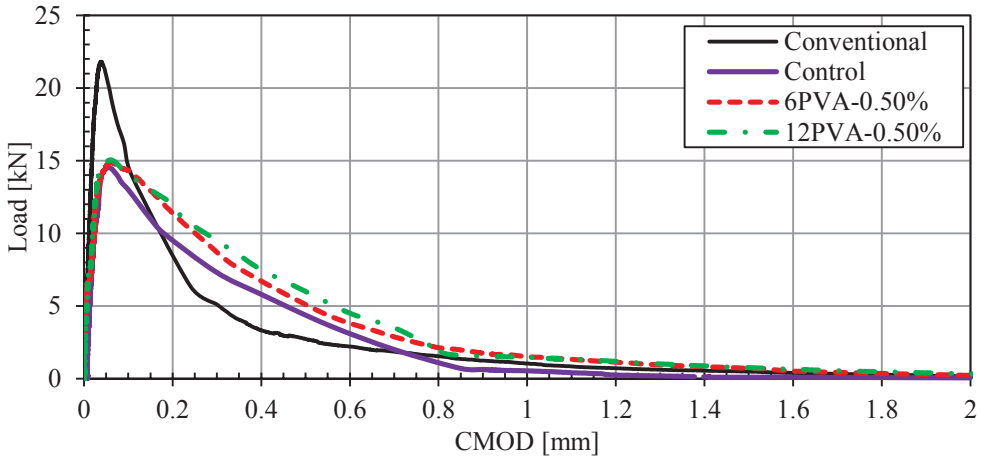

Figure 68. Load-CMOD curves of FRCs versus control

From the results of three-point bending tests over notched prisms at the age of 28 days carried out in this study, the load-crack mouth opening displacement (F-CMOD) relationship has been established (Figure 68). The tests were performed on control mix and FRCs with fibre content of 0.5%. Conventional concrete mix (avoiding FA and

fibres) is also tested to evaluate the influence of incorporating FA to the mix (Figure 69).

From these relationships, the load at the limit of proportionality (F_L) of concrete samples can be evaluated. According to the definition stated in EN 14651:2005, F_L is equal to the highest value of the load recorded up to a CMOD of 0.05 mm. Thus, concrete limit of proportionality (LOP) can be calculated using the expression given below;

$$f_{ct}^{f}L = \frac{3F_L l}{2bh_{sp}^2} \tag{15}$$

where $f_{ct}^{f}L$ is the limit of proportionality (LOP) in MPa, F_L is the load corresponding to the LOP in Newtons, b (150 mm) and l (500 mm) are the width and span length of the specimen and h_{sp} (125 mm) is the distance between the tip of the notch and the top of the specimen. All these expressions were defined assuming a linear stress distribution on the cross section.

Figure 69. Residual flexural tensile strength test

From the analysis of the F-CMOD relationship of conventional concrete (avoiding FA and fibres), the value of 21.8 kN can be characterised for F_L and LOP was calculated as 7.0 MPa using the above mentioned equation. Following the same analysis for the other three concrete series, F_L and LOP are calculated and the results presented in Table 30. F_L can be defined as the load corresponding to the first crack and limit of proportionality (LOP) is the stress at first crack (Giaccio et al. 2008).

Table 30. Limit of proportionality and residual flexural strength of control and FRCs at 28 days

Mix reference	F_L [kN]	LOP [MPa]	F_1 [kN]	$f_{R,1}$ [MPa]
Control	14.5	4.6	4.2	1.3
6PVA-0.50%	15.0	4.8	5.0	1.6
12PVA-0.50%	15.5	5.0	6.0	1.9
Conventional	21.8	7.0	2.7	0.9

From the load-CMOD curve, residual flexural tensile strength which represents the load carrying capacity at different CMODs (Figure 70) can also be calculated as;

$$f_{R,j} = \frac{3F_j l}{2bh_{sp}^2} \tag{16}$$

where $f_{R,j}$ is the residual flexural tensile strength corresponding to CMOD = $CMOD_j$ (j = 1,2,3,4) in MPa and F_j is the load corresponding to $CMOD_j$ in Newtons. The value of different CMODs are defined in Figure 70 which are; $CMOD_1$ = 0.5 mm, $CMOD_2$ = 1.5 mm, $CMOD_3$ = 2.5 mm and $CMOD_4$ = 3.5 mm.

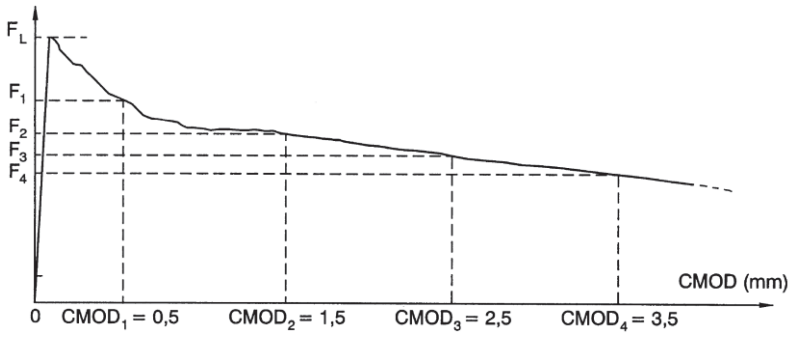

Figure 70. Typical Load-CMOD curve and definition of the reference points on the curve (EN 14651:2005)

According to the above mentioned standard, the residual flexural tensile strength values are calculated by assuming a linear elastic distribution of stresses at the fracture point.

The load-CMOD curves of all concrete mixes indicate that after the peak load, a load decay has occurred and the value of F_j corresponding to $CMOD_2$ = 1.5 mm is approximately equal to zero, which gives zero residual flexural tensile strength. The only $f_{R,j}$ which can be calculated is related to $CMOD_1$ = 0.5 mm. The results for $f_{R,1}$ of different concretes are presented in Table 30.

Based on the test results, conventional concrete shows higher F_L and limit of proportionality compared to all other mixes, while control and FRCs have approximately the same values. This can be due to the higher compressive and tensile strength of conventional concrete in comparison with the other mixes.

However, in terms of residual strength, it can be observed that control concrete and FRCs, which have 30% FA in their matrix, show a higher value of residual flexural tensile strength at $CMOD_1$ compared to the conventional concrete (avoiding FA). This observation confirms the fact that FA concretes exhibit lower load bearing capacity but larger crack mouth opening displacement and final mid-span deflection. This has been previously reported by lam et al. (Lam et al. 1998). They have indicated that an increase in FA content reduces compressive strength but improves the fracture properties.

Comparing FRCs with control, it can be concluded that the residual flexural tensile strength corresponding to crack opening of 0.5 mm improves to some extent. However, a noticeable drop in strength after the first peak is observed, which is mostly the case for synthetic fibres. This can be due to the elastomeric nature and intrinsic properties of synthetic fibres. Once concrete begins to crack, synthetic fibres require a large deformation to occur before fibres are stretched enough and begin to carry the load (Sukontasukkul et al. 2010). These results also comply with a previous study (Meddah & Bencheikh 2009) which indicates that shorter and low volumes of fibres do not significantly affect the crack initiation, crack propagation and also post peak response of concrete.

4.3.6 *Dynamic properties of materials*

From the results of the impact resonant frequency test (Figure 71), the material dynamic properties of FRCs and control concrete, including three primary characteristics; fundamental resonant frequency, dynamic modulus of elasticity and damping ratio, are calculated for transverse and longitudinal modes of vibration.

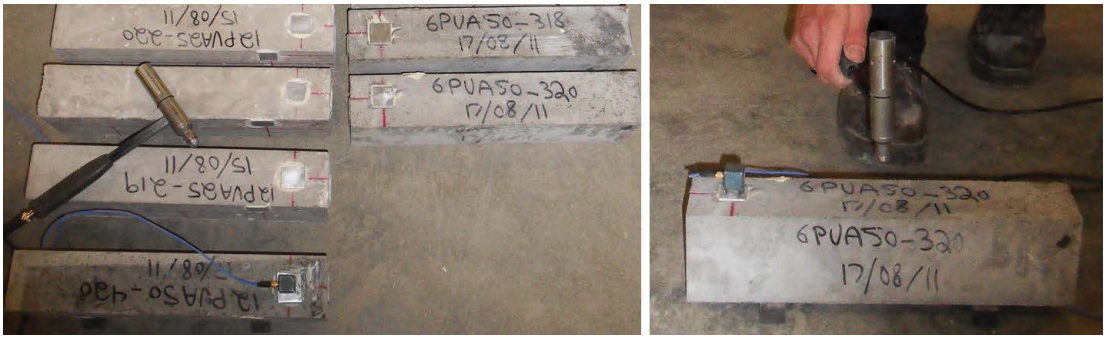

Figure 71. Impact resonant frequency test

The hammer force and acceleration response signals during the tests were recorded using a computer based data acquisition system. Data processing, including Fast Fourier Transform (FFT) and Frequency Response Function (FRF) calculations were then executed using a specifically developed MATLAB programme. From recorded dynamic response time histories, using FFT, the auto spectrum of the given signal can be obtained and the FRF can be computed.

For each mix design, 30 samples (15 for transverse and 15 for longitudinal) were gathered to calculate the damping ratio and 30 samples (15 × 2) to measure the fundamental first mode frequency in transverse and longitudinal modes. Among these number of samples, some needed filtering for more accurate calculations, since they did not show very smooth curves. This may be due to outside noises on the system or some test irregularities.

Filtering is usually performed to reduce the noise and unwanted frequencies which affect the smoothness of the signal. Frequency filters process the Fourier transformed data image in the frequency domain. This image is multiplied by the function defined as filter function and is then re-transformed into time domain. The filter used in this study is the 'Butterworth' filter in 'LABVIEW'.

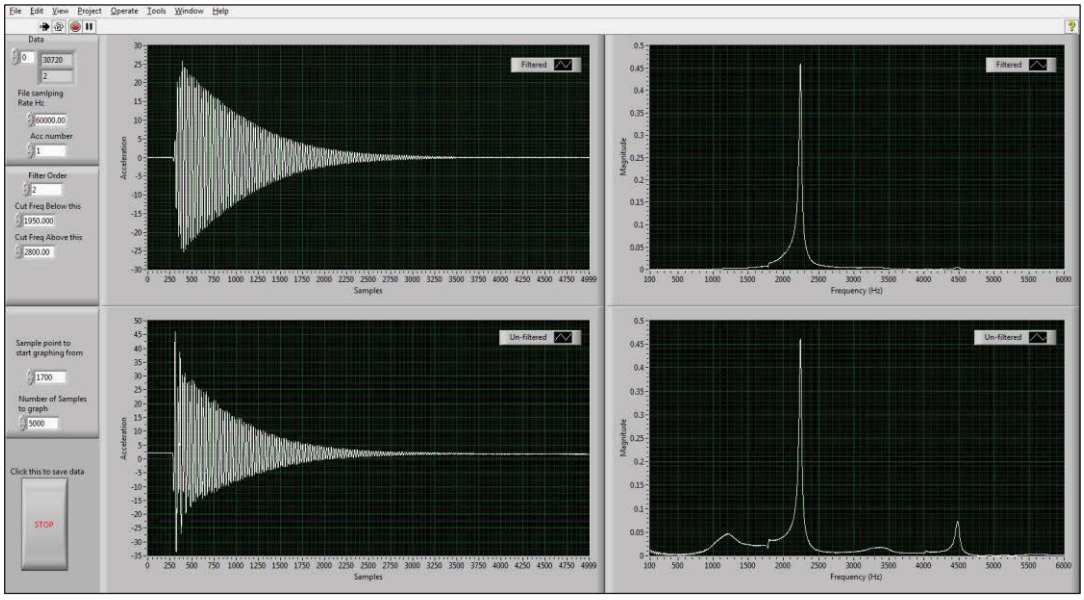

Figure 72. Sample filtered signal using 'Butterworth' filter in 'LABVIEW'

In filtering, maintaining the frequency of the first mode was of great importance as not to lose the main response of the concrete samples. An example of the filtered transverse signal data is presented in Figure 72. Two bottom images show unfiltered data whereas

top images show the filtered signals. In order to be able to read accurate data from the filtered signals, data has been transferred to an Excel file and programmed to plot the graphs for easier visualisation and readings of the data.

As mentioned earlier in section 2.6, logarithmic decrement (δ) which simply provides a measure of the rate of decay of oscillation is used to find the damping ratio (ξ), based on the assumption of viscous damping. For this reason, the acceleration-time histories for transverse and longitudinal modes are used and damping ratio (ξ) of concrete samples is calculated using Equation (17);

$$\xi = \frac{1}{2\pi m} \ln \frac{U_n}{U_{n+m}} \tag{17}$$

where U_n is the amplitude of a successive peak, U_{n+m} is the amplitude of a peak after m cycles and m is the number of cycles between the two successive positive peaks.

A sample acceleration-time history in free vibration is illustrated in Figure 73. One example of acceleration-time history for transverse and longitudinal modes of each mix design at the age of 14 and 28 days are presented in Appendix A.

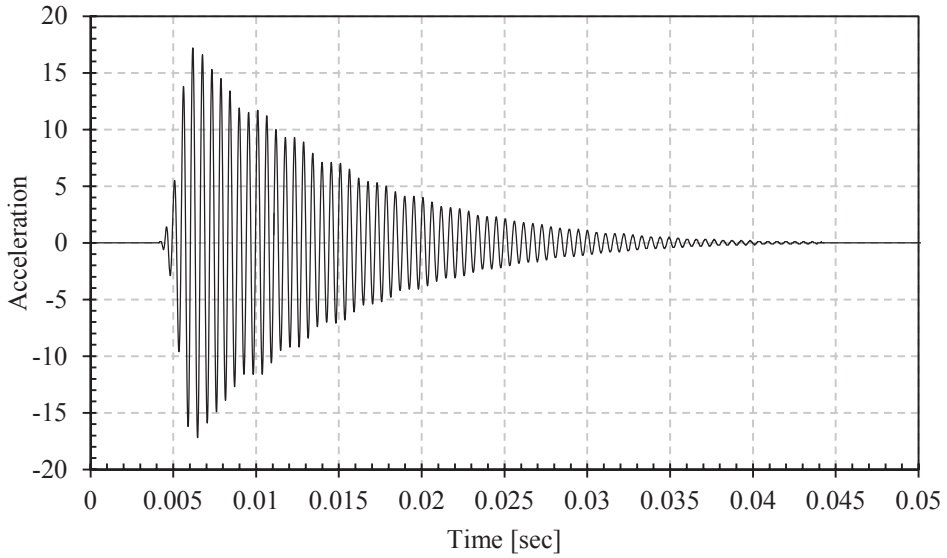

Figure 73. Sample PVA-FRC acceleration-time history

Figure 74 to Figure 77 show the damping ratio of control and FRCs in transverse and longitudinal modes of vibration at the age of 14 and 28 days. For each concrete mix design, 45 samples were measured for damping ratio. These 45 samples were calculated from the acceleration-time history of 5 hammer strikes over 3 specimens. From each

acceleration-time history, 3 damping ratios were calculated from 3 different parts of the graph, to minimise the measurement error. To follow the same procedure for calculating the damping ratios and minimising measurement errors, 'U_{n+m}' was taken as half the value of 'U_n'. In Figure 74 to Figure 77, the horizontal short dash mark, '—', indicates the average value of damping for each mix.

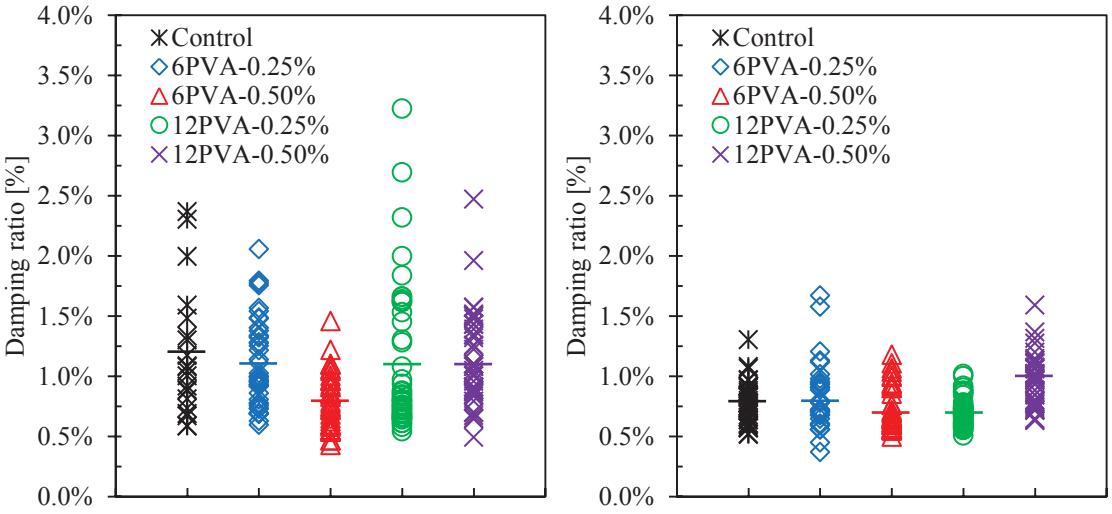

Figure 74. Damping ratio of FRCs versus control concrete in transverse mode at the age of; 14 days (left) 28 days (right)

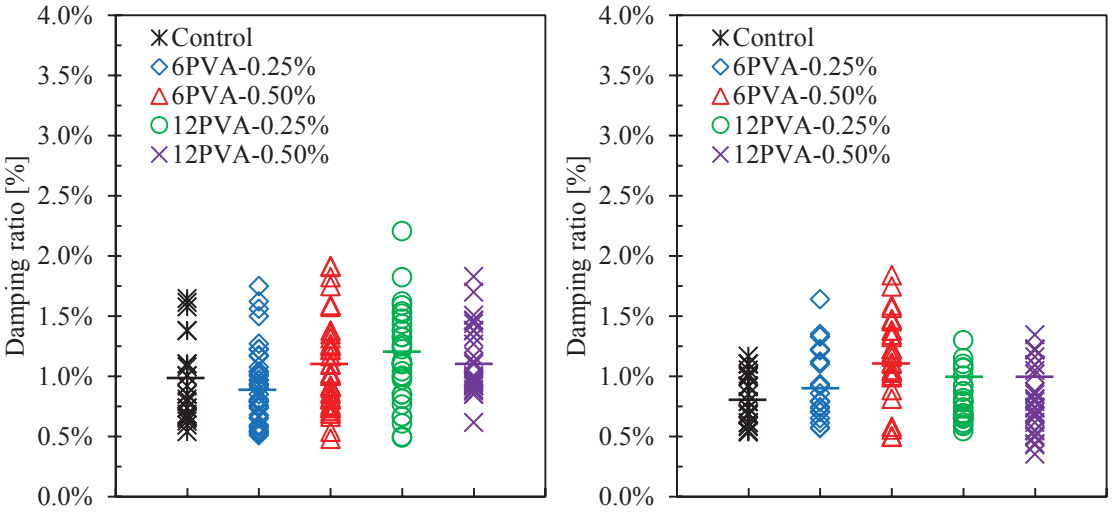

Figure 75. Damping ratio of FRCs versus control concrete in longitudinal mode at the age of; 14 days (left) 28 days (right)

It has previously been (Yan et al. 2000a) reported that concrete has damping ratios more than 0.5% of critical which can be used as a good reference point. Damping ratio of all concretes was observed to decrease with increased age which is in line with previous investigations (Amick & Monteiro 2006; Cole & Spooner 1965; Swamy & Rigby 1971;

Yan et al. 2000a). According to these results, it can be mentioned that addition of PVA fibres in low volume fraction has no significant effect on concrete damping ratio.

Comparing the results for damping ratio of conventional and control concrete in transverse and longitudinal modes, illustrated in Figure 76 and Figure 77, show that replacing 30% Portland cement with fly ash leads to a lower damping ratio of concrete for transverse mode with much larger standard deviation at 14 days of age. The damping ratios are almost the same for the longitudinal direction.

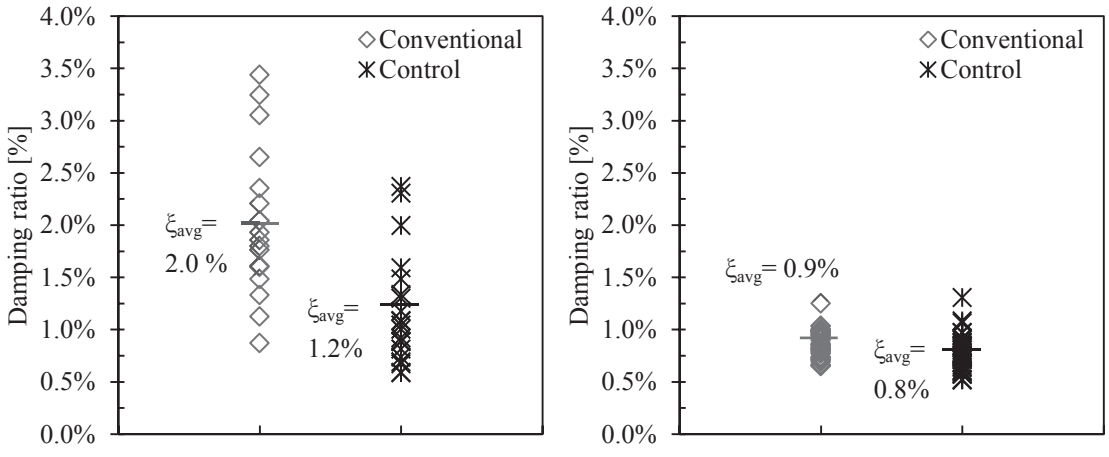

Figure 76. Damping ratio of control versus conventional concrete in transverse mode at the age of; 14 days (left) 28 days (right)

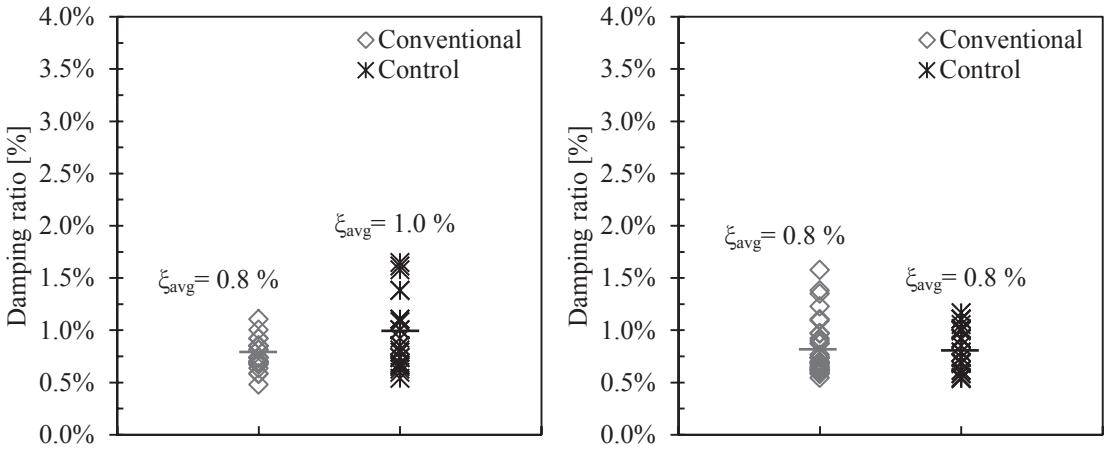

Figure 77. Damping ratio of control versus conventional concrete in longitudinal mode at the age of; 14 days (left) 28 days (right)

Dynamic modulus of elasticity of concrete samples as described earlier in section 3.6.10, are calculated from fundamental transverse (n) and longitudinal (n') frequencies using Equations (18) and (19). These frequencies can be obtained from the FRF curves.

$$DMOE_{transverve} = CMn^2 \quad (18)$$

$$DMOE_{longitudinal} = DM(n')^2 \quad (19)$$

where M is the mass of specimen in kg and C and D are factors equal to 1122.6 and 213.3, respectively (details mentioned in section 3.6.10).

Samples of transverse and longitudinal FRF for a PVA-FRC are shown in Figure 78 and Figure 79. One example of FRF frequency-magnitude curve for transverse and longitudinal modes of each mix design at the age of 14 and 28 days are presented in Appendix A.

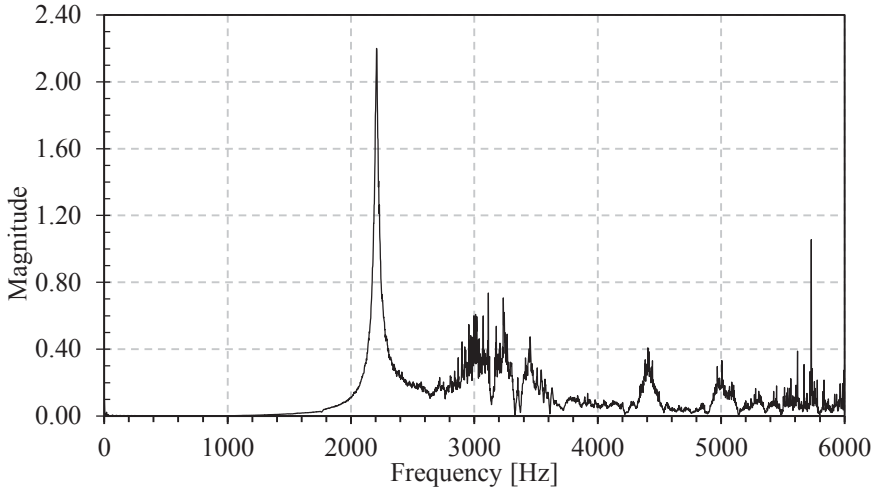

Figure 78. Sample PVA-FRC transverse Frequency Response Function (FRF)

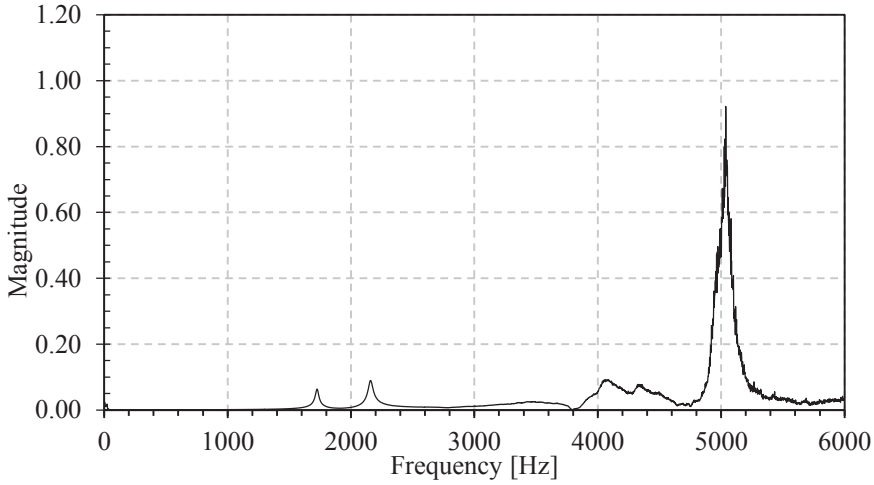

Figure 79. Sample PVA-FRC longitudinal Frequency Response Function (FRF)

The results of all above calculations for transverse and longitudinal modes of vibration are summarised in Table 31 and Table 32. Each value for damping ratio listed in the tables, is the average of 45 samples as shown in Figure 74 to Figure 77.

Table 31. Dynamic properties of control and FRCs for transverse mode

Mix Reference	Resonant frequency [Hz ± SD[1]]		Dynamic-MOE [GPa ± SD]		Damping ratio (ξ) [% ± SD]	
	14 day	28 day	14 day	28 day	14 day	28 day
Control	2206 ± 11	2245 ± 10	40.2 ± 0.4	41.5 ± 0.4	1.2 ± 0.5	0.8 ± 0.2
6PVA-0.25%	2240 ± 29	2260 ± 37	41.5 ± 1.1	42.0 ± 1.4	1.1 ± 0.4	0.8 ± 0.3
6PVA-0.50%	2210 ± 14	2240 ± 7	40.5 ± 0.5	41.5 ± 0.3	0.8 ± 0.2	0.7 ± 0.2
12PVA-0.25%	2230 ± 22	2240 ± 12	41.0 ± 0.8	41.5 ± 0.4	1.1 ± 0.6	0.7 ± 0.1
12PVA-0.50%	2190 ± 34	2220 ± 37	39.5 ± 1.3	40.5 ± 1.4	1.1 ± 0.4	1.0 ± 0.2
Conventional	2273 ± 19	2312 ± 13	42.7 ± 0.7	44.0 ± 0.5	2.0 ± 0.7	0.9 ± 0.1

[1] SD: Standard deviation

Table 32. Dynamic properties of control and FRCs for longitudinal mode

Mix Reference	Resonant frequency [Hz ± SD[1]]		Dynamic-MOE [GPa ± SD]		Damping ratio (ξ) [% ± SD]	
	14 day	28 day	14 day	28 day	14 day	28 day
Control	5056 ± 19	5096 ± 32	40.1 ± 0.3	40.7 ± 0.3	1.0 ± 0.3	0.8 ± 0.2
6PVA-0.25%	5027 ± 40	5163 ± 25	39.7 ± 0.6	41.9 ± 0.4	0.9 ± 0.3	0.9 ± 0.3
6PVA-0.50%	5039 ± 34	5034 ± 8	39.9 ± 0.5	39.8 ± 0.1	1.1 ± 0.4	1.1 ± 0.4
12PVA-0.25%	5048 ± 52	5111 ± 13	40.0 ± 0.8	41.0 ± 0.2	1.2 ± 0.4	0.8 ± 0.2
12PVA-0.50%	5016 ± 13	5054 ± 9	39.5 ± 0.2	40.1 ± 0.1	1.1 ± 0.3	0.8 ± 0.3
Conventional	5205 ± 21	5271 ± 47	42.5 ± 0.3	44.6 ± 0.4	0.8 ± 0.1	0.8 ± 0.3

[1] SD: Standard deviation

Figure 80 and Figure 81 show the resonant frequency of control and FRCs at the age of 14 and 28 days. Results show that resonant frequency of plain and fibre reinforced concrete increases by age as concrete gets stiffer with increasing age which complies with previous investigations (Hassan & Jones 2012). Furthermore, in a same fibre volume fraction for both transverse and longitudinal modes of vibration, longer fibre mostly reduces the resonant frequency of concrete slightly more than that of shorter fibre. It is also observed that for each fibre type, resonant frequency decreases with increase in fibre volume fraction which has been previously proven by other researchers (Nili & Afroughsabet 2012).

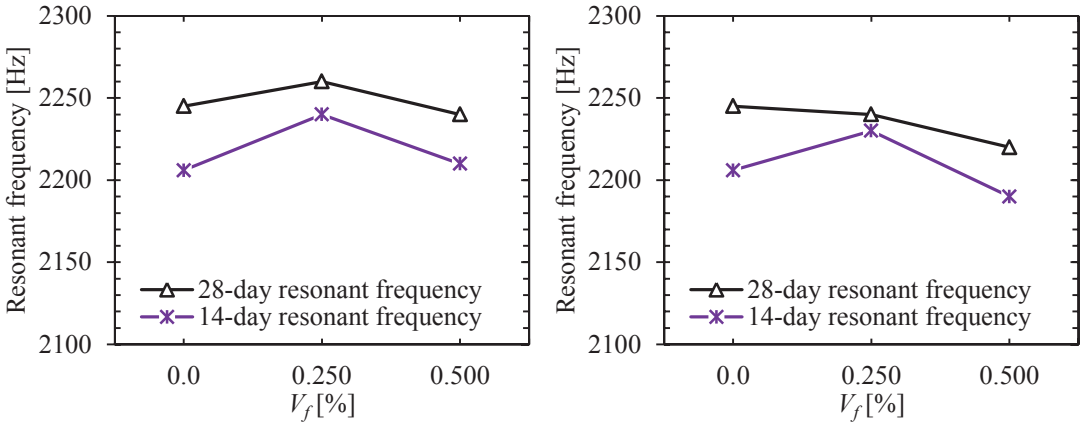

Figure 80. Transverse resonant frequency of FRCs and control at the age of 14 and 28 days; FRCs with 6 mm fibres (left) FRCs with 12 mm fibres (right)

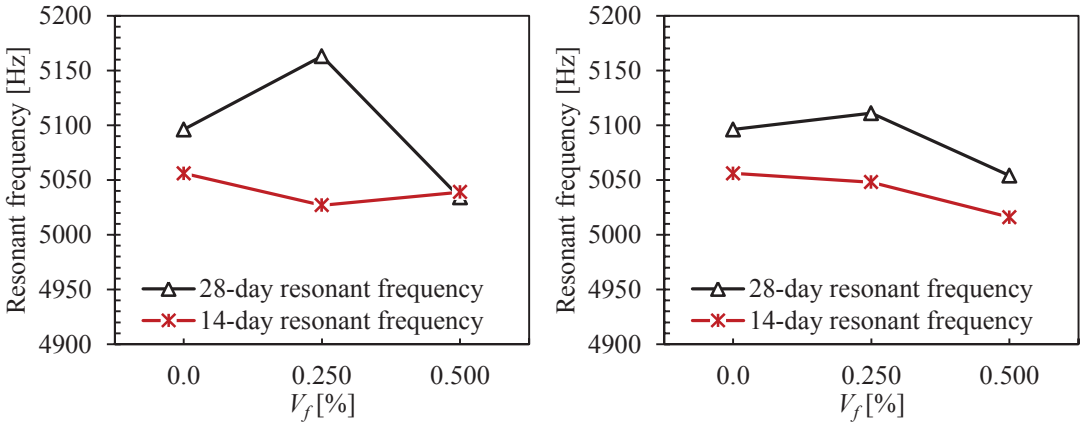

Figure 81. Longitudinal resonant frequency of FRCs and control at the age of 14 and 28 days; FRCs with 6 mm fibres (left) FRCs with 12 mm fibres (right)

By comparing the 28 day dynamic-MOE with that of static chord-MOE at the same age (Figure 82), a high level of consistency in the results can be observed. Both the static and dynamic MOE values follow the same trend, although the dynamic-MOEs are slightly higher. ASTM C 215, states that, in general, the dynamic-MOE is greater than the static-MOE, depending on the strength level of concrete. This was also previously observed by other researchers (Hassan & Jones 2012) that the dynamic MOE may be up to about 10% higher than static MOE.

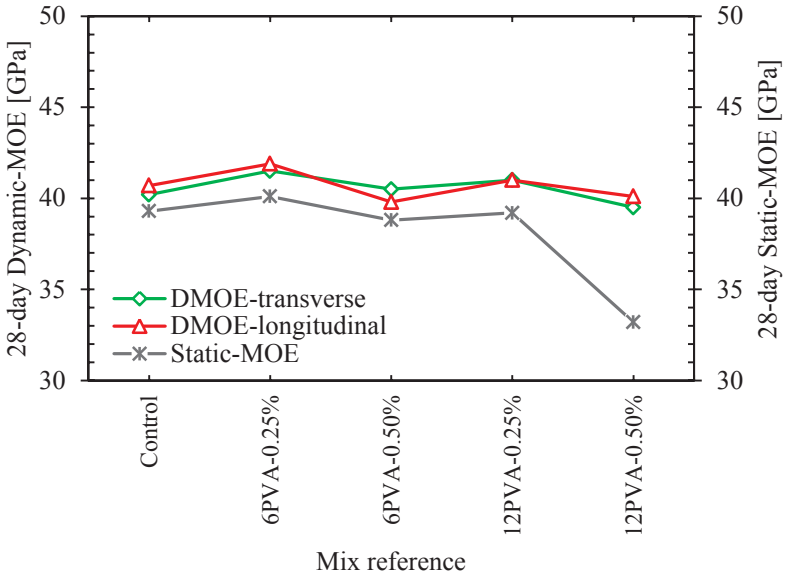

Figure 82. Dynamic MOE versus static chord MOE at the age of 28 days

4.4 Structural Properties

4.4.1 *4-point flexural test*

Although creating a perfect engineered construction material is of great achievement, it should also be applicable to structures to reap the benefits from the structural point of view, as well. Accordingly, the structural properties of RC beams incorporating polyvinyl alcohol (PVA) fibre as intrinsic reinforcement are investigated. As mentioned earlier, five RC beams made out of three different concrete mix designs and two different steel reinforcement arrangements, as detailed further in Table 33, are tested for 4-point flexure.

Table 33. Beam designations

Beam label	Reinforcement arrangement	Fibre length [mm]	V_f [%]
Control (A)	Type A	-	-
Control (B)	Type B	-	-
6PVA-0.25% (A)	Type A	6	0.25
12PVA-0.50% (A)	Type A	12	0.50
12PVA-0.50% (B)	Type B	12	0.50

The compressive strength of concrete beams were also measured at the age of 28 days and the beam test day, using cylindrical specimens. These compressive strengths, in addition to the other concrete properties measured previously in the material section, are summarised in Table 34.

Table 34. Concrete properties of RC beams

Beam label	$f_{c,28}$ [MPa]	$f_{c,test\ day}$ [MPa]	$E_{c,56}$ [GPa]	$f_{ct.f,56}$ [MPa]
Control (A)	68.0 ± 4.3	84.0 ± 6.4	41.4	7.1
Control (B)	58.0 ± 1.2	80.0 ± 3.1	41.4	7.1
6PVA-0.25% (A)	72.0 ± 2.7	85.5 ± 6.0	41.9	8.3
12PVA-0.50% (A)	61.5 ± 2.2	80.5 ± 5.1	38.7	6.6
12PVA-0.50% (B)	66.5 ± 3.9	75.0 ± 3.3	38.7	6.6

As stated before, values of the applied load and the beam deflections at each loading step were measured by means of LVDTs and results are compared. Strain gauges were also used to create a strain profile along the depth of the beam. The plane sections were assumed to remain plane. Therefore, the strain profile results could be used to determine the curvature. Strain gauges were used until their readings became unreliable due to cracking in the underlying concrete. The moment-curvature of the cross-section calculated was used for sectional analysis. Moreover, the crack propagation was monitored and recorded during the test. In addition, the impact resonance test was conducted before, during and after the flexural test.

4.4.1-a Load-deflection

From the comprehensive set of data collected, the net load-deflection curves as shown in Figure 83 and Figure 84 were calculated from the raw data captured by two load-cells mounted on loading jacks and an LVDT was placed at mid-span to measure the deflection. As shown below, the beam's deflection until the initiation of cracks increased linearly and was proportional to load. After the initial cracking, the slope of the load-deflection curve decreased although the relation still seems to be linear until the steel reinforcements' yield. From the yield point, the deflection increased nonlinearly until the ultimate load was reached.

The term ductility in seismic design is used to explain the ability of a structure to withstand large amplitude cyclic deformations in the inelastic range without a considerable strength reduction (Park 1988). Ductility factor, which is defined as the maximum deformation divided by the corresponding deformation when yielding occurs, permits the maximum deformation to be expressed in non-dimensional terms. This can be used as an index of inelastic deformation for seismic design and analysis. Ductility factor is generally known as the various response parameters related to deformations, namely displacement, rotation and curvature (Park 1988).

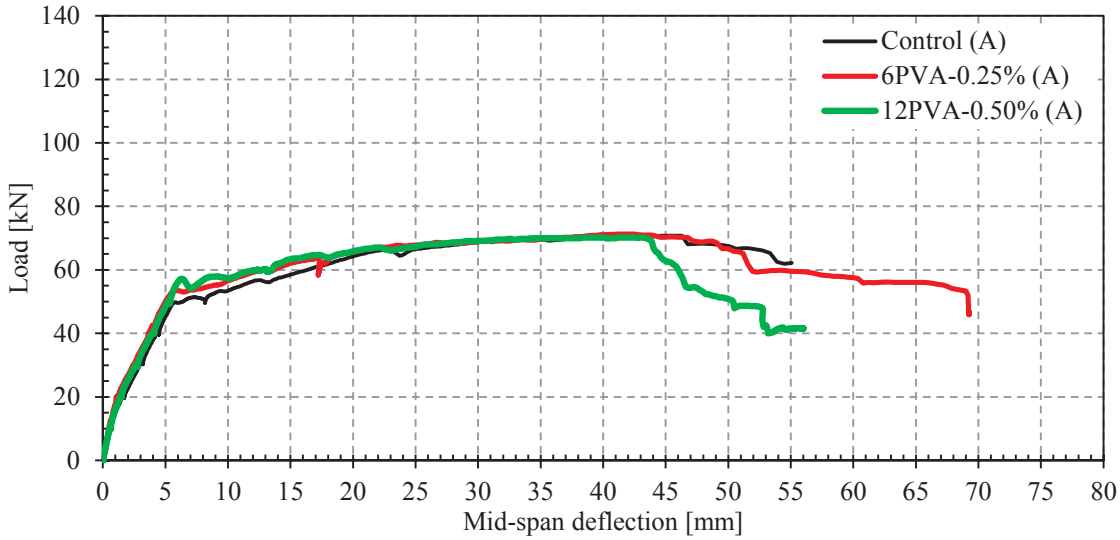

Figure 83. Load-defection curves of PVA-FRC and control beams of series A

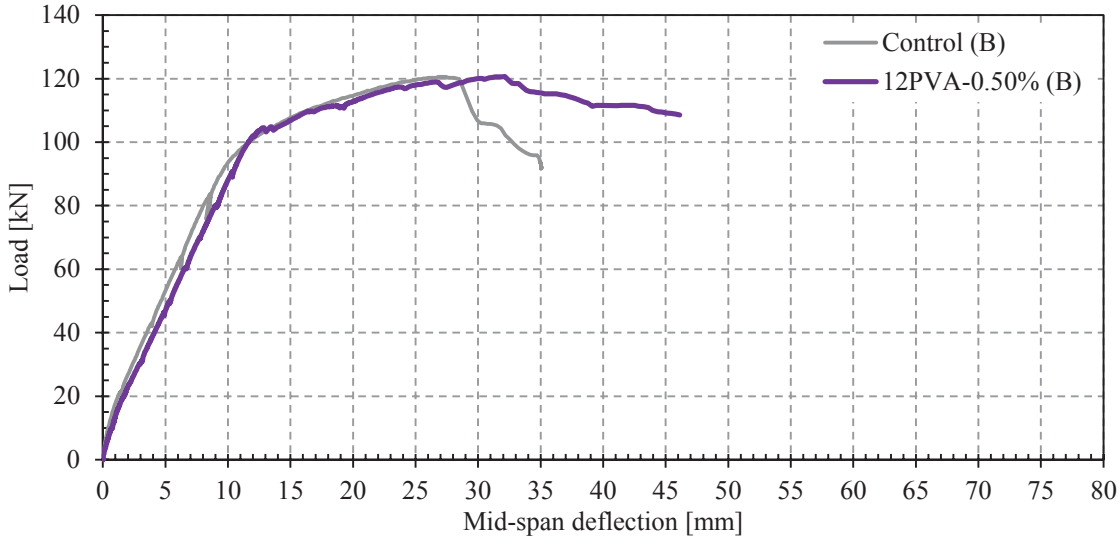

Figure 84. Load-defection curves of PVA-FRC and control beams of series B

The displacement ductility factor (μ), which is usually determined in inelastic time history dynamic analysis, may vary between 1 for elastically responding structures to as high as 7 for ductile structures. However, it is typically ranging from 3 to 6 (Park 1988). The displacement ductility factor can be calculated using below mentioned Equation;

$$\mu = \frac{\delta_u}{\delta_y} \tag{20}$$

where δ_u is the ultimate (maximum) displacement and δ_y is the yield displacement.

The definition of yield displacement often causes difficulty since the load-displacement relationship may not have a well-defined yield point. This may happen because of

several reasons such as; non-linear behaviour of materials, various moment levels needed for longitudinal bars at different depths in a reinforced concrete section to reach yield and different load levels required to form plastic hinges in different parts of a structure (Park 1988). Figure 85 demonstrates variations of definitions used by researchers to estimate the yield displacement. Figure 85.a, shows the displacement when yielding first occurs and Figure 85.b, illustrates the yield displacement of the equivalent elastoplastic system with the same elastic stiffness and ultimate load as the real system. Figure 85.c and Figure 85.d, explain the yield displacement of the equivalent elasto-plastic system with the same energy absorption as the real system and the yield displacement of the equivalent elasto-plastic system with reduced stiffness found as the secant stiffness at 75% of the ultimate load of the real system, respectively (Park 1988).

The latter definition (Figure 85.d), takes the secant stiffness as explained before, to take into account the reduction in stiffness due to cracking which happens near the end of the elastic range. This description may be considered as the most realistic definition of the yield displacement for reinforced concrete structures (Park 1988).

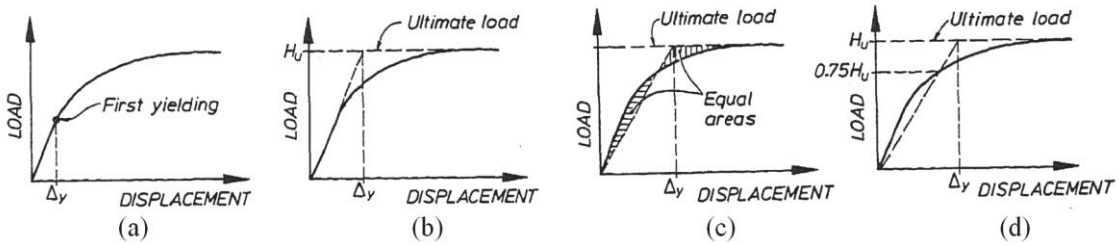

Figure 85. Alternative definitions of yield displacement (Park 1988)

The ultimate (maximum) displacement has also been estimated using divergent assumptions, some of which are shown in Figure 86. These possible estimates as explained by Park (Park 1988) involve; the displacement corresponding to a particular limiting value for the concrete compressive strain (Figure 86.a), the displacement corresponding to the peak of the load-displacement relation (Figure 86.b), the post-peak displacement when the load bearing capacity has undergone a small reduction (Figure 86.c), and the displacement when the transverse or longitudinal reinforcing steel fractures or the longitudinal compression reinforcement buckles (Figure 86.d). In order to consider the most appropriate definition, it is noteworthy to take into account the fact that most structures have some capacity to withstand deformation beyond the peak load

without considerable reduction in strength. It would be reasonable to recognise at least part of this post-peak deformation capacity. Therefore, the most accurate and realistic definition for the ultimate displacement would be the criteria shown in Figure 86.c and d (Park 1988).

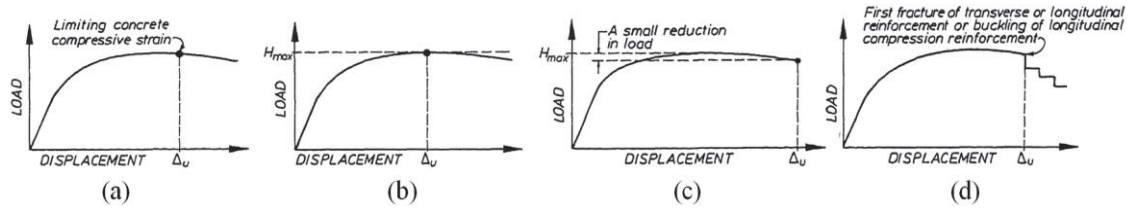

Figure 86. Alternative definitions of ultimate (maximum) displacement (Park 1988)

In order to calculate the ductility factor, displacement at yield point (δ_y) and ultimate displacement (δ_u) of all RC beams are calculated, using above mentioned definitions.

For beams of series A, having low strength longitudinal tensile reinforcement, the secant modulus at 75% ultimate load is observed not to be the best fit representing the stiffness prior to yield. It has been found that secant modulus at about 70% ultimate load provides the best achievable estimation of stiffness. Accordingly, this value (70% ultimate load) was selected for further calculations. However, in the case of series B beams including high strength longitudinal tensile reinforcement, secant modulus at 75% ultimate load was used to measure displacement at yield.

The ultimate displacement (δ_u) in this study is taken as the displacement of the beam when the load has dropped to 70% of the peak load, after reaching the peak, for series A beam and 85% for RC beams of series B.

In accordance with the above mentioned, ductility factor of all five concrete beams of series A and B were calculated as shown in Figure 87 to Figure 91.

For a RC beam, the proportionality limit is defined as the load below which the material is essentially linearly elastic. This limit is also often referred to as the elastic limit or the "first crack strength" of the composite.

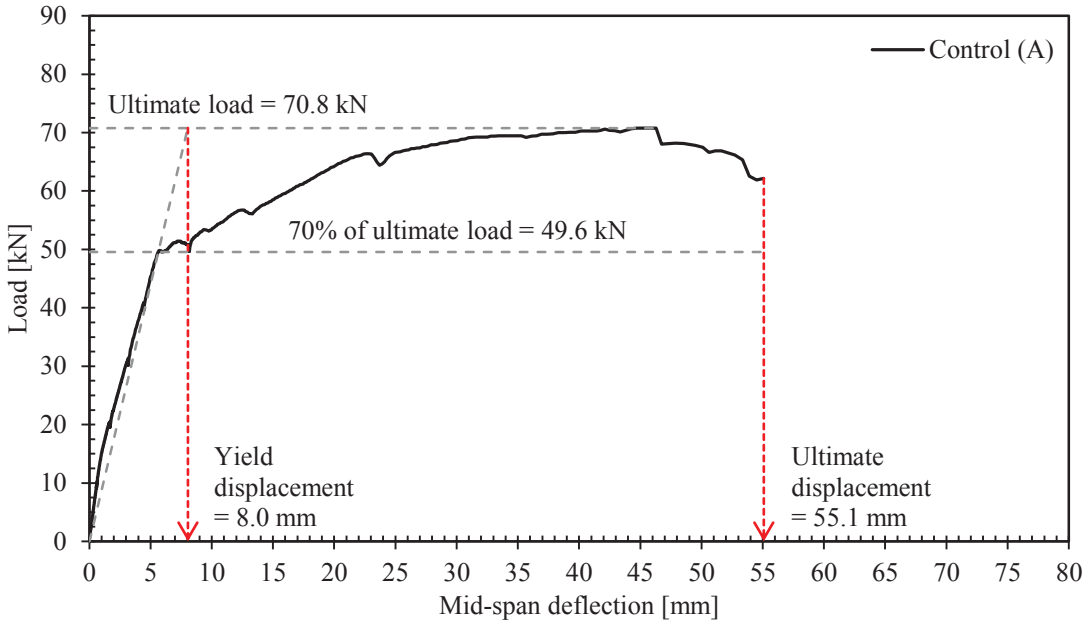

Figure 87. Equivalent yield displacement and ultimate displacement of control (A) beam

According to Figure 87, ductility of beam control (A) can be calculated as;

Yield displacement = 8.0 mm

Ultimate displacement = 55.1 mm

By means of Equation (20) ductility factor is equal to;

$$\mu = \frac{\delta_u}{\delta_y} = \frac{55.1}{8.0} = 6.9$$

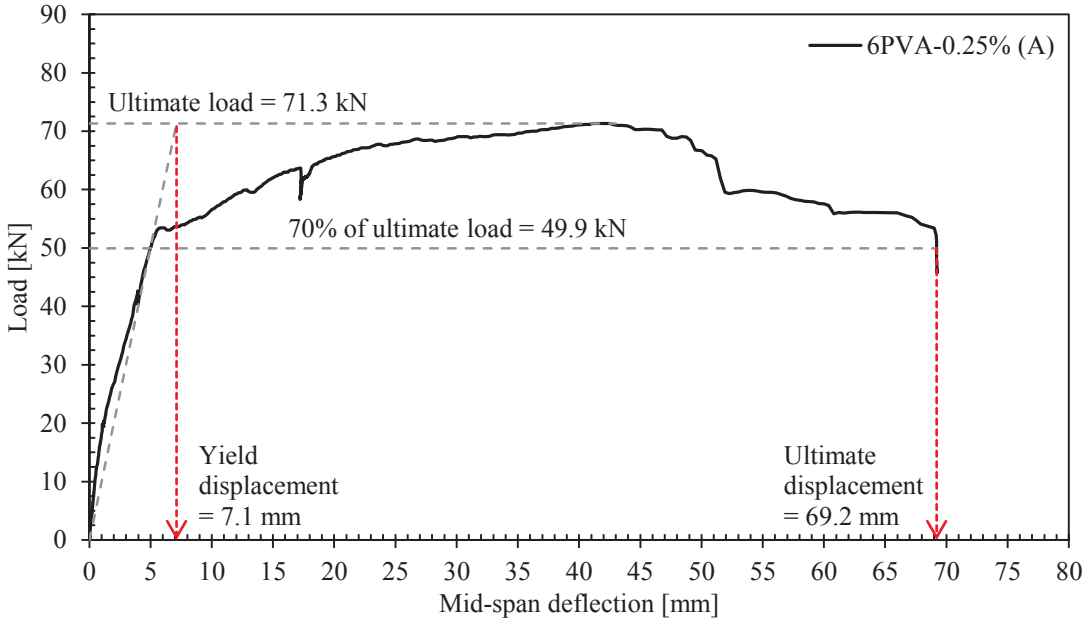

Figure 88. Equivalent yield displacement and ultimate displacement of 6PVA-0.25% (A) beam

According to Figure 88 ductility of beam 6PVA-0.25% (A) can be calculated as;

Yield displacement = 7.1 mm

Ultimate displacement = 69.2 mm

By means of Equation (20) ductility factor is equal to;

$$\mu = \frac{\delta_u}{\delta_y} = \frac{69.2}{7.1} = 9.7$$

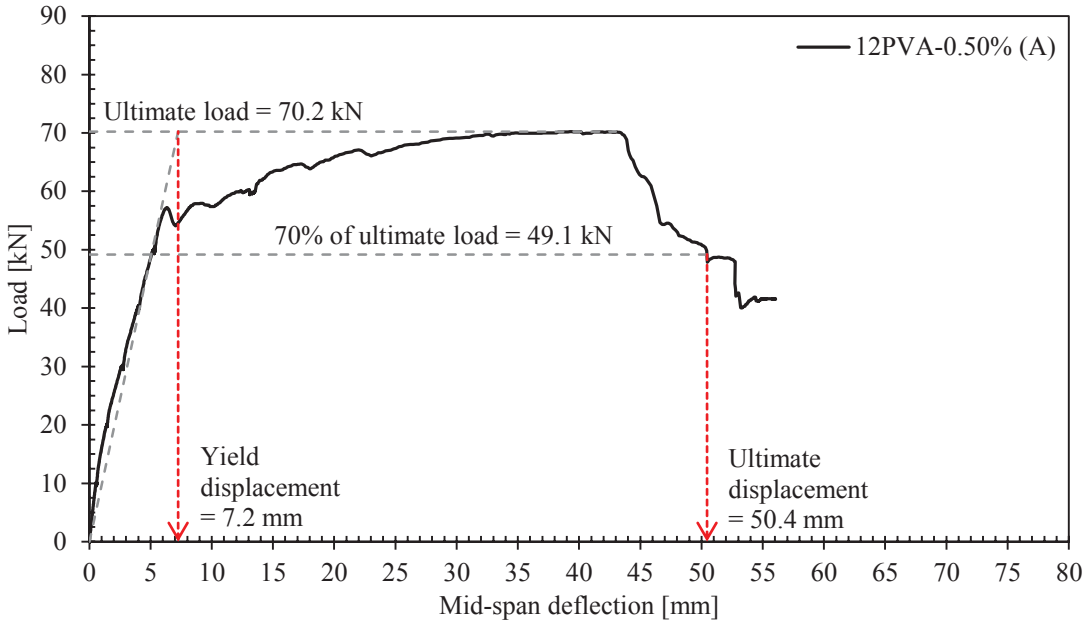

Figure 89. Equivalent yield displacement and ultimate displacement of 12PVA-0.5% (A) beam

According to Figure 89, ductility of beam 12PVA-0.50% (A) can be calculated as;

Yield displacement = 7.2 mm

Ultimate displacement = 50.4 mm

By means of Equation (20) ductility factor is equal to;

$$\mu = \frac{\delta_u}{\delta_y} = \frac{50.4}{7.2} = 7.0$$

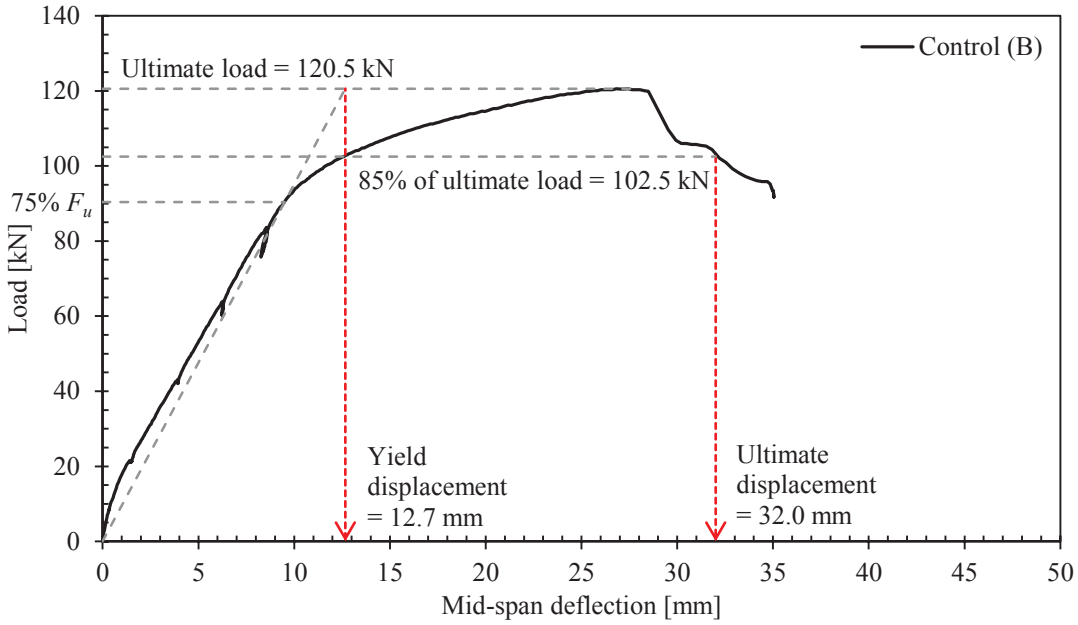

Figure 90. Equivalent yield displacement and ultimate displacement of control (B) beam

According to Figure 90, ductility of beam control (B) can be calculated as;

Yield displacement = 12.7 mm

Ultimate displacement = 32.0 mm

By means of Equation (20) ductility factor is equal to;

$$\mu = \frac{\delta_u}{\delta_y} = \frac{32.0}{12.7} = 2.5$$

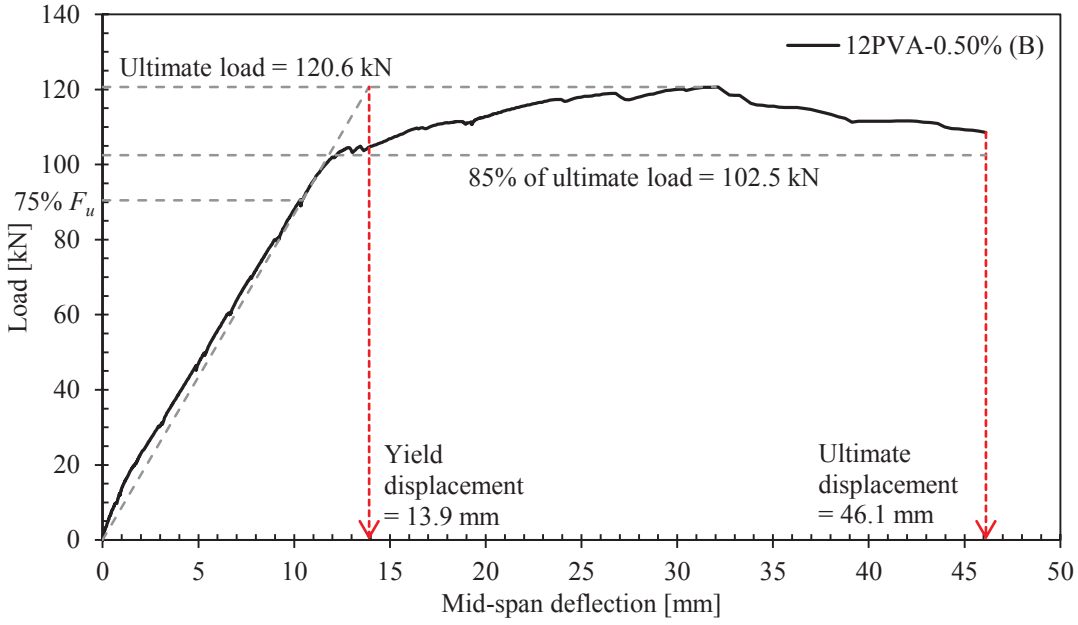

Figure 91. Equivalent yield displacement and ultimate displacement of 12PVA-0.5% (B) beam

According to Figure 91, ductility of beam 12PVA-0.50% (B) can be calculated as;

Yield displacement = 13.9 mm

Ultimate displacement = 46.1 mm

By means of Equation (20) ductility factor is equal to;

$$\mu = \frac{\delta_u}{\delta_y} = \frac{46.1}{13.9} = 3.3$$

The summary of all above calculations are presented in Table 35.

Table 35. Ductility factor of control and FRC beams

No.	Beam label	Reinforcement[1]	Fibre		f_c [2]	F_u [3]	δ_y	δ_u	μ
			L_f [mm]	V_f [%]	[MPa]	[kN]	[mm]	[mm]	
1	Control (A)	f_y = 250 MPa	-	-	84.0	70.8	8.0	55.1	6.9
2	6PVA-0.25% (A)	f_y = 250 MPa	6	0.25	85.5	71.3	7.1	69.2	9.7
3	12PVA-0.50% (A)	f_y = 250 MPa	12	0.50	80.5	70.2	7.2	50.4	7.0
4	Control (B)	f_y = 500 MPa	-	-	80.0	120.5	12.7	32.0	2.5
5	12PVA-0.50% (B)	f_y = 500 MPa	12	0.50	75.0	120.6	13.9	46.1	3.3

[1] Longitudinal tensile reinforcement
[2] Compressive strength of concrete (cylindrical samples) at test day (> 56 days)
[3] Ultimate (maximum) load applied

The results show that, amongst all concrete beams of series A, 6PVA-0.25% (A) beam ranked first in terms of ductility and post-peak behaviour. A 40% higher value of ductility factor was recorded for this beam including 0.25% volume fraction of 6 mm fibre compared to the control. However, beam number 3 having 0.50% volume fraction of 12 mm PVA fibres demonstrated almost the same ductility as control.

In concrete beams of series B, FRC beam including 0.50% volume fraction of 12 mm fibre showed approximately 30% higher ductility compared to control beam.

4.4.1-b Moment-curvature

In order to plot the strain distribution diagrams of the reinforced concrete beams, compressive and tensile strain, captured by means of several strain gauges mounted on the beam face and imbedded in concrete (details described in section 3.6.11 and in Figure 35), were used. The compressive strain used was obtained from the top strain gauge attached to the concrete face at mid-span (SG-C.3) while the tensile strain was partially obtained from the bottom strain gauge attached to the concrete face (SG-C.1) and the strain gauge attached to the steel bar, both at mid-spans (SG-S.1). The readings of SG-C.1 was only used up to the point where the first crack happens and for the rest

the reading of SG-S.1 was used. In some cases, since the readings of SG-C.1 seemed to be inaccurate, all tensile strains were obtained from SG-S.1.

The strain profile for concrete beams of series A and B are shown in Figure 94 and Figure 96. If the readings of any strain gauge appeared to be inaccurate at a load level close to the beam failure, due to the strain gauge damage or other reasons, the strain diagram is only plotted up to the load stage where reasonable readings for strain gauges were obtained.

To evaluate the flexural behaviour of reinforced concrete beams under loading and to analyse their non-linear behaviour, the moment-curvature relationship can be used. Using this structural characteristic, the non-linear analysis of RC beams can be conducted because most of the deformation in beams arise from the strains associated with flexure (Kwak & Kim 2002). Studying the non-linear behaviour of a structural element ,e.g. an RC beam, can help to find the non-linear behaviour of a structure since any structure is composed of several structural elements (Kwak & Kim 2002).

Curvature (κ or Ø), a measure of local bending deformation, is the rotation per unit length ($\delta\theta/\delta x$). This value, as shown in Figure 92, can be obtained either by inverse of the radius of curvature measured at the neutral axis ($\kappa=1/R$) or from the slope (gradient) of the strain profile (Warner et al. 2007).

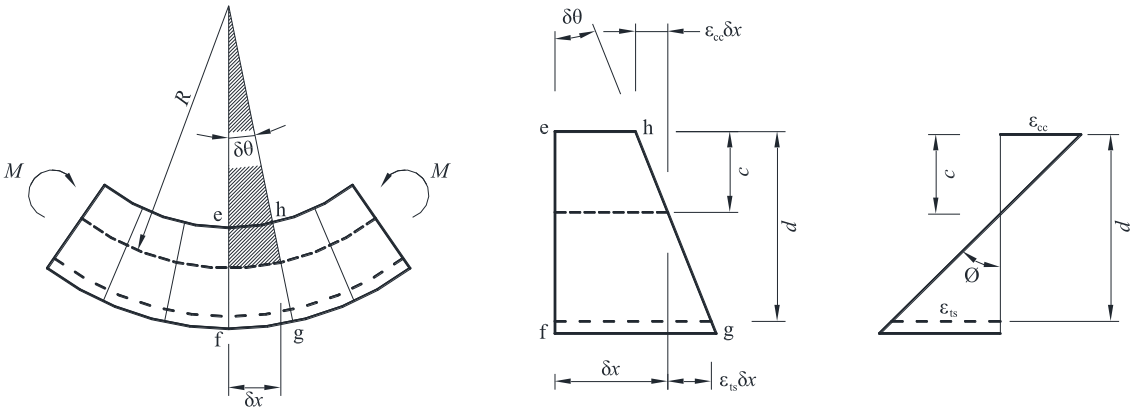

Figure 92. flexural deformation and curvature (Warner et al. 2007)

$$\kappa = \emptyset = \frac{\delta\theta}{\delta x} = \frac{1}{R} = \frac{\varepsilon_{cc} + \varepsilon_{ts}}{d} \tag{21}$$

The moment and curvature calculations for concrete beams of series A and B are summarised in Table 36 to Table 40. These values are calculated for loading levels starting from 5 kN up to the failure with 5kN increments in applied load.

Table 36. Moment and curvature calculations for beam control (A)

Load [kN]	Moment [kN.m]	Strain in compression (SG-C.3[1]) [×10^6]	Strain in tension (SG-S.1[1]) [×10^6]	Curvature [1/m]
0	0.0	0.0	0.0	0.0000
5	1.5	34.0	-93.3	0.0003
10	3.0	64.4	-183.3	0.0007
15	4.5	98.8	-275.9	0.0010
20	6.0	140.2	-603.8	0.0027
25	7.5	178.4	-928.4	0.0044
30	9.0	217.4	-1237.4	0.0060
35	10.5	260.8	-1633.9	0.0081
40	12.0	299.4	-1999.4	0.0100
45	13.5	340.8	-2427.2	0.0123
50	15.0	384.2	-3217.5	0.0167
55	16.5	426.8	-4117.6	0.0217
60	18.0	471.4	-5038.6	0.0269
65	19.5	512.6	-6037.6	0.0325

[1] Refer to Figure 35 for more details on Strain gauge labelling and locations

Table 37. Moment and curvature calculations for beam 6PVA0.25% (A)

Load [kN]	Moment [kN.m]	Strain in compression (SG-C.3[1]) [×10^6]	Strain in tension (SG-S.1[1]) [×10^6]	Curvature [1/m]
0	0.0	0.0	0.0	0.0000
5	1.5	4.7	-66.6	0.0003
10	3.0	63.0	-187.4	0.0007
15	4.5	101.3	-276.4	0.0010
20	6.0	148.5	-634.2	0.0029
25	7.5	245.4	-1042.3	0.0047
30	9.0	304.3	-1481.2	0.0069
35	10.5	364.5	-1852.0	0.0088
40	12.0	419.4	-2273.9	0.0109
45	13.5	477.9	-2663.6	0.0129
50	15.0	538.3	-3725.8	0.0188
55	16.5	591.2	-4906.6	0.0254
60	18.0	670.7	-6234.3	0.0327
65	19.5	731.8	-7785.0	0.0415

Table 38. Moment and curvature calculations for beam 12PVA0.50% (A)

Load [kN]	Moment [kN.m]	Strain in compression (SG-C.3[1]) [×10^6]	Strain in tension (SG-S.1[1]) [×10^6]	Curvature [1/m]
0	0.0	0.0	0.0	0.0000
5	1.5	40.4	-103.8	0.0004
10	3.0	74.4	-201.8	0.0007
15	4.5	121.3	-300.5	0.0011
20	6.0	184.4	-627.9	0.0026
25	7.5	248.2	-956.5	0.0042
30	9.0	310.3	-1297.4	0.0058
35	10.5	364.9	-1595.9	0.0072
40	12.0	411.9	-1923.0	0.0089
45	13.5	464.2	-2300.2	0.0108
50	15.0	515.4	-3199.6	0.0158
55	16.5	569.4	-4309.4	0.0220
60	18.0	620.4	-5720.4	0.0300
65	19.5	673.2	-7173.2	0.0382

Table 39. Moment and curvature calculations for beam Control (B)

Load [kN]	Moment [kN.m]	Strain in compression (SG-C.3[1]) [×10^6]	Strain in tension (SG-S.1[1]) [×10^6]	Curvature [1/m]
0	0.0	0.0	0.0	0.0000
5	1.5	38.9	-97.4	0.0003
10	3.0	87.2	-204.7	0.0007
15	4.5	158.6	-333.7	0.0010
20	6.0	224.6	-761.4	0.0032
25	7.5	285.9	-1135.9	0.0050
30	9.0	347.2	-1440.1	0.0064
35	10.5	404.5	-1777.6	0.0081
40	12.0	460.7	-2160.7	0.0100
45	13.5	518.6	-2514.3	0.0117
50	15.0	579.7	-2897.9	0.0136
55	16.5	637.7	-3309.1	0.0157
60	18.0	701.6	-3701.6	0.0176
65	19.5	755.5	-4037.7	0.0193
70	21.0	813.0	-4383.0	0.0210
75	22.5	876.0	-4701.0	0.0225
80	24.0	937.0	-5017.0	0.0240
85	25.5	1013.7	-5348.7	0.0255
90	27.0	1087.4	-6487.4	0.0318
95	28.5	1178.4	-7638.4	0.0380
100	30.0	1326.0	-8717.3	0.0435

Table 40. Moment and curvature calculations for beam 12PVA0.50% (B)

Load [kN]	Moment [kN.m]	Strain in compression (SG-C.3[1]) [×10^6]	Strain in tension (SG-S.1[1]) [×10^6]	Curvature [1/m]
0	0.0	0.0	0.0	0.0000
5	1.5	26.3	-87.6	0.0004
10	3.0	54.9	-178.1	0.0007
15	4.5	85.7	-269.1	0.0011
20	6.0	117.9	-363.7	0.0014
25	7.5	156.8	-794.3	0.0038
30	9.0	204.5	-1224.5	0.0060
35	10.5	251.3	-1679.3	0.0084
40	12.0	290.7	-2064.6	0.0104
45	13.5	331.2	-2417.6	0.0123
50	15.0	371.9	-2800.5	0.0143
55	16.5	410.2	-3215.2	0.0165
60	18.0	447.8	-3602.5	0.0186
65	19.5	490.7	-4017.3	0.0207
70	21.0	533.9	-4414.3	0.0228
75	22.5	581.9	-4785.2	0.0247
80	24.0	627.8	-5161.2	0.0267
85	25.5	670.3	-5541.1	0.0287
90	27.0	712.3	-7087.3	0.0375
95	28.5	757.8	-8448.3	0.0452
100	30.0	803.3	-10076.1	0.0545

The moment-curvature relationships and strain distribution profiles of concrete beams of series A and B are illustrated in Figure 93 to Figure 96.

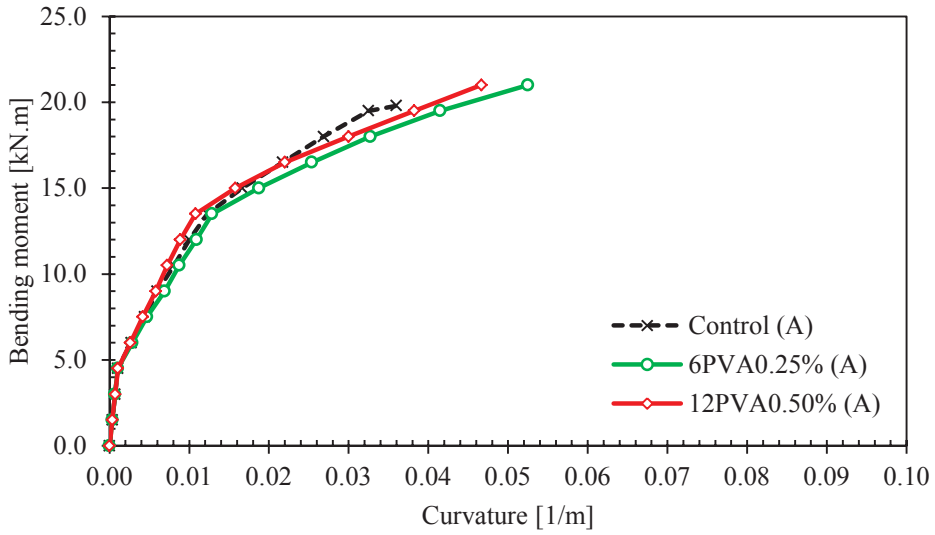

Figure 93. Moment-curvature relationship of concrete beams of series A

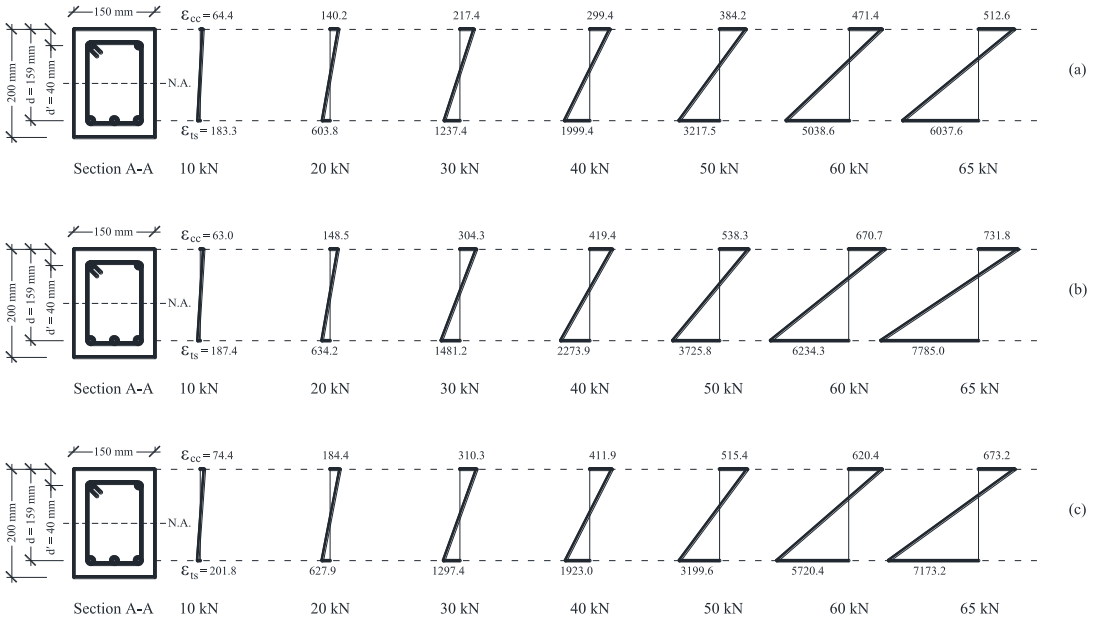

Figure 94. Strain diagrams of concrete beams of series A at different loading stages (a) Control (A), (b) 6PVA0.25% (A) and (c) 12PVA0.50% (A)

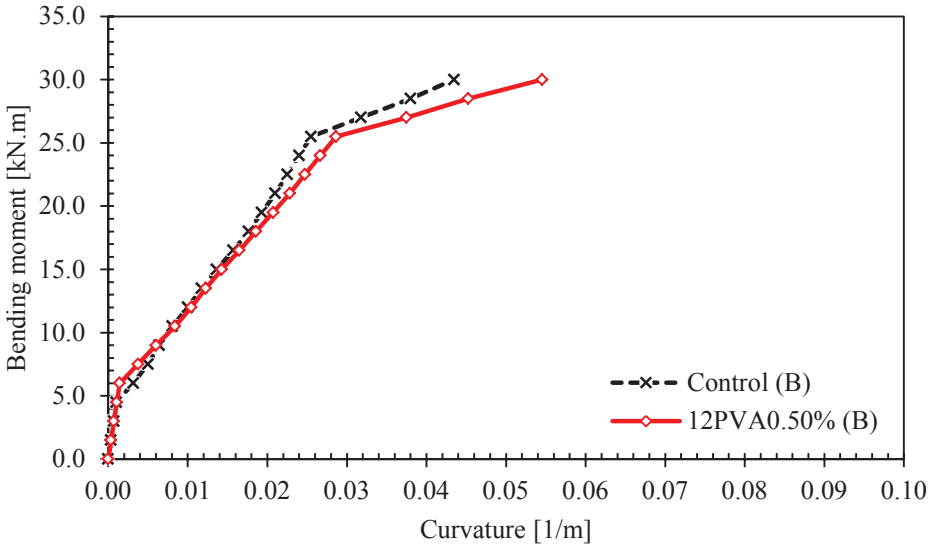

Figure 95. Moment-curvature relationship of concrete beams of series B

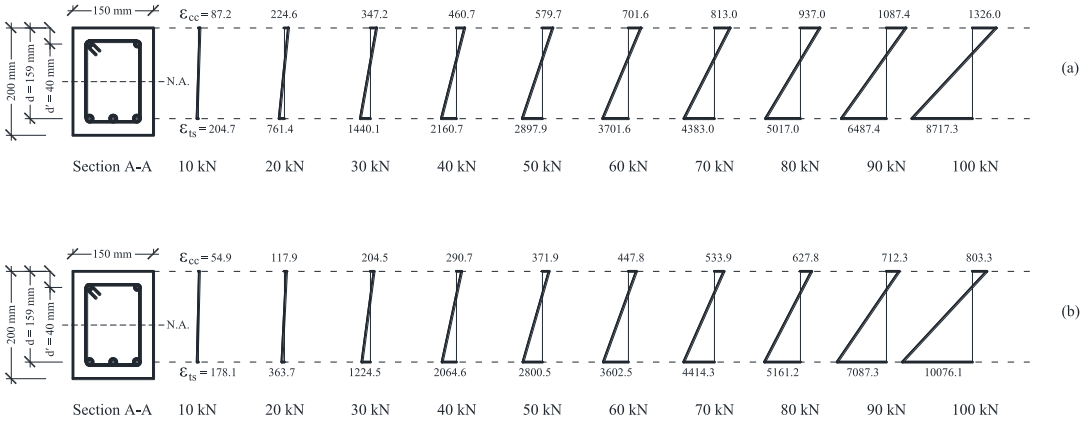

Figure 96. Strain diagrams of concrete beams of series B at different loading stages (a) Control (B) and (b) 12PVA0.50% (B)

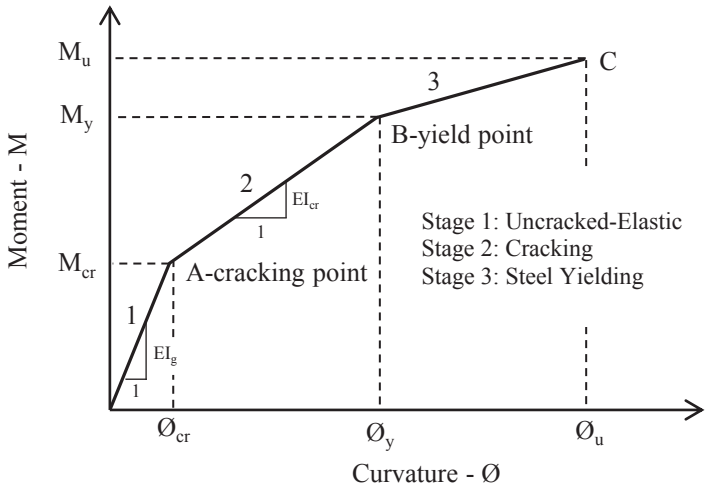

Figure 97. Idealized moment-curvature relationship of RC section (Kwak & Kim 2002)

The typical moment-curvature relation of an RC section can be idealized as shown in Figure 97. The first stage is related to the uncracked-elastic range of behaviour. At the end of this stage (point A) the flexural tension cracking will occur. The first crack happens when the stress in the extreme tension fibre equals to the concrete modulus of rupture ($f_{ct.f}$) (Wight & MacGregor 2011). Within this stage and up to the point A, the moment-curvature relationship is linear and concrete behaves elastically. The moment and curvature at cracking can be calculated directly from the elastic flexural theory (Wight & MacGregor 2011) as shown in Equations (22) to (24).

$$I_g = \frac{bh^3}{12} + (n-1)A_{st}(d-c)^2 + (n-1)A_{sc}(c-d')^2 \tag{22}$$

$$M_{cr} = \frac{f'_{ct.f} I_g}{(h-c)} \tag{23}$$

$$\emptyset_{cr} = \frac{M_{cr}}{E_c I_g} \tag{24}$$

where I_g is the second moment of area of the uncracked cross-section in mm^4, M_{cr} is the cracking moment in N.mm, $\emptyset_{cr}$ is the curvature corresponding to the cracking moment (M_{cr}) in 1/mm, $n=E_s/E_c$ is the modular ratio, b and h are the width and height of the cross-section, respectively, in mm, d is the effective depth of the cross-section in mm, d' is the distance from the extreme compressive fibre to the centroid of the compression steels in mm, c is the distance from the extreme compression fibre to the neutral axis in

mm, A_{st} and A_{sc} are the areas of tension and compression steels, respectively, in mm^2, $f'_{ct,f}$ is the concrete characteristic modulus of rupture in MPa and E_c is the concrete modulus of elasticity in MPa.

In stage 2 (cracking) and after the cracking point (point A), as the moment applied to the section continuous to increase, the tensile stress in the reinforcement and compression stress in the concrete compression zone will steadily increase. Finally, either the steel or the concrete will reach its capacity and start to yield (in case of steel) or crush (in case of concrete). Since the section considered here is assumed to be the ideal case which is under-reinforced, the steel will yield before the concrete crushes and reaches its maximum usable strain. This point (point B) which represents the end of the elastic range of behaviour is called the yield point.

In order to calculate the moment and curvature values for the yield point, the tension at tension reinforcement is set equal to the steel yield strain;

$$\varepsilon_{sy} = \frac{f_{sy}}{E_s} \tag{25}$$

At this stage of flexural behaviour, the concrete in tension can be disregarded since its contribution is not significant for section equilibrium. When the section equilibrium is established, the neutral axis and the section moment called the yield moment (M_y) can then be determined. The moment of inertia of the cracked section (I_{cr}) and the yield curvature ($\emptyset_y$) which is the slope of the strain profile can also be calculated as below;

$$I_{cr} = \frac{bc^3}{3} + (n-1)A_{st}(d-c)^2 + (n-1)A_{sc}(c-d')^2 \tag{26}$$

$$\emptyset_y = \frac{\varepsilon_{sy}}{d-c} \tag{27}$$

The stage 3 of the moment-curvature is related to the limit of useful strain in the concrete. After the yield point and where the steel yields, a large increase in curvature happens and the moment rises slowly to a maximum and then decreases.

The gradient of the moment-curvature curve represents the elastic bending stiffness (EI) which includes all the section characteristics in a typical loading condition (Kwak &

Kim 2002). Accordingly, the elastic bending stiffness of uncracked (EI_g) and cracked (EI_{cr}) sections can be calculated following Equation (29) and (30).

$$EI = \frac{\Delta M}{\Delta \emptyset} \tag{28}$$

$$EI_g = \frac{M_{cr}}{\emptyset_{cr}} \tag{29}$$

$$EI_{cr} = \frac{M_y - M_{cr}}{\emptyset_y - \emptyset_{cr}} \tag{30}$$

According to the theory explained above, the properties of uncracked and cracked sections of the control and FRC beams were calculated.

Uncracked Section

For the uncracked section, by using the transformed section method (Figure 98) the location of section neutral axis can be calculated as shown in Table 41.

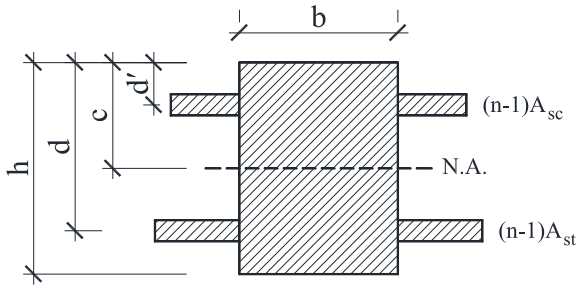

Figure 98. Uncracked transformed section of RC beam

$$c = \frac{1}{2} \times \frac{bh^2 + 2(n-1)A_{st}d + 2(n-1)A_{sc}d'}{bh + (n-1)A_{st} + (n-1)A_{sc}} \tag{31}$$

Table 41. Neutral axis calculation for uncracked section of RC beams

Beam label	b [mm]	h [mm]	d [mm]	d′ [mm]	A_{st} [mm^2]	A_{sc} [mm^2]	E_s [GPa]	E_c [GPa]	n	c [mm]
Control (A)	150	200	159	40	226	157	200	41.4	4.8	100.48
Control (B)	150	200	159	40	226	157	200	41.4	4.8	100.48
6PVA-0.25% (A)	150	200	159	40	226	157	200	41.9	4.8	100.47
12PVA-0.50% (A)	150	200	159	40	226	157	200	38.7	5.2	100.52
12PVA-0.50% (B)	150	200	159	40	226	157	200	38.7	5.2	100.52

Thereafter, by using the Equations (22) to (24) and (29), the EI_g, M_{cr} and $\emptyset_{cr}$ can be calculated. These values are summarised in Table 44.

The concrete characteristic flexural tensile strength or modulus of rupture ($f'_{ct.f}$) can be obtained from the below equation (AS3600 - 2009, clause 3.1.1.2);

$$f'_{ct.f} = 0.6\sqrt{f'_c} \tag{32}$$

According to the Australian Standard; AS 3600 (2009), characteristic compressive strength (f'_c) which is the value of the concrete strength exceeded by 95% of the concrete samples (assessed by standard test), can be calculated using Equation (33);

$$f'_c = f_{cm} - k.SD \tag{33}$$

Where f_{cm} is the mean value of the samples compressive strength, k is the acceptance constant depending on the number of samples, but in all cases at least 1.645, and *SD* is the standard deviation. The characteristic compressive strength of all concrete beams are presented in Table 42.

Table 42. Characteristic compressive and flexural tensile strength of RC beams

Beam label	$f_{c.28}$ [MPa]	*SD* [MPa]	f'_c [MPa]	$f'_{ct.f}$ [MPa]
Control (A)	68.0	4.3	60.9	4.7
Control (B)	58.0	1.2	56.0	4.5
6PVA-0.25% (A)	72.0	2.7	67.6	4.9
12PVA-0.50% (A)	61.5	2.2	57.9	4.6
12PVA-0.50% (B)	66.5	3.9	60.1	4.7

* k is taken as equal to 1.645 in all cases

Cracked Section

For the cracked section, again by using the transformed section method (Figure 99) the location of section neutral axis can be calculated as shown in Table 43.

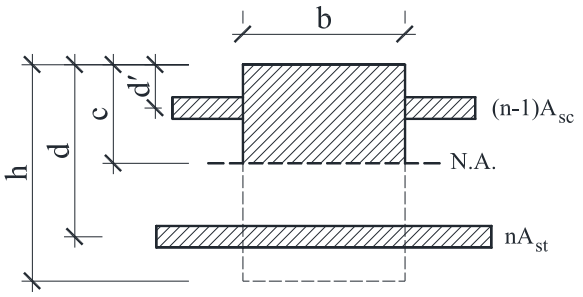

Figure 99. Cracked transformed section of RC beam

$$c = \frac{\sqrt{[(n-1)A_{sc} + nA_{st}]^2 + 2b[(n-1)A_{sc}d' + nA_{st}d]} - [(n-1)A_{sc} + nA_{st}]}{b}$$

In order to determine the modular ratio (n) of the cracked section, the concrete secant modulus of elasticity ($E_{c.sec}$) should be used instead of the initial modulus of elasticity (E_{ci} or E_c). The concrete secant modulus of elasticity from the origin to the peak compressive stress (Figure 100) can be calculated using the relation suggested in CEB-FIP Model Code 90, clause 2.1.4.4.1 (Béton 1993) as shown in Equation (34).

$$E_{c.sec} = \frac{f_{cm}}{0.0022} \tag{34}$$

where $E_{c.sec}$ is the concrete secant modulus of elasticity in MPa and f_{cm} is concrete compressive strength (the peak value of the concrete compressive stress shown in Figure 100) in MPa.

In this relation, the value of 0.0022 is the concrete strain corresponding to the peak compressive stress (f_{cm}).

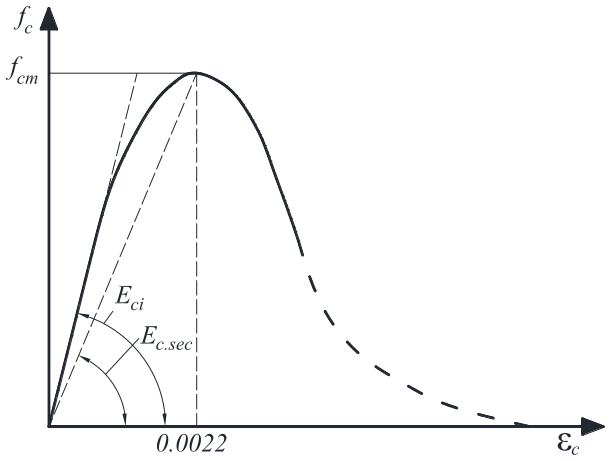

Figure 100. Concrete stress-strain diagram for uniaxial compression (Béton 1993)

Table 43. Neutral axis calculation for cracked section of RC beams

Beam label	b [mm]	h [mm]	d [mm]	d′ [mm]	A_{st} [mm^2]	A_{sc} [mm^2]	E_s [GPa]	$E_{c.sec}$ [GPa]	n	c [mm]
Control (A)	150	200	159	40	226	157	200	30.9	6.5	46.2
Control (B)	150	200	159	40	226	157	200	26.3	7.6	48.9
6PVA-0.25% (A)	150	200	159	40	226	157	200	32.7	6.1	45.2
12PVA-0.50% (A)	150	200	159	40	226	157	200	28.0	7.2	47.9
12PVA-0.50% (B)	150	200	159	40	226	157	200	30.2	6.6	46.6

Thereafter, by using the Equations (27) and (30), the EI_{cr} and $Ø_{cr}$ can be calculated. M_y is also calculated using the cracked section properties. These values are summarised in Table 44.

Table 44. Analytical uncracked and cracked section properties of RC beams

Beam label	$Ø_{cr}$ [1/m]	M_{cr} [kN.m]	$Ø_y$ [1/m]	M_y [kN.m]	EI_g [kN.m^2]	EI_{cr}
Control (A)	0.0011	4.95	0.0129	12.13	4354	613
Control (B)	0.0011	4.74	0.0268	25.23	4354	797
6PVA-0.25% (A)	0.0012	5.21	0.0127	12.02	4403	590
12PVA-0.50% (A)	0.0012	4.85	0.0131	12.31	4088	629
12PVA-0.50% (B)	0.0012	4.94	0.0262	24.77	4088	792

Comparing the analytical results calculated for uncracked and cracked section (Table 44) with moment-curvature relations from the experimental tests (Figure 93 and Figure 95) shows approximately the same values for M_{cr} and M_y. Furthermore, the same value and trend for stiffness change in beam elements of series A and B could be observed.

Results show that for concrete beams of series B, in both uncracked and cracked sections, the beams including PVA fibres show slightly lower stiffness. However, in beam elements of series A, the beam incorporating 6 mm PVA fibre shows marginally higher stiffness for uncracked section. In terms of cracked section, a higher value of stiffness was recorded for beam 12PVA-0.50% (A) made with 12 mm fibres.

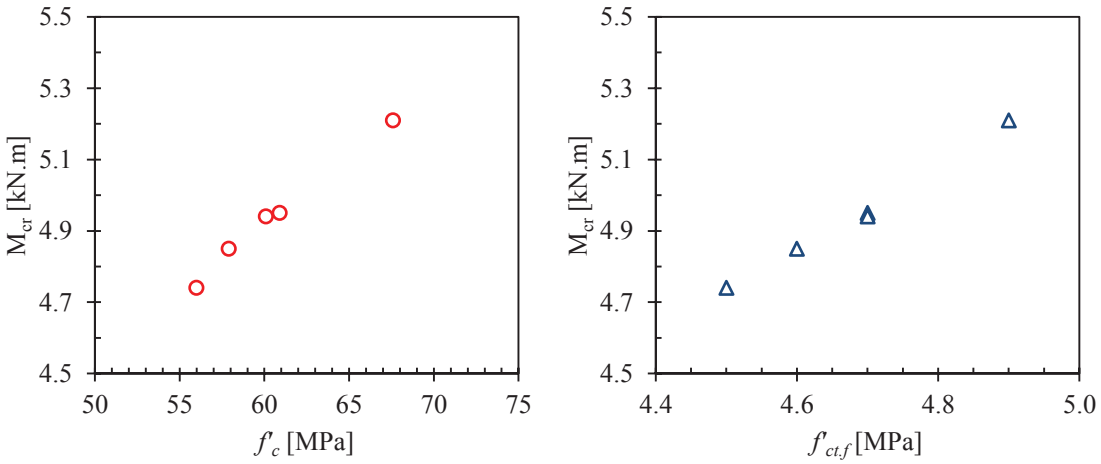

Figure 101. Characteristic strength versus cracking behaviour of RC beams

Figure 101 shows the characteristic compressive strength and modulus of rupture of control and FRC beams versus their cracking moment. From the results, it can be stated that the cracking moment of RC beams is enhanced by increase in compressive and flexural strength of concrete. Accordingly, since PVA-FRC provides a higher modulus of rupture (section 3.6.7), it significantly enhances the cracking moment of RC beams. For instance, the cracking moment of beam 6PVA0.25% (A) incorporating 0.25% of 6

mm PVA fibre is 5.21 kN.m where this value is 4.95 kN.m for beam control (A) with no fibre.

4.4.1-c Crack propagation

The tracings given in Figure 102 to Figure 105 show the cracking patterns for the RC beams. The numbers on the cracks indicate the load of each individual loading jack (P/2), in kN, at which the loading was stopped and the cracks mapped. Hence, the actual load applied to the beam (P) is twice the value recorded on the cracks. The rate of load increment was 5 kN.

From the cracking patterns of the beams it can be stated that the crack initiation was observed at 20 kN for the control beam, where in the case of FRC beams the first crack was observed to happen between 30 and 40 kN. This is possibly due to the higher FRC's modulus of rupture compared to that of the control. The failure mode of each concrete beam is also displayed.

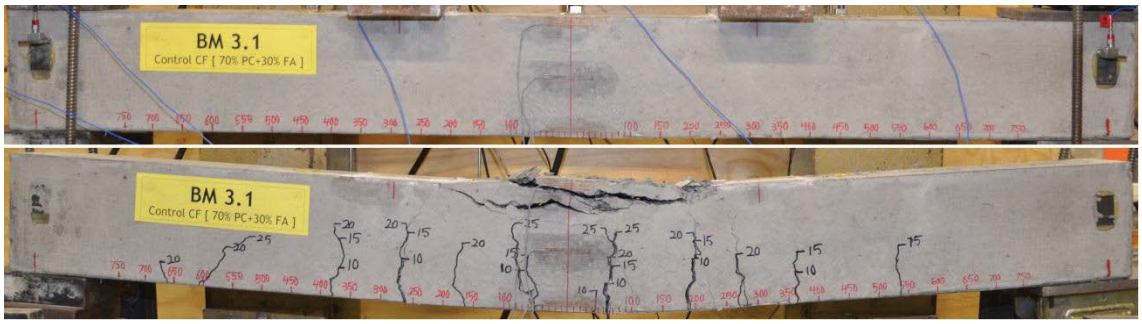

Figure 102. Cracking patterns of beam Control (A)

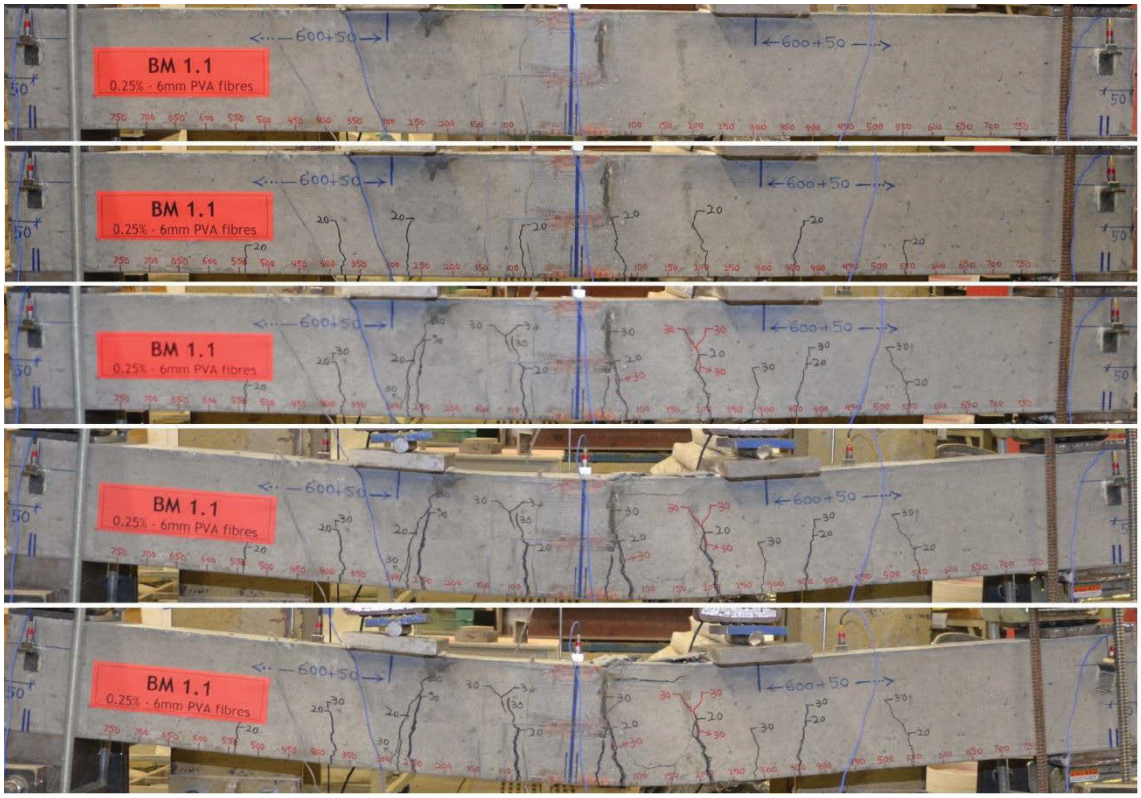

Figure 103. Cracking patterns of beam 6PVA0.25% (A)

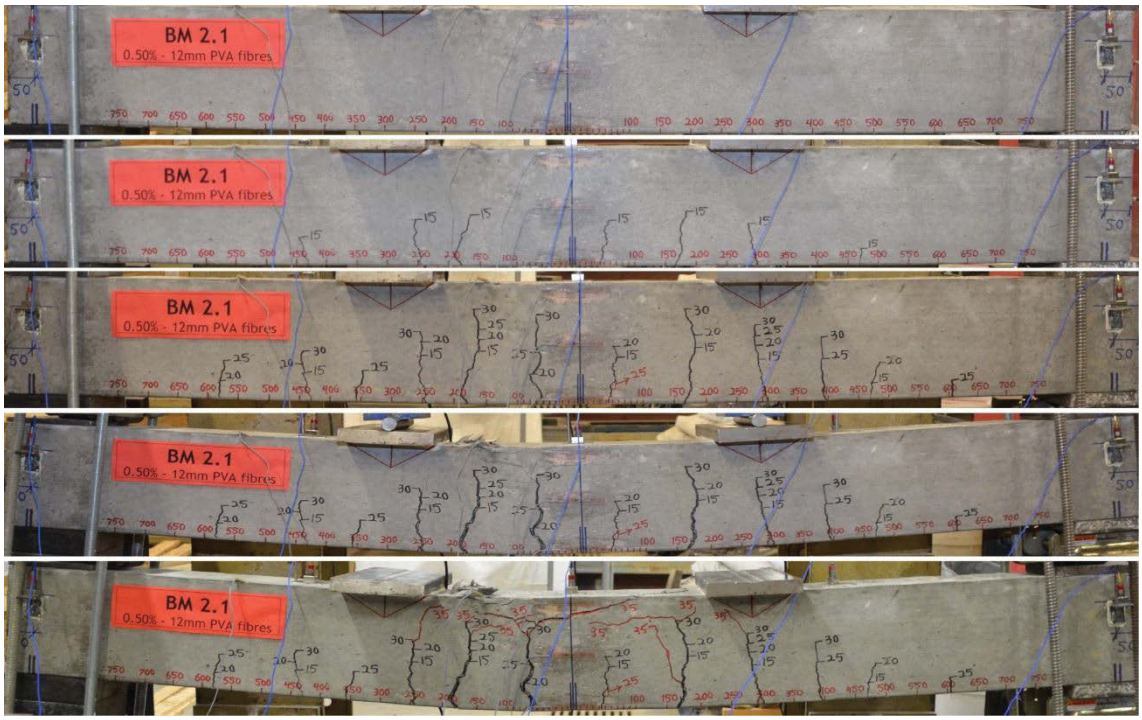

Figure 104. Cracking patterns of beam 12PVA0.50% (A)

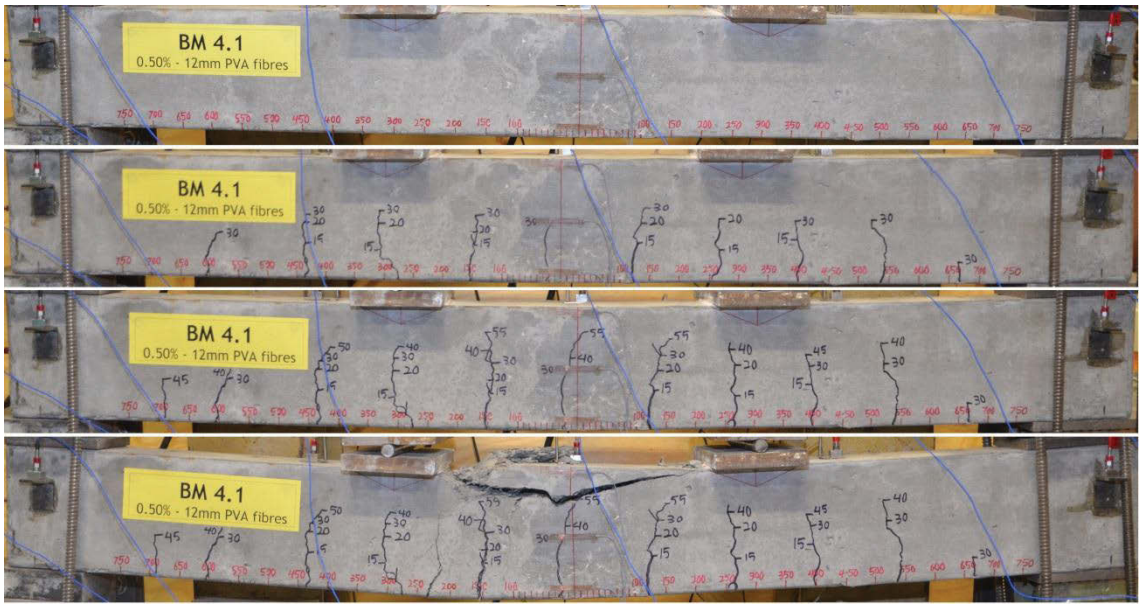

Figure 105. Cracking patterns of beam 12PVA0.50% (B)

4.4.1-d Impact resonant frequency test

In this section, findings from an investigation into the damping characteristics of FRC reinforced beam elements are presented. As previously stated in details in section 3.6.10, a hammer test has been conducted on the beams before loading (uncracked section) and in sequence of every 10 kN loading until failure (cracked section). The beam natural frequency change during the test has been calculated and results for uncracked and cracked sections are presented in Table 45. A natural frequency shift in a system can conclude that changes have happened in the system. The magnitude of this change is also an indicator of the severity or state of the change experienced (Razak & Choi 2001).

Since the complete analysis of this test, which is mainly related to the concept of damage detection in system, is out the scope of this study, only calculating the frequency of transverse mode (which is the most important dynamic characteristic of a concrete beam under flexure) is focused in the following. Accordingly, as shown in Figure 106, only the results of accelerometer A3 mounted at mid-span is used to calculate the natural frequency of the beams for hits at mid-span at each loading stage. For the transverse mode of captured vibration, the number of data per second is 1000 as the frequency is low and data has been captured for 30 seconds. Each value of natural frequency presented is the average of 5 hits on the beam.

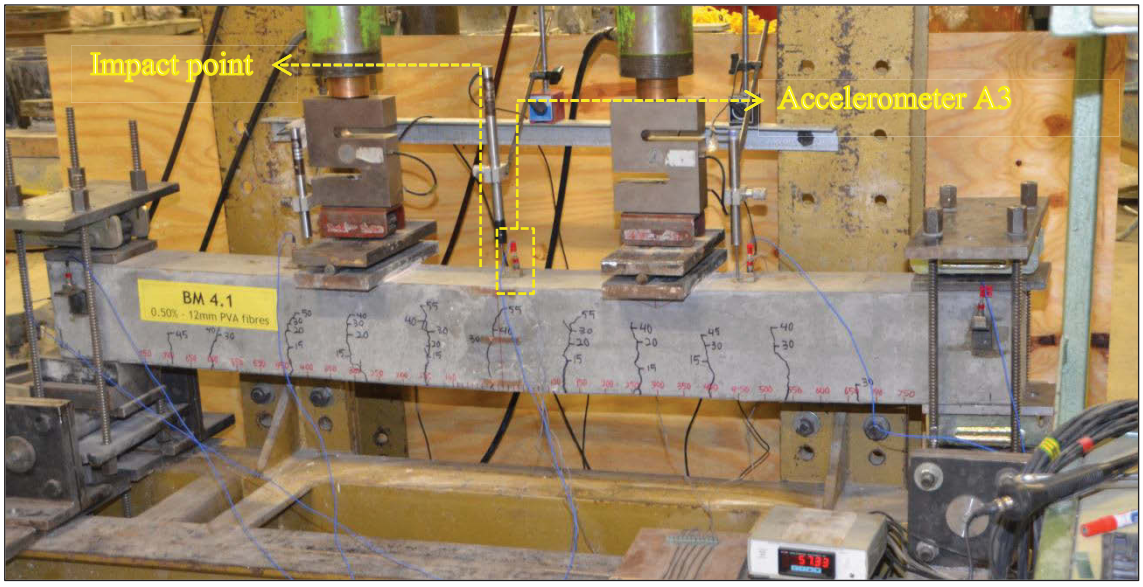

Figure 106. Impact resonance test set up

Table 45. Natural frequency of uncracked and cracked sections for transverse mode

Beam label	Natural frequency-Uncracked [Hz ± SD[1]]	Natural frequency-Cracked [Hz ± SD]
Control (A)	76.7 ± 0.2	39.9 ± 0.3
Control (B)	77.1 ± 0.3	40.1 ± 0.2
6PVA-0.25% (A)	77.3 ± 0.1	40.0 ± 0.1
12PVA-0.50% (A)	68.5 ± 1.0	34.9 ± 1.0
12PVA-0.50% (B)	75.2 ± 0.2	39.5 ± 0.2

[1] SD: Standard deviation

The test results show that the beams natural frequency for uncracked section remained constant until the cracking happens. Thereafter, a sudden drop in frequency was observed due to damage in the structure. For the cracked section, the frequency was approximately the same, while more loading was imposed, until failure.

Furthermore, for each concrete series of A and B, as shown in Figure 107 and Figure 108, the frequency of RC beams changes due to change in stiffness (for beams stiffness (EI) values refer to Table 44). This is in line with previous studies (Razak & Choi 2001) that the natural frequency of a beam element is proportional to its stiffness (EI). Consequently, a reduction in stiffness leads to reduction in the natural frequencies.

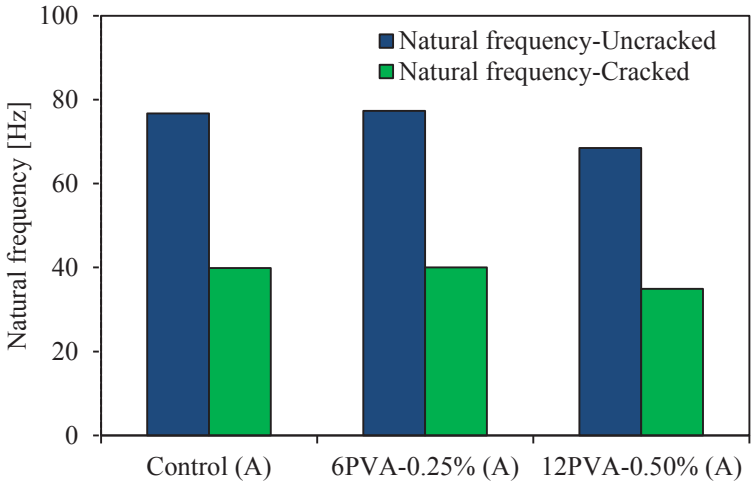

Figure 107. Transverse mode natural frequency for uncracked and cracked beams of series A

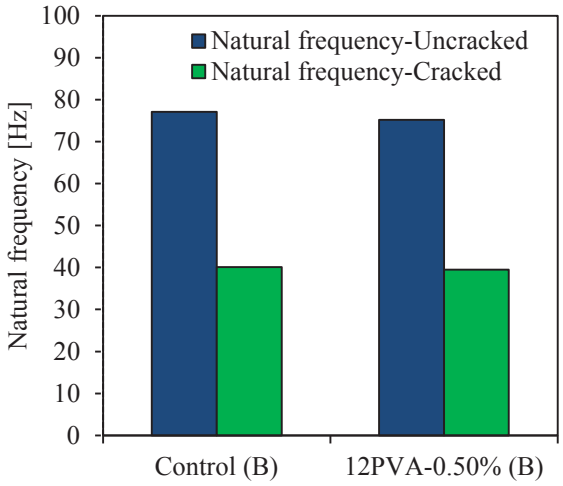

Figure 108. Transverse mode natural frequency for uncracked and cracked beams of series B

Natural frequencies of a simply supported beam subjected to flexural free vibration, can be predicted from the physical properties of the beam using Equation (35) (Zheng et al. 2008). These values, as shown in Table 46, are comparable to those captured from the experimental tests as shown in Figure 109.

$$f_n = \frac{n^2\pi}{2}\sqrt{\frac{EI}{mL^4}} \tag{35}$$

where f_n is the frequency of the nth mode, n is the mode number (for fundamental frequency, n = 1), E is the dynamic modulus of elasticity in MPa, I is the moment of inertial in m^4, L is the length of simply supported beam in m, and m is the mass of the beam per unit length (kg/m).

Table 46. Theoretical natural frequency calculation for transverse mode (uncracked section)

Beam label	EI [kN.m^2]	m [kg/m]	L [m]	Natural frequency-Theoretical [Hz]
Control (A)	4354	145.1	1.9	75.4
Control (B)	4354	145.1	1.9	75.4
6PVA-0.25% (A)	4403	142.8	1.9	76.4
12PVA-0.50% (A)	4088	136.5	1.9	75.3
12PVA-0.50% (B)	4088	136.5	1.9	75.3

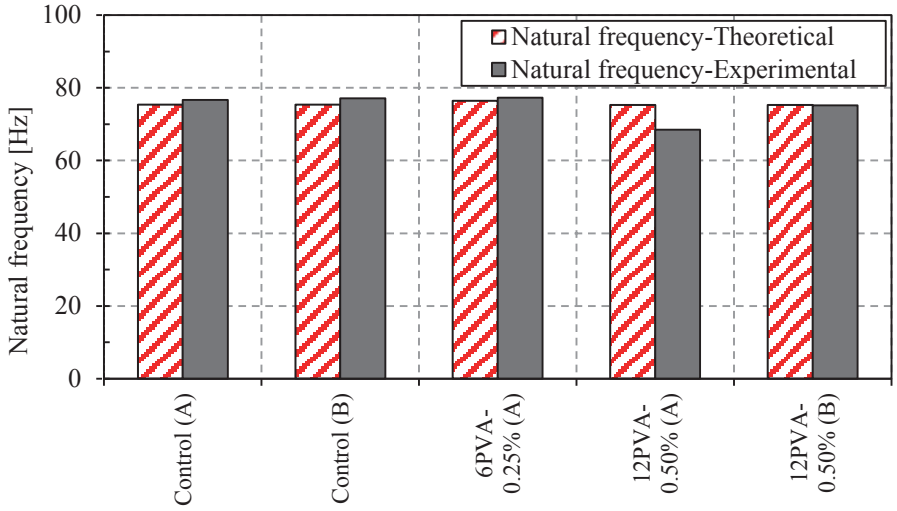

Figure 109. Comparison of theoretical and experimental natural frequency of RC beams for uncracked section

4.4.2 *3-point cyclic test*

In order to evaluate the energy absorption capacity of different RC beams and also calculating the damping characteristics of the beam elements, a series of concrete beams including three fibre reinforced RC beams and two non-fibre reinforced RC beams, with details mentioned previously in section 3.6.12, have been tested for 3-point cyclic bending as shown in Figure 110.

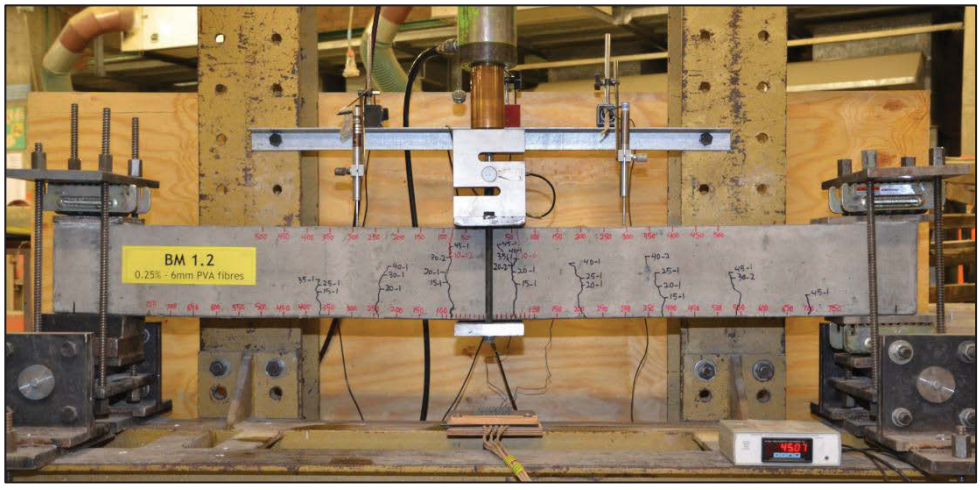

Figure 110. 3-point cyclic test set up

Since the concrete beams were designed for the positive moment only, the compression reinforcement ratio, ρ'_s , (top reinforcements) is not equal to the tension reinforcement ratio, ρ_s , (bottom reinforcements). Accordingly, as stated in section 3.6.12, to avoid beam failure under negative moment, the positive and negative loading at each cycle

were not applied symmetrically. The positive loading (resulting in positive moments) was gradually increased from one cycle to another, where the negative loading (resulting in negative moments) was kept constant within a certain limit for all the loading cycles.

The load-deflection curves of the beam element under positive loadings are presented in Figure 111 to Figure 115.

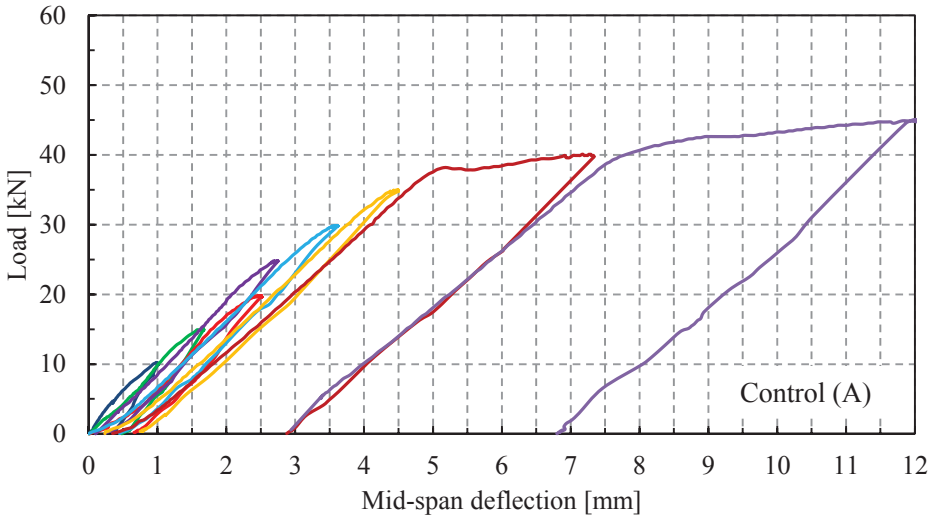

Figure 111. Hysteretic curves for beam Control (A)

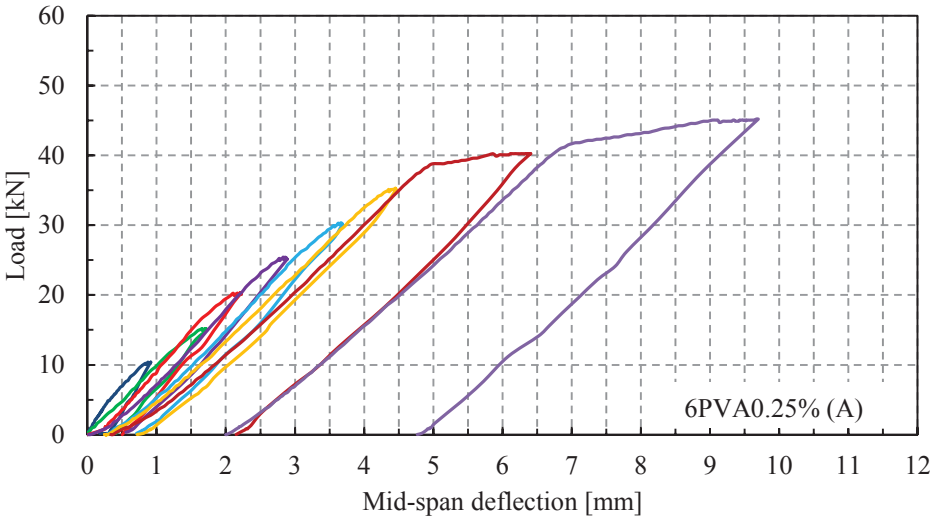

Figure 112. Hysteretic curves for beam 6PVA0.25% (A)

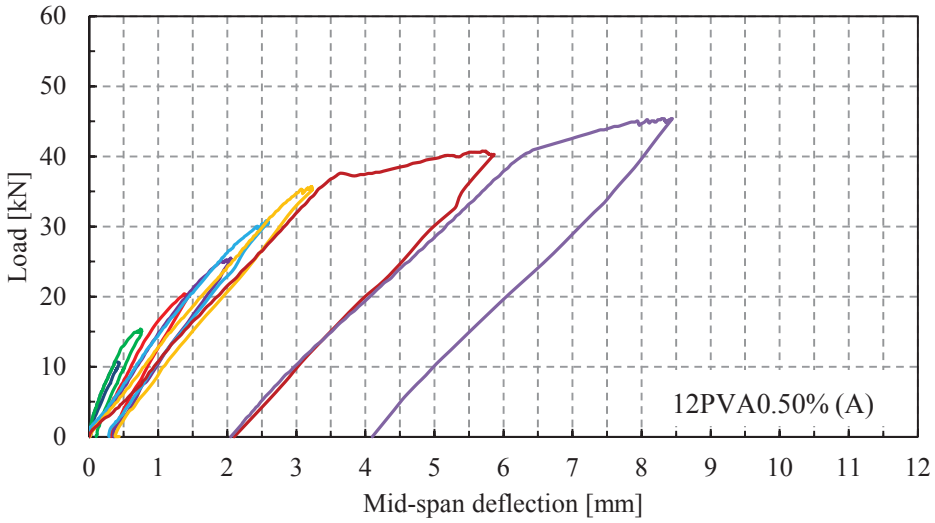

Figure 113. Hysteretic curves for beam 12PVA0.50% (A)

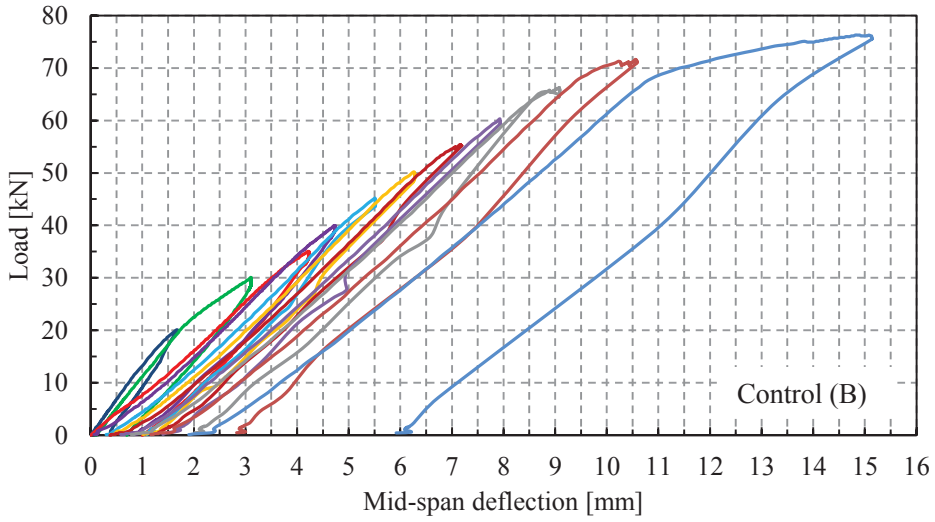

Figure 114. Hysteretic curves for beam Control (B)

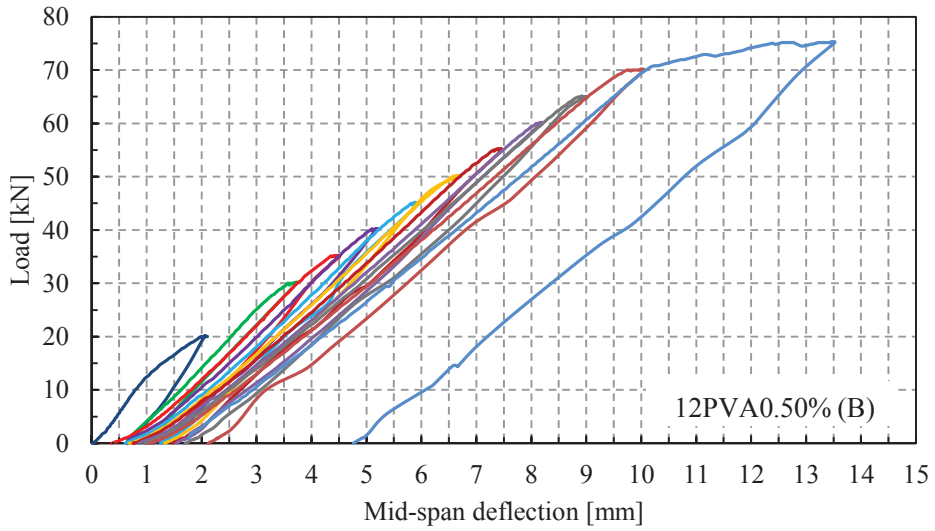

Figure 115. Hysteretic curves for beam 12PVA0.50% (B)

As stated in section 2.6 (page 31) with details described in Figure 13 and Figure 14, to calculate the energy absorption and damping ratio of each cycle following Equation (5), a hysteresis loop including both positive and negative load-deflection curves is required. Since in this study, the positive and negative loading of each cycle was not symmetrical which consequently results in an unsymmetrical hysteresis loop, the original load-deflection curve for the negative loading is replaced with the mirrored positive load-deflection curve. In this case, it is assumed that the beams would behave similarly in both positive and negative loadings and all calculations in this section are based on this assumption.

Accordingly, the full hysteretic curves of RC beams can be obtained as shown in Figure 116 to Figure 120. Furthermore, the load-deflection curves of each cycle of loading for all concrete beams are presented in Appendix B.

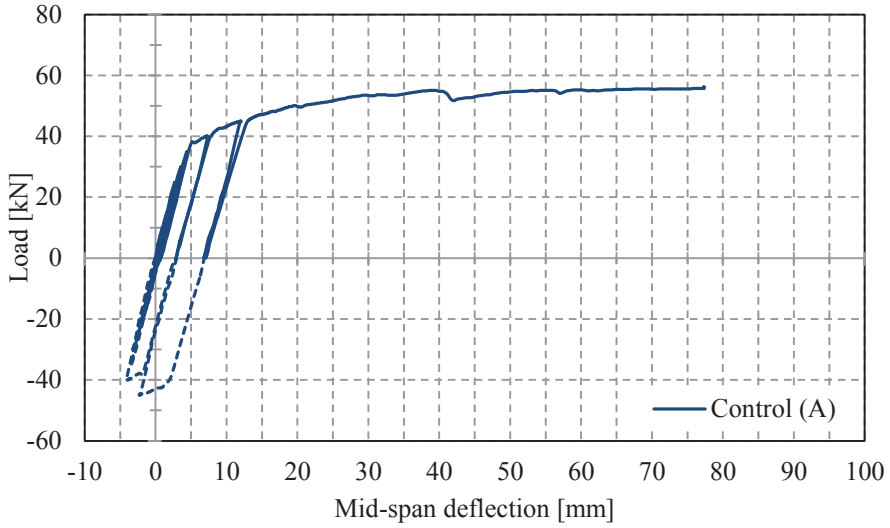

Figure 116. Load-deflection curves for beam Control (A) under cyclic loading until failure

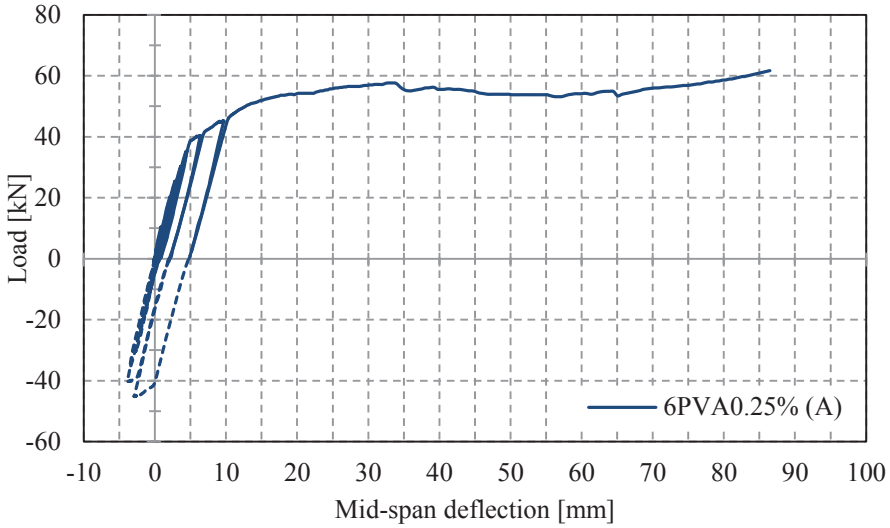

Figure 117. Load-deflection curves for beam 6PVA0.25% (A) under cyclic loading until failure

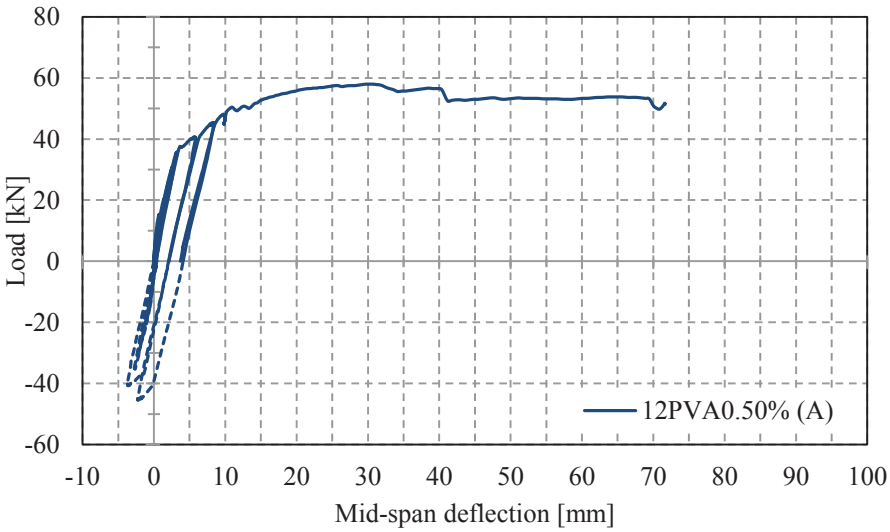

Figure 118. Load-deflection curves for beam 12PVA0.50% (A) under cyclic loading until failure

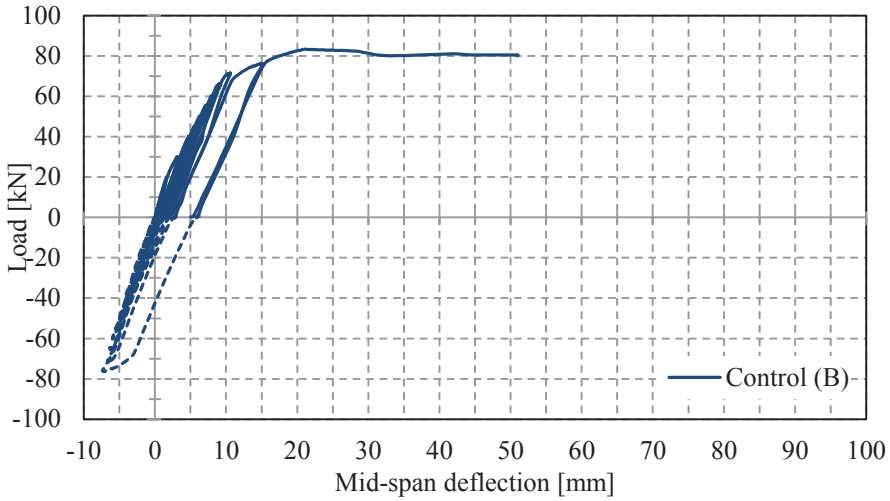

Figure 119. Load-deflection curves for beam Control (B) under cyclic loading until failure

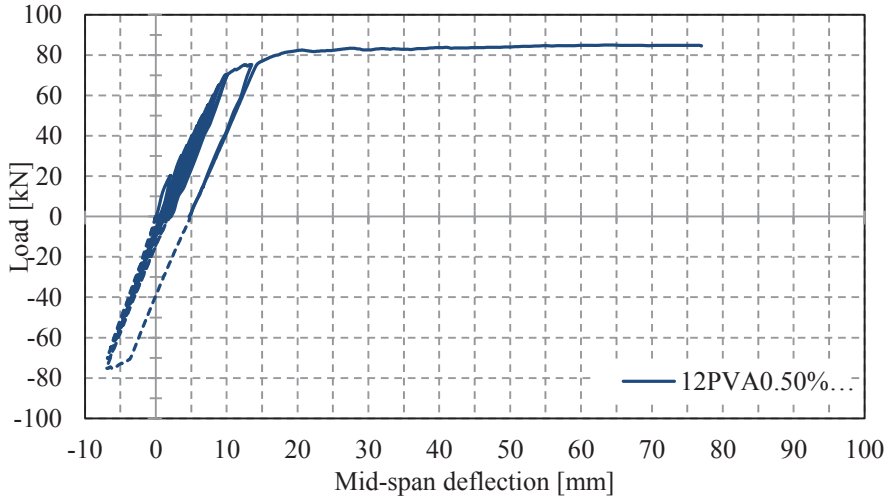

Figure 120. Load-deflection curves for beam 12PVA0.50% (B) under cyclic loading until failure

In cyclic loading, the load-deflection curves give an indication of the energy dissipated within each loading cycle. Following the theory of hysteresis loop method described in section 2.6, the energy dissipated in each cycle (E_D), the strain energy (E_{S0}) and finally the damping ratio (ξ) can be calculated using below equations.

$$\xi = \frac{1}{2\pi}\frac{E_D}{E_{S0}} \tag{36}$$

$$E_{S0} = \frac{k\,{u_0}^2}{2} \tag{37}$$

where E_D is equal to the area enclosed within each hysteretic loop, u_0 is equal to the maximum deformation in each cycle and k is the peak-to-peak secant stiffness for each complete loading cycle (Figure 121).

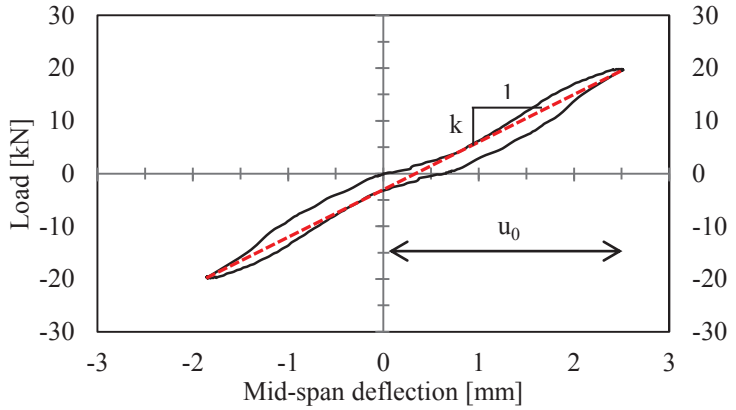

Figure 121. Peak-to-peak secant stiffness k

The summary of damping ratio and dissipated energy calculations for concrete beams of series A and B are tabulated in Table 47 to Table 51.

Table 47. Hysteretic energy and damping calculations for beam Control (A)

Cycle No.	Max load [kN]	u_0 [mm]	k[1] [kN/mm]	E_{s0} [kN.mm]	Area - positive [kN.mm]	E_D [kN.mm]	ζ
1	10.2	1.0	10.1	5.2	2.8	5.5	0.17
2	15.1	1.7	9.0	12.6	5.3	10.6	0.13
3	19.8	2.5	7.9	24.9	7.1	14.3	0.09
4	24.8	2.7	9.3	32.9	6.3	12.5	0.06
5	29.8	3.6	8.2	53.9	9.2	18.5	0.05
6	35.0	4.3	8.2	74.5	10.6	21.2	0.05
7	40.1	7.0	5.7	140.2	88.4	176.9	0.20
8	45.1	9.1	5.0	205.0	168.8	337.6	0.26

[1] Peak-to-peak secant stiffness

Table 48. Hysteretic energy and damping calculations for beam 6PVA0.25% (A)

Cycle No.	Max load [kN]	u_0 [mm]	k [kN/mm]	E_{s0} [kN.mm]	Area - positive [kN.mm]	E_D [kN.mm]	ζ
1	10.4	0.9	11.4	4.8	2.6	5.2	0.17
2	15.2	1.7	8.8	13.1	4.6	9.2	0.11
3	20.3	2.2	9.1	22.5	6.3	12.6	0.09
4	25.4	2.9	8.9	36.5	7.9	15.8	0.07
5	30.3	3.4	8.8	51.8	10.0	20.0	0.06
6	35.3	4.2	8.4	74.3	13.3	26.6	0.06
7	40.2	6.1	6.6	122.1	59.3	118.7	0.15
8	45.2	7.7	5.9	174.0	113.0	225.9	0.21

Table 49. Hysteretic energy and damping calculations for beam 12PVA0.50% (A)

Cycle No.	Max load [kN]	u_0 [mm]	k [kN/mm]	E_{s0} [kN.mm]	Area - positive [kN.mm]	E_D [kN.mm]	ζ
1	10.7	0.4	24.6	2.3	0.5	1.0	0.07
2	15.4	0.8	20.2	5.8	2.2	4.5	0.12
3	20.4	1.5	14.0	14.8	4.7	9.4	0.10
4	25.5	2.1	12.4	26.2	7.1	14.2	0.09
5	30.8	2.6	11.9	39.9	8.3	16.5	0.07
6	35.7	3.2	11.1	57.5	10.2	20.4	0.06
7	40.8	5.9	6.9	119.5	83.0	165.9	0.22
8	45.4	6.4	7.1	145.2	85.1	170.2	0.19

Table 50. Hysteretic energy and damping calculations for beam Control (B)

Cycle No.	Max load [kN]	u_0 [mm]	k [kN/mm]	E_{s0} [kN.mm]	Area - positive [kN.mm]	E_D [kN.mm]	ζ
1	20.1	1.7	12.0	16.9	5.5	11.0	0.10
2	30.1	3.0	10.0	45.3	19.2	38.5	0.14
3	35.0	4.2	8.3	74.1	25.7	51.5	0.11
4	40.0	4.7	8.6	93.4	21.9	43.8	0.07
5	45.2	5.2	8.7	118.0	19.5	39.1	0.05
6	50.2	5.9	8.5	148.0	23.2	46.5	0.05
7	55.3	6.8	8.1	188.7	25.2	50.4	0.04
8	60.3	7.4	8.2	221.9	21.3	42.6	0.03
9	66.3	8.3	8.0	275.1	39.3	78.7	0.05
10	71.6	9.4	7.6	337.4	65.4	130.8	0.06
11	76.3	13.2	5.8	505.0	247.9	495.7	0.16

Table 51. Hysteretic energy and damping calculations for beam 12PVA0.50% (B)

Cycle No.	Max load [kN]	u_0 [mm]	k [kN/mm]	E_{s0} [kN.mm]	Area - positive [kN.mm]	E_D [kN.mm]	ζ
1	20.2	2.1	9.7	21.0	10.9	21.8	0.17
2	30.2	3.1	9.8	46.5	8.3	16.6	0.06
3	35.1	4.1	8.5	72.9	14.3	28.7	0.06
4	40.2	4.5	8.9	91.4	15.1	30.3	0.05
5	45.2	5.4	8.4	121.1	15.7	31.3	0.04
6	50.2	6.0	8.4	150.8	12.7	25.4	0.03
7	55.2	6.7	8.2	185.1	21.2	42.3	0.04
8	60.2	7.3	8.2	220.6	19.9	39.9	0.03
9	65.1	8.0	8.1	261.8	27.5	55.1	0.03
10	70.2	9.0	7.8	316.2	47.6	95.2	0.05
11	75.3	11.8	6.4	442.9	222.8	445.7	0.16

The damping ratios of all loading cycles for beams of series A and B are shown in Figure 122 and Figure 123. Results show that the damping ratios of fibre reinforced RC beams are very close to that of conventional (control) RC beams for both beam elements of series A and B. However, FRC beams of series A generally show slightly higher damping ratios compared to the control beam, except for the first and last cycle, where in beams of series B, the control beam shows higher damping values. Furthermore, it is worth noting that in most cases the damping ratios of the first cycle (about first cracking) and the last cycle (about failure) are by far higher than that of other cycles.

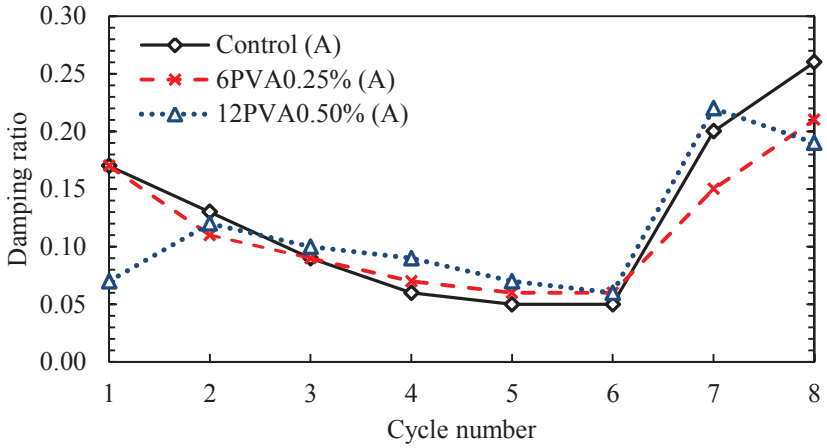

Figure 122. Damping ratio at each cycle for beams of series A

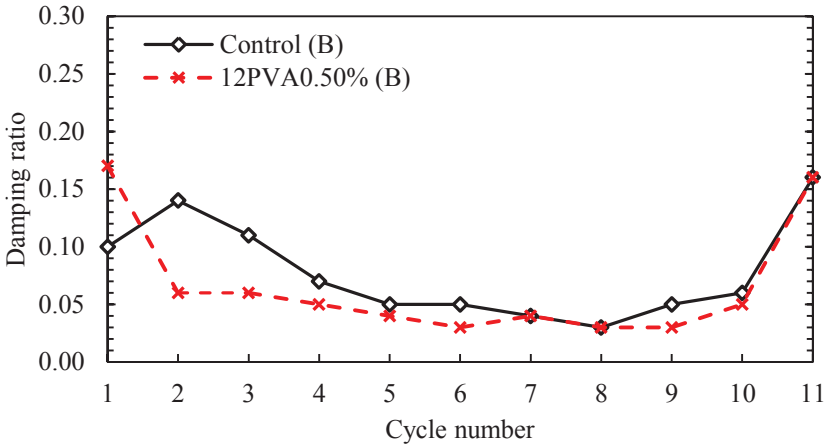

Figure 123. Damping ratio at each cycle for beams of series B

The amount of energy dissipated during the test for beams of series A and B are shown in Figure 124 and Figure 125. From the results it can be stated that little energy has been dissipated before concrete cracking and also during the elasto-plastic phase. However, the energy dissipation capacity is significantly increased within the last two cycles of loading. It could generally be mentioned that the energy dissipation capacity of all RC beams with and without PVA fibres have slightly increased by increasing loads until about the end of elasto-plastic phase. And at the last stage of cyclic loading, where the steel reinforcements start to yield, a large amount of energy has been dissipated.

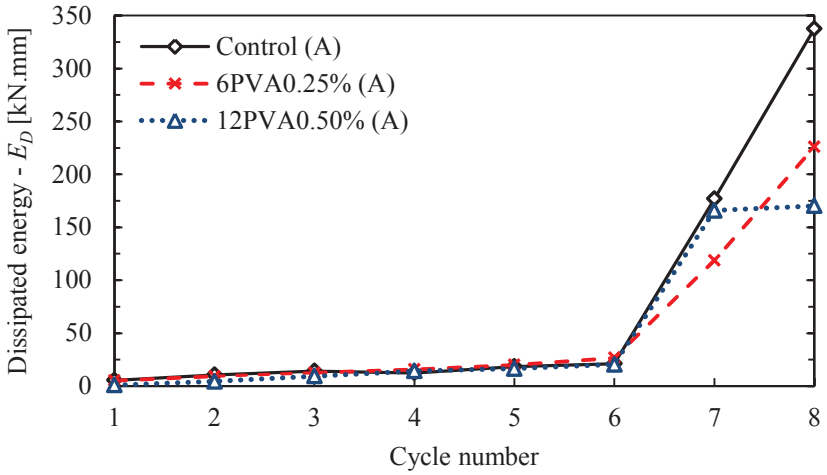

Figure 124. Energy dissipated in each cycle for beams of series A

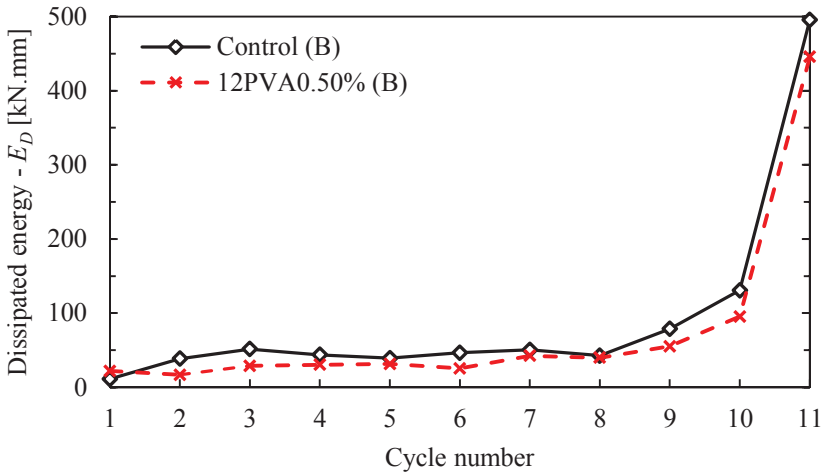

Figure 125. Energy dissipated in each cycle for beams of series B

Beside the energy dissipation capacity and damping properties, stiffness degradation rate can also be investigated from the results of the cyclic test. Peak to peak secant stiffness (k) for each loading cycle of concrete beams of series A and B are shown in Figure 126 and Figure 127. In Table 52, the initial and ultimate stiffness of all concrete beams are summarised. For concrete beams of series A with low strength longitudinal tensile reinforcements (f_y = 250 MPa), higher initial stiffness (k_0) is observed for beams incorporating PVA fibres compared to that of control concrete. However, for beams of series B with high strength longitudinal tensile reinforcements (f_y = 500 MPa), the control beam (devoid of PVA fibre) shows slightly higher initial stiffness. It is worth noting that all FRC beams show higher ultimate stiffness compared to the control beams which is due to the presence of fibres.

Table 52. Initial and ultimate stiffness of concrete beams of series A and B

Beam lable	k_0[1] [kN/mm]	k_u[2] [kN/mm]	k_u/k_0 [%]
Control (A)	10.1	5.0	49.5
6PVA0.25% (A)	11.4	5.9	51.8
12PVA0.50% (A)	24.6	7.1	28.9
Control (B)	12.0	5.8	48.3
12PVA0.50% (B)	9.7	6.4	66.0

[1] Initial peak-to-peak secant stiffness
[2] Ultimate (collapse) peak-to-peak secant stiffness

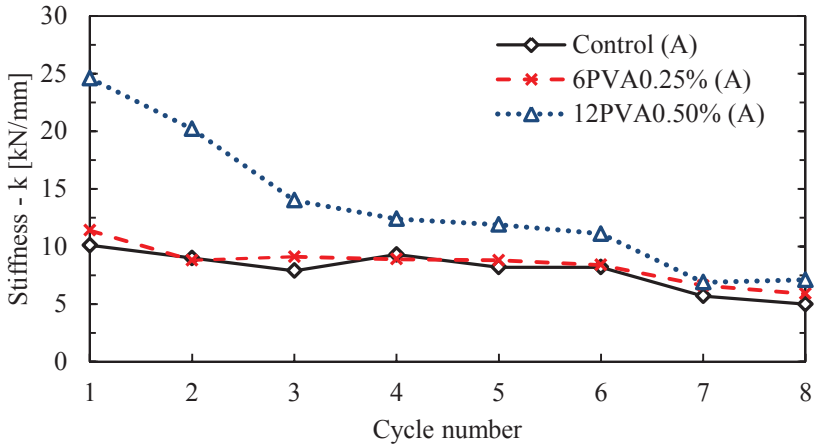

Figure 126. Peak-to-peak secant stiffness of each cycle for beams of series A

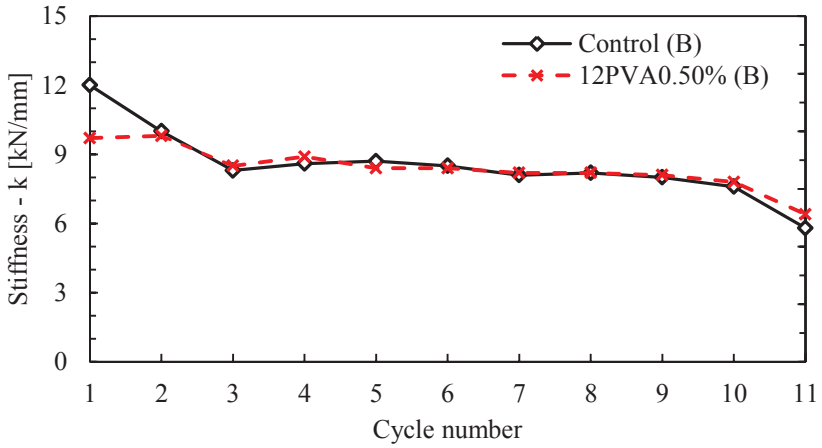

Figure 127. Peak-to-peak secant stiffness of each cycle for beams of series B

In addition, the normalized stiffness of each loading cycle with respect to the initial stiffness for beams of series A and B are shown in Figure 128 and Figure 129.

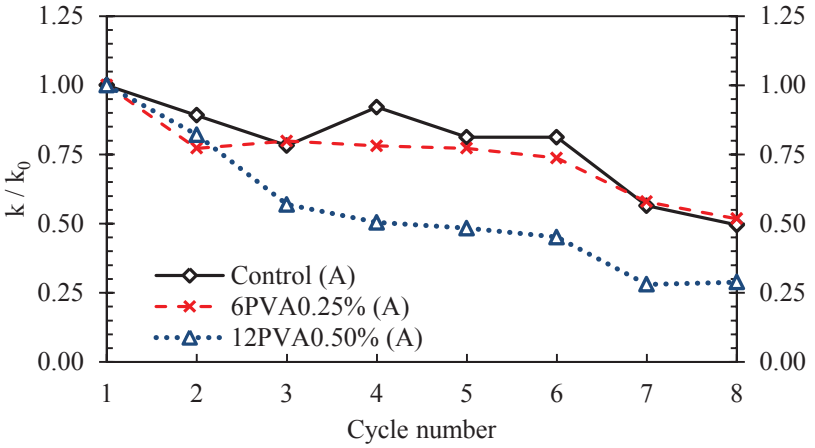

Figure 128. Stiffness degradation for beams of series A

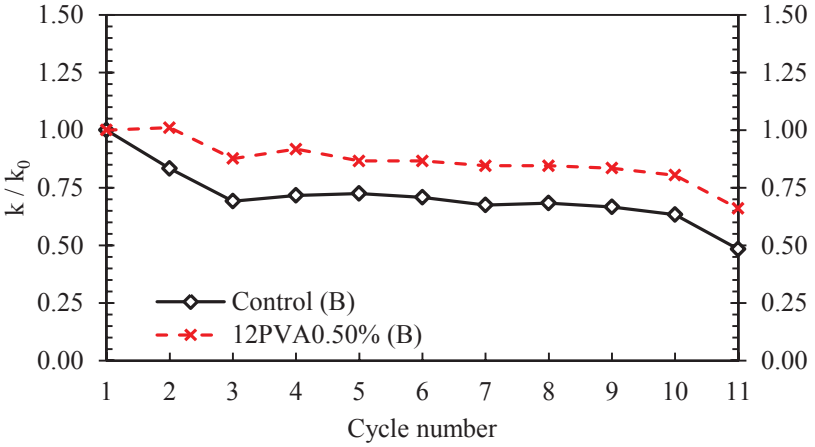

Figure 129. Stiffness degradation for beams of series B

From the results reported above regarding the stiffness of RC beams, it can be stated that in concrete beams of series A, the beams incorporating PVA fibres show higher initial and ultimate stiffness compared to the control beam. FRC beams also have higher stiffness degradation rate (slope of the curve) within the first two cycles of loading, however, after that point they show higher capacity to maintain their stiffness during the test.

In concrete beams of series B, the beam incorporating 12 mm PVA fibres show lower initial stiffness but higher ultimate stiffness compared to the control beam. Furthermore, the addition of PVA fibres in beams of series B decreases the stiffness degradation rate. As shown in Table 52, the beam having 0.5% of 12 mm PVA fibres maintained 66% of its initial stiffness where this value (k_u/k_0) is less than 50% for control beam.

It is specified in most reinforced concrete building codes (e.g. ACI-318-11 and DIN 1045-1) that a cracked beam shall remain at 50% of their initial stiffness properties to

develop and maintain their flexural capacity. As can be observed from the results presented in Table 52, beam 6PVA0.25%-A and beam 12PVA0.50%-B would be able to fulfil this requirement since they kept 51.8% and 66% of their original stiffness at the ultimate stage, respectively.

4.5 Concluding Remarks

The following conclusions can be drawn from the results and discussion obtained in this chapter:

- Less workability is observed for mixes having more fibre content and higher amount of HWR. Mixes with longer fibre length demonstrate lower slump compared to shorter fibre length for the same fibre volume addition. As a result, it can be stated that adding hydrophilic PVA fibre decreases concrete slump.
- Air content remained constant by introducing PVA fibres into concrete, although a slight increase in air content can be observed.
- Mass per unit volume of concrete is seen to decrease by adding fibres to the mix. This is due to the lower density of the fibres contributing to a lower volume density.
- Compressive strength at 28 days ($f_{c,28}$) increases with increasing fibre addition and the optimum fibre volume fraction was found to be 0.25% with 12% improvement noted in $f_{c,28}$. It can also be concluded that shorter fibres increase compressive strength further compared to longer-length fibre.
- FRCs provide for a more ductile mode of failure compared to control concrete devoid of fibre additions and strain at ultimate stress behaviour is observed to be higher with higher fibre contents.
- An ideal concrete can be produced for seismic region structures, if the post peak behaviour of concrete can also be improved and a strain softening behaviour and high ductility be achieved. This may be attainable by using longer fibres which can be targeted as future works.
- The same trend as compressive strength is also observed for tensile and flexural strength. The average additional strength development of 20% in flexure and 30% in splitting tensile at 0.25% volume fraction shows how PVA fibre can improve the properties of plain concrete.
- MOE test results show that, PVA fibres in low volume fractions used in this study (0.25% and 0.50%) do not significantly affect the modulus of elasticity of concrete. Some variations are noticed at early ages (7 and 28 days) while at 56

days most FRCs have very close values to that of control. However, it is anticipated that within the FRCs, adding more fibres will lead to a decrease in concrete modulus of elasticity and in a same fibre content longer fibres have lower MOE.

- Residual flexural tensile strength results demonstrate that, prior to the peak, response of all concrete series is almost similar and showing the same stiffness. However, a slight improvement in post-peak flexural response of concrete having FA was observed compared to the conventional concrete (devoid of FA). Furthermore, the post-peak behaviour of PVA-FRCs was found to be approximately the same as control although a subtle improvement had occurred.
- Damping ratio of all concretes is observed to decrease by ageing from 14 to 28 days. Moreover, it can be mentioned that addition of PVA fibres in low volume fraction used in this study has no significant effect on concrete damping ratio. However, comparing the results for damping ratio of conventional (devoid of FA) and control (including FA) concrete show that replacing 30% PC with FA leads to a lower damping ratio of concrete.
- Results of 4-point flexural tests show that, amongst all concrete beams of series A, 6PVA-0.25% (A) beam is ranked first in terms of ductility and post-peak behaviour. 40% higher value of ductility factor is recorded for this beam containing 0.25% volume fraction of 6 mm fibre compared to the control. In concrete beams of series B, the FRC beam containing 0.50% volume fraction of 12 mm fibre showed approximately 30% higher ductility compared to the control beam.
- From the cracking patterns of the beams tested under 4-point bending, it can be stated that the crack initiation occures at 20 kN for the control beam, whereas in the case of FRC beams the first crack was observed to happen between 30 to 40 kN. This is possibly due to the higher FRC's modulus of rupture compared to that of control.

a) The test results show that the RC beams (with and without PVA fibres) natural frequency for uncracked section have remained constant until the cracking happens. Thereafter, a sudden drop in frequency was observed due to damage in

the structure and drop in flexural stiffness. For the cracked section, the frequency remained approximately the same with increasing load until failure.

- Furthermore, for each concrete series of A and B, the frequency of RC beams changed due to change in stiffness. This shows that the natural frequency of a beam element is proportional to its stiffness (EI). Consequently, a reduction in stiffness leads to a reduction in the natural frequencies.
- Results of 3-point cyclic test over concrete beams of series A and B show that little energy has been dissipated before concrete cracking and also during the elasto-plastic phase. The energy dissipation capacity of all RC beams with and without PVA fibres slightly increased by increasing loads until about the end of elasto-plastic phase. At the last stage of cyclic loading, where the steel reinforcements start to yield, a large amount of energy has been dissipated. It is also observed that the damping ratio of fibre reinforced RC beams are very close to that of conventional (control) RC beams. In most cases the damping ratios at the first cycle (about first cracking) and the last cycle (about failure) are by far much higher than those of other cycles.
- RC beams of series A incorporating PVA fibres have higher initial and ultimate stiffness compared to the control beam. FRC beams also have higher stiffness degradation rate within the first two cycles of loading, however, after that point they show higher capacity to maintain their stiffness during the test. Furthermore, they generally show slightly higher damping ratios compared to the control beam, except for the first and last cycles.
- In concrete beams of series B, the beam incorporating 12 mm PVA fibres show lower initial stiffness but higher ultimate stiffness compared to the control beam. Moreover, the addition of PVA fibres in beams of series B decreases the stiffness degradation rate. The beam having 0.5% of 12 mm PVA fibres maintained 66% of its initial stiffness whereas this value (k_u/k_0) is less than 50% for control beam. Furthermore, it is worth noting that the control beam shows slightly higher damping values compared to fibre reinforced RC beams.

Chapter 5

Finite Element Modelling and Analysis

5 FINITE ELEMENT MODELLING AND ANALYSIS

5.1 Preface

The finite element method (FEM) is a numerical technique for finding approximate solutions to a problem. The finite element analysis of any structure usually follows three well defined steps. First, the constitutive modelling of the material behaviour, which are the stress-strain behaviour and the associated failure criteria. Second, the finite element discretization of the structure in which the structure to be analysed is divided into a finite number of elements, connected only at their nodes. Figure 130 shows a model for a beam that is divided into 10 elements. And third, the numerical solution of the resulting system of equations that yields the nodal displacements and therefore the strains and stresses throughout the structure (Tadjiogueu 1980).

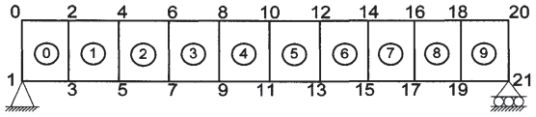

Figure 130. Discretization of a beam; numbers at the corners are node numbers, and the circled numbers are element numbers (Yeung 2008).

In this study, FEM was used to find the numerical results and approximate behaviour of reinforced concrete beams under 4-point bending test and to compare these results with those of experimental obtained from the tests.

The computer program (software) used for the purpose of the current study is called 'ATENA. This software has been utilised since it is mainly designed for concrete structures and is known to have more accurate analysis algorithms. ATENA is a program with the general governing continuum equations for non-linear analysis. The constitutive model in ATENA used in this study to model the reinforced concrete beams is called SBETA which is described further in details below. The name SBETA comes from the former program, in which this material model was first used. It is the abbreviation for the analysis of reinforced concrete in German language - StahlBETonAnalyse.

5.2 Constitutive Model SBETA[1]

5.2.1 *Basic assumptions*

The formulation of constitutive relations is considered in the plane stress state. A smeared approach is used to model the material properties, such as cracks or distributed reinforcement. This means that material properties defined for a material point are valid within a certain material volume, which is, in this case, associated with the entire finite element. The constitutive model is based on the stiffness and is described by the equation of equilibrium at a material point:

$$s = De, s = \{\sigma_x, \sigma_y, \tau_{xy}\}^T, e = \{\varepsilon_x, \varepsilon_y, \gamma_{xy}\}^T \quad (38)$$

where s is the stress vector, D is the material stiffness matrix and e is a strain vector. The stress and strain vectors are composed of the stress components of the plane stress state σ_x, σ_y, τ_{xy} (Figure 131) and the strain components ε_x, ε_y, γ_{xy} (Figure 132), where γ_{xy} is the engineering shear strain. The strains are common for all materials. The stress vector (s) and the material matrix (D) can be decomposed into the material components due to concrete and reinforcement as:

$$s = s_c + s_s, D = D_c + D_s \quad (39)$$

The stress vector s and both component stress vectors s_c, s_s are related to the total cross sectional area. The concrete stress s_c is acting on the material area of concrete A_c, which is approximately set equal to the cross section of the composite material, $A_c \approx A$ (the area of concrete occupied by reinforcement is not subtracted).

The matrix D has a form of the Hooke's law for either isotropic or orthotropic material, as will be shown later.

[1] The contents of this section is derived from the ATENA handbook guide (Červenka et al. 2012)

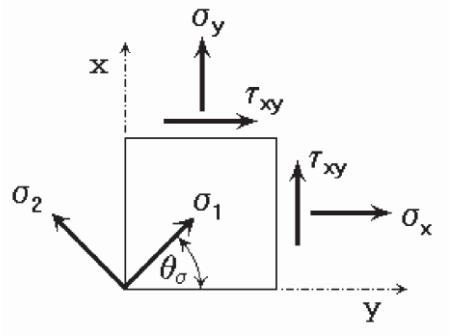

Figure 131. Components of plane stress state (Červenka et al. 2012)

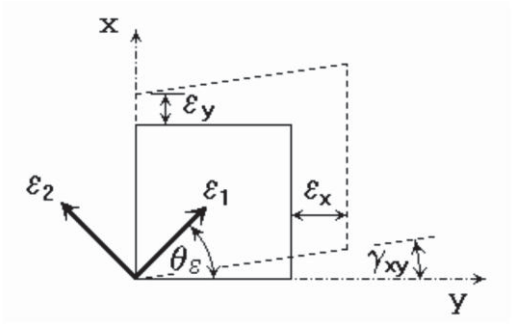

Figure 132. Components of plane strain state (Červenka et al. 2012)

The reinforcement stress vector s_s is the sum of stresses of all the smeared reinforcement components:

$$s_s = \sum_{i=1}^{n} s_{si} \tag{40}$$

where n is the number of the smeared reinforcement components. For the i^{th} reinforcement, the global component reinforcement stress s_{si} is related to the local reinforcement stress σ_{si} by the transformation:

$$s_{si} = T_\sigma p_i \sigma_{si} \tag{41}$$

where p_i is the reinforcing ratio $p_i = \frac{A_{si}}{A_c}$, A_{si} is the reinforcement cross sectional area.

The local reinforcement stress σ_{si} is acting on the reinforcement area A_{si}.

The stress and strain vectors are transformed according to the equations (42) and (45) in the plane stress state. New axes u, v are rotated from the global x, y axes by the angle α. The angle α is positive in the counter clockwise direction, as shown in Figure 133.

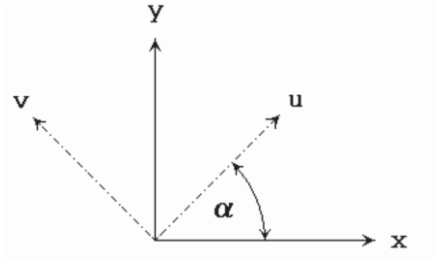

Figure 133. Rotation of reference coordinate axes (Červenka et al. 2012)

The transformation of the stresses is governed by,

$$s_{(u)} = T_\sigma s_{(x)} \tag{42}$$

$$\mathbf{T}_\sigma = \begin{bmatrix} \cos(\alpha)^2 & \sin(\alpha)^2 & 2\cos(\alpha)\sin(\alpha) \\ \sin(\alpha)^2 & \cos(\alpha)^2 & -2\cos(\alpha)\sin(\alpha) \\ -\cos(\alpha)\sin(\alpha) & \cos(\alpha)\sin(\alpha) & \cos(\alpha)^2 - \sin(\alpha)^2 \end{bmatrix} \tag{43}$$

$$s_{(u)} = \{\sigma_u, \sigma_v, \tau_{uv}\}^T, s_{(x)} = \{\sigma_x, \sigma_y, \gamma_{xy}\}^T \tag{44}$$

The transformation of the strains is governed by,

$$e_{(u)} = T_\sigma e_{(x)} \tag{45}$$

$$\mathbf{T}_\varepsilon = \begin{bmatrix} \cos(\alpha)^2 & \sin(\alpha)^2 & \cos(\alpha)\sin(\alpha) \\ \sin(\alpha)^2 & \cos(\alpha)^2 & -\cos(\alpha)\sin(\alpha) \\ -2\cos(\alpha)\sin(\alpha) & 2\cos(\alpha)\sin(\alpha) & \cos(\alpha)^2 - \sin(\alpha)^2 \end{bmatrix} \tag{46}$$

$$e_{(u)} = \{\varepsilon_u, \varepsilon_v, \tau_{uv}\}^T, s_{(x)} = \{\varepsilon_x, \varepsilon_y, \gamma_{xy}\}^T \tag{47}$$

The angles of principal axes of the stresses and strains, Figure 131, Figure 132, are found from the equations:

$$\tan(2\vartheta_\sigma) = \frac{2\tau_{xy}}{\sigma_x - \sigma_y}, \tan(2\vartheta_\varepsilon) = \frac{\gamma_{xy}}{\varepsilon_x - \varepsilon_y} \tag{48}$$

where ϑ_σ is the angle of the first principal stress axis and ϑ_ε is the angle of the first principal strain axis.

In case of isotropic material (un-cracked concrete) the principal directions of the stress and strains are identical; in case of anisotropic material (cracked concrete) they can be

different. The sign convention for the normal stresses, employed within this program, uses the positive values for the tensile stress (strain) and negative values for the compressive stress (strain). The shear stress (strain) is positive if acting upwards on the right face of a unit element.

The material model SBETA includes the following effects of concrete behaviour:

- Non-linear behaviour in compression including hardening and softening,
- Fracture of concrete in tension based on the nonlinear fracture mechanics,
- Biaxial strength failure criterion,
- Reduction of compressive strength after cracking,
- Tension stiffening effect,
- Reduction of the shear stiffness after cracking (variable shear retention),
- Two crack models: fixed crack direction and rotated crack direction.

Perfect bond between concrete and reinforcement is assumed within the smeared concept. No bond slip can be directly modelled except for the one included inherently in the tension stiffening. However, on a macro-level, a relative slip displacement of reinforcement with respect to concrete over a certain distance can arise, if concrete is cracked or crushed. This corresponds to a real mechanism of bond failure in case of the bars with ribs. The reinforcement in both forms, smeared and discrete, is in the uniaxial stress state and its constitutive law is a multi-linear stress-strain diagram.

The material matrix is derived using the nonlinear elastic approach. In this approach the elastic constants are derived from a stress-strain function called here the "equivalent uniaxial law". This approach is similar to the nonlinear hypoelastic constitutive model, except that different laws are used here for loading and unloading, causing the dissipation of energy exhausted for the damage of material. The detailed treatment of the theoretical background of this subject can be found, for example, in the book by Chen (1982). This approach can also be regarded as an isotropic damage model, with the unloading modulus representing the damage modulus.

5.2.2 *Stress-Strain Relations for Concrete*

The nonlinear behaviour of concrete in the biaxial stress state is described by means of the so-called effective stress σ_c^{ef}, and the equivalent uniaxial strain ε^{eq}. The effective stress is in most cases a principal stress.

The equivalent uniaxial strain is introduced in order to eliminate the Poisson's effect in the plane stress state.

$$\varepsilon^{eq} = \frac{\sigma_{ci}}{E_{ci}} \tag{49}$$

The equivalent uniaxial strain can be considered as the strain, that would be produced by the stress σ_{ci} in a uniaxial test with modulus E_{ci} associated with direction i. Within this assumption, the nonlinearity representing a damage is caused only by the governing stress σ_{ci}. The details can be found in Chen (1982).

The complete equivalent uniaxial stress-strain diagram for concrete is shown in Figure 134.

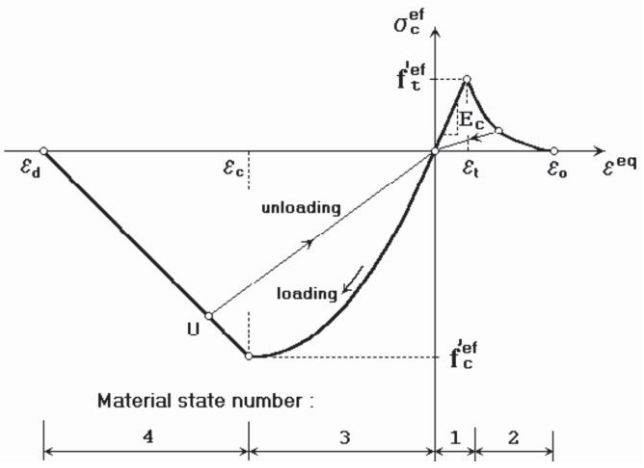

Figure 134. Concrete uniaxial stress-strain diagram (Červenka et al. 2012)

The numbers on the diagram in Figure 134 (material state numbers) are used in the results of the analysis to indicate the state of damage of concrete.

Unloading is a linear function to the origin. An example of the unloading point U is shown in Figure 134. Thus, the relation between stress σ_c^{ef} and strain ε^{eq} is not unique and depends on a load history. A change from loading to unloading occurs when the

increment of the effective strain changes the sign. If subsequent reloading occurs the linear unloading path is followed until the last loading point U is reached again. Then, the loading function is resumed. The peak values of stress in compression $f_c'^{ef}$ and in tension $f_t'^{ef}$ are calculated according to the biaxial stress state as will be shown later. Thus, the equivalent uniaxial stress-strain law reflects the biaxial stress state.

The above defined stress-strain relation is used to calculate the elastic modulus for the material stiffness matrices. The secant modulus is calculated as

$$E_c^s = \frac{\sigma_c}{\varepsilon^{eq}} \tag{50}$$

It is used in the constitutive equation to calculate stresses for the given strain state.

The tangent modulus E_c^t is used in the material matrix D_c for construction of an element stiffness matrix for the iterative solution. The tangent modulus is the slope of the stress-strain curve at a given strain which is always positive. In cases when the slope of the curve is less than the minimum value $E_{\min}^t$, the value of the tangent modulus is set at $E_c^t = E_{\min}^t$. This occurs in the softening ranges and near the compressive peak.

Detailed description of the stress-strain law is given in the following subsections.

5.2.2.a Tension before Cracking

The behaviour of concrete in tension without cracks is assumed linear elastic. E_c is the initial elastic modulus of concrete, $f_t'^{ef}$ is the effective tensile strength derived from the biaxial failure function.

$$\sigma_c^{ef} = E_c \varepsilon^{eq}, \qquad 0 \le \sigma_c \le f_t'^{ef} \tag{51}$$

5.2.2.b Tension after Cracking

Two types of formulations are used for the crack opening:

1. A fictitious crack model based on a crack-opening law and fracture energy. This formulation is suitable for modelling of crack propagation in concrete. It is used in combination with the crack band.

2. A stress-strain relation in a material point. This formulation is not suitable for normal cases of crack propagation in concrete and should be used only in some special cases.

In the following, five softening models included in SBETA material model are described.

- *Exponential crack opening law*

This function of crack opening was derived experimentally by HORDIJK (1991).

$$\frac{\sigma}{f'^{ef}_t} = \left\{1 + \left(c_1 \frac{w}{w_c}\right)^3\right\} exp\left(-c_2 \frac{w}{w_c}\right) - \frac{w}{w_c}(1 + c_1^3) exp(-c_2) \qquad (52)$$

where w is the crack opening, $w_c = 5.14 \frac{G_f}{f'^{ef}_t}$ is the crack opening at the complete release of stress, σ is the normal stress in the crack (crack cohesion). Values of the constants are, $c_1 = 3$, $c_2 = 6.93$. G_f is the fracture energy needed to create a unit area of stress-free crack, $f_t'^{ef}$ is the effective tensile strength derived from a failure function. The crack opening displacement w is derived from strains according to the crack band theory.

- *Linear crack opening law*

$$\frac{\sigma_c^{ef}}{f'^{ef}_t} = \frac{f'_t}{w_c}(w_c - w), \qquad w_c = \frac{2G_f}{f'_t} \qquad (53)$$

- *Linear softening based on local strain*

The descending branch of the stress-strain diagram is defined by the strain c_3 (Figure 135) corresponding to zero stress (complete release of stress).

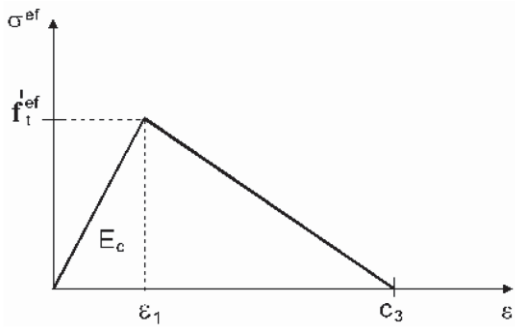

Figure 135. Linear softening based on strain (Červenka et al. 2012)

- *SFRC based on fracture energy (Refer to Figure 136)*

Parameters:

$$c_1 = \frac{f_1}{f'^{ef}_t}, \qquad c_2 = \frac{f_2}{f'^{ef}_t}, \qquad w_c = \frac{2G_f}{f_1 + f_2} \tag{54}$$

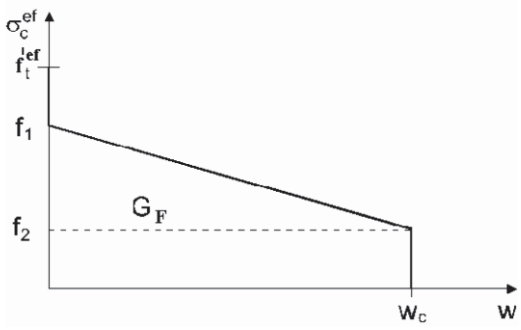

Figure 136. Steel fiber reinforced concrete based on fracture energy (Červenka et al. 2012)

- *SFRC based on strain*

Parameters:

$$c_1 = \frac{f_1}{f'^{ef}_t}, \qquad c_2 = \frac{f_2}{f'^{ef}_t} \tag{55}$$

Parameters c_1 and c_2 are relative positions of stress levels, and c_3 is the end strain as seen in Figure 137.

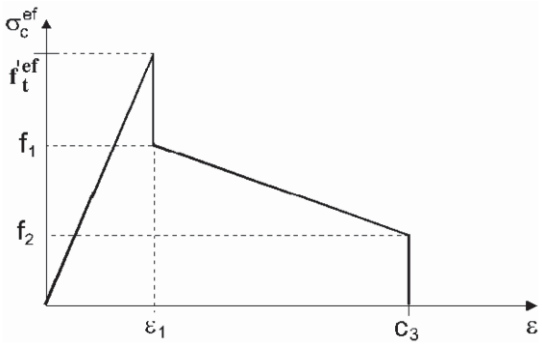

Figure 137. Steel fiber reinforced concrete based on strain (Červenka et al. 2012)

5.2.2.c Compression before peak stress

The formula recommended by CEB-FIP Model Code 90 has been adopted for the ascending branch of the concrete stress-strain law in compression, Figure 138. This formula enables a wide range of curve forms, from linear to curved, and is appropriate for normal as well as high strength concrete.

$$\sigma_c^{ef} = f'^{ef}_c \frac{kx - x^2}{1 + (k-2)x}, \qquad x = \frac{\varepsilon}{\varepsilon_c}, \qquad k = \frac{E_0}{E_c} \tag{56}$$

Meaning of the symbols in the above formula are:

σ_c^{ef} concrete compressive stress

f'^{ef}_c concrete effective compressive strength

x normalized strain

ε strain

ε_c strain at the peak stress f'^{ef}_c

k shape parameter

E_o initial elastic modulus

E_c secant elastic modulus at the peak stress, $E_c = \dfrac{f'^{ef}_c}{\varepsilon_c}$

Parameter k may have any positive value greater than or equal to 1. Examples: k = 1 linear, k = 2 parabola.

As a consequence of the above assumption, distributed damage is considered before the peak stress is reached, contrary to the localized damage, which is considered after the peak.

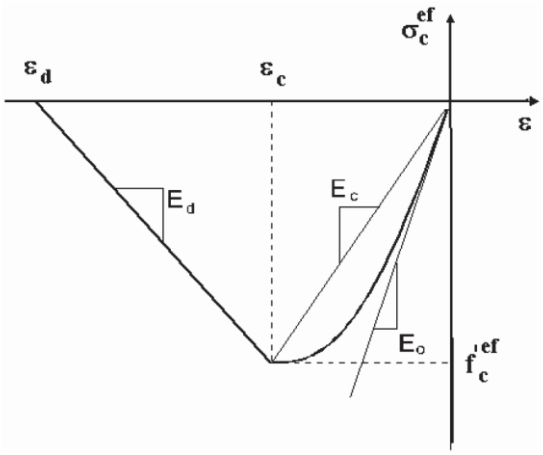

Figure 138. Compressive stress-strain diagram (Červenka et al. 2012)

5.2.2.d Compression after peak stress

The softening law in compression is linearly descending. There are two models of strain softening in compression, one based on dissipated energy, and the other based on local strain softening.

- *Fictitious Compression Plane Model*

The fictitious compression plane model is based on the assumption that compression failure is localized in a plane normal to the direction of compressive principal stress. All post-peak compressive displacements and energy dissipation are localized in this plane. It is assumed that this displacement is independent of the size of the structure. This hypothesis is supported by experiments conducted by Van MIER (1986).

This assumption is analogous to the Fictitious Crack Theory for tension, where the shape of the crack-opening law and the fracture energy are defined and are considered as material properties.

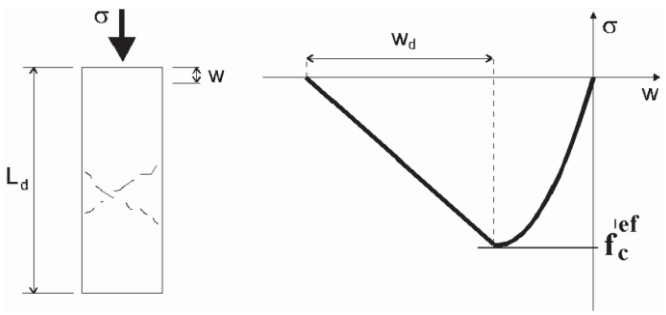

Figure 139. Softening displacement law in compression (Červenka et al. 2012)

In case of compression, the end point of the softening curve is defined by means of the plastic displacement w_d. In this way, the energy needed for generation of a unit area of the failure plane is indirectly defined. From the experiments of Van MIER (1986), the value of w_d = 0.5 mm for normal concrete. This value is used as default for the definition of the softening in compression.

The softening law is transformed from a fictitious failure plane, Figure 139, to the stress-strain relation valid for the corresponding volume of continuous material, Figure 138. The slope of the softening part of the stress-strain diagram is defined by two points: a peak of the diagram at the maximal stress and a compressive strain limit ε_d at the zero stress. This strain is calculated from a plastic displacement w_d and a band size L'_d according to the following expression:

$$\varepsilon_d = \varepsilon_c + \frac{w_d}{L'_d} \tag{57}$$

The advantage of this formulation is the reduced dependency on finite element mesh.

- *Compression Strain Softening Law Based on Strain*

A slope of the softening law is defined by means of the softening modulus E_d. This formulation is dependent on the size of the finite element mesh.

5.2.3 *Localization Limiters*

The so-called localization limiter controls localization of deformations in the failure state. It is a region (band) of material which represents a discrete failure plane in the finite element analysis. In tension it is a crack, in compression it is a plane of crushing. In reality these failure regions have some dimensions. However, since according to the experiments, the dimensions of the failure regions are independent of the structural size, they are assumed as fictitious planes. In case of tensile cracks, this approach is known as rack the "crack band theory", BAZANT, OH (1983). Here the same concept is also used for the compression failure. The purpose of the failure band is to eliminate two deficiencies, which occur in connection with the application of the finite element model: element size effect and element orientation effect (see Figure 140).

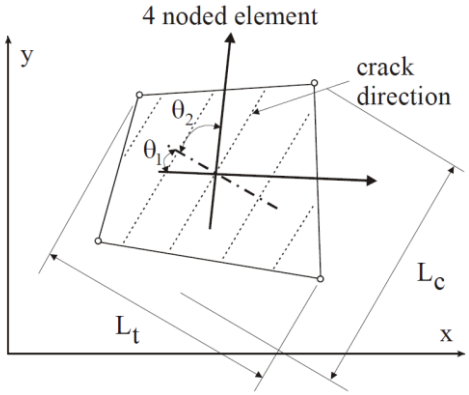

Figure 140. Definition of localization bands (Červenka et al. 2012)

5.2.4 *Fracture process, crack width*

The process of crack formation can be divided into three stages, Figure 141. The uncracked stage is before tensile strength is reached. The crack formation takes place in the process zone of a potential crack with decreasing tensile stress on a crack face due to a bridging effect. Finally, after a complete release of the stress, the crack opening continues without the stress.

The crack width w is calculated as a total crack opening displacement within the crack band.

$$w = \varepsilon_{cr} L'_t \tag{58}$$

where w_{cr} is the crack opening strain, which is equal to the strain normal to the crack direction in the cracked state after the complete stress release.

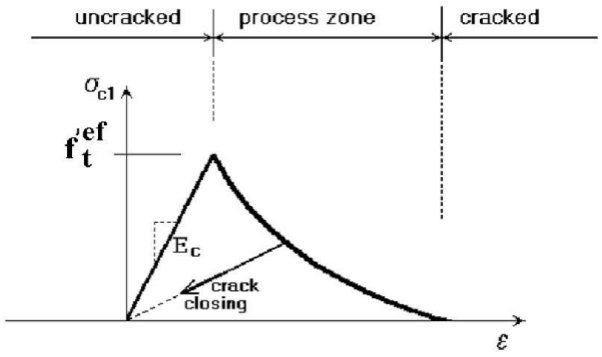

Figure 141. Stages of crack opening (Červenka et al. 2012)

It has been shown that the smeared model based on the refined crack band theory can successfully describe the discrete crack propagation in plain, as well as reinforced concrete (CERVENKA et al. 1991, 1992, and 1995).

It is also possible that the second stress, parallel to the crack direction, exceeds the tensile strength. Then the second crack, in the direction orthogonal to the first one, is formed using the same softening model as the first crack. (Note: The second crack may not be shown in a graphical post-processing. It can be identified by the concrete state number in the second direction at the numerical output.)

5.2.5 *Biaxial Stress Failure Criterion of Concrete*

5.2.5.a Compressive Failure

A biaxial stress failure criterion according to KUPFER et al. (1969) is used as shown in Figure 142.

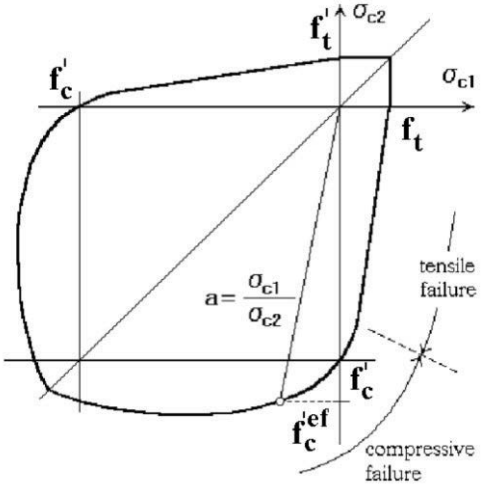

Figure 142. Biaxial failure function for concrete (Červenka et al. 2012)

In the compression-compression stress state the failure function is;

$$f'^{ef}_c = \frac{1+3.65a}{(1+a)^2} f'_c, \qquad a = \frac{\sigma_{c1}}{\sigma_{c2}} \tag{59}$$

where σ_{c1} and σ_{c2} are the principal stresses in concrete and f_c' is the uniaxial cylinder strength. In the biaxial stress state, the strength of concrete is predicted under the assumption of a proportional stress path.

In the tension-compression state, the failure function continues linearly from the point $\sigma_{c1} = 0$ and $\sigma_{c2} = f_c'$ into the tension-compression region with linearly decreasing strength:

$$f'^{ef}_c = f_c' r_{ec}, \qquad r_{ec} = \left(1 + 5.3278 \frac{\sigma_{c1}}{f_c'}\right), \qquad 1.0 \geq r_{ec} \geq 0.9 \tag{60}$$

where r_{ec} is the reduction factor of the compressive strength in the principal direction 2 due to the tensile stress in the principal direction 1.

5.2.5.b Tensile Failure

In the tension-tension state, the tensile strength is constant and equal to the uniaxial tensile strength f_t'. In the tension-compression state, the tensile strength is reduced by the relation:

$$f'^{ef}_t = f' r_{et} \tag{61}$$

where r_{et} is the reduction factor of the tensile strength in the direction 1 due to the compressive stress in the direction 2. The reduction function has one of the following forms, Figure 143.

$$r_{et} = 1 - 0.95 \frac{\sigma_{c2}}{f'_c} \tag{62}$$

$$r_{et} = \frac{A + (A-1)B}{AB}, \qquad B = Kx + A, \qquad x = \frac{\sigma_{c2}}{f'_c} \tag{63}$$

The relation in Equation (62) is the linear decrease of the tensile strength and Equation (63) is the hyperbolic decrease.

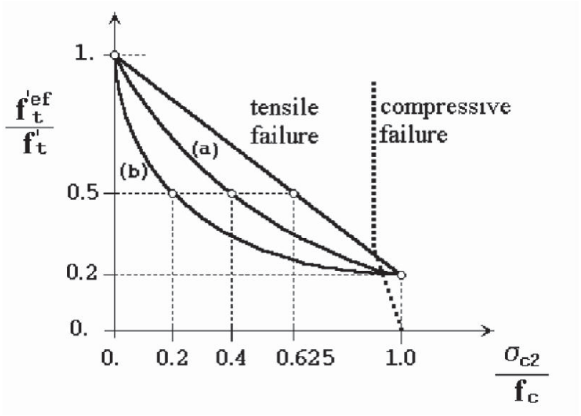

Figure 143. Tension-compression failure function for concrete (Červenka et al. 2012)

Two predefined shapes of the hyperbola are given by the position of an intermediate point *r* and *x*. Constants *K* and *A* define the shape of the hyperbola. The values of the constants for the two positions of the intermediate point are given in the following table.

Table 53. The values of constants related to Equation (63)

Type	Point		Parameters	
	r	x	A	K
a	0.5	0.4	0.75	1.125
b	0.5	0.2	1.0625	6.0208

5.2.6 *Crack modelling*

The smeared crack approach for modelling of the cracks is adopted in the model SBETA. Within the smeared concept, two options are available for crack models: the fixed crack model and the rotated crack model. In both models the crack is formed when the principal stress exceeds the tensile strength. It is assumed that the cracks are uniformly distributed within the material volume. This is reflected in the constitutive model by an introduction of orthotropy.

5.2.7 *Compressive Strength of Cracked Concrete*

A reduction of the compressive strength after cracking in the direction parallel to the cracks is done by a similar way as found from experiments of Vecchio and Collins (1982) and formulated in the Compression Field Theory. However, a different function is used for the reduction of concrete strength here, in order to allow for user's adjustment of this effect. This function has the form of the Gauss's function, Figure 144. The parameters of the function were derived from the experimental data published by

Kolleger et al. (1988), which included also data of Vecchio and Collins (Vecchio et al. 1982)

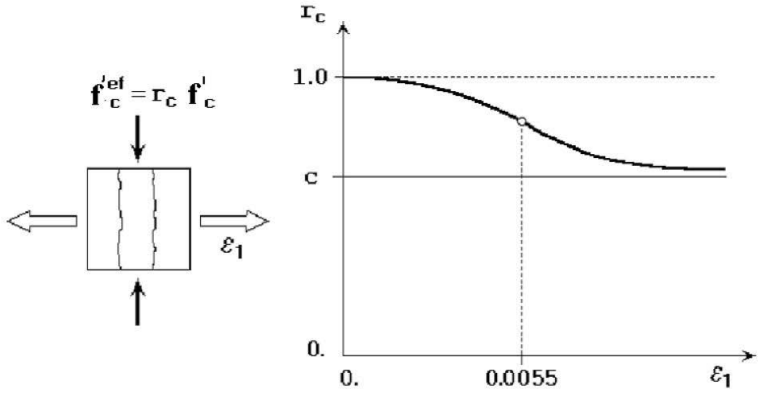

Figure 144. Compressive strength reduction of cracked concrete (Červenka et al. 2012)

$$f'^{ef}_c = r_c f'_c, \qquad r_c = c + (1-c)e^{-(128\varepsilon_u)^2} \tag{64}$$

For the zero normal strain (ε_υ) there is no strength reduction, and for the large strains, the strength is asymptotically approaching to the minimum value $f_c'^{ef} = cf_c'$.

The constant *c* represents the maximal strength reduction under the large transverse strain. From the experiments by Kolleger et al. (1988), the value *c* = 0.45 was derived for the concrete reinforced with the fine mesh. The other researchers (Dyngeland 1989) found the reductions not less than *c* = 0.8. The value of *c* can be adjusted by input data according to the actual type of reinforcing.

However, the reduction of compressive strength of the cracked concrete does not have to be effected only by the reinforcing. In the plain concrete, when the strain localizes in one main crack, the compressive concrete struts can cross this crack, causing so-called "bridging effect". The compressive strength reduction of these bridges is also captured by the above model.

5.2.8 *Tension Stiffening in Cracked Concrete*

The tension stiffening effect can be described as a contribution of cracked concrete to the tensile stiffness of reinforcing bars. This stiffness is provided by the uncracked concrete or not fully opened cracks and is generated by the strain localization process. It

was verified by simulation experiments of Hartl, G. (1977) and published in the paper (Margoldova et al. 1998).

Including an explicit tension stiffening factor would result in an overestimation of this effect. Therefore, in the ATENA versions up to1.2.0 no explicit tension stiffening factor is possible in the input.

5.2.9 *Material Stiffness Matrices*

5.2.9.a Uncracked Concrete

The material stiffness matrix for the uncracked concrete has the form of an elastic matrix of an isotropic material. It is written in the global coordinate system *x* and *y* as,

$$\mathbf{D}_c = \frac{E}{1-\nu^2}\begin{bmatrix} 1 & \nu & 0 \\ \nu & 1 & 0 \\ 0 & 0 & \frac{1-\nu}{2} \end{bmatrix} \tag{65}$$

In the above, *E* is the concrete elastic modulus derived from the equivalent uniaxial law. The Poisson's ratio (ν) is a constant.

5.2.9.b Cracked Concrete

For the cracked concrete, the matrix has the form of the elastic matrix for the orthotropic material. The matrix is formulated in a coordinate system *m1* and *m2,* which is coincident with the crack direction. This local coordinate system is referred to with superscript *L* later. The direction 1 is normal to the crack and the direction 2 is parallel to the crack. The definition of the elastic constants for the orthotropic material in the plane stress state follows from the flexibility relation:

$$\begin{Bmatrix} \varepsilon_1 \\ \varepsilon_2 \\ \gamma \end{Bmatrix} = \begin{bmatrix} \frac{1}{E_1} & -\frac{\nu_{21}}{E_2} & 0 \\ -\frac{\nu_{12}}{E_1} & \frac{1}{E_2} & 0 \\ 0 & 0 & \frac{1}{G} \end{bmatrix} \begin{Bmatrix} \sigma_1 \\ \sigma_2 \\ \tau \end{Bmatrix} \tag{66}$$

First we eliminate the orthotropic Poisson's ratios for the cracked concrete, because they are commonly not known. For this we use the symmetry relation $\nu_{12}E_2 = \nu_{21}E_1$.

Therefore, in Equation (66) there are only three independent elastic constants E_1, E_2 and v_2. Assuming that $\nu_{21} = \nu$ is the Poisson's ratio of the uncracked concrete and using the symmetry relation, we obtain;

$$\nu_{12} = \frac{E_1}{E_2}\nu \tag{67}$$

The stiffness matrix D_c^L is found as the inverse of the flexibility matrix in Equation (67):

$$\mathbf{D}_c{}^L = H\begin{bmatrix} \xi & \nu\xi & 0 \\ \nu\xi & 1 & 0 \\ 0 & 0 & G \end{bmatrix} \tag{68}$$

where;

$$\xi = \frac{E_1}{E_2}, \qquad H = E_1(1 - \xi\nu^2) \tag{69}$$

In the above relation E_2 must be non-zero. If E_2 is zero and E_1 is non-zero, then an alternative formulation is used with the inverse parameter; $\frac{1}{\zeta} = \frac{E_2}{E_1}$. In the case that both elastic moduli are zero, the matrix D_c^L is set equal to the null matrix.

The matrix D_c^L is transformed into the global coordinate system using the transformation matrix T_ε from Equation (46).

$$D_c = T_\varepsilon^T D_c^L T_\varepsilon \tag{70}$$

The angle α is between the global axis x and the 1st material axis m_1, which is normal to the crack.

5.2.9.c Smeared Reinforcement

The material stiffness matrix of the i^{th} smeared reinforcement is;

$$\mathbf{D}_{si} = p_i E_{si} \begin{bmatrix} \cos(\beta_i)^4 & \cos(\beta_i)^2 \sin(\beta_i)^2 & \cos(\beta_i)^3 \sin(\beta_i) \\ \cos(\beta_i)^2 \sin(\beta_i)^2 & \sin(\beta_i)^4 & \cos(\beta_i) \sin(\beta_i)^3 \\ \cos(\beta_i)^3 \sin(\beta_i) & \cos(\beta_i) \sin(\beta_i)^3 & \cos(\beta_i)^2 \sin(\beta_i)^2 \end{bmatrix} \quad (71)$$

The angle β is between the global axis x and the i^{th} reinforcement direction, and E_{si} is the elastic modulus of reinforcement. The reinforcing ratio $p_i = A_s / A_c$.

5.2.9.d Material Stiffness of Composite Material

The total material stiffness of the reinforced concrete is the sum of material stiffness of concrete and smeared reinforcement:

$$D = D_c + \sum_{i=1}^{n} D_{si} \quad (72)$$

The summation is over n smeared reinforcing components. In ATENA the smeared reinforcement is not added at the constitutive level, but is modelled by separate layers of elements whose nodes are connected to those of the concrete elements. This corresponds to the assumption of perfect bond between the smeared reinforcement and concrete.

Note: The material stiffness matrices are either secant or tangent, depending on the type of elastic modulus used. The secant material stiffness matrix is used to calculate the stresses for the given strains. The tangent material stiffness matrix is used to construct the element stiffness matrix.

5.2.10 *Analysis of Stresses*

The stresses in concrete are obtained using the actual secant component material stiffness matrix

$$S_c = D_c^s e \quad (73)$$

Where D_c^s is the secant material stiffness matrix for the uncracked or cracked concrete depending on the material state. The stress components are calculated in the global as well as in the local material coordinates (the principal stresses in the uncracked concrete and the stresses on the crack planes).

The stress in reinforcement and the associated tension stiffening stress is calculated directly from the strain in the reinforcement direction.

5.2.11 *Parameters of Constitutive Model*

The SBETA constitutive model of concrete includes 20 material parameters. These parameters are specified for the problem under consideration by user. In case the parameters are not known, automatic generation can be done using the default formulas (some of which are given in Table 54). In such a case, only the cube strength of concrete f'_{cu} (nominal strength) is specified and the remaining parameters are calculated as functions of the cube strength. The formulas for these functions are taken from the CEB-FIP Model Code 90 and other research sources. Used units are MPa.

Note: when simulating a real behaviour, the parameters should be chosen as close as possible to the properties of real materials. The best way is to determine these properties from mechanical tests on material sample specimens.

Table 54. Default formulas of material parameters (Červenka et al. 2012)

Parameter	Formula
Cylinder strength	$f'_c = -0.85 f'_{cu}$
Tensile strength	$f'_t = 0.24 f'^{2/3}_{cu}$
Initial elastic modulus	$E_c = (6000 - 15.5 f'_{cu}) \sqrt{f'_{cu}}$
Poisson's ratio	$\nu = 0.2$
Compressive strength in cracked concrete	$c = 0.8$
Tension stiffening stress	$\sigma_{st} = 0$
Fracture energy G_f according to VOS 1983	$G_F = 0.000025 f'^{ef}_t \left[MN/m\right]$

5.3 Finite element modelling

The beam geometry and 4-point monotonic test set up was first modelled in ATENA. The beam supports are the pin rollers which allow movement alongside the beam's horizontal axis. Since in real cases (experimental) the supports were not simple nodes and steel plates with a specific width were used, the same steel plates were modelled to simulate the real conditions. It should be noted that the beams rotate over one end of the steel plate. The loads were applied at one-third spans. Because the loads could not be applied as real point loads in the real condition and there is a width for the applied load, this simulation is also modelled as a small distributed load on each third span (Figure 145). The length of each distributed load is equal to the plates located under the load cells in the experimental tests.

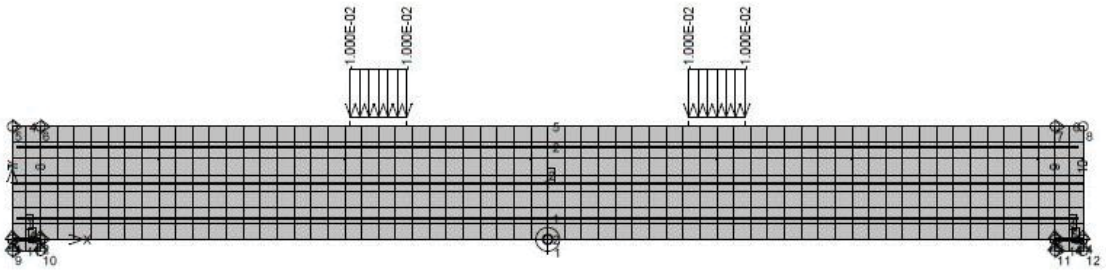

Figure 145. RC beam schematic modelled in ATENA

In the next stage, the material properties were allocated to the model. For the concrete material, the 'SBETA Material' as described in details in section 5.2 is utilised. The concrete properties presented in section 4.4.1 are assigned to the SBETA Material for each concrete beam. A screen shot is shown in Figure 146

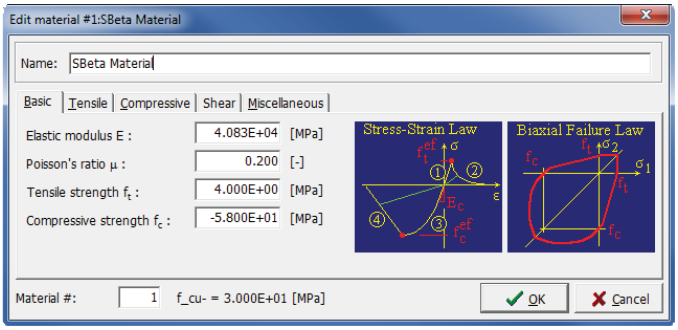

Figure 146. SBETA Material used in FE modelling

For the steel reinforcement, the 'Reinforcement' bilinear model with hardening as shown in Figure 147 is used. The mechanical properties of steel reinforcements are gathered from the test results presented in section 3.2.7.

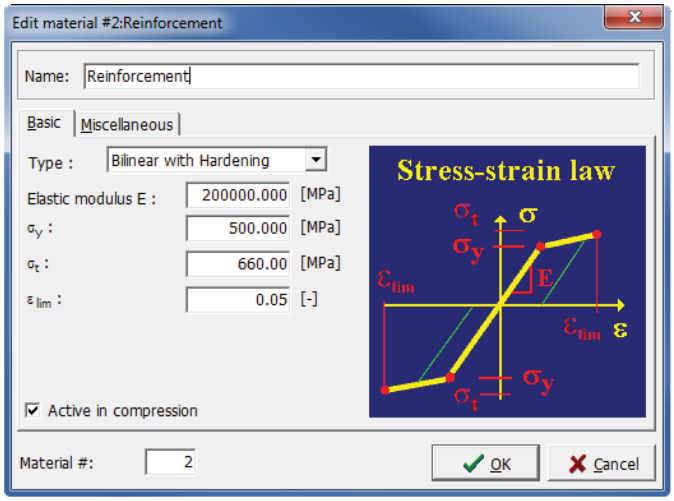

Figure 147. Reinforcement model used in FE modelling

Thereafter, the macro-element (mesh) sizes and analysis steps (load steps) are defined and model is run.

5.4 Mesh sensitivity analysis results

The physical mesh size may have a considerable effect on the element performance and influence the failure of structural elements. When analysing, the elements are broken into small pieces (sections) called mesh and the program analyses each section. The smaller the mesh, the more accurate the analysis can be.

It should be noted that very small mesh sizes may not necessarily give more accurate results i.e. where mesh size is very small the strain at failure may increase.

In this section, the mesh size effect is investigated to work out the limit up to which the results can be trusted. The original mesh size used for the analysis in this study is 30 mm. A mesh sensitivity analysis is performed for the mesh sizes; 10 mm, 30 mm and 50 mm. the results of this analysis are plotted in Figure 148.

From the graph, it can be observed that for the 50 mm mesh size, the results start to deviate from the maximum stress and is obviously generating incorrect data. The results of 10 and 30 mm mesh sizes seem to be very close showing that both mesh sizes are almost generating the same results and are reliable compared to the real test results.

However, since the analysis with mesh size of 10 mm takes much more time compared to that of the 30 mm mesh, the latter mesh size was selected for all the analyses in this study.

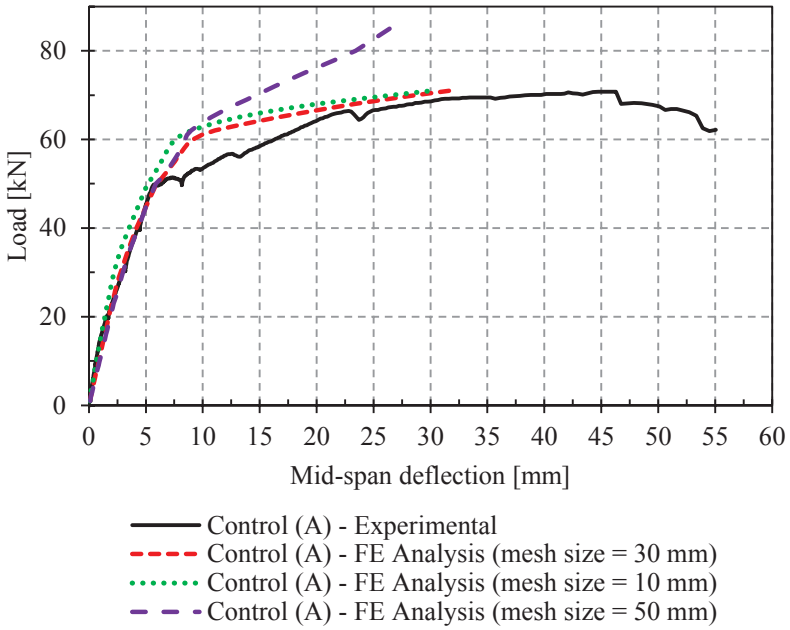

Figure 148. FE modelling result of beam Control (A)

5.5 Finite element analysis results

From the FE analyses, the results are derived and compared to those obtained from the experiments as shown in Figure 149 to Figure 153. The results show that by using ATENA, fairly accurate results can be gained. In the case of RC beams incorporating PVA fibres, since there is no built-in option in the software to model the synthetic fibre reinforced concrete, it was very complicated to model the post peak behaviour of FRC beams. Due to this fact, in such cases, the modelling was done by introducing only the mechanical properties of FRC concretes in the software (same as control concrete). In order to obtain more accurate results, the effects of pre-existing cracks as well as the temporal effects of creep and shrinkage were also considered in the model. To model these effects, beams were initially loaded up to a point before the cracking and unloaded back to zero.

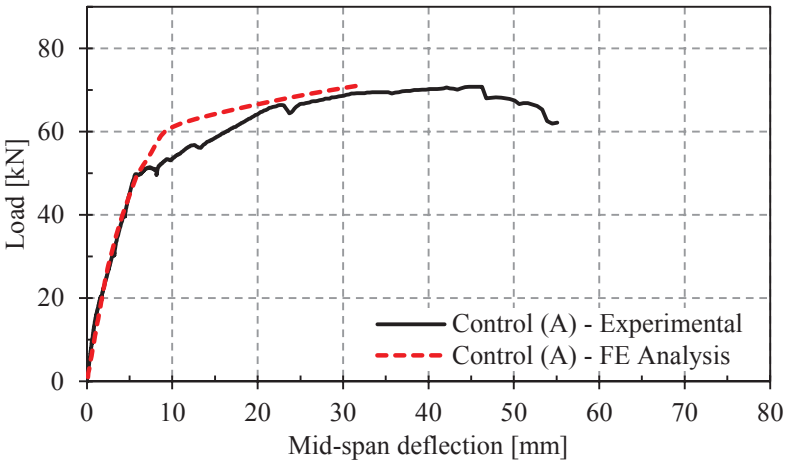

Figure 149. FE modelling result of beam Control (A)

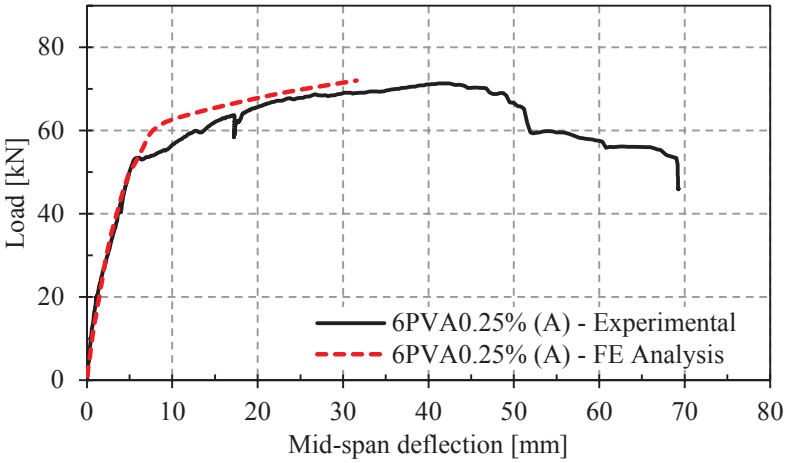

Figure 150. FE modelling result of beam 6PVA0.25% (A)

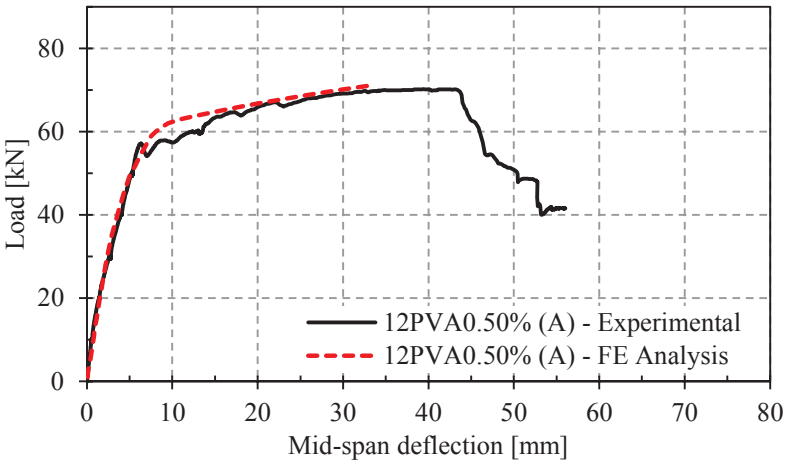

Figure 151. FE modelling result of beam 12PVA0.50% (A)

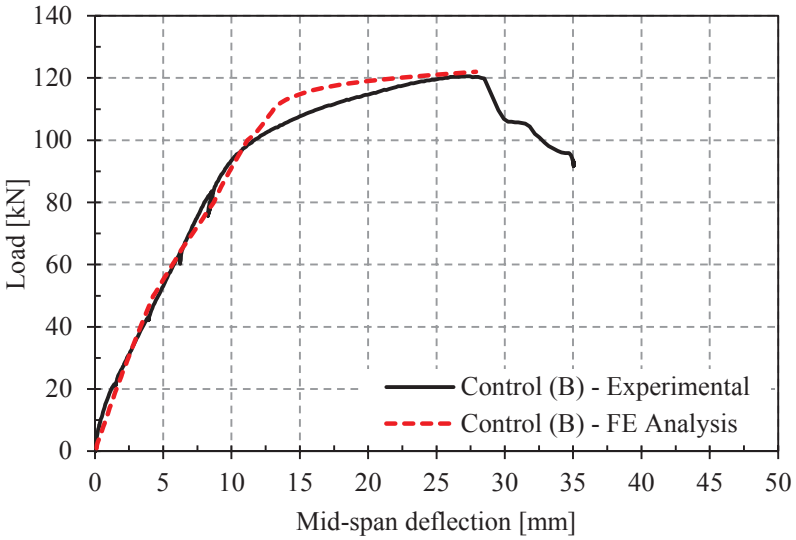

Figure 152. FE modelling result of beam Control (B)

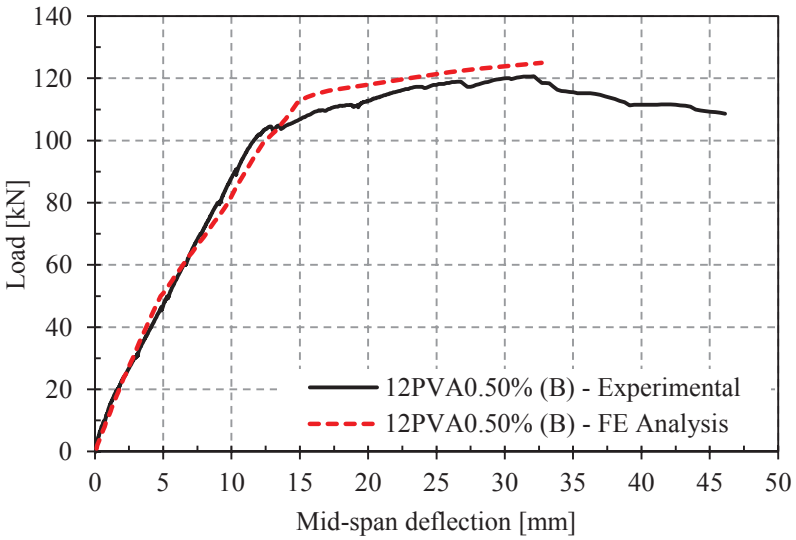

Figure 153. FE modelling result of beam 12PVA0.50% (B)

5.6 Concluding remarks

The results of finite element analysis using ATENA show that in both cases of non-FRC beams and FRC beams, fairly accurate results can be gained. However, it should be mentioned that the post peak behaviour of FRC beams is not captured by using this model. A developed model which could simulate each individual PVA fibre and it's effect when used in concrete matrix to produce more accurate data is worth considering in future studies.

Chapter 6

Summary and Conclusions

6.1 General remarks

6.2 Fresh properties of PVA-FRC

6.3 Mechanical (material) properties of PVA-FRC

6.4 Structural (static and dynamic) properties of PVA-FRC beam elements

6.5 Future works

6 SUMMARY AND CONCLUSSIONS

6.1 General Remarks

A systematic and comprehensive investigation has been undertaken on the effect of PVA fibre addition on mechanical and structural properties of conventional concrete incorporating fly ash.

Concrete mixes containing PVA fibres of varying length (6 and 12 mm) in different fibre volume fractions ranging from 0.125% - 1% were prepared and tested for their fresh and hardened properties. The optimum fibre contents in terms of FRC performance were selected to cast concrete beams. These beams have been tested for 4-point monotonic and 3-point cyclic in flexure, to assess their structural properties. Impact resonant frequency test was also conducted to evaluate the dynamic characteristics of Non-FRC and FRC specimens as well as RC beams.

The outcomes of the current research on PVA-FRC are presented under the following:

- ✓ Fresh Properties of PVA-FRC
- ✓ Mechanical (material) properties of PVA-FRC
- ✓ Structural (static and dynamic) properties of PVA-FRC beam elements

6.2 Fresh Properties of PVA-FRC

The overall objective of the fresh property tests was to investigate the effect of PVA fibre addition on the properties of freshly mixed concrete. The following conclusions can be drawn from the results obtained:

a) Less workability is observed for mixes having more fibre content and higher amount of HWR. Mixes with longer fibre length demonstrate lower slump compared to shorter fibre length for the same fibre volume addition. As a result, it can be stated that adding hydrophilic PVA fibre decreases concrete slump.

b) Compacting factor results show that the low additions of PVA fibres are insignificant in contributing to the concrete self-compaction characteristics, although a small decrease in the compaction factor has been recorded for FRCs compared to the control concrete.

c) Air content is slightly increased by introducing PVA fibres into concrete. (1.0 - 1.4% in case of FRCs compared to 1.0% for control concrete)

d) Mass per unit volume of concrete is seen to decrease by adding fibres to the mix (1% – 6% lower density for FRCs compared to the control). This is due to the lower density of the fibres contributing to a lower volume density.

6.3 Mechanical (material) properties of PVA-FRC

Evaluating the mechanical properties of PVA-FRCs is one of the main objectives of this research work. The following outcomes were achieved from the material testings and investigations:

a) Compressive strength at 28 days ($f_{c,28}$) increases with increasing PVA fibre addition and the optimum fibre volume fraction is found to be 0.25% with 12% improvement noted in $f_{c,28}$. It can also be concluded that shorter fibres increase compressive strength more compared to longer-length fibre. The average 28-day compressive strength of FRCs made with different volume fractions of 6 mm PVA fibre is shown to be 6.5% higher than that of control, while this value is 2.5% for FRCs made with 12 mm fibres.

b) PVA-FRCs provide for a more ductile mode of failure compared to control concrete devoid of fibre additions and strain at ultimate stress behaviour is observed to be higher with higher fibre contents. FRCs strain at peak stress (ε_{cu}) was ranging between 0.0026 to 0.0035 compared to 0.0025 for control concrete.

c) The same trend as compressive strength is also observed for tensile and flexural strength. The average additional strength development of 20% in flexure and 30% in splitting tensile at 0.25% volume fraction shows how PVA fibre can improve the properties of plain concrete.

d) MOE test results show that, PVA fibres in low volume fractions used in this study (0.25% and 0.50%) do not significantly affect the modulus of elasticity of concrete. Some variations are noticed at early ages (7 and 28 days) while at 56 days most FRCs have very close values (38.7 – 41.9 GPa) to that of control (41.4 GPa). However, it is anticipated that within the FRCs, adding more fibres will lead to a decrease in concrete modulus of elasticity and in a same fibre content longer fibres have lower MOE.

e) Residual flexural tensile strength results demonstrate that, prior to the peak, response of all concrete series is almost similar, showing the same stiffness. However, a slight improvement in post-peak flexural response of concrete having FA was observed compared to the conventional concrete (devoid of FA). It is worth noting that the limit of proportionality (LOP) of PVA-FRCs made with 0.5% of 6 and 12 mm fibres is found to be slightly higher than that of control concrete (4.8 and 5.0 MPa for FRCs compared to 4.6 MPa for control). Furthermore, the post-peak behaviour of PVA-FRCs was found to be approximately the same as control although a subtle improvement had occurred.

f) Damping ratio of all concretes is observed to decrease by ageing from 14 to 28 days. Moreover, it can be mentioned that addition of PVA fibres in low volume fraction used in this study has no significant effect on concrete damping ratio. The 28-day damping ratio of FRCs for transverse mode of vibration is ranging between 0.7 – 1.0 % which is very close to that of control (0.8%). However, comparing the results for damping ratio of conventional (devoid of FA) and control (including FA) concrete show that replacing 30% PC with FA leads to a lower damping ratio of concrete (comparing 0.9% for conventional concrete with 0.8% for control for 28-day transverse mode damping ratio).

6.4 Structural (static and dynamic) properties of PVA-FRC beam elements

In terms of structural properties, a detailed theoretical and experimental study was undertaken involving RC beam elements with and without PVA fibres with the following outcomes:

b) Results of 4-point flexural tests show that, amongst all concrete beams of series A, beam 6PVA-0.25% (A) ranked first in terms of ductility and post-peak behaviour. 40% higher value of ductility factor is recorded for this beam including 0.25% volume fraction of 6 mm fibre compared to the control. In concrete beams of series B, FRC beam including 0.50% volume fraction of 12 mm fibre showed approximately 30% higher ductility compared to the control beam.

c) From the cracking patterns of the beams tested for 4-point bending, it can be stated that the crack initiation was observed to happen at 20 kN for the control beam, while in the case of FRC beams the first crack was observed to happen between 30

to 40 kN. This is possibly due to the higher FRC's modulus of rupture compared to that of the control.

d) The test results show that RC beams (with and without PVA fibres) natural frequency for uncracked section remained constant until the cracking happens. Thereafter, a sudden drop in frequency was observed due to damage in the structure. For the cracked section, the frequency remained approximately the same with increasing load until failure.

e) Furthermore, for each concrete series of A and B, the frequency of RC beams changed by change in stiffness. This shows that the natural frequency of a beam element is proportional to its stiffness (EI). Consequently, a reduction in stiffness leads to a reduction in the natural frequencies.

f) Results of 3-point cyclic tests over concrete beams of series A and B show that little energy has been dissipated before concrete cracking and also during the elasto-plastic phase. The energy dissipation capacity of all RC beams, with and without PVA fibres, slightly increased by increasing loads until about the end of elasto-plastic phase. At the last stage of cyclic loading, where the steel reinforcements start to yield, a large amount of energy is dissipated. It is also observed that the damping ratios of fibre reinforced RC beams are very close to that of conventional (control) RC beams. In most cases the damping ratios in the first cycle (about first cracking) and the last cycle (about failure) are by far much higher than that of other cycles.

g) RC beams of series A, incorporating PVA fibres, have higher initial stiffness (11.4 and 24.6 kN/mm) and ultimate stiffness (5.9 and 7.1 kN/mm) compared to the control beam (initial stiffness; 10.1 kN/mm and ultimate stiffness; 5 kN/mm). FRC beams also have higher stiffness degradation rate within the first two cycles of loading, however, after that point they show higher capacity to maintain their stiffness during the test. Furthermore, they generally show slightly higher damping ratios compared to the control beam, except for the first and last cycles.

h) In concrete beams of series B, the beam incorporating 12 mm PVA fibre shows lower initial stiffness (9.7 kN/mm compared to 12 kN/mm) but higher ultimate stiffness compared to the control beam (6.4 kN/mm compared to 5.8 kN/mm). Moreover, the addition of PVA fibres in beams of series B decreases the stiffness

degradation rate. The beam having 0.5% of 12 mm PVA fibre maintained 66% of its initial stiffness where this value (k_u/k_0) is less than 50% for control beam. Furthermore, it is worth noting that the control beam shows slightly higher damping values compared to fibre reinforced RC beam.

i) The results of finite element analysis using ATENA show that in both cases of non-FRC beams and FRC beams, fairly accurate results can be gained.

6.5 Future works

A number of future research works beyond the scope of this study are suggested below;

a) In order to utilise the maximum achievable capacity of FRC composites, the fibre-matrix interaction is of great significance. Hence, a supplementary study investigating the effect of coated PVA fibres of higher diameters and longer length with adjusted bond characteristics is greatly encouraged. Carrying out the mentioned study, the ideal FRC composite behaviour may be achieved. In this case and at the fracture point, fibres pull out of the matrix while elongating and consequently, the highest achievable amount of energy will be dissipated within the material (Li et al. 2002).

b) An investigation on the mechanical and structural properties of PVA fibre reinforced self-compacting concrete (PVA-FRSCC) is warranted.

c) In order to reduce potential sustainability issues arising from the cement consumption in concrete, an investigation on PVA-FRC mixes incorporating higher amounts of supplementary cementitious materials such as FA and slag is highly recommended. This is also in line with the perspective of the ” Green Building Council Australia” ('*Green Building Council Australia*').

d) A long-term study into the creep performance of PVA-FRC structural elements is warranted. This is particularly valuable for the prestressed and post-tensioned concrete behaviour.

e) An investigation on fire exposed properties of PVA-FRC, including; the effect of PVA fibres on mitigating explosive spalling, the effects of PVA fibres on compressive strength at high temperatures (roughly 500 °C to 700 °C) and also the effects of PVA fibres on the residual strength (ambient strength after fire exposure) is recommended.

REFRENCES

Alhozaimy, A.M., Soroushian, P. & Mirza, F. 1996, 'Mechanical properties of polypropylene fiber reinforced concrete and the effects of pozzolanic materials', *Cement and Concrete Composites*, vol. 18, no. 2, pp. 85-92.

Alsayed, S.H. 1993, 'Flexural Deflection of Reinforced Fibrous Concrete Beams', *ACI Structural Journal*, vol. 90, no. 1, pp. 72-6.

Álvarez, M., Salas, J. & Veras, J. 1988, 'Properties of concrete made with fly ash', *International Journal of Cement Composites and Lightweight Concrete*, vol. 10, no. 2, pp. 109-20.

Amick, H. & Monteiro, P.J.M. 2005, 'Modification of concrete damping properties for vibration control in technology facilities', *Proceedings of SPIE - The International Society for Optical Engineering*, vol. 5933, pp. 1-12.

Amick, H. & Monteiro, P.J.M. 2006, 'Experimental determination of model damping in concrete beams', *ACI material Journal*, vol. 103, no. 3, pp. 153-60.

Anderson, T.L. 2005, *Fracture Mechanics: Fundamentals and Applications*, Third Edition edn, CRC Press, Colorado, USA.

Arisoy, B. 2002, 'Development and fracture evaluation of high performance fiber reinforced lightweight concrete', Wayne State University.

Arisoy, B. & Wu, H.-C. 2008, 'Material characteristics of high performance lightweight concrete reinforced with PVA', *Construction and Building Materials*, vol. 22, no. 4, pp. 635-45.

Arivalagan & Kandasamy 2009, 'Energy Abrorption Capacity of Composite Beams', *Engineering Science and Technology Review*, vol. 2, pp. 145-50.

Askegaard, V. & Langsoe, H.E. 1986, 'Correlation between changes in dynamic properties and remaining carrying capacity: Laboratory tests with reinforced concrete beams', *Material and Structures (RILEM)*, vol. 19, no. 109, pp. 11-9.

Bai, J., Wild, S., Ware, J.A. & Sabir, B.B. 2003, 'Using neural networks to predict workability of concrete incorporating metakaolin and fly ash', *Advances in Engineering Software*, vol. 34, no. 11–12, pp. 663-9.

Bai, W., Zhang, J., Yan, P. & Wang, X. 2009, 'Study on vibration alleviating properties of glass fiber reinforced polymer concrete through orthogonal tests', *Materials & Design*, vol. 30, no. 4, pp. 1417-21.

Balaguru, P.N. & Shah, S.P. 1992, *Fiber Reinforced Cement Composites*, McGraw Hill.

Bangi, M.R. & Horiguchi, T. 2012, 'Effect of fibre type and geometry on maximum pore pressures in fibre-reinforced high strength concrete at elevated temperatures', *Cement and Concrete Research*, vol. 42, no. 2, pp. 459-66.

Batson, G., Jenkins, E. & Spatney, R. 1972, 'Steel Fibers As Shear Reinforcement In Beams', *ACI Journal*, vol. 69, no. 10, pp. 640-4.

Bayasi, Z. & Zeng, J. 1993, 'Properties of Polypropylene Fiber Reinforced Concrete', *American Concrete Institute*, vol. 90, no. 6, pp. 605-10.

Bencardino, F., Rizzuti, L., Spadea, G. & Swamy, R.N. 2012, 'Implications of test methodology on post-cracking and fracture behaviour of Steel Fibre Reinforced Concrete', *Composites Part B: Engineering*, no. 0.

Bentur, A. & Mindess, S. 1983, 'Concrete beams reinforced with conventional steel bars and steel fibres: properties in static loading', *International Journal of Cement Composites and Lightweight Concrete*, vol. 5, no. 3, pp. 199-202.

Bentur, A. & Mindess, S. 1990, *Fiber Reinforced Cementitious Composites*, Elsevier Applied Science.

Bentur, A. & Mindess, S. 2007, *Fibre Reinforced Cementitious Composites*, second edn, Taylor & Francis, Abingdon, England.

Bentur, A., Peled, A. & Yankelevsky, D. 1997, 'Enhanced Bonding of Low Modulus Polymer Fibres-Cement Matrix By Means of Crimped Geometry', *Cement and Concrete Research*, vol. 27, no. 7, pp. 1099-111.

Béton, C.E.-I.d. 1993, *Ceb-Fip Model Code 1990: Design Code*, Thomas Telford.

Betterman, L.R., Ouyang, C. & Shah, S.P. 1995, 'Fiber-matrix interaction in microfiber-reinforced mortar', *Advanced Cement Based Materials*, vol. 2, no. 2, pp. 53-61.

Bouzoubaâ, N., Zhang, M.H. & Malhotra, V.M. 2001, 'Mechanical properties and durability of concrete made with high-volume fly ash blended cements using a coarse fly ash', *Cement and Concrete Research*, vol. 31, no. 10, pp. 1393-402.

Brandt, A.M. 1986, 'Influence of the fibre orientation on the energy absorption at fracture of SFRC specimens', in A.M. Brandt & I.H. Marshall (eds), *Brittle Matrix Composites I*, Elsevier Applied Science Publishers, London, pp. 403-20.

Buratti, N., Mazzotti, C. & Savoia, M. 2011, 'Post-cracking behaviour of steel and macro-synthetic fibre-reinforced concretes', *Construction and Building Materials*, vol. 25, no. 5, pp. 2713-22.

Carneiro, J.O., Demelo, F.J., Jalili, S., Teixera, V. & Tomas, M. 2006, 'The use of pseudo-dynamic method in the evaluation of damping characteristics in reinforced concrete beams having variable bending stiffness', *Mechanics Research Communications*, vol. 33, no. 5, pp. 601-13.

Červenka, V., Libor Jendele & Červenka, J. 2012, *ATENA Program Documentation-Part 1-Theory* Cervenka Consulting Ltd.

Chopra, A.K. 1995, *Dynamics of Structures: Theory and Applications to Earthquake Engineering*, Prentice Hall, New Jersey.

Chowdhury, S.H. 1999, 'Damping Characteristics of Reinforced and Partially Prestressed Concrete Beams', Griffith University, Gold Coast.

Cole, D.G. 1966, 'The damping capacity of hardened cement paste, mortar and concrete specimens', *Symposium Organised by the National Section of the International Association for Earthquake Engineering*, Imperial College of Science and Technology, London, pp. 235-347.

Cole, D.G. & Spooner, D.C. 1965, 'The damping capacity of hardened cement paste and mortar in specimens vibrating at very low frequencies', *Proceedings of American Society for Testing and Materials*, pp. 661-7.

Cooper, G.A. & Kelly, A. 1970, 'The contribution to the work of fracture of a composite material of pull-out fibres', in F.W. Wendt, H. Liebowitz & N. Perrone (eds), *Mechanics of composite materials*, Pergamon, Oxford, U.K., pp. 653-61.

Corinaldesi, V. & Moriconi, G. 2011, 'Characterization of self-compacting concretes prepared with different fibers and mineral additions', *Cement and Concrete Composites*, vol. 33, no. 5, pp. 596-601.

Craig, R. 1987, 'Flexural behaviour and design of reinforced fiber concrete members', paper presented to the *American Concrete Institute*, Fiber Reinforced Concrete Properties and Applications

De Nicolo, B., Pani, L. & Pozzo, E. 1994, 'Strain of concrete at peak compressive stress for a wide range of compressive strengths', *Materials and Structures*, vol. 27, no. 4, pp. 206-10.

Debs, E., Mounir, Montedor, C., L., Hanai, d. & B., J.o. 2006, 'Compression tests of cement-composite bearing pads for precast concrete connections', *Cement and Concrete Composites*, vol. 28, no. 7, pp. 621-9.

Di Maggio, R., Franchini, M., Guerrini, G., Poli, S. & Migliaresi, C. 1997, 'Fibre-matrix adhesion in fibre reinforced CAC-MDF composites', *Cement and Concrete Composites*, vol. 19, no. 2, pp. 139-47.

Fanella, D.A. & Naaman, A.E. 1985, 'Stress-strain properties of fiber reinforced mortar in compression', *ACI Journal proceedings*, vol. 82, ACI.

Feldman, D. 1989, *Polymeric Building Materials*, Elsevier Applied Science, London.

Felekoğlu, B., Tosun, K. & Baradan, B. 2009, 'Effects of fibre type and matrix structure on the mechanical performance of self-compacting micro-concrete composites', *Cement and Concrete Research*, vol. 39, no. 11, pp. 1023-32.

Feng, X. & Krark, B. 2001, 'Evaluation of the Physical and Chemical Properties of Fly Ash Products for Use in Portland Cement Concrete', *World of Coal Ash Conferance*, vol. Denver.

Fischer, G. & Li, V.C. 2007, 'Effect of fiber reinforcement on the response of structural members', *Engineering Fracture Mechanics*, vol. 74, no. 1–2, pp. 258-72.

Flores-Johnson, E.A. & Li, Q.M. 2012, 'Structural behaviour of composite sandwich panels with plain and fibre-reinforced foamed concrete cores and corrugated steel faces', *Composite Structures*, vol. 94, no. 5, pp. 1555-63.

Fraay, A.L.A., Bijen, J.M. & de Haan, Y.M. 1989, 'The reaction of fly ash in concrete a critical examination', *Cement and Concrete Research*, vol. 19, no. 2, pp. 235-46.

Frances Cyr, M. 2003, 'Hybrid-fibre reinforcement in extruded cementitious composites and cast concrete'.

Fu, S.-Y. & Lauke, B. 1996, 'Effects of fiber length and fiber orientation distributions on the tensile strength of short-fiber-reinforced polymers', *Composites Science and Technology*, vol. 56, no. 10, pp. 1179-90.

Fu, X. & Chung, D.D.L. 1996, 'Vibration damping admixtures for cement', *Cement and Concrete Research*, vol. 26, no. 1, pp. 69-75.

Gencel, O., Koksal, F., Ozel, C. & Brostow, W. 2012, 'Combined effects of fly ash and waste ferrochromium on properties of concrete', *Construction and Building Materials*, vol. 29, no. 0, pp. 633-40.

Gencturk, B.E., Amr S. 2011, *Multi-objective optimal seismic design of building using advanced engineering materials*, Research and Publications from the Mid-America Earthquake Center

Ghosni, N. 2012, 'Evaluation of Static and Dynamic Behaviour of Fibre reinforced Concrete Incorporating Polypropylene Fibres', University of Technology Sydney (UTS), Sydney.

Giaccio, G., Tobes, J.M. & Zerbino, R. 2008, 'Use of small beams to obtain design parameters of fibre reinforced concrete', *Cement and Concrete Composites*, vol. 30, no. 4, pp. 297-306.

Giner, V.T., Baeza, F.J., Ivorra, S., Zornoza, E. & Galao, Ó. 2012, 'Effect of steel and carbon fiber additions on the dynamic properties of concrete containing silica fume', *Materials & Design*, vol. 34, no. 0, pp. 332-9.

Gopalaratnam, V., Shah, S. & Batson, G. 1991, 'Fracture toughness of fiber reinforced concrete', *Material Journal*, vol. 88, no. 4, pp. 339-53.

Gopalaratnam, V.S. & Gettu, R. 1995, 'On the characterization of flexural toughness in fiber reinforced concretes', *Cement and Concrete Composites*, vol. 17, no. 3, pp. 239-54.

'*Green Building Council Australia*', *Green Building Council Australia*, *<http://www.gbca.org.au/green-star/>*.

Hamoush, S., Abu-Lebdeh, T. & Cummins, T. 2010, 'Deflection behavior of concrete beams reinforced with PVA micro-fibers', *Construction and Building Materials*, vol. 24, no. 11, pp. 2285-93.

Han, C.-G., Han, M.-C. & Heo, Y.-S. 2009, 'Improvement of residual compressive strength and spalling resistance of high-strength RC columns subjected to fire', *Construction and Building Materials*, vol. 23, no. 1, pp. 107-16.

Hannant, D.J. 1980, 'Polymer fibre reinforced cement and concrete', *Advances in Cement-Matrix Composites*, eds D.M. Roy, A.J. Majumdar, S.P. Shah & J.A. Manson, Materials Research Society, Pittsburgh, PA, pp. 171-80.

Hannant, D.J. 2003, 'Fibre-reinforced concrete', in J. Newman & B.S. Choo (eds), *Advanced Concrete Technology Set*, Butterworth-Heinemann, Oxford, pp. 6/1-6/17.

Hannant, D.J., Zonsveld, J.J. & Hughes, D.C. 1978, 'Polypropylene film in cement based materials', *Composites*, vol. 9, no. 2, pp. 83-8.

Hassan, A.M.T. & Jones, S.W. 2012, 'Non-destructive testing of ultra high performance fibre reinforced concrete (UHPFRC): A feasibility study for using ultrasonic and resonant frequency testing techniques', *Construction and Building Materials*, vol. 35, no. 0, pp. 361-7.

Heo, Y.-S., Sanjayan, J.G., Han, C.-G. & Han, M.-C. 2012, 'Relationship between inter-aggregate spacing and the optimum fiber length for spalling protection of concrete in fire', *Cement and Concrete Research*, vol. 42, no. 3, pp. 549-57.

Hota, S. & Naaman, A.E. 1997, 'Bond Stress-Slip Response of Reinforcing Bars Embedded in FRC Matrices under Monotonic and Cyclic Loading ', *ACI Structural Journal* vol. 94, no. 5, pp. 525-37.

James, M. & Lutes, L. 1964, 'Damping proprties of reinfored and prestresed concrete structural components', *American Concrete Institute*, vol. 61, no. 11, pp. 1359-81.

Jastrzebski, J.D. 1977, *The Nature and Properties of Engineering Materials*, Second edition edn, John Wiley & Sons, New York.

Jeong, S.M. 1994, 'Evaluation of ductility in prestressed concrete beams using fiberreinforced plastic tendons', University of Michigan, Ann Arbor, Michigan, US.

Jinping, O., Tiejun, L. & Jilong, L. 2008, 'Dynamic and Seismic property experiments of high damping concrete and its frame models', *Jurnal of Wuhan university of technology-Mater.Si.Ed*

Jones, R. 1957, 'The effect of frequency on the damping modulus and damping coefficient of concrete', *Magazine of Concrete Research*, vol. 9, no. 26, pp. 69-72.

Jordan, R.W. 1980, 'The effect of stress,frequency, curing , mix and age upon the damping of concrete', *Magazine of Concrete Research*, vol. 23, no. 113, pp. 195-205.

Kesler, C.E. & Y.Higuchi 1954, 'Problems in the sonic test of concrete', paper presented to the *The international symposium on the non-destructuve testing of materials and structures*, Paris.

Kong, H.-J., Bike, S.G. & Li, V.C. 2003, 'Constitutive rheological control to develop a self-consolidating engineered cementitious composite reinforced with hydrophilic poly(vinyl alcohol) fibers', *Cement and Concrete Composites*, vol. 25, no. 3, pp. 333-41.

Kou, S.-C. & Poon, C.-S. 2010, 'Properties of concrete prepared with PVA-impregnated recycled concrete aggregates', *Cement and Concrete Composites*, vol. 32, no. 8, pp. 649-54.

Krenchel, H. & Shah, S.P. 1986, *Synthetic fibre for tough and durable concrete*, RILEM Symp., Sheffield.

Kwak, H.-G. & Kim, S.-P. 2002, 'Nonlinear analysis of RC beams based on moment–curvature relation', *Computers & Structures*, vol. 80, no. 7–8, pp. 615-28.

Lam, L., Wong, Y.L. & Poon, C.S. 1998, 'Effect of Fly Ash and Silica Fume on Compressive and Fracture Behaviors of Concrete', *Cement and Concrete Research*, vol. 28, no. 2, pp. 271-83.

Lepech, M.D. & Li, V.C. 2009, 'Water permeability of engineered cementitious composites', *Cement and Concrete Composites*, vol. 31, no. 10, pp. 744-53.

Li, D., Hai, C. & Jinping, O. 2012, 'Fracture behavior and damage evaluation of polyvinyl alcohol fiber concrete using acoustic emission technique', *Materials & Design*, vol. 40, no. 0, pp. 205-11.

Li, Q. & Xu, S. 2009, 'Experimental investigation and analysis on flexural performance of functionally graded composite beam crack-controlled by ultrahigh toughness cementitious composites', *Science in China Series E: Technological Sciences*, vol. 52, no. 6, pp. 1648-64.

Li, V.C. 1992, 'A simplified micromechanical model of compressive strength of fiber-reinforced cementitious composites', *Cement and Concrete Composites*, vol. 14, no. 2, pp. 131-41.

Li, V.C. 1998, 'Engineered Cementitious Composites-Tailored Composites Through Micromechanical Modeling', in N. Banthia, A. Bentur & a.A. Mufti (eds), *Fiber Reinforced Concrete: Present and the Future*, Canadian Society for Civil Engineering, Montreal, pp. 64-97.

Li, V.C. 2003, 'On Engineered Cementitious Composites (ECC); A Review of the Material and Its Applications', *Journal of Advanced Concrete Technology*, vol. 1, no. 3, pp. 215-30.

Li, V.C. 2008, *Engineered cementitious composites (ECC) material, structural and durability performance*, CRC Press.

Li, V.C., Kanda, T. & Lin, Z. 1997, 'The influence of fibre/matrix interface properties on complementary energy and composite damage tolerance', *3rd Conference on Fracture and Strength of Solids*, Hong Kong, pp. 456-72.

Li, V.C. & Maalej, M. 1996, 'Toughening in cement based composites. Part II: Fiber reinforced cementitious composites', *Cement and Concrete Composites*, vol. 18, no. 4, pp. 239-49.

Li, V.C. & Stang, H. 1997, 'Interface property characterization and strengthening mechanisms in fiber reinforced cement based composites', *Advanced Cement Based Materials*, vol. 6, no. 1, pp. 1-20.

Li, V.C. & Wang, S. 2006, 'Microstructure variability and macroscopic composite properties of high performance fiber reinforced cementitious composites', *Probabilistic Engineering Mechanics*, vol. 21, no. 3, pp. 201-6.

Li, V.C., Wang, S. & Wu, C. 2001, 'Tensile strain-hardening behavior or polyvinyl alcohol engineered cementitious composite (PVA-ECC)', *ACI Materials Journal*, vol. 98, no. 6, pp. 483-92.

Li, V.C., Wang, Y. & Backer, S. 1991, 'Fibre-Reinforced Cementitious Materials', *Materials Research Society Symposium Proceeding (S. Mindess and J. Skalny Eds.),*, vol. 211.

Li, V.C., Ward, R. & Hamza, A.M. 1992, 'Steel And Synthetic Fibers As Shear Reinforcement', *J. Materials, American Concrete Institute*, vol. 89, no. 4, pp. 499-508.

Li, V.C., Wu, C., Wang, S., Ogawa, A. & Saito, T. 2002, 'Interface Tailoring for Strain-Hardening Polyvinyl Alcohol-Engineered Cementitious Composite (PVA-ECC)', *ACI Materials Journal*, vol. 99, no. 5, pp. 463-72.

Lim, T., Paramasivam, P. & Lee, S. 1987, 'Behavior of Reinforced Steel Fiber Concrete Beams in Flexure', *Journal of Structural Engineering*, vol. 113, no. 12, pp. 2439-58.

Lin, Z. & Li, V.C. 1997, 'Crack bridging in fibre reinforced cementitious composites with slip-hardening interfaces', *Journal of the Mechanics and Physics of Solids*, vol. 45, no. 5, pp. 763-87.

Low, N.M.P. & Beaudoin, J.J. 1994, 'The flexural toughness and ductility of portland cement-based binders reinforced with wollastonite micro-fibres', *Cement and Concrete Research*, vol. 24, no. 2, pp. 250-8.

Malhotra, V.M. 1990, 'Durability of concrete incorporating high-volume of low-calcium (ASTM Class F) fly ash', *Cement and Concrete Composites*, vol. 12, no. 4, pp. 271-7.

Manolis, G.D., Gareis, P.J., Tsonos, A.D. & Neal, J.A. 1997, 'Dynamic properties of polypropylene fiber-reinforced concrete slabs', *Cement and Concrete Composites*, vol. 19, no. 4, pp. 341-9.

Manz, O.E. 1999, 'Coal fly ash: a retrospective and future look', *Fuel*, vol. 78, no. 2, pp. 133-6.

Mechtcherine, V., Millon, O., Butler, M. & Thoma, K. 2011, 'Mechanical behaviour of strain hardening cement-based composites under impact loading', *Cement and Concrete Composites*, vol. 33, no. 1, pp. 1-11.

Meda, A., Minelli, F. & Plizzari, G.A. 2012, 'Flexural behaviour of RC beams in fibre reinforced concrete', *Composites Part B: Engineering*, vol. 43, no. 8, pp. 2930-7.

Meddah, M.S. & Bencheikh, M. 2009, 'Properties of concrete reinforced with different kinds of industrial waste fibre materials', *Construction and Building Materials*, vol. 23, no. 10, pp. 3196-205.

Mehta, P.K. & Monteiro, P.J.M. 2005, *Concrete: Microstructure, Properties, and Materials*, 3 edn, McGraw-Hill Professional.

Menefy, L. 2007, 'Investigation of reactive powder concrete and it's damping characteristics when utilised in beam elements', Griffith University, Gold Coast.

Meyer, C. 2009, 'The greening of the concrete industry', *Cement and Concrete Composites*, vol. 31, no. 8, pp. 601-5.

Midwest-Research-Institute 1994, *Emission Factor Documentation for AP-42 Section 11.6,Portland Cement Manufacturing*, U. S. Environmental Protection Agency Office of Air Quality Planning and Standards Emission Inventory Branch.

Mindess 2007a, *Thirty years of Fibre Reinforced Concrete research at the UWM British Colombia*, Sustainable construction materials and technologies.

Mindess, S. 2007b, *Fibre Reinforced Cementitious Composites*, Taylor & Francis.

Mindess, S., Banthia, N. & Bentur, A. 1986, 'The response of reinforced concrete beams with a fibre concrete matrix to impact loading', *International Journal of Cement Composites and Lightweight Concrete*, vol. 8, no. 3, pp. 165-70.

Mobasher, B., Stang, H. & Shah, S. 1990, 'Microcracking in fibre reinforced concrete', *Cement and Concrete Research*, vol. 20, pp. 665-76.

Naaman, A.E., Buschow, K.H.J., Robert, W.C., Merton, C.F., Bernard, I., Edward, J.K., Subhash, M. & Patrick, V. 2001, 'Reinforced Concrete', in, *Encyclopedia of Materials: Science and Technology*, Elsevier, Oxford, pp. 8095-109.

Naaman, A.E. & Reinhardt, H.W. 1996, 'High performance fibre reinforced cementitious composites', *RILEM proc. 31*, E & FN Spon, London.

Nelson & Hancock 1979, 'Interfacial slip and damping in fibre reinforced composites', *Journal of Materials Science*, vol. 13, no. 3, pp. 2429-40.

Neville, A. 1991, *Properties of Concrete*, Fourth And Final Edition edn.

Nili, M. & Afroughsabet, V. 2012, 'The long-term compressive strength and durability properties of silica fume fiber-reinforced concrete', *Materials Science and Engineering: A*, vol. 531, no. 0, pp. 107-11.

Ong, K.C.G., Basheerkhan, M. & Paramasivam, P. 1999, 'Resistance of fibre concrete slabs to low velocity projectile impact', *Cement and Concrete Composites*, vol. 21, no. 5-6, pp. 391-401.

Ou, J.P. 2002, 'Smart Concrete Products and structural Systems', *Control and Health monitoring of Structures*, pp. 4-5.

Padron, I. & Zollo, R.F. 1990, 'Effect of synthetic fibers on volume stability and cracking of Portland cement concrete and mortar', *ACI J.*, vol. 87, no. 4, pp. 327-32.

Pantazopoulou, S.J. & Zanganeh, M. 2001, 'Triaxial Tests of Fiber-Reinforced Concrete', *Journal of Materials in Civil Engineering*, vol. 13, no. 5, pp. 340-8.

Park, R. 1988, 'Ductility evaluation from laboratory and analytical testing', *The 9th world conference on earthquake engineering*, vol. 8, pp. 605-16.

Patton, M.E. & Whittaker, W.L. 1990, 'Effect of Fiber Content and Damaging Load of Steel Fiber Reinforced Concrete Stiffness', *ACI Journal*, vol. 80, no. 1, pp. 13-6.

Penzien, J. 1964, 'Damping characterisitics of prestressed concrete', *Journal of the American Concrete Institude*, vol. 61, no. 9, pp. 1125-48.

Penzien, J. & Hansen, R.J. 1954, 'Static and dynamic elastic behaviour of reinforced concrete beams', *American Concrete Institute*, vol. 50, no. 7, pp. 545-67.

Perumalsamy, N.B. & Surendra, P.S. 1992, *Fiber-reinforced cement composites*, McGraw-Hill, New York.

Purkiss, J.A. & Blagojević, P. 1993, 'Comparison between the short and long term behaviour of fibre reinforced and unreinforced concrete beams', *Composite Structures*, vol. 25, no. 1–4, pp. 45-9.

Radtke, F., Simone, A. & Sluys, L. 2012, 'A computational model for failure analysis of fibre reinforced concrete with discrete treatment of fibres', *Engineering Fracture Mechanics*, vol. 77, pp. 597-620.

Ramadevi, K. & Venkatesh Babu, D.L. 2012, 'Flexural Behavior of Hybrid (Steel-Polypropylene) Fibre Reinforced Concrete Beams ', *European Journal of Scientific Research*, vol. 70, no. 1, pp. 81-7.

Ramamurty, K. & Narayanan, N. 2000, 'Factors influencing the density and compressive strength of aerated concrete', *Magazine of Concrete Research*, vol. 52, no. 3, pp. 163–8.

Raphael, J.M. 1984, 'Tensile strength of concrete', *Concrete International*, vol. 81, no. 2, pp. 158-65.

Razak, H.A. & Choi, F.C. 2001, 'The effect of corrosion on the natural frequency and modal damping of reinforced concrete beams', *Engineering Structures*, vol. 23, no. 9, pp. 1126-33.

Redon, C., Li, V.C., Wu, C., Hoshiro, H., Saito, T. & Ogawa, A. 2001, 'Measuring and modifying interface properties of PVA fibres in ECC matrix', *ASCE Journal of Materials in Civil Engineering*, vol. 13, no. 6, pp. 399-406.

Redon, C., Li, V.C., Wu, C., Hoshiro, H., Saito, T. & Ogawa, A. 2004, 'Measuring and modifying interface properties of PVA fibers in ECC matrix', *ASCE Journal of Materials in Civil Engineering*.

Rinaldi, Z., Grimaldi, A., Fischer, G. & Li, V. 2006, 'Influence of high performance fiber reinforced concrete on the ductility of beam elements', *International RILEM Workshop on High Performance Fiber Reinforced Cementitious Composites in Structural Applications*, RILEM Publications SARL, pp. 433-41.

Romualdi & Batson 1963, 'Mechanics of crack arrest in Concrete', *ASCE Journal of Engineering Mechanics* vol. 89, pp. 147-68.

Romualdi & Mandel 1964, "Tensile strength of concrete affected by uniformly distributed closely spaced short length of wire reinforcement', *American concrete institute*, vol. 61, no. 657-671.

Şahin, R., Demirboğa, R., Uysal, H. & Gül, R. 2003, 'The effects of different cement dosages, slumps and pumice aggregate ratios on the compressive strength and densities of concrete', *Cement and Concrete Research*, vol. 33, no. 8, pp. 1245-9.

Şahmaran, M., Lachemi, M., Hossain, K.M.A. & Li, V.C. 2009, 'Internal curing of engineered cementitious composites for prevention of early age autogenous shrinkage cracking', *Cement and Concrete Research*, vol. 39, no. 10, pp. 893-901.

Şahmaran, M. & Li, V.C. 2007, 'De-icing salt scaling resistance of mechanically loaded engineered cementitious composites', *Cement and Concrete Research*, vol. 37, no. 7, pp. 1035-46.

Şahmaran, M. & Li, V.C. 2008, 'Durability of mechanically loaded engineered cementitious composites under highly alkaline environments', *Cement and Concrete Composites*, vol. 30, no. 2, pp. 72-81.

Şahmaran, M. & Li, V.C. 2009, 'Durability properties of micro-cracked ECC containing high volumes fly ash', *Cement and Concrete Research*, vol. 39, no. 11, pp. 1033-43.

Şahmaran, M., Özbay, E., Yücel, H.E., Lachemi, M. & Li, V.C. 2012, 'Frost resistance and microstructure of Engineered Cementitious Composites: Influence of fly ash and micro poly-vinyl-alcohol fiber', *Cement and Concrete Composites*, vol. 34, no. 2, pp. 156-65.

Sakulich, A.R. & Li, V.C. 2011, 'Nanoscale characterization of engineered cementitious composites (ECC)', *Cement and Concrete Research*, vol. 41, no. 2, pp. 169-75.

Shen, B., Hubler, M., Paulino, G.H. & Struble, L.J. 2008, 'Functionally-graded fiber-reinforced cement composite: Processing, microstructure, and properties', *Cement and Concrete Composites*, vol. 30, no. 8, pp. 663-73.

Shimizu, K., Kanakubo, T., Kanda, T. & Nagai, S. 2004, 'Shear behaviour of steel reinforced PVA-ECC beams', paper presented to the *13th World Conference on Earthquake Engineering*, Vancouver, B.C., Canada.

Siddique, R. 2004, 'Performance characteristics of high-volume Class F fly ash concrete', *Cement and Concrete Research*, vol. 34, no. 3, pp. 487-93.

Sivakuram, A. & Sathanam, M. 2007, 'Mechanical properties of high strength concrete reinforced with metallic and non-metallic fibers', *Cement and Concrete Composites*, vol. 29, pp. 603-8.

Smith, J.W. 1988, *Vibration of Structures: Application in civil engineering design*, Chapman and Hall, London.

Soliman, A.E.-k.S. & Osman, M.a.-m. 2012, 'Efficiency of using discrete fibers on the shear behavior of R.C. beams', *Ain Shams Engineering Journal*, vol. 3, no. 3, pp. 209-17.

Soroushian, P. & Bayasi, Z. 1991, 'Fiber Type Effects on the Performance of Steel Fiber Reinforced Concrete ', *Fiber Type Effects on the Performance of Steel Fiber Reinforced Concrete* vol. 88, no. 2, pp. 359-66.

Standard, A. 2010, *General purpose and blended cements*, vol. AS 3972, Australian Standard.

Stang, H. & Aarre, T. 1992, 'Evaluation Of Crack Width In FRC With Conventional Reinforcement', *Cement & Concrete Composite*, vol. 14, no. 2, pp. 143-54.

Stang, H., Li, V.C. & Krenchel, H. 1995, 'Design And Structural Applications Of Stress-Crack Width Relations In Fiber Reinforced Concrete', *RILEM J. of Materials and Structures*, vol. 28, pp. 210-9.

Sukontasukkul, P., Pomchiengpin, W. & Songpiriyakij, S. 2010, 'Post-crack (or post-peak) flexural response and toughness of fiber reinforced concrete after exposure to high temperature', *Construction and Building Materials*, vol. 24, no. 10, pp. 1967-74.

Sun, C.T., Chaturvedi, S.K. & Gibson, R.F. 1985, 'Internal damping of short-fiber reinforced polymer matrix composites', *Computers & Structures*, vol. 20, no. 1â€“3, pp. 391-400.

Sun, P. & Wu, H.-C. 2008, 'Transition from brittle to ductile behavior of fly ash using PVA fibers', *Cement and Concrete Composites*, vol. 30, no. 1, pp. 29-36.

Sun, W., Chen, H., Luo, X. & Qian, H. 2001, 'The effect of hybrid fibers and expansive agent on the shrinkage and permeability of high-performance concrete', *Cement and Concrete Research*, vol. 31, no. 4, pp. 595-601.

Swamy, N. & Rigby, G. 1971, 'Dynamic properties of hardened paste, mortar and concrete', *Materials and Structures*, vol. 4, no. 1, pp. 13-40.

Swamy, R. 1974, 'The technology of steel fibre-reinforced concrete for practical applications', *Proceedings of the Institution of Civil Engineers, London, May 1994*, vol. 56(1), no. 1, pp. pp.143-59.

Swamy, R.N. 1970, 'Damping mechanism in cementitious systems', paper presented to the *Dynamic waves in civil engineering*, University College of Swansea.

Swamy, R.N. & Al-Ta'an, S.A. 1981, 'Deformation and Ultimate Strength in Flexure of Reinforced Concrete Beams Made with Steel Fiber Concrete', *ACI Journal*, vol. 78, no. 5, pp. 395-405.

Swamy, R.N. & Mangat, P.S. 1974, 'Influence of fiber geometry on the properties of steel fiber reinforced concrete', *Cement and Concrete Research*, vol. 4, no. 3, pp. 451-65.

Tadjiogueu, E.W. 1980, 'NONLINEAR ANALYSIS OF REINFORCED CONCRETE BEAMS BY THE FINITE-ELEMENT METHOD', Ph.D. thesis, State University of New York at Buffalo, Ann Arbor.

Tasdemir, M.A., Tasdemir, C., Akyüz, S., Jefferson, A.D., Lydon, F.D. & Barr, B.I.G. 1998, 'Evaluation of strains at peak stresses in concrete: A three-phase composite model approach', *Cement and Concrete Composites*, vol. 20, no. 4, pp. 301-18.

Tedesco, J.W., McDougal, W.G. & Ross, C.A. 1999, *Structural Dynamics: Theory and Applications*, Addison-Wesley.

Thomson, W.T. 1940, 'Measuring changes in physical properties of concrete by the dynamic method', vol. 40, proceeding of the American Society of Testing and Materials, pp. 1113-8.

Toutanji, H., Xu, B., Gilbert, J. & Lavin, T., 'Properties of poly(vinyl alcohol) fiber reinforced high-performance organic aggregate cementitious material: Converting brittle to plastic', *Construction and Building Materials*, vol. 24, no. 1, pp. 1-10.

Vandenberghe, R.E., de Resende, V.G., da Costa, G.M. & De Grave, E. 2010, 'Study of loss-on-ignition anomalies found in ashes from combustion of iron-rich coal', *Fuel*, vol. 89, no. 9, pp. 2405-10.

Wang, Y., Backer, S. & Li, V.C. 1989, 'A statistical tensile model of fibre reinforced cementitious composites', *Composites*, vol. 20, no. 3, pp. 265-74.

Wang, Z., Man, X., Finch, R.D. & Jansen, B.H. 1998, 'Dynamic behaviour and vibration monitoring of reinforced concrete beams', *Journal of Testing and Evaluation*, vol. 26, no. 5, pp. 405-19.

Warner, R.F., Foster, S.J. & Kilpatrick, A.E. 2007, *Reinforced Concrete Basics: Analysis and Design of Reinforced Concrete Structures*, Pearson Prentice Hall.

Wight, J.K. & MacGregor, J.G. 2011, *Reinforced Concrete: Mechanics and Design*, Pearson Education, Limited.

Wu, H.C. & Sun, P. 2003, *High performance masonry units from 100% fly ash: synergistic approach*, Wayne State University.

Xu, B., Toutanji, H.A. & Gilbert, J. 2010, 'Impact resistance of poly(vinyl alcohol) fiber reinforced high-performance organic aggregate cementitious material', *Cement and Concrete Research*, vol. 40, no. 2, pp. 347-51.

Yan, L., Jenkins, C.H. & Pendleton, R.L. 2000a, 'Polyolefin fiber-reinforced concrete composites: Part I. Damping and frequency characteristics', *Cement and Concrete Research*, vol. 30, no. 3, pp. 391-401.

Yan, L., Jenkins, C.H. & Pendleton, R.L. 2000b, 'Polyolefin fiber-reinforced concrete composites: Part II. Damping and interface debonding', *Cement and Concrete Research*, vol. 30, no. 3, pp. 403-10.

Yang, E.-H. & Li, V.C. 2012, 'Tailoring engineered cementitious composites for impact resistance', *Cement and Concrete Research*, vol. 42, no. 8, pp. 1066-71.

Yang, E.H. 2008, 'Designing added functions in Engineered cementitious composites', The University of Michigan.

Yeung, L.S.Y. 2008, 'A new finite element for reinforced concrete beam analyses including shear', M.A.Sc. thesis, University of Toronto (Canada), Ann Arbor.

Zensveld, J.J. 1975, 'Properties and testing of concrete containing fibres other than steel', *Fibre Reinforced Cement and Concrete*, ed. A. Neville, The Construction Press, Lancaster, England, pp. 217-26.

Zhang, J. & Li, V.C. 2002, 'Monotonic and fatigue performance in bending of fiber-reinforced engineered cementitious composite in overlay system', *Cement and Concrete Research*, vol. 32, no. 3, pp. 415-23.

Zheng, L., Sharon Huo, X. & Yuan, Y. 2008, 'Experimental investigation on dynamic properties of rubberized concrete', *Construction and Building Materials*, vol. 22, no. 5, pp. 939-47.

Zheng, W., Li, H. & Wang, Y. 2012, 'Compressive behaviour of hybrid fiber-reinforced reactive powder concrete after high temperature', *Materials & Design*, vol. 41, no. 0, pp. 403-9.

Zheng, Z. & Feldman, D. 1995, 'Synthetic fibre-reinforced concrete', *Progress in Polymer Science*, vol. 20, no. 2, pp. 185-210.

Zollo, R.F. 1997, 'Fiber-reinforced concrete: an overview after 30 years of development', *Cement and Concrete Composites*, vol. 19, no. 2, pp. 107-22.

APPENDIX A

One sample of acceleration-time history and three samples of Frequency Response Function (FRF) graphs for each of the control and FRC mixes, in transverse and longitudinal modes of vibration, at the testing ages of 14 and 28 days are presented in this appendix.

Note: Regarding the material's transverse and longitudinal fundamental frequencies, the first or the most dominant frequency peak in the FRF graph is taken as the frequency of the first mode.

A.1 Transverse and longitudinal mode acceleration-time history

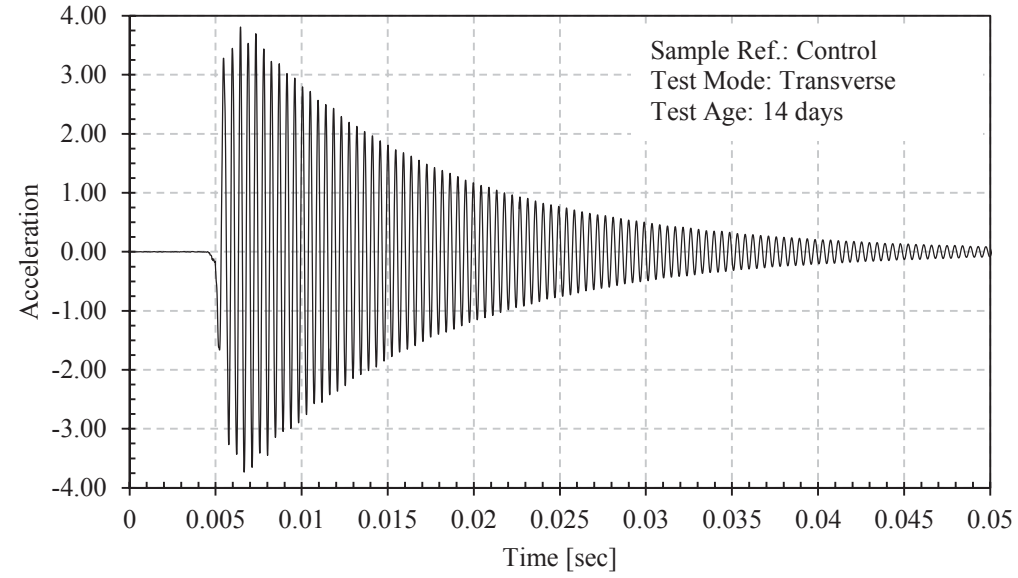

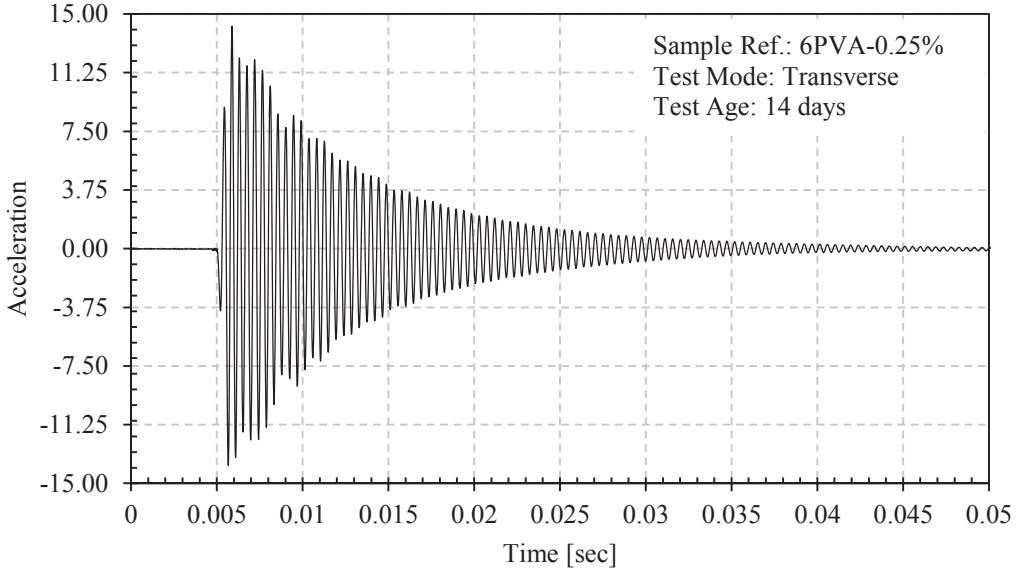

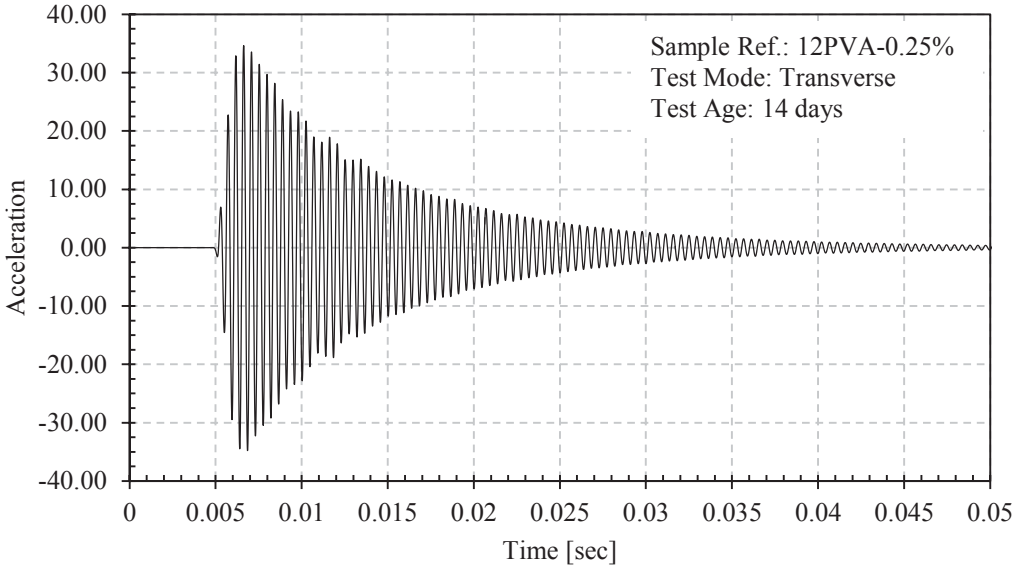
Sample Ref.: 12PVA-0.25%
Test Mode: Transverse
Test Age: 14 days
Acceleration
40.00
30.00
20.00
10.00
0.00
-10.00
-20.00
-30.00
-40.00
0
0.005
0.01
0.015
0.02
0.025
0.03
0.035
0.04
0.045
0.05
Time [sec]

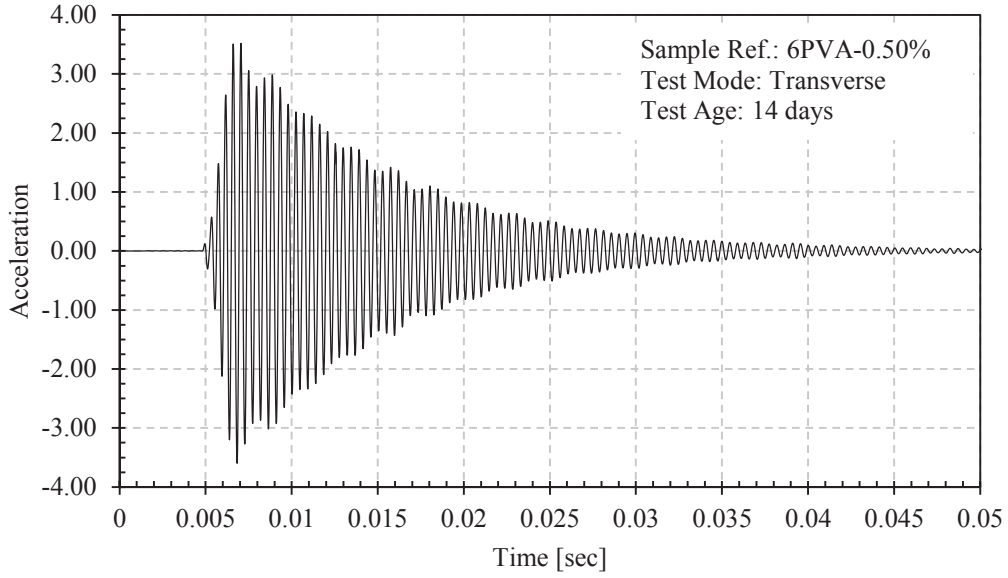
Sample Ref.: 6PVA-0.50%
Test Mode: Transverse
Test Age: 14 days
Acceleration
4.00
3.00
2.00
1.00
0.00
-1.00
-2.00
-3.00
-4.00
0
0.005
0.01
0.015
0.02
0.025
0.03
0.035
0.04
0.045
0.05
Time [sec]

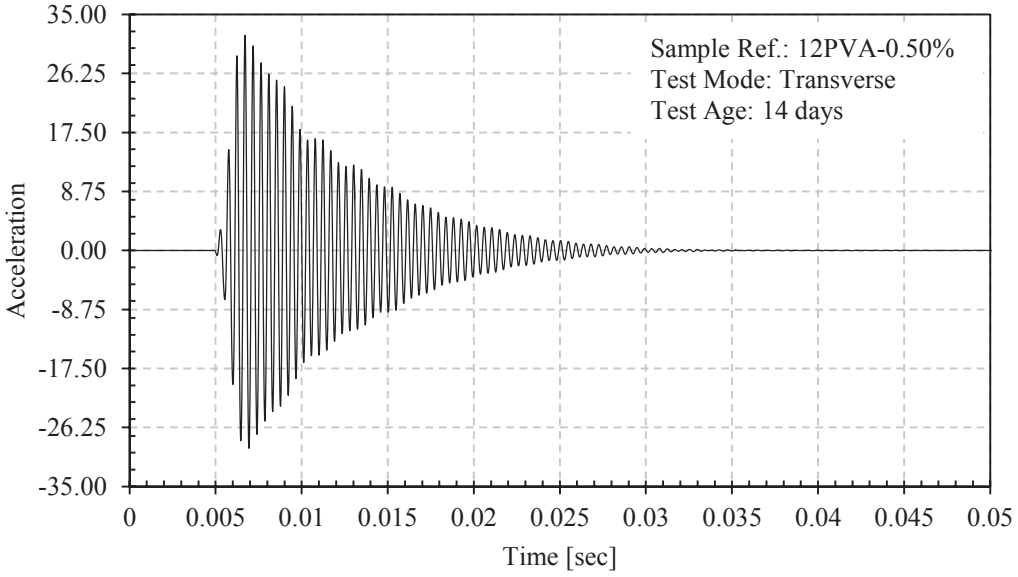
Sample Ref.: 12PVA-0.50%
Test Mode: Transverse
Test Age: 14 days
Acceleration
35.00
26.25
17.50
8.75
0.00
-8.75
-17.50
-26.25
-35.00
0
0.005
0.01
0.015
0.02
0.025
0.03
0.035
0.04
0.045
0.05
Time [sec]

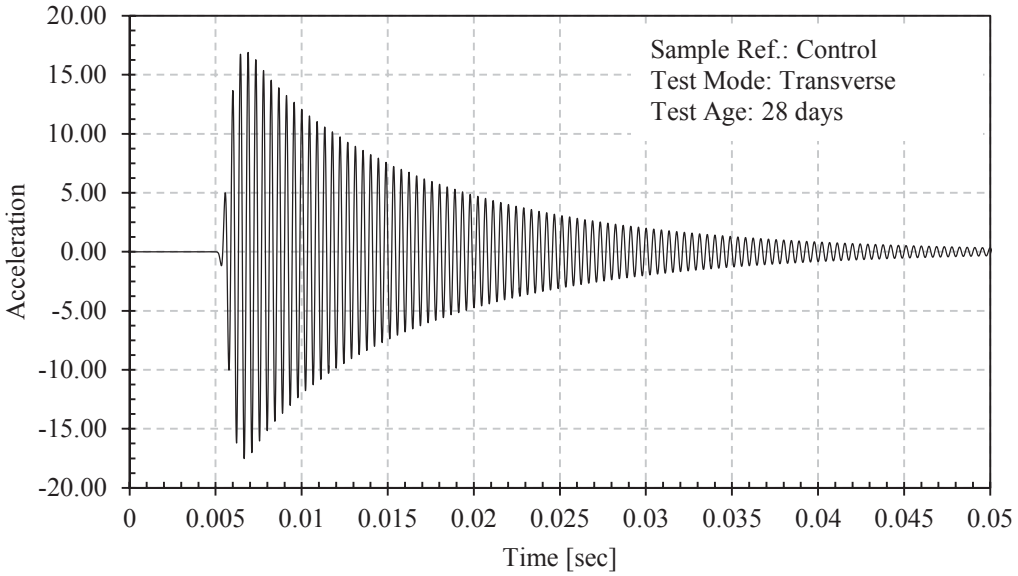
Sample Ref.: Control
Test Mode: Transverse
Test Age: 28 days
Acceleration
Time [sec]
20.00
15.00
10.00
5.00
0.00
-5.00
-10.00
-15.00
-20.00
0
0.005
0.01
0.015
0.02
0.025
0.03
0.035
0.04
0.045
0.05

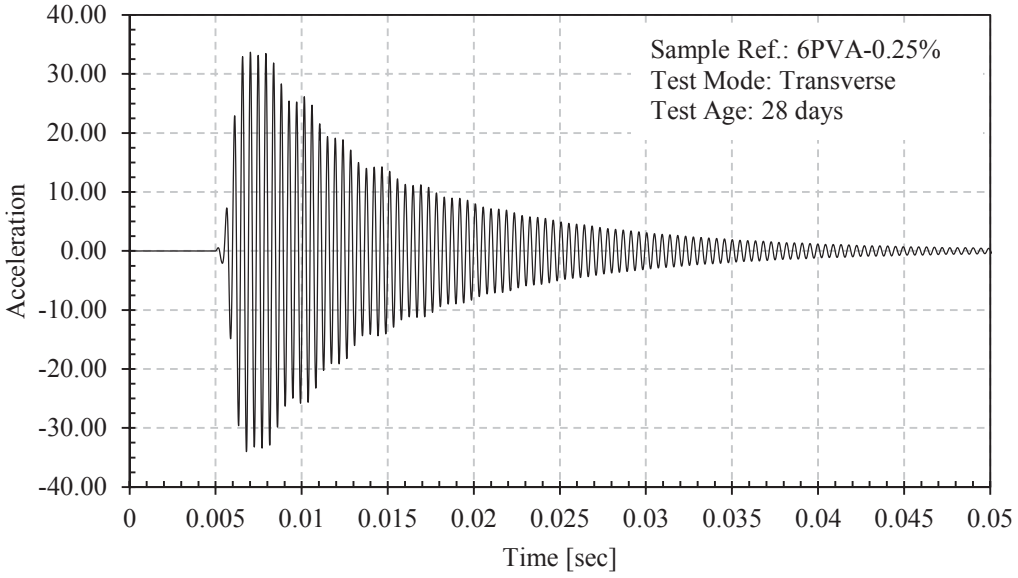
Sample Ref.: 6PVA-0.25%
Test Mode: Transverse
Test Age: 28 days
Acceleration
Time [sec]
40.00
30.00
20.00
10.00
0.00
-10.00
-20.00
-30.00
-40.00
0
0.005
0.01
0.015
0.02
0.025
0.03
0.035
0.04
0.045
0.05

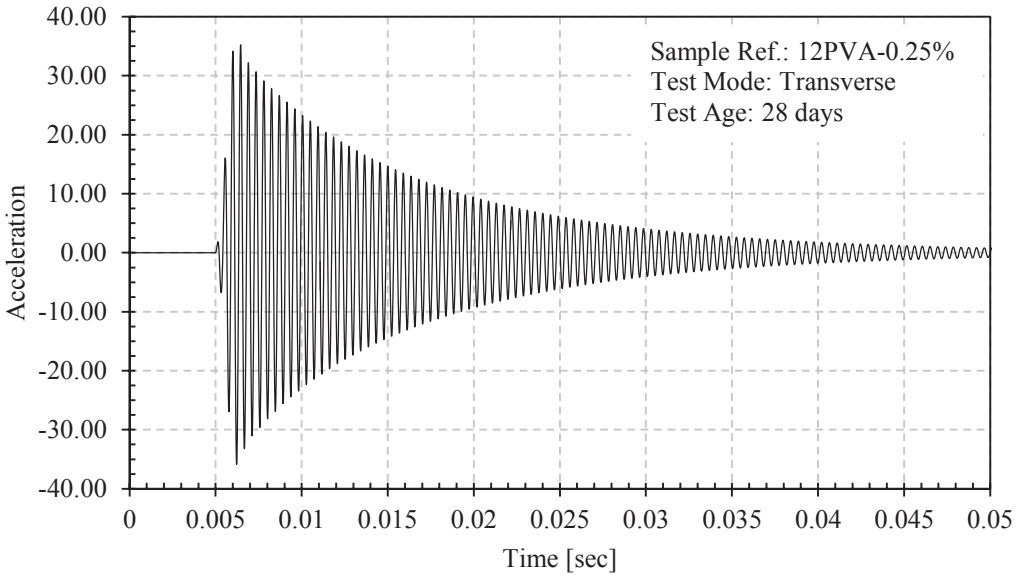
Sample Ref.: 12PVA-0.25%
Test Mode: Transverse
Test Age: 28 days
Acceleration
Time [sec]
40.00
30.00
20.00
10.00
0.00
-10.00
-20.00
-30.00
-40.00
0
0.005
0.01
0.015
0.02
0.025
0.03
0.035
0.04
0.045
0.05

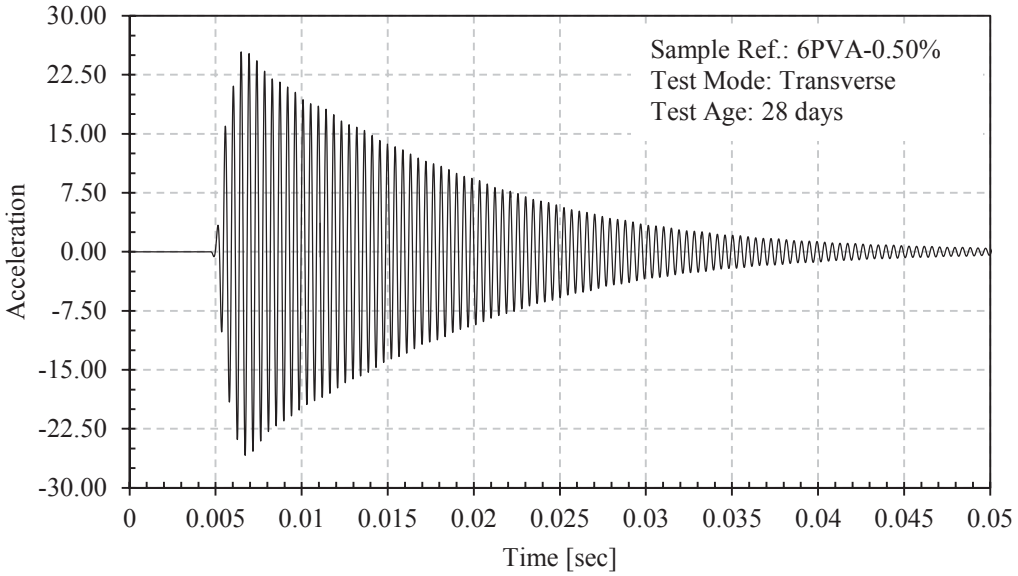
Sample Ref.: 6PVA-0.50%
Test Mode: Transverse
Test Age: 28 days
Acceleration
30.00
22.50
15.00
7.50
0.00
-7.50
-15.00
-22.50
-30.00
0
0.005
0.01
0.015
0.02
0.025
0.03
0.035
0.04
0.045
0.05
Time [sec]

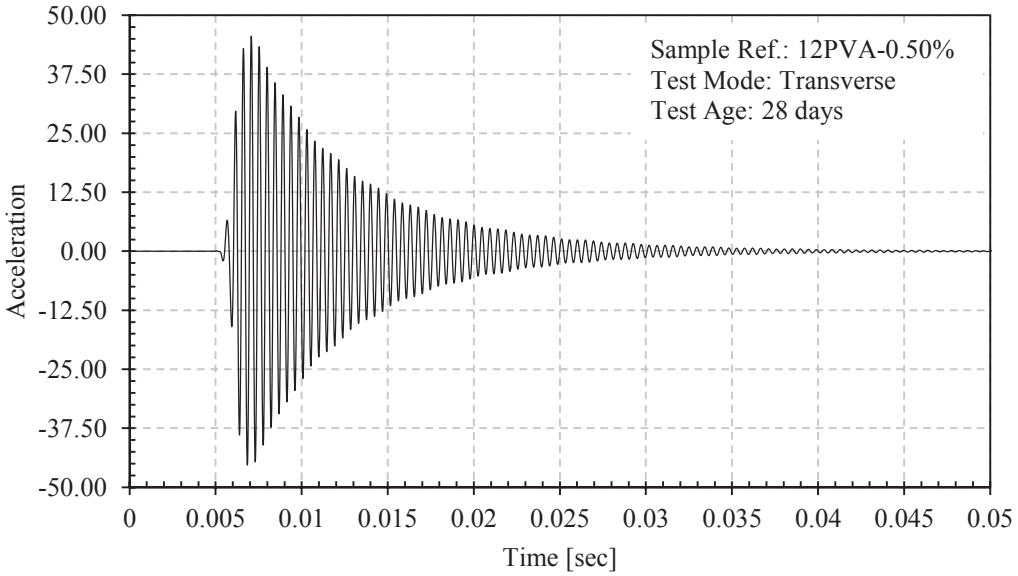
Sample Ref.: 12PVA-0.50%
Test Mode: Transverse
Test Age: 28 days
Acceleration
50.00
37.50
25.00
12.50
0.00
-12.50
-25.00
-37.50
-50.00
0
0.005
0.01
0.015
0.02
0.025
0.03
0.035
0.04
0.045
0.05
Time [sec]

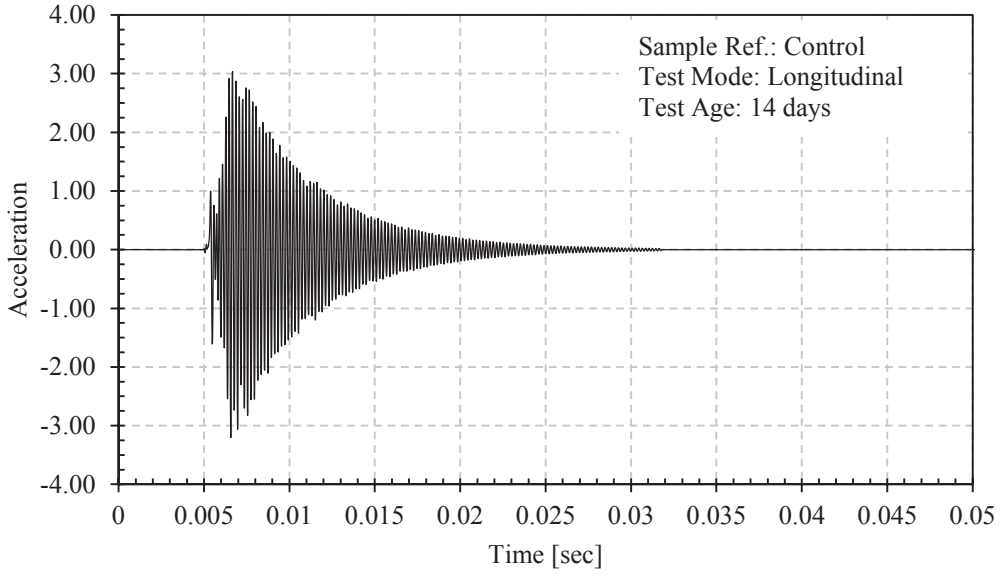
Sample Ref.: Control
Test Mode: Longitudinal
Test Age: 14 days
Acceleration
4.00
3.00
2.00
1.00
0.00
-1.00
-2.00
-3.00
-4.00
0
0.005
0.01
0.015
0.02
0.025
0.03
0.035
0.04
0.045
0.05
Time [sec]

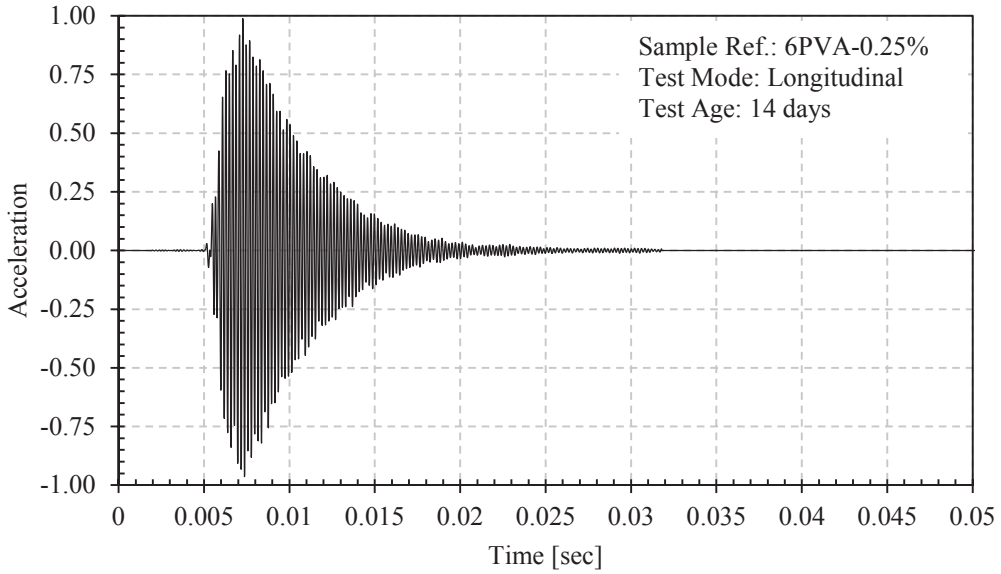
Sample Ref.: 6PVA-0.25%
Test Mode: Longitudinal
Test Age: 14 days
Acceleration
1.00
0.75
0.50
0.25
0.00
-0.25
-0.50
-0.75
-1.00
0
0.005
0.01
0.015
0.02
0.025
0.03
0.035
0.04
0.045
0.05
Time [sec]

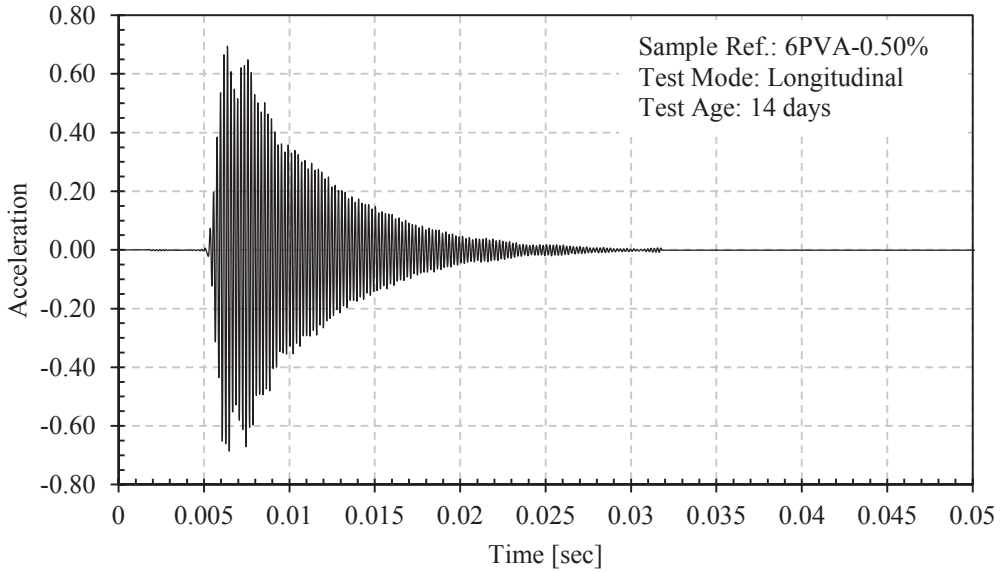
Sample Ref.: 6PVA-0.50%
Test Mode: Longitudinal
Test Age: 14 days
Acceleration
0.80
0.60
0.40
0.20
0.00
-0.20
-0.40
-0.60
-0.80
0
0.005
0.01
0.015
0.02
0.025
0.03
0.035
0.04
0.045
0.05
Time [sec]

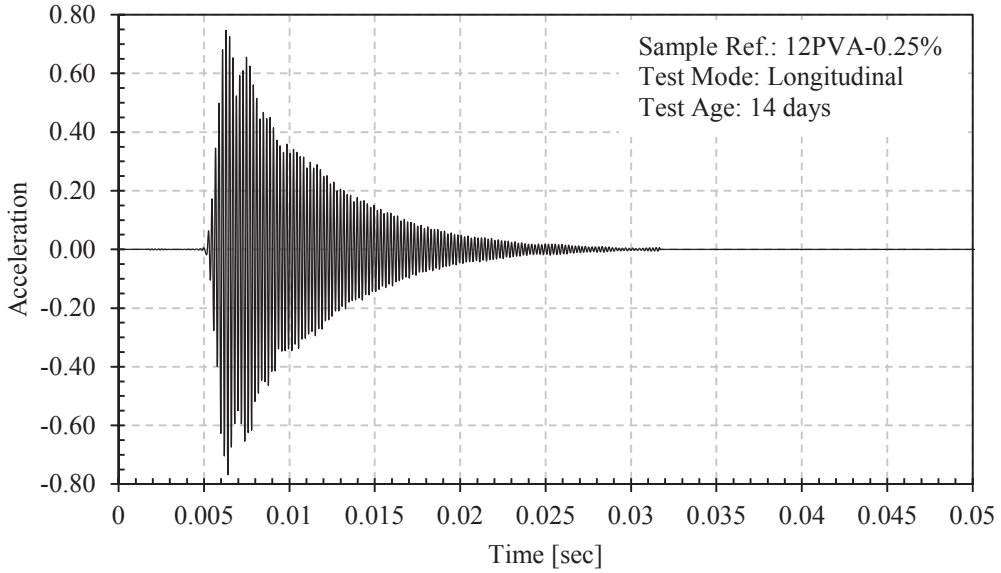
Sample Ref.: 12PVA-0.25%
Test Mode: Longitudinal
Test Age: 14 days
Acceleration
0.80
0.60
0.40
0.20
0.00
-0.20
-0.40
-0.60
-0.80
0
0.005
0.01
0.015
0.02
0.025
0.03
0.035
0.04
0.045
0.05
Time [sec]

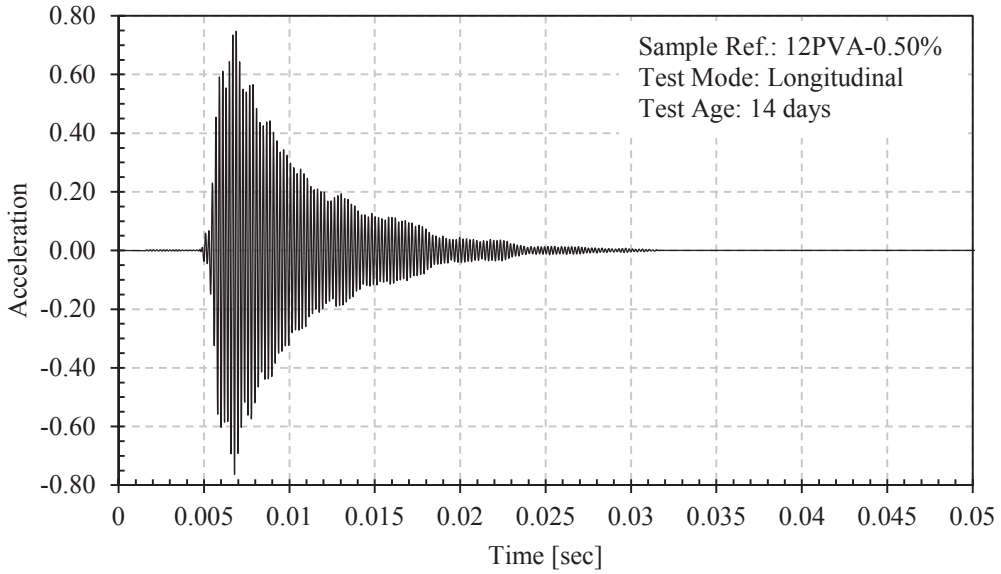
Sample Ref.: 12PVA-0.50%
Test Mode: Longitudinal
Test Age: 14 days
Acceleration
0.80
0.60
0.40
0.20
0.00
-0.20
-0.40
-0.60
-0.80
0
0.005
0.01
0.015
0.02
0.025
0.03
0.035
0.04
0.045
0.05
Time [sec]

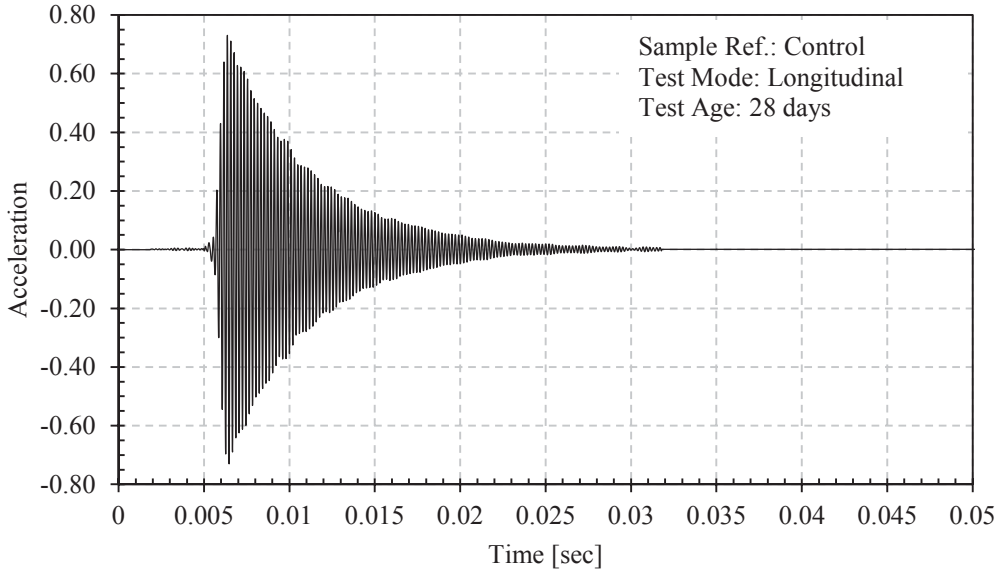
Sample Ref.: Control
Test Mode: Longitudinal
Test Age: 28 days
Acceleration
0.80
0.60
0.40
0.20
0.00
-0.20
-0.40
-0.60
-0.80
0
0.005
0.01
0.015
0.02
0.025
0.03
0.035
0.04
0.045
0.05
Time [sec]

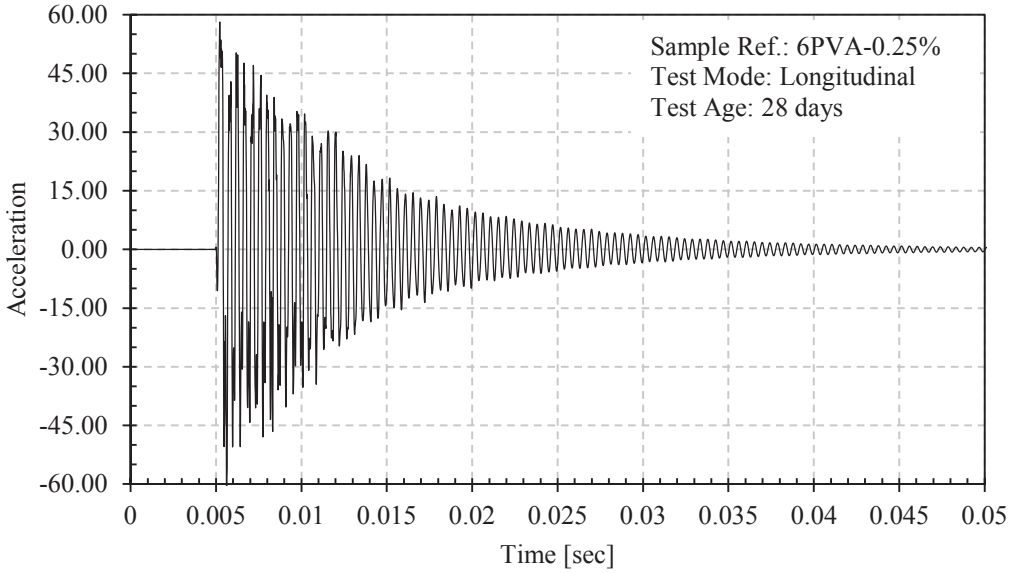
Sample Ref.: 6PVA-0.25%
Test Mode: Longitudinal
Test Age: 28 days
Acceleration
60.00
45.00
30.00
15.00
0.00
-15.00
-30.00
-45.00
-60.00
0
0.005
0.01
0.015
0.02
0.025
0.03
0.035
0.04
0.045
0.05
Time [sec]

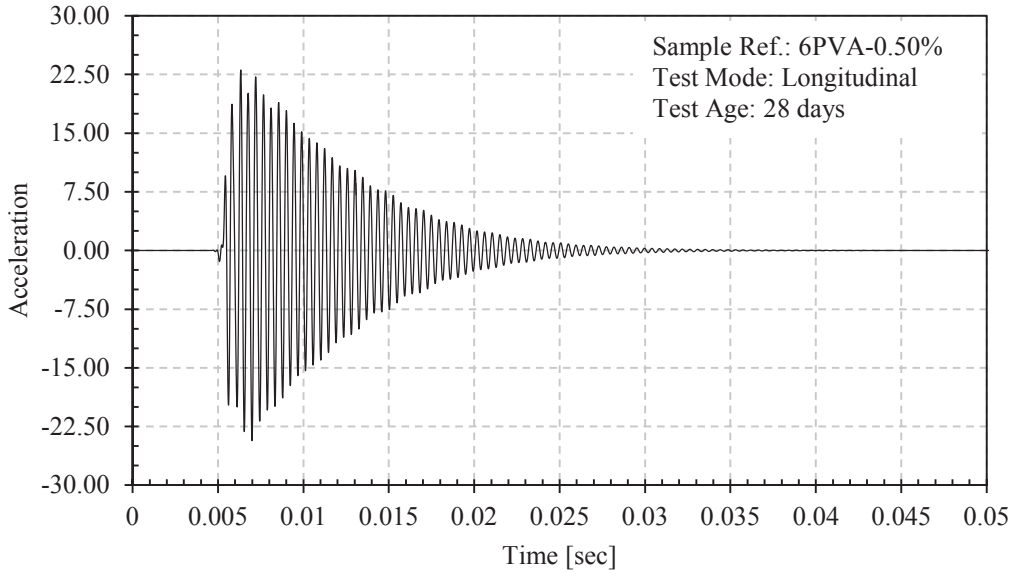
Sample Ref.: 6PVA-0.50%
Test Mode: Longitudinal
Test Age: 28 days
Acceleration
Time [sec]
30.00
22.50
15.00
7.50
0.00
-7.50
-15.00
-22.50
-30.00
0
0.005
0.01
0.015
0.02
0.025
0.03
0.035
0.04
0.045
0.05

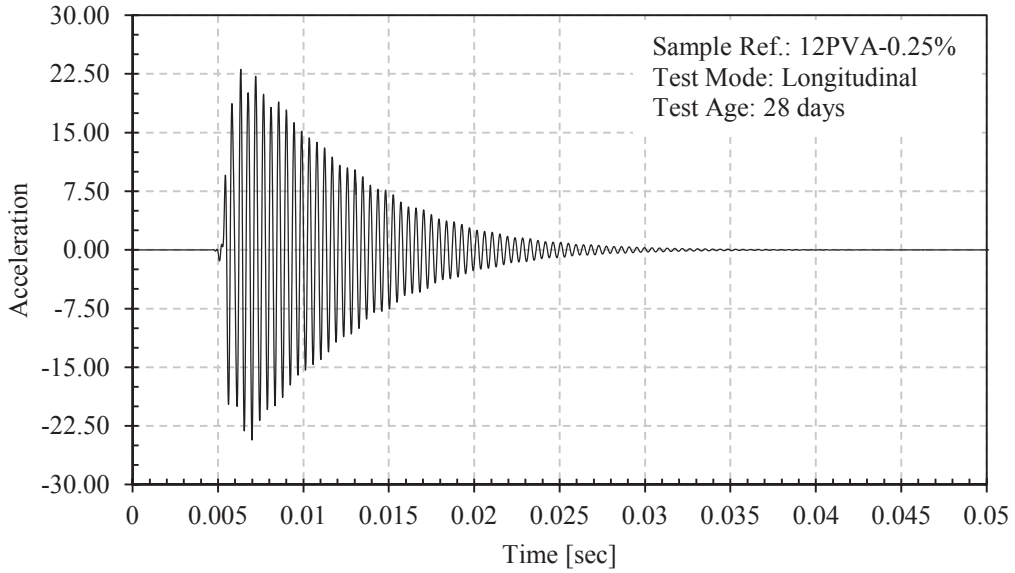
Sample Ref.: 12PVA-0.25%
Test Mode: Longitudinal
Test Age: 28 days
Acceleration
Time [sec]
30.00
22.50
15.00
7.50
0.00
-7.50
-15.00
-22.50
-30.00
0
0.005
0.01
0.015
0.02
0.025
0.03
0.035
0.04
0.045
0.05

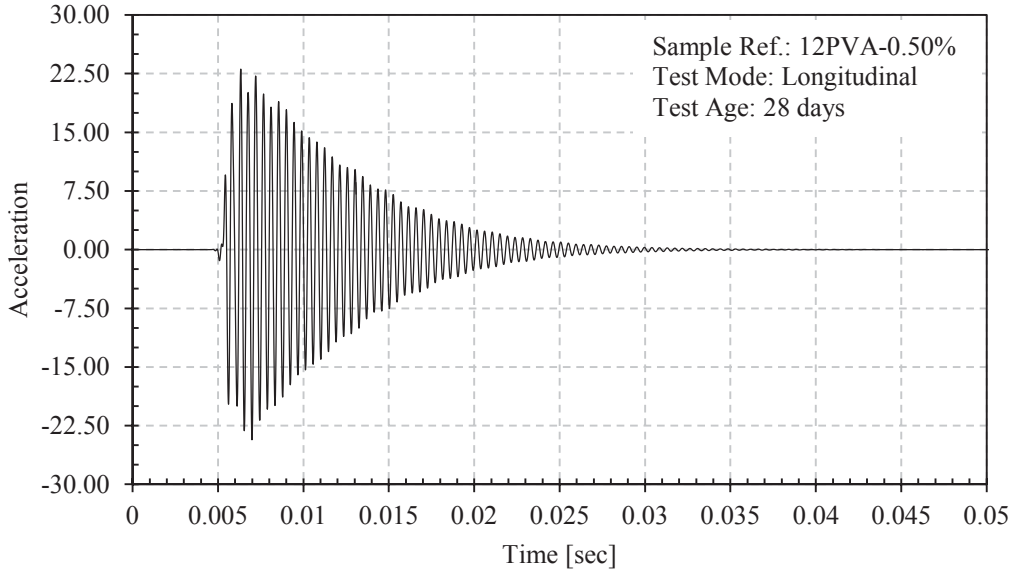
Sample Ref.: 12PVA-0.50%
Test Mode: Longitudinal
Test Age: 28 days
Acceleration
Time [sec]
30.00
22.50
15.00
7.50
0.00
-7.50
-15.00
-22.50
-30.00
0
0.005
0.01
0.015
0.02
0.025
0.03
0.035
0.04
0.045
0.05

A.2 Transverse mode Frequency Response Functions (FRF)

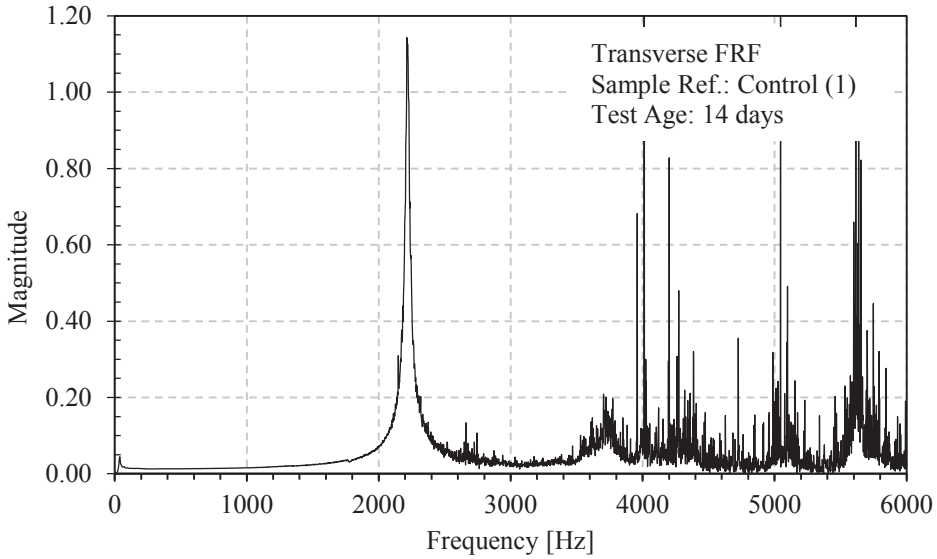

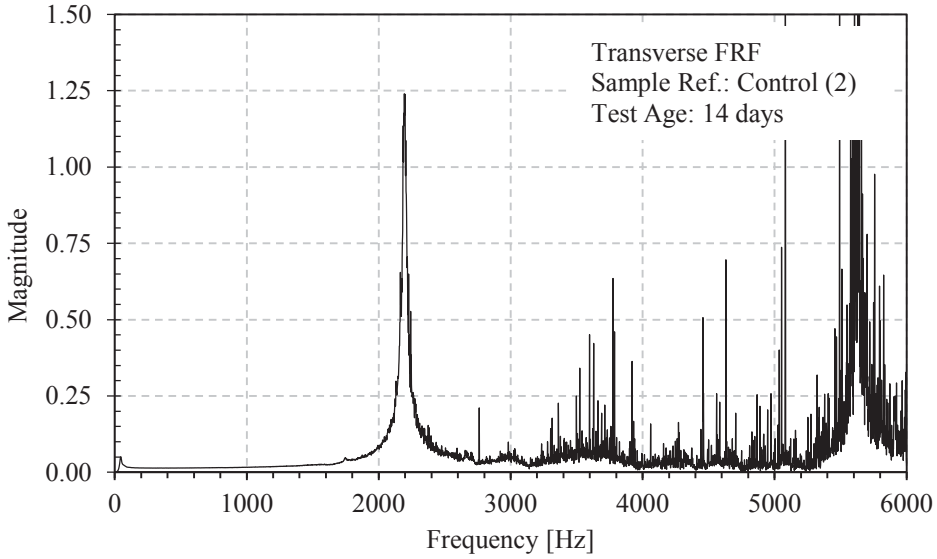

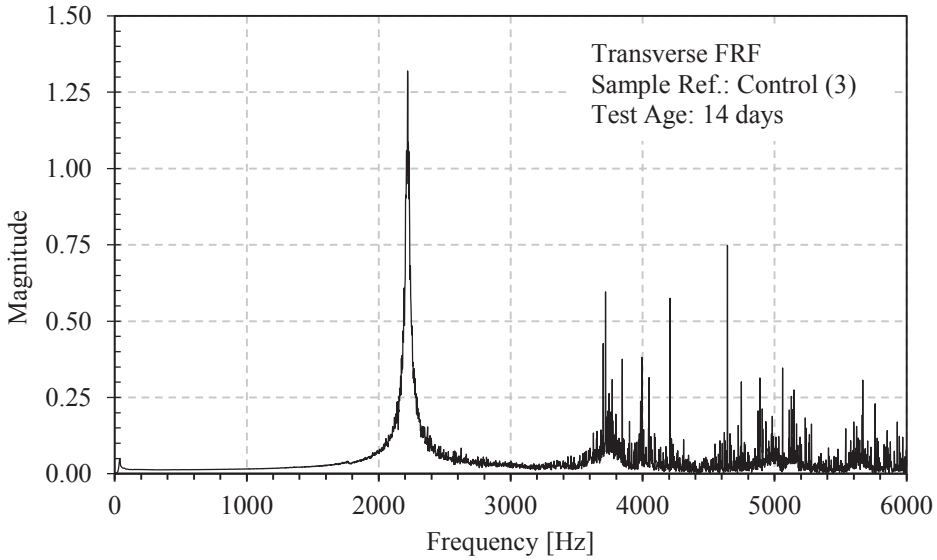

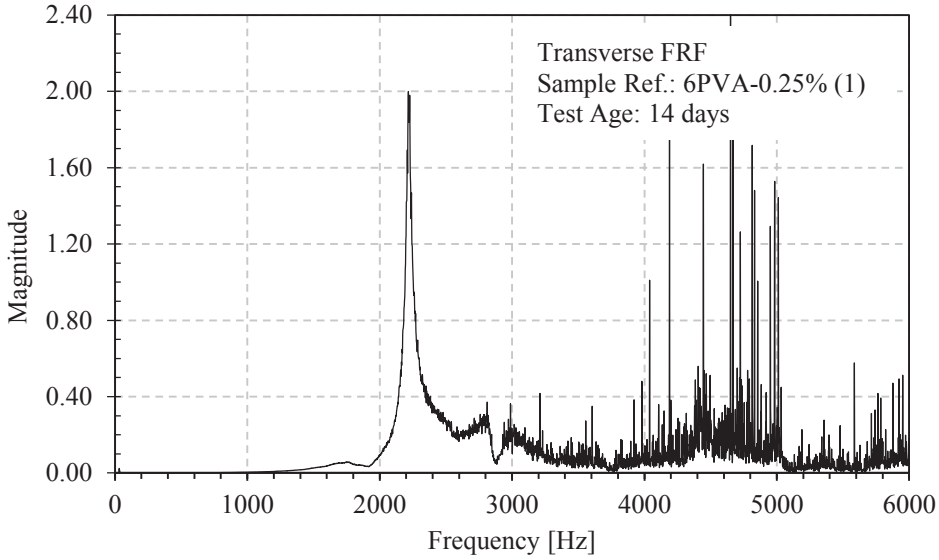
Transverse FRF
Sample Ref.: 6PVA-0.25% (1)
Test Age: 14 days
Magnitude
Frequency [Hz]
0.00
0.40
0.80
1.20
1.60
2.00
2.40
0
1000
2000
3000
4000
5000
6000

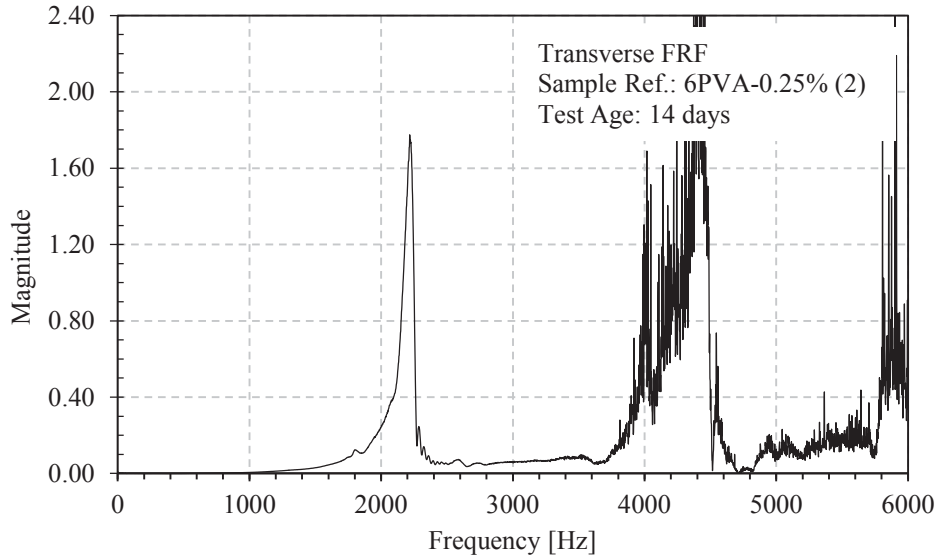
Transverse FRF
Sample Ref.: 6PVA-0.25% (2)
Test Age: 14 days
Magnitude
Frequency [Hz]
0.00
0.40
0.80
1.20
1.60
2.00
2.40
0
1000
2000
3000
4000
5000
6000

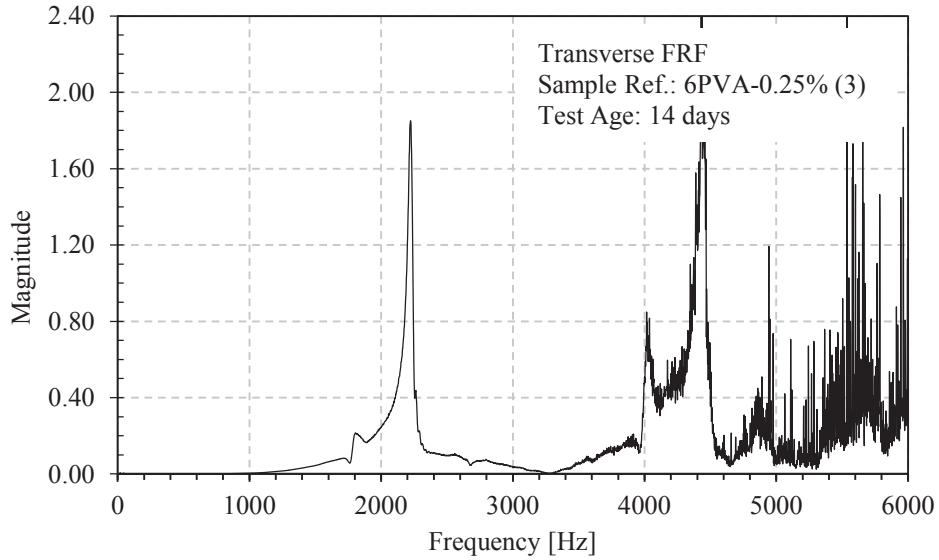
Transverse FRF
Sample Ref.: 6PVA-0.25% (3)
Test Age: 14 days
Magnitude
Frequency [Hz]
0.00
0.40
0.80
1.20
1.60
2.00
2.40
0
1000
2000
3000
4000
5000
6000

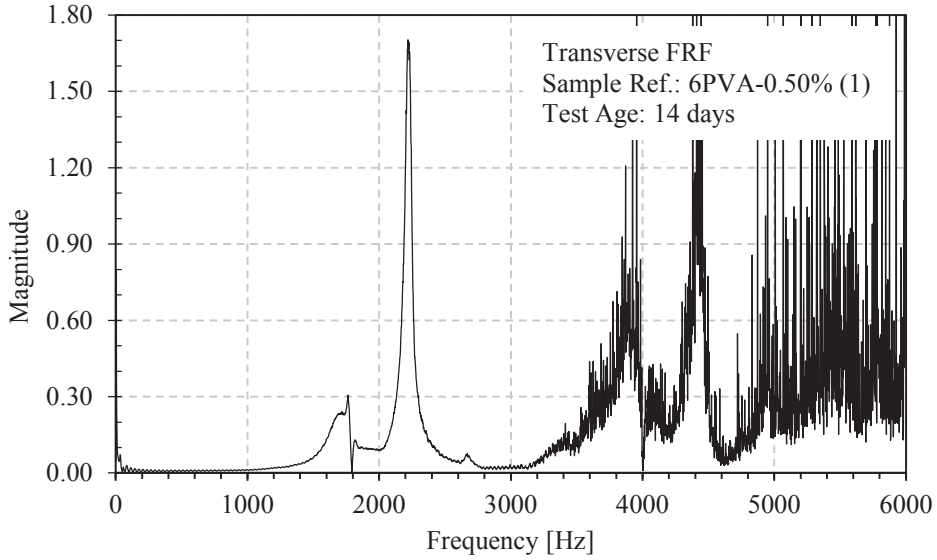
Transverse FRF
Sample Ref.: 6PVA-0.50% (1)
Test Age: 14 days
Magnitude
Frequency [Hz]
0.00
0.30
0.60
0.90
1.20
1.50
1.80
0
1000
2000
3000
4000
5000
6000

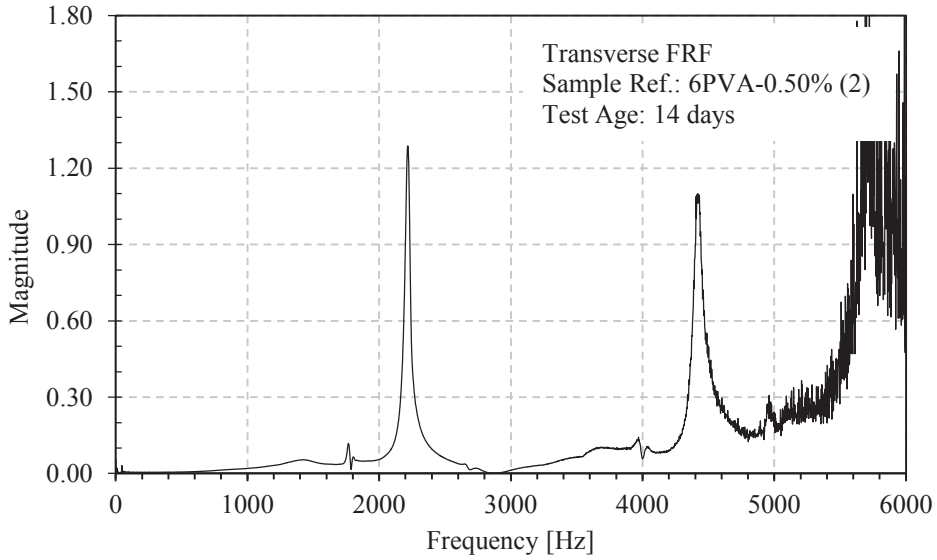
Transverse FRF
Sample Ref.: 6PVA-0.50% (2)
Test Age: 14 days
Magnitude
Frequency [Hz]
0.00
0.30
0.60
0.90
1.20
1.50
1.80
0
1000
2000
3000
4000
5000
6000

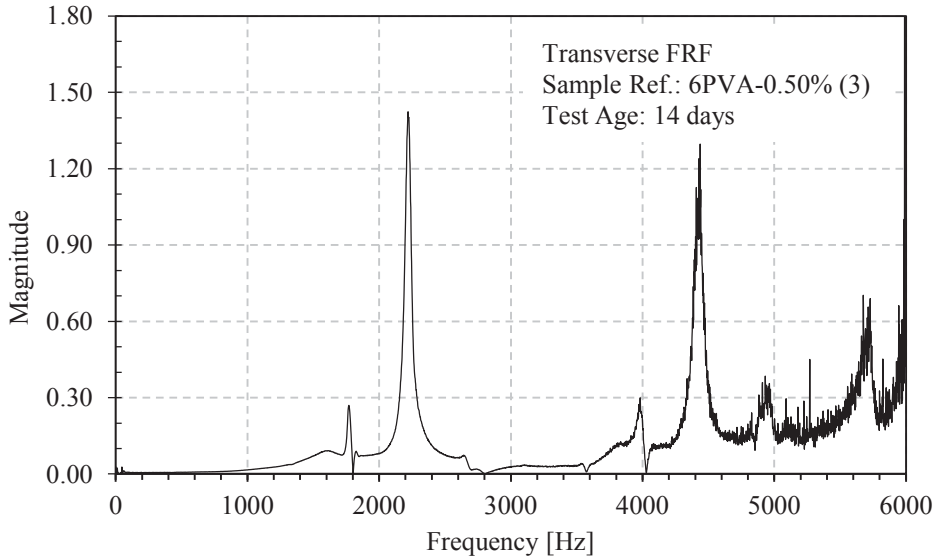
Transverse FRF
Sample Ref.: 6PVA-0.50% (3)
Test Age: 14 days
Magnitude
Frequency [Hz]
0.00
0.30
0.60
0.90
1.20
1.50
1.80
0
1000
2000
3000
4000
5000
6000

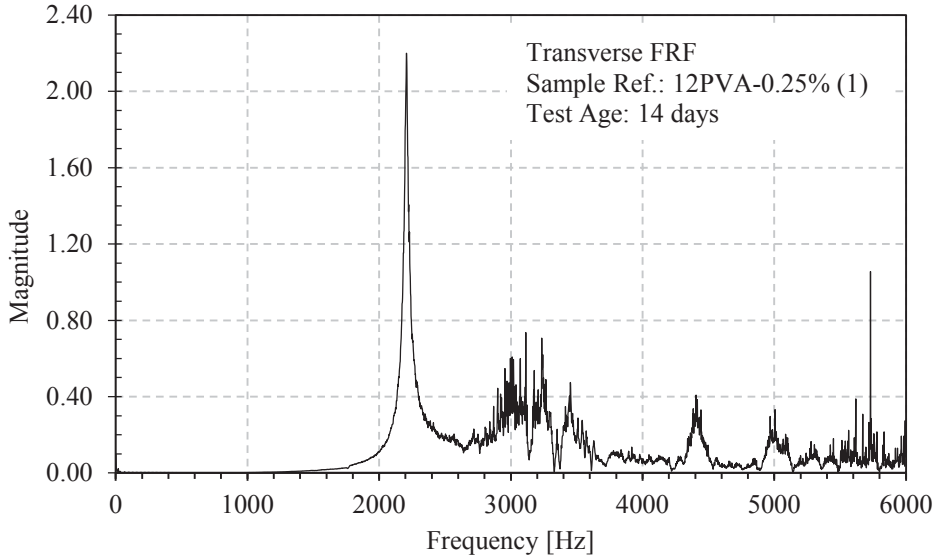
Transverse FRF
Sample Ref.: 12PVA-0.25% (1)
Test Age: 14 days
Magnitude
Frequency [Hz]
0.00
0.40
0.80
1.20
1.60
2.00
2.40
0
1000
2000
3000
4000
5000
6000

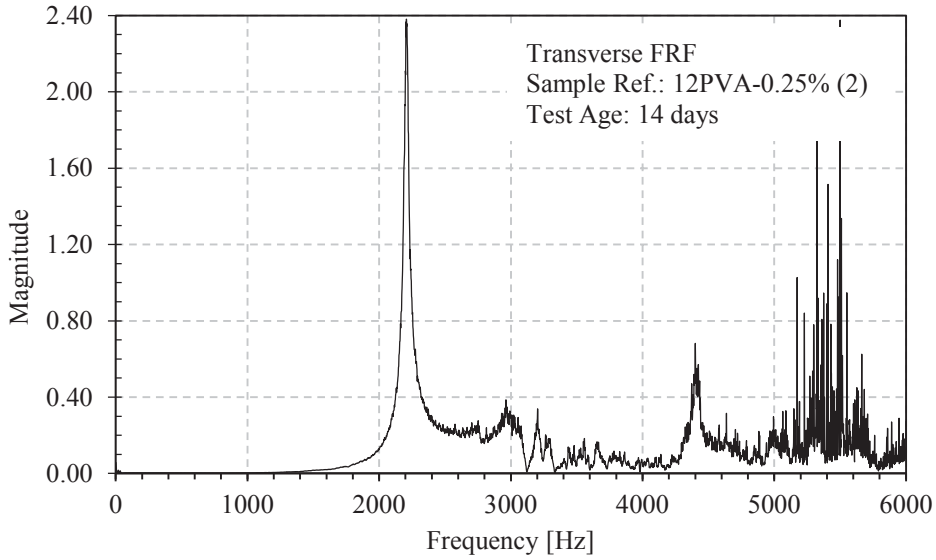
Transverse FRF
Sample Ref.: 12PVA-0.25% (2)
Test Age: 14 days
Magnitude
Frequency [Hz]
0.00
0.40
0.80
1.20
1.60
2.00
2.40
0
1000
2000
3000
4000
5000
6000

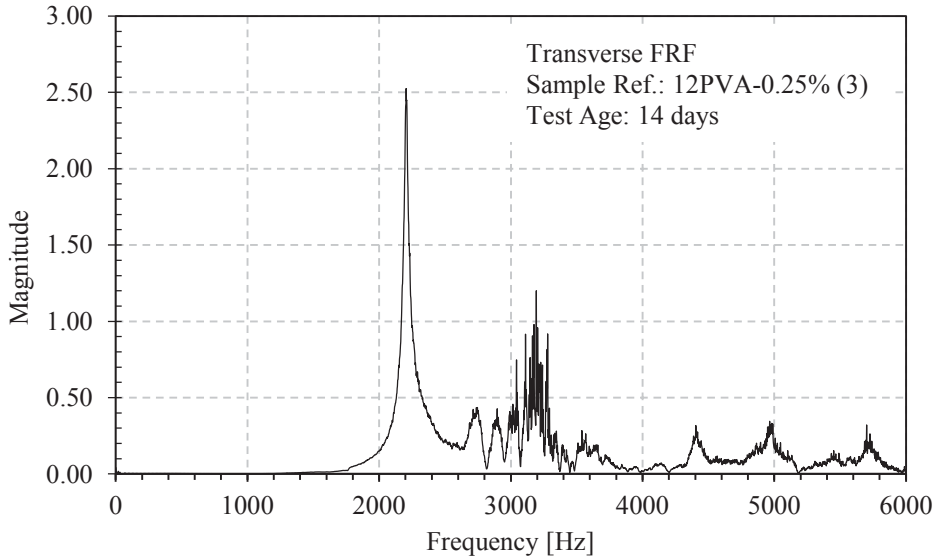
Transverse FRF
Sample Ref.: 12PVA-0.25% (3)
Test Age: 14 days
Magnitude
Frequency [Hz]
0.00
0.50
1.00
1.50
2.00
2.50
3.00
0
1000
2000
3000
4000
5000
6000

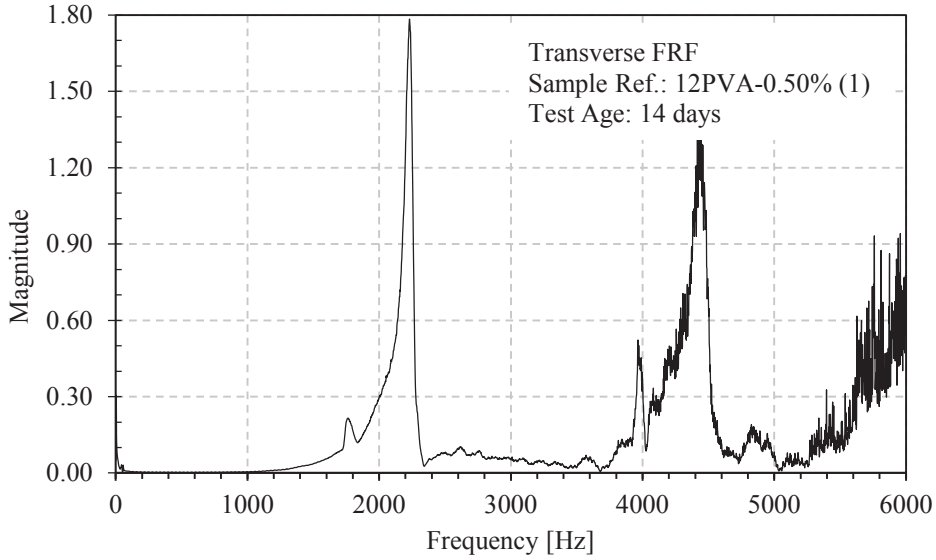
Transverse FRF
Sample Ref.: 12PVA-0.50% (1)
Test Age: 14 days
Magnitude
Frequency [Hz]
0.00
0.30
0.60
0.90
1.20
1.50
1.80
0
1000
2000
3000
4000
5000
6000

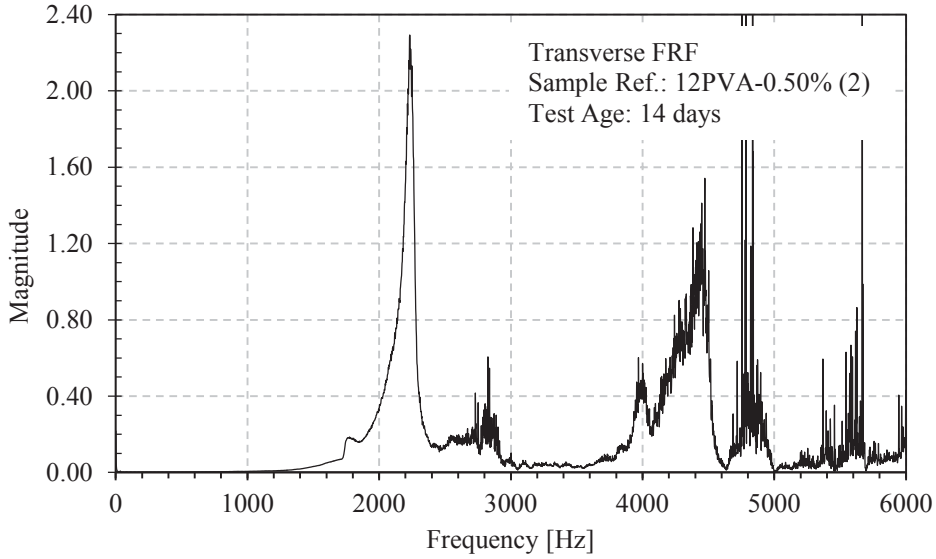
Transverse FRF
Sample Ref.: 12PVA-0.50% (2)
Test Age: 14 days
Magnitude
Frequency [Hz]
0.00
0.40
0.80
1.20
1.60
2.00
2.40
0
1000
2000
3000
4000
5000
6000

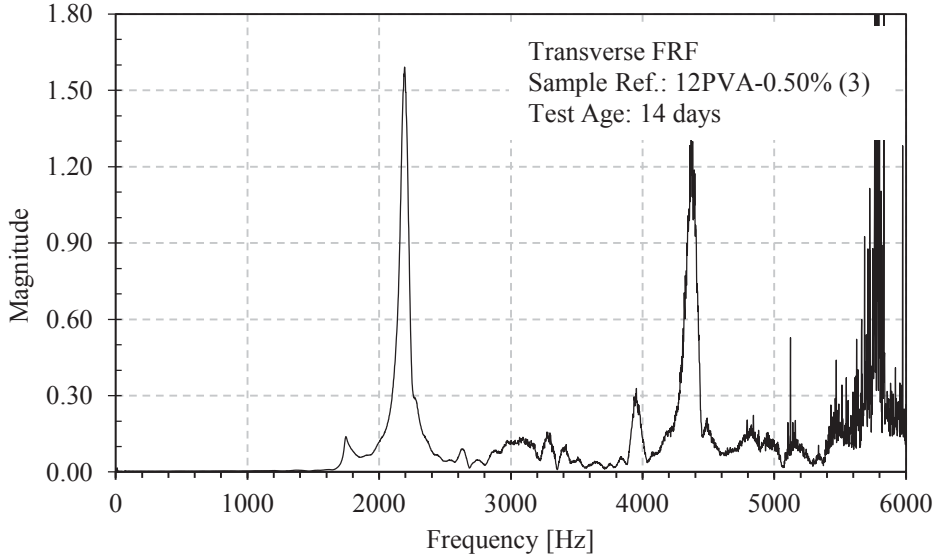
Transverse FRF
Sample Ref.: 12PVA-0.50% (3)
Test Age: 14 days
Magnitude
Frequency [Hz]
0.00
0.30
0.60
0.90
1.20
1.50
1.80
0
1000
2000
3000
4000
5000
6000

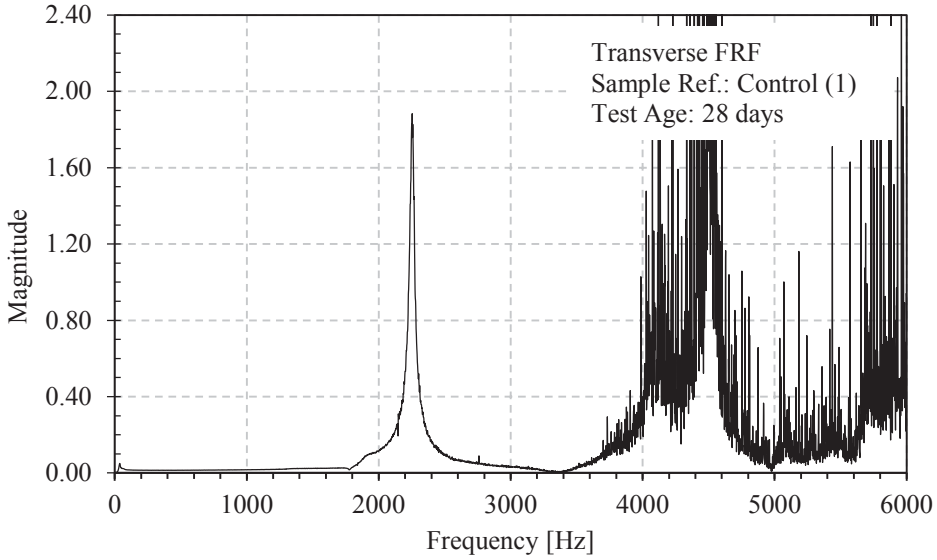
Transverse FRF
Sample Ref.: Control (1)
Test Age: 28 days
Magnitude
Frequency [Hz]
0.00
0.40
0.80
1.20
1.60
2.00
2.40
0
1000
2000
3000
4000
5000
6000

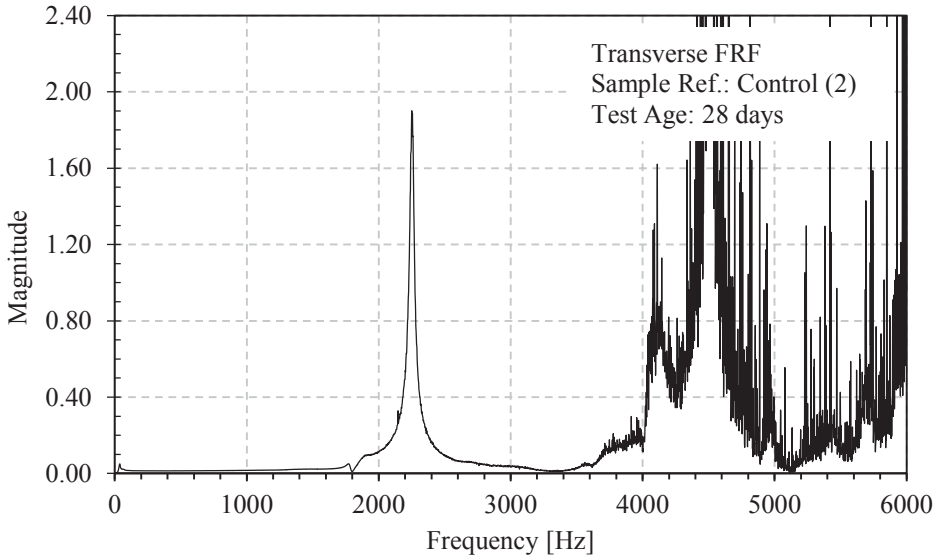
Transverse FRF
Sample Ref.: Control (2)
Test Age: 28 days
Magnitude
Frequency [Hz]
0.00
0.40
0.80
1.20
1.60
2.00
2.40
0
1000
2000
3000
4000
5000
6000

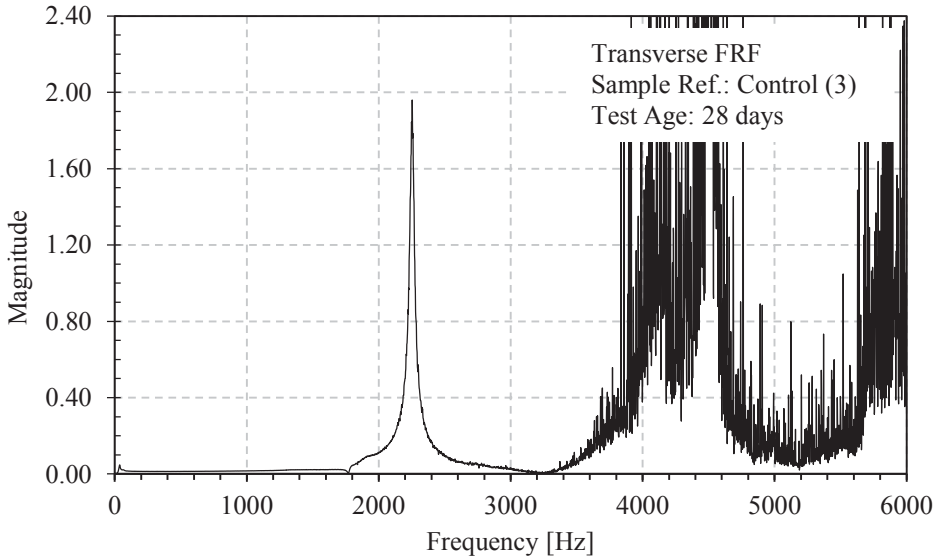
Transverse FRF
Sample Ref.: Control (3)
Test Age: 28 days
Magnitude
Frequency [Hz]
0.00
0.40
0.80
1.20
1.60
2.00
2.40
0
1000
2000
3000
4000
5000
6000

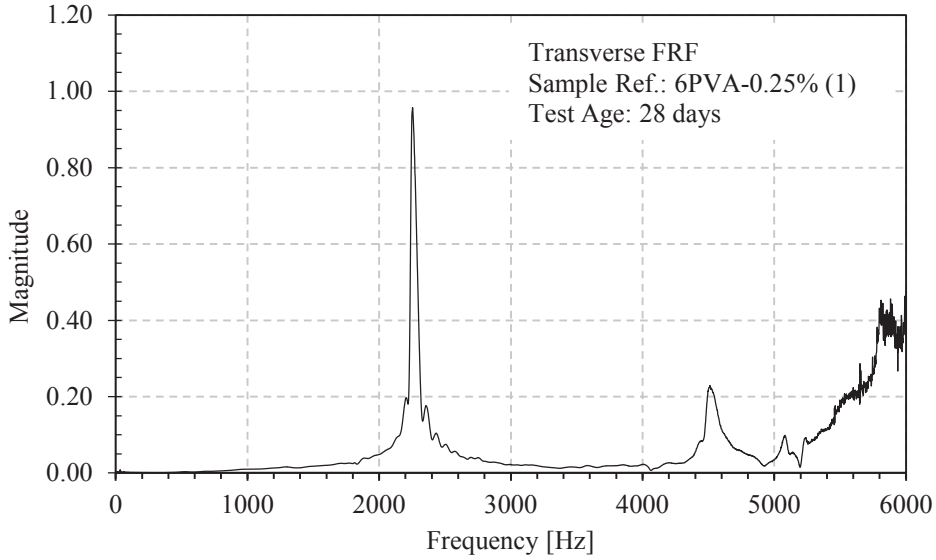
Transverse FRF
Sample Ref.: 6PVA-0.25% (1)
Test Age: 28 days
Magnitude
Frequency [Hz]
0.00
0.20
0.40
0.60
0.80
1.00
1.20
0
1000
2000
3000
4000
5000
6000

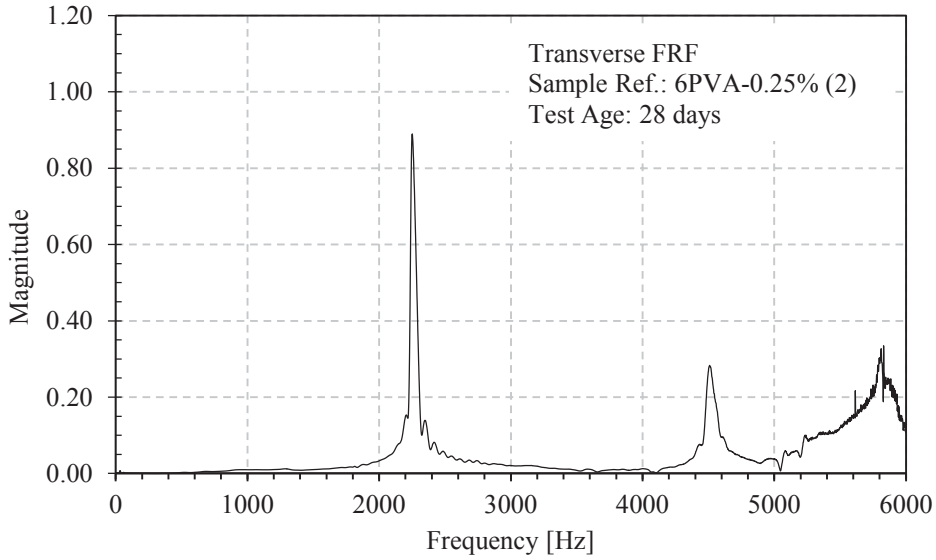
Transverse FRF
Sample Ref.: 6PVA-0.25% (2)
Test Age: 28 days
Magnitude
Frequency [Hz]
0.00
0.20
0.40
0.60
0.80
1.00
1.20
0
1000
2000
3000
4000
5000
6000

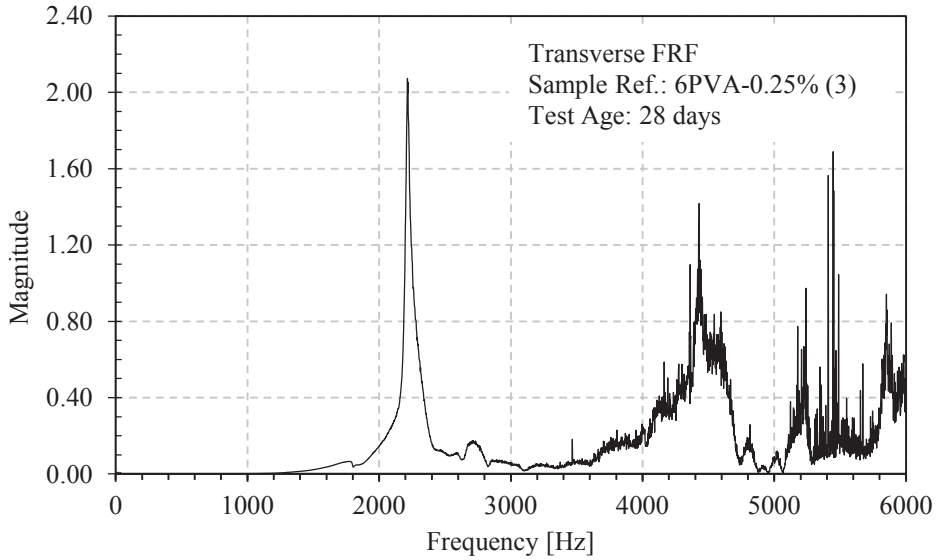
Transverse FRF
Sample Ref.: 6PVA-0.25% (3)
Test Age: 28 days
Magnitude
Frequency [Hz]
0.00
0.40
0.80
1.20
1.60
2.00
2.40
0
1000
2000
3000
4000
5000
6000

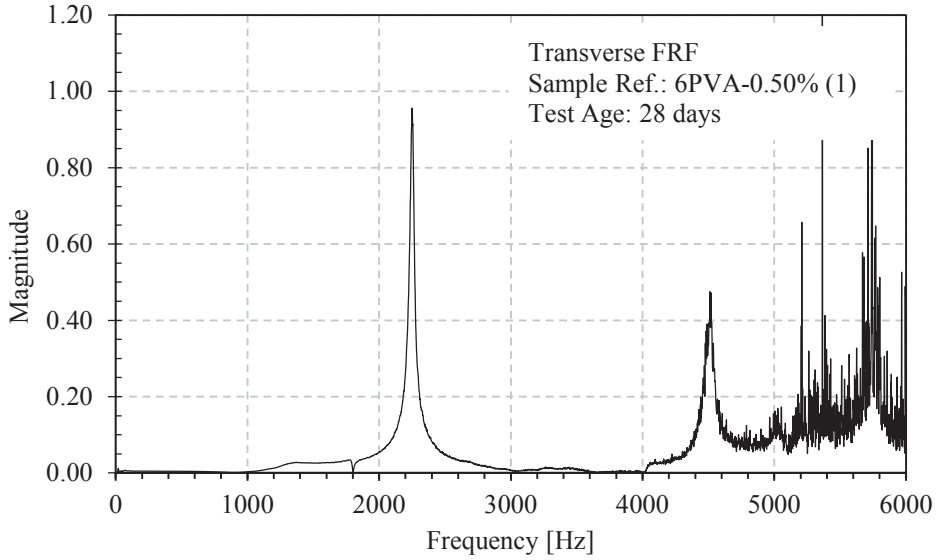
Transverse FRF
Sample Ref.: 6PVA-0.50% (1)
Test Age: 28 days
Magnitude
Frequency [Hz]
0.00
0.20
0.40
0.60
0.80
1.00
1.20
0
1000
2000
3000
4000
5000
6000

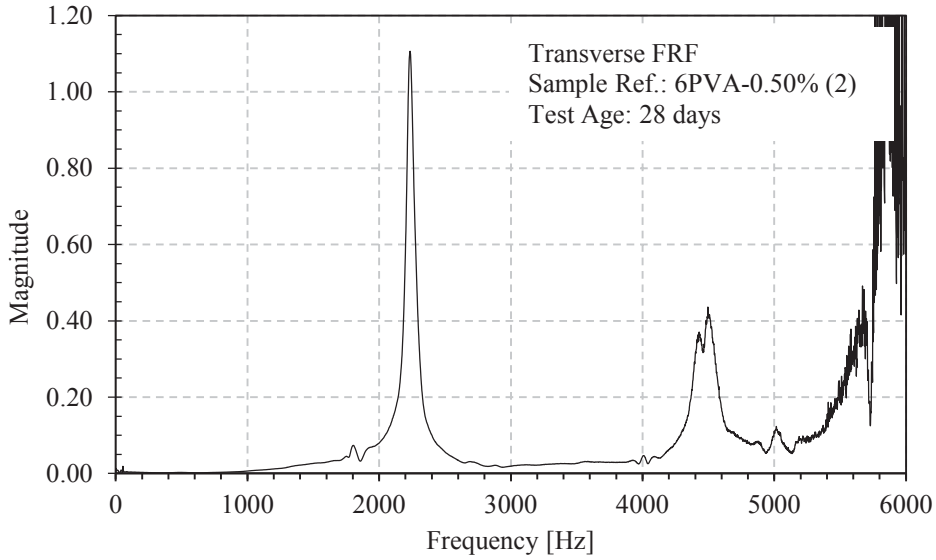
Transverse FRF
Sample Ref.: 6PVA-0.50% (2)
Test Age: 28 days
Magnitude
Frequency [Hz]
0.00
0.20
0.40
0.60
0.80
1.00
1.20
0
1000
2000
3000
4000
5000
6000

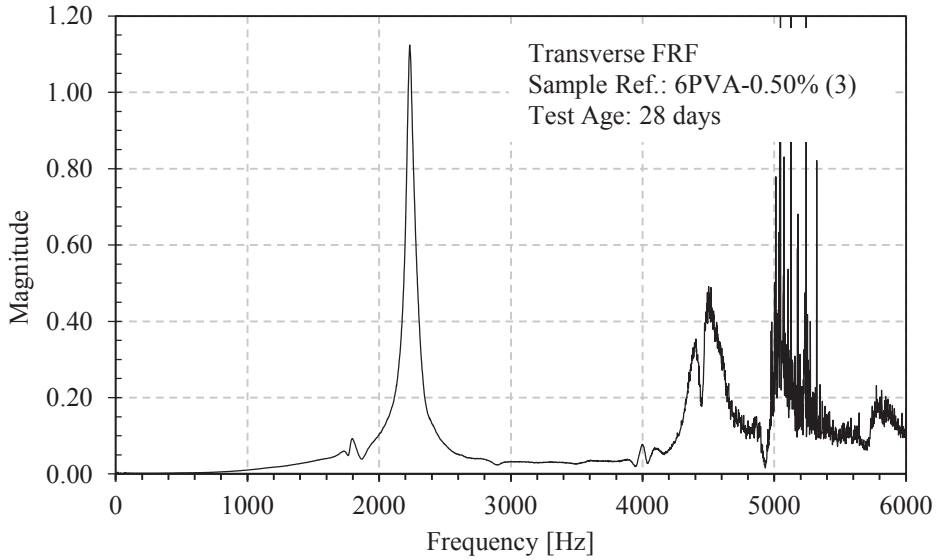
Transverse FRF
Sample Ref.: 6PVA-0.50% (3)
Test Age: 28 days
Magnitude
Frequency [Hz]
0.00
0.20
0.40
0.60
0.80
1.00
1.20
0
1000
2000
3000
4000
5000
6000

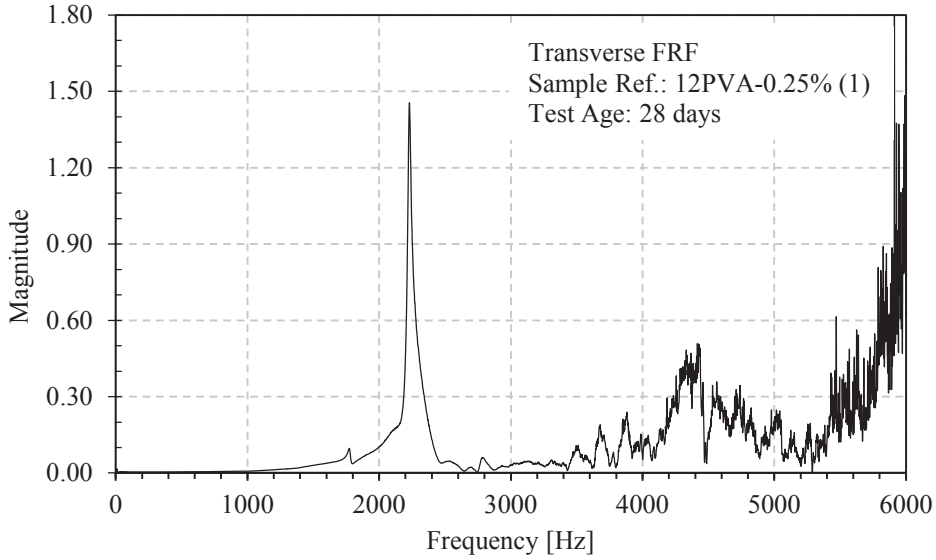
Transverse FRF
Sample Ref.: 12PVA-0.25% (1)
Test Age: 28 days
Magnitude
Frequency [Hz]
0.00
0.30
0.60
0.90
1.20
1.50
1.80
0
1000
2000
3000
4000
5000
6000

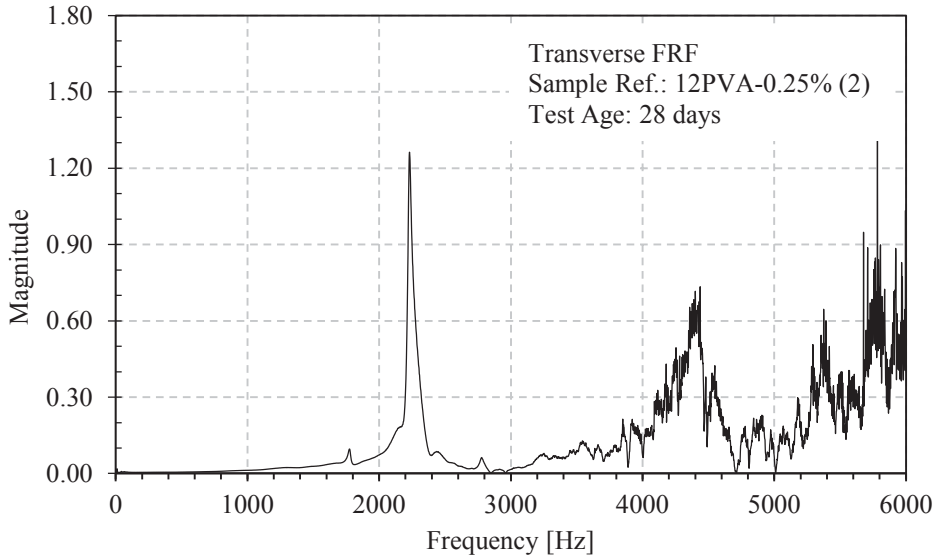
Transverse FRF
Sample Ref.: 12PVA-0.25% (2)
Test Age: 28 days
Magnitude
Frequency [Hz]
0.00
0.30
0.60
0.90
1.20
1.50
1.80
0
1000
2000
3000
4000
5000
6000

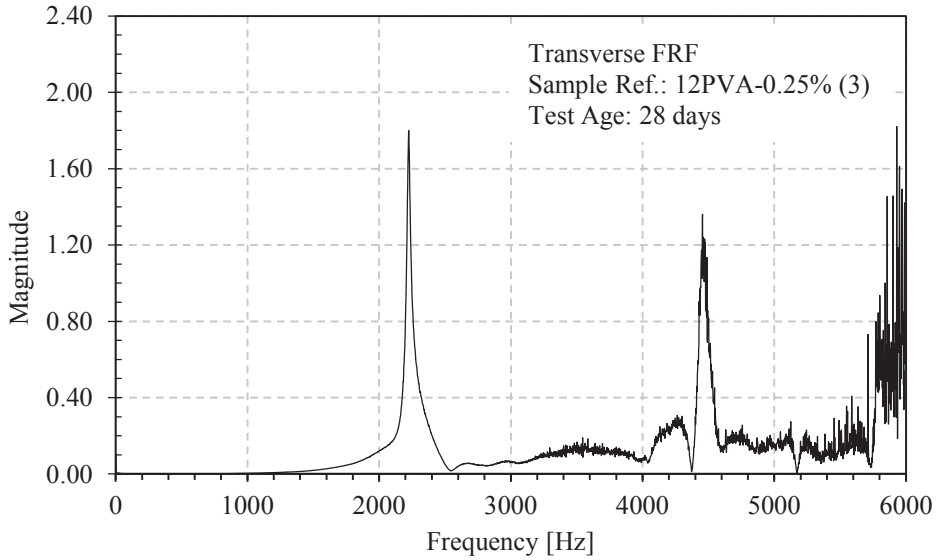
Transverse FRF
Sample Ref.: 12PVA-0.25% (3)
Test Age: 28 days
Magnitude
Frequency [Hz]
0.00
0.40
0.80
1.20
1.60
2.00
2.40
0
1000
2000
3000
4000
5000
6000

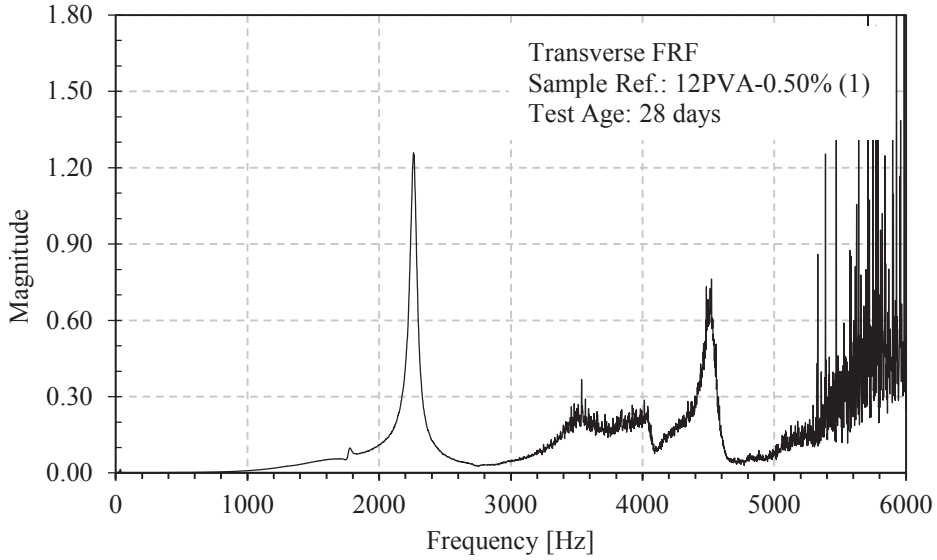
Transverse FRF
Sample Ref.: 12PVA-0.50% (1)
Test Age: 28 days
Magnitude
Frequency [Hz]
0.00
0.30
0.60
0.90
1.20
1.50
1.80
0
1000
2000
3000
4000
5000
6000

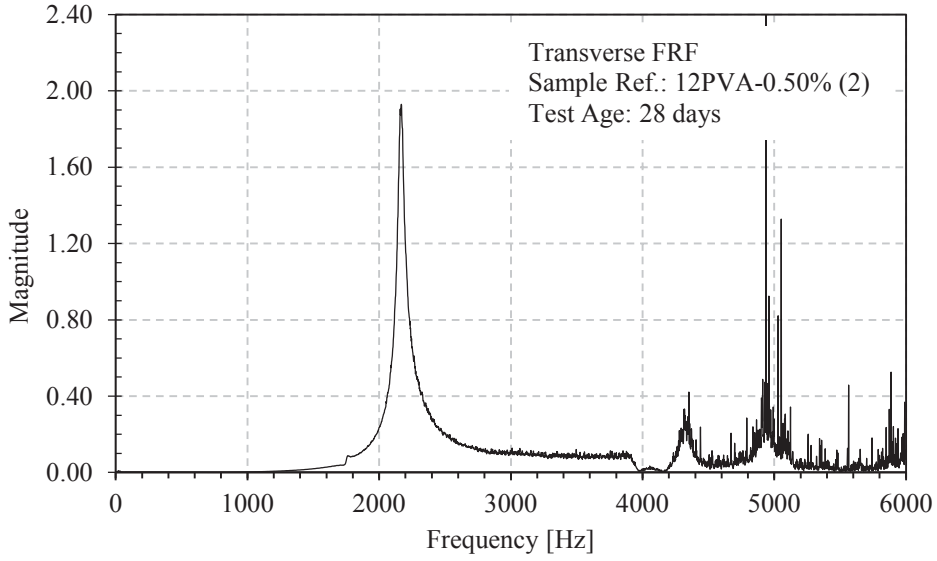
Transverse FRF
Sample Ref.: 12PVA-0.50% (2)
Test Age: 28 days
Magnitude
Frequency [Hz]
0.00
0.40
0.80
1.20
1.60
2.00
2.40
0
1000
2000
3000
4000
5000
6000

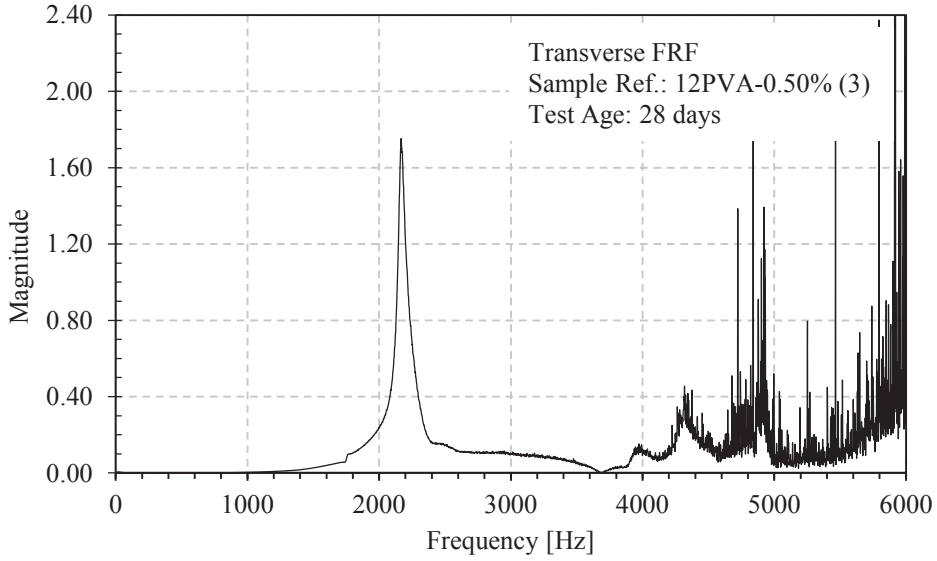
Transverse FRF
Sample Ref.: 12PVA-0.50% (3)
Test Age: 28 days
Magnitude
Frequency [Hz]
0.00
0.40
0.80
1.20
1.60
2.00
2.40
0
1000
2000
3000
4000
5000
6000

A.3 Longitudinal mode Frequency Response Functions (FRF)

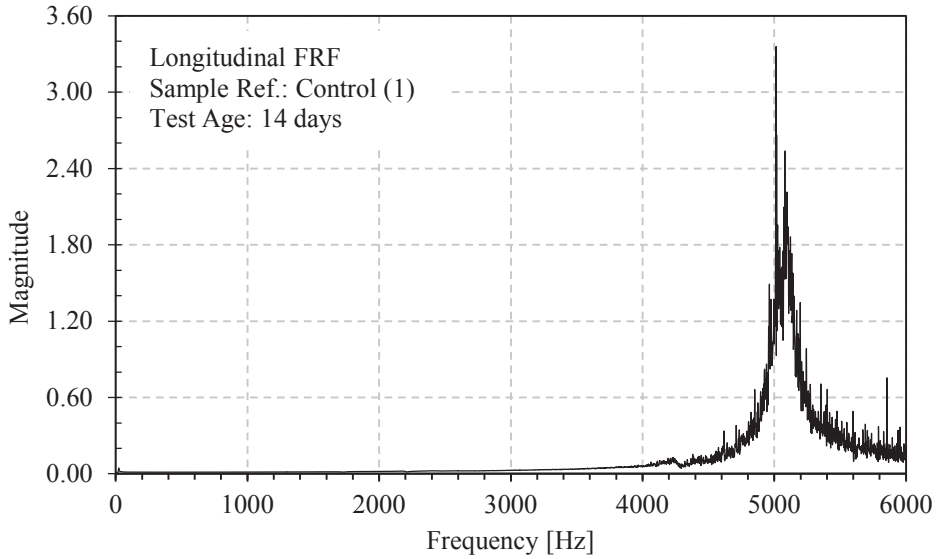

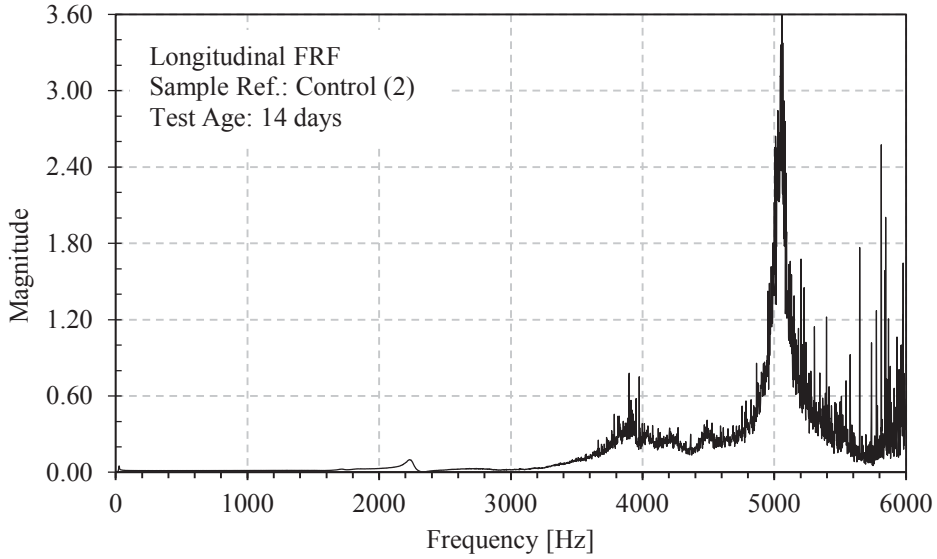

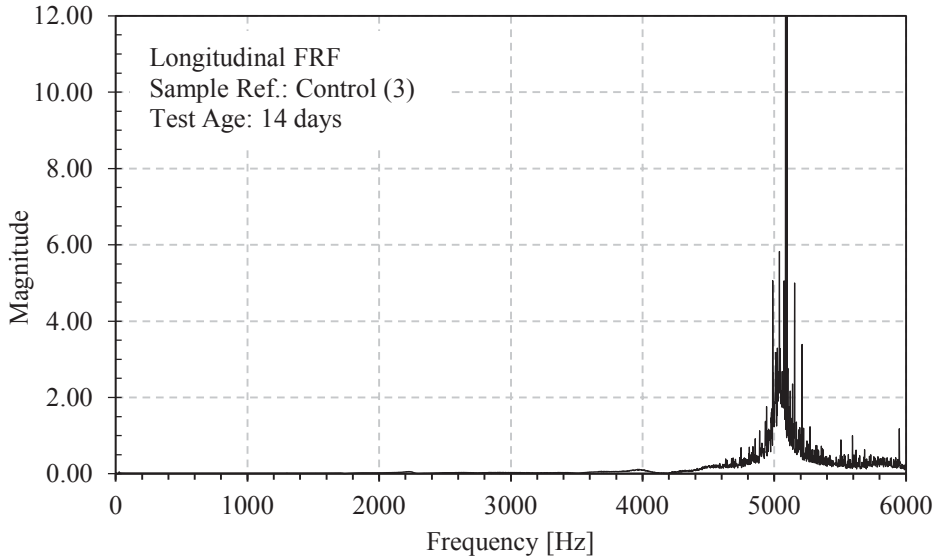

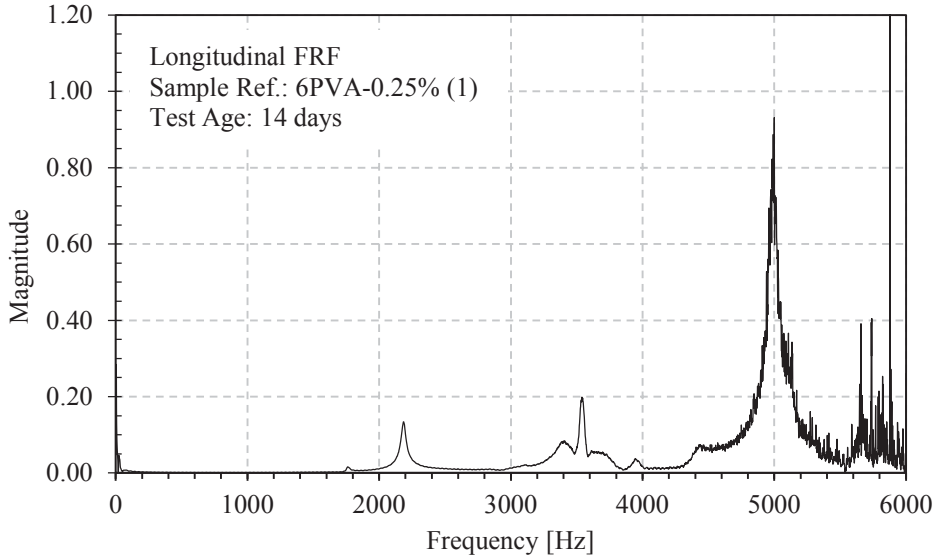
Longitudinal FRF
Sample Ref.: 6PVA-0.25% (1)
Test Age: 14 days
Magnitude
Frequency [Hz]
0.00
0.20
0.40
0.60
0.80
1.00
1.20
0
1000
2000
3000
4000
5000
6000

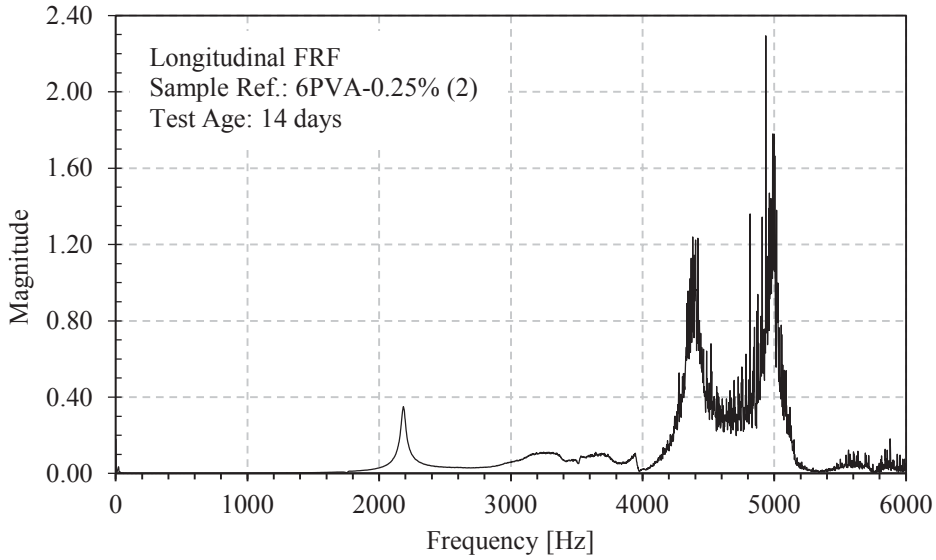
Longitudinal FRF
Sample Ref.: 6PVA-0.25% (2)
Test Age: 14 days
Magnitude
Frequency [Hz]
0.00
0.40
0.80
1.20
1.60
2.00
2.40
0
1000
2000
3000
4000
5000
6000

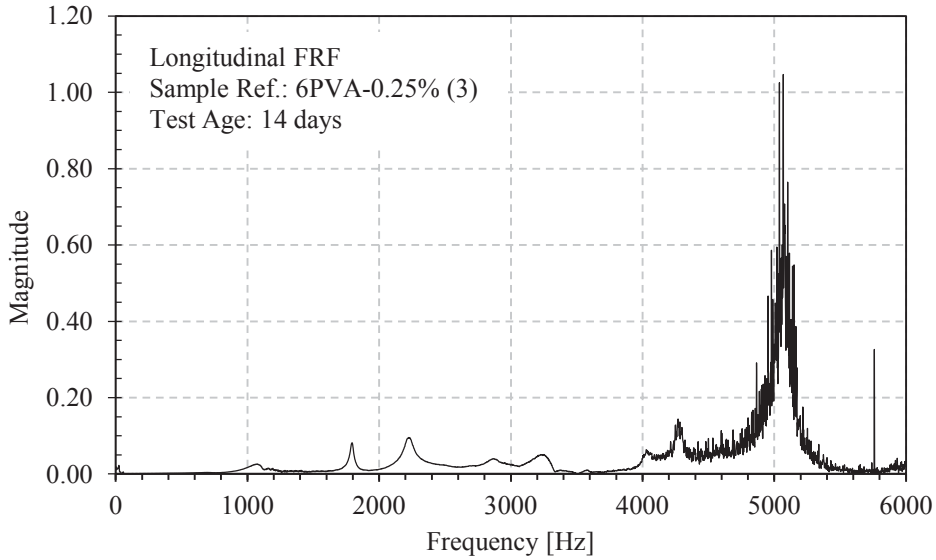
Longitudinal FRF
Sample Ref.: 6PVA-0.25% (3)
Test Age: 14 days
Magnitude
Frequency [Hz]
0.00
0.20
0.40
0.60
0.80
1.00
1.20
0
1000
2000
3000
4000
5000
6000

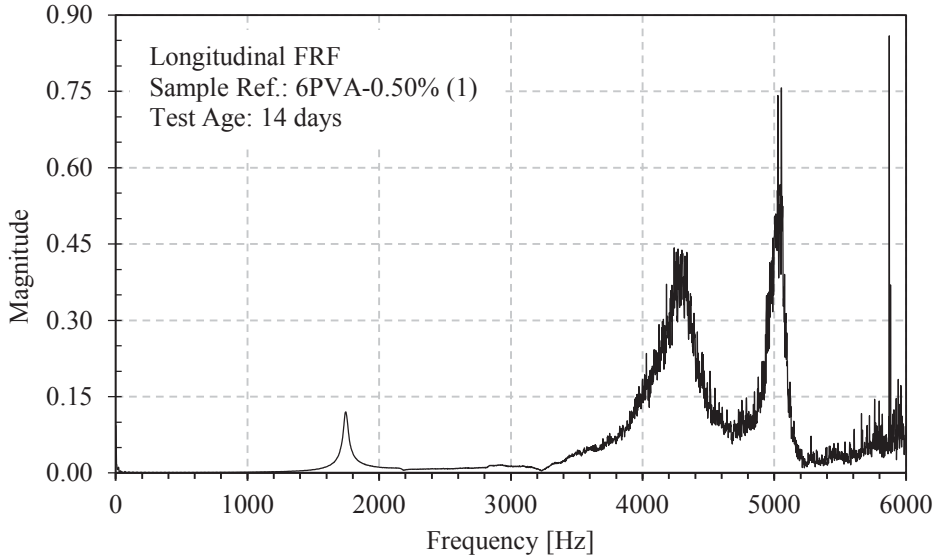
Longitudinal FRF
Sample Ref.: 6PVA-0.50% (1)
Test Age: 14 days
Magnitude
0.90
0.75
0.60
0.45
0.30
0.15
0.00
0
1000
2000
3000
4000
5000
6000
Frequency [Hz]

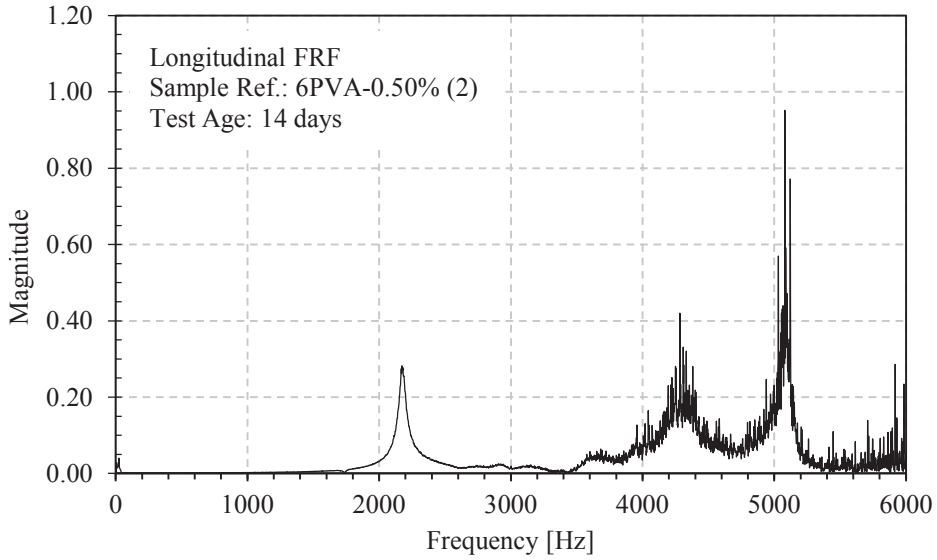
Longitudinal FRF
Sample Ref.: 6PVA-0.50% (2)
Test Age: 14 days
Magnitude
1.20
1.00
0.80
0.60
0.40
0.20
0.00
0
1000
2000
3000
4000
5000
6000
Frequency [Hz]

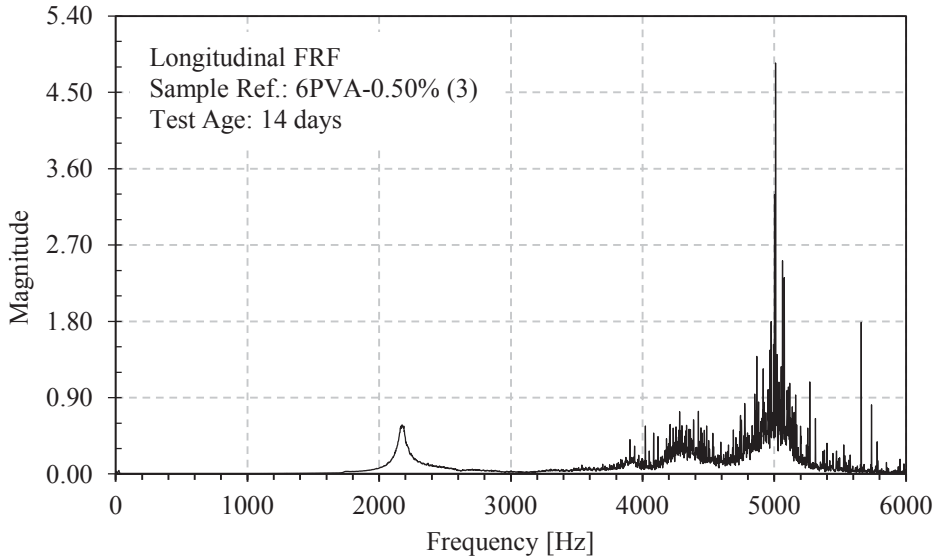
Longitudinal FRF
Sample Ref.: 6PVA-0.50% (3)
Test Age: 14 days
Magnitude
5.40
4.50
3.60
2.70
1.80
0.90
0.00
0
1000
2000
3000
4000
5000
6000
Frequency [Hz]

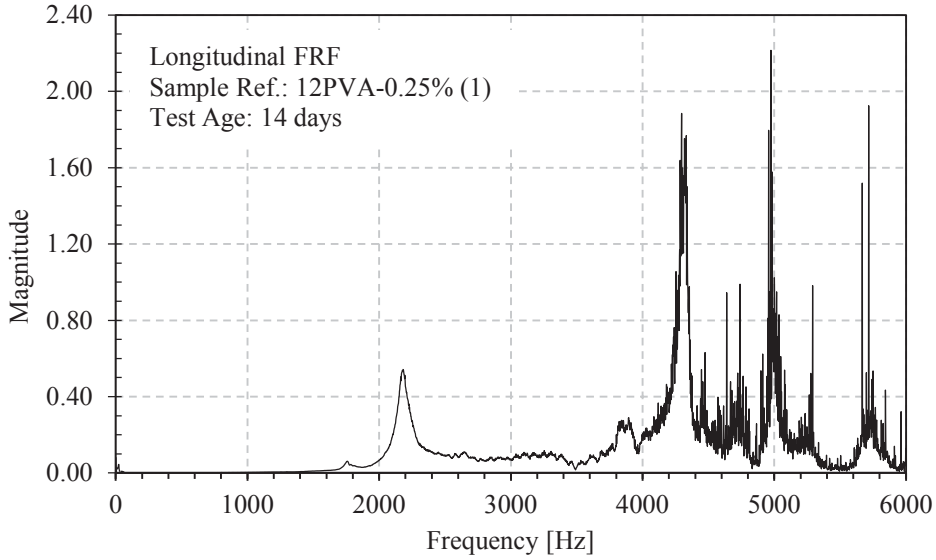
Longitudinal FRF
Sample Ref.: 12PVA-0.25% (1)
Test Age: 14 days
Magnitude
Frequency [Hz]
0.00
0.40
0.80
1.20
1.60
2.00
2.40
0
1000
2000
3000
4000
5000
6000

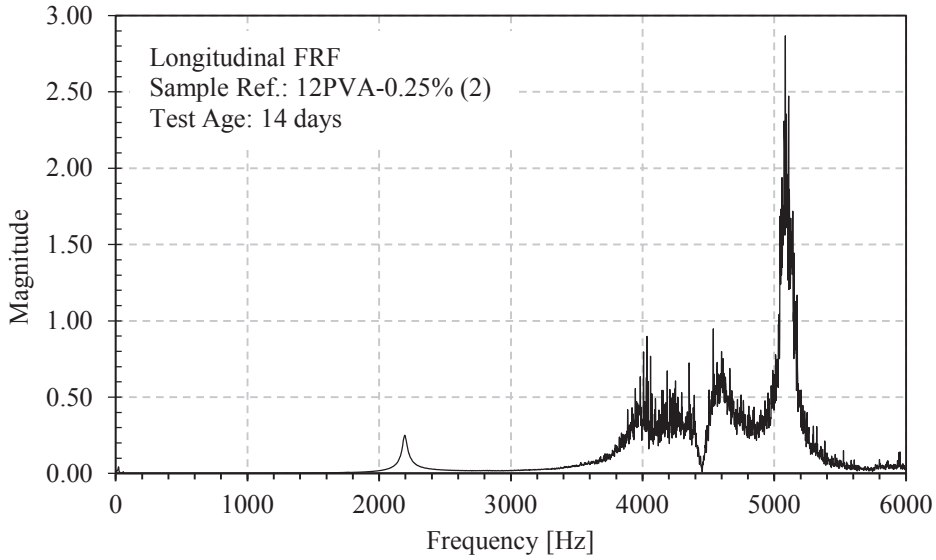
Longitudinal FRF
Sample Ref.: 12PVA-0.25% (2)
Test Age: 14 days
Magnitude
Frequency [Hz]
0.00
0.50
1.00
1.50
2.00
2.50
3.00
0
1000
2000
3000
4000
5000
6000

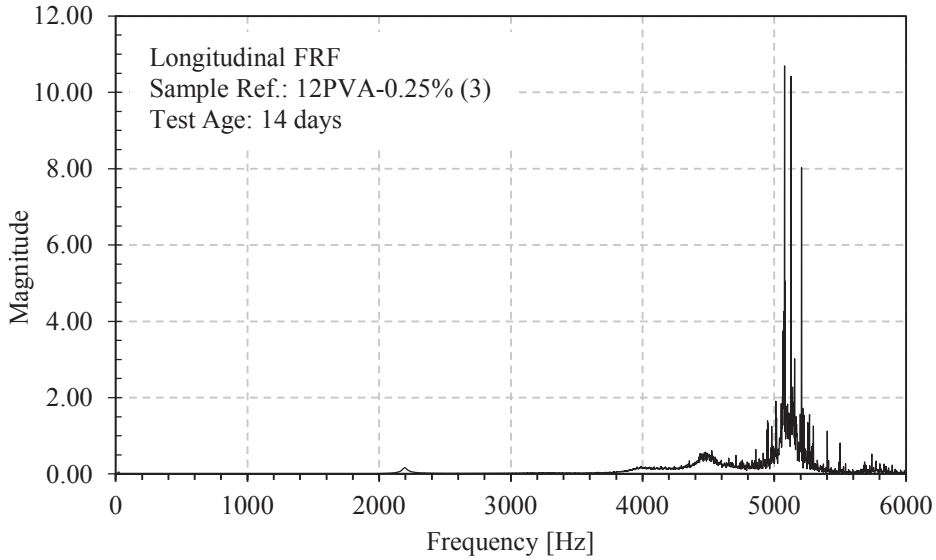
Longitudinal FRF
Sample Ref.: 12PVA-0.25% (3)
Test Age: 14 days
Magnitude
Frequency [Hz]
0.00
2.00
4.00
6.00
8.00
10.00
12.00
0
1000
2000
3000
4000
5000
6000

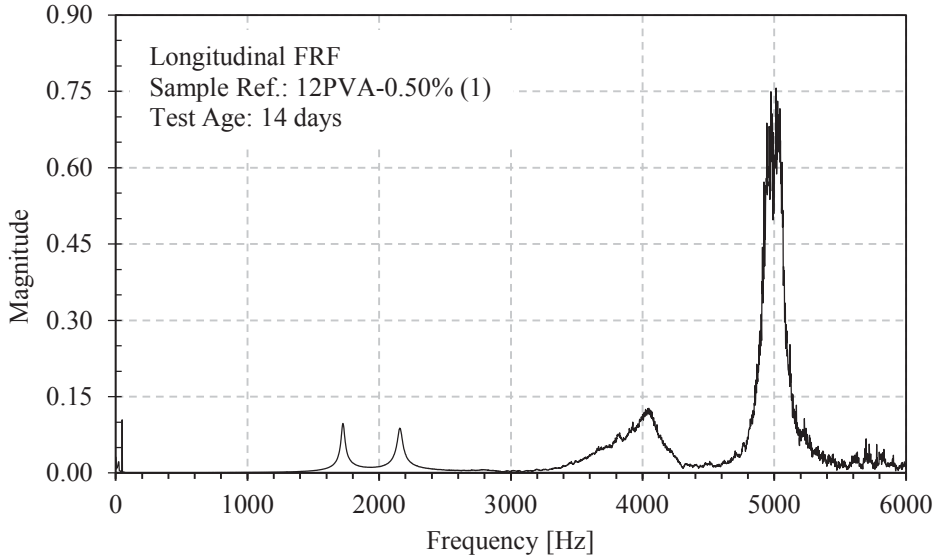
Longitudinal FRF
Sample Ref.: 12PVA-0.50% (1)
Test Age: 14 days
Magnitude
0.90
0.75
0.60
0.45
0.30
0.15
0.00
0
1000
2000
3000
4000
5000
6000
Frequency [Hz]

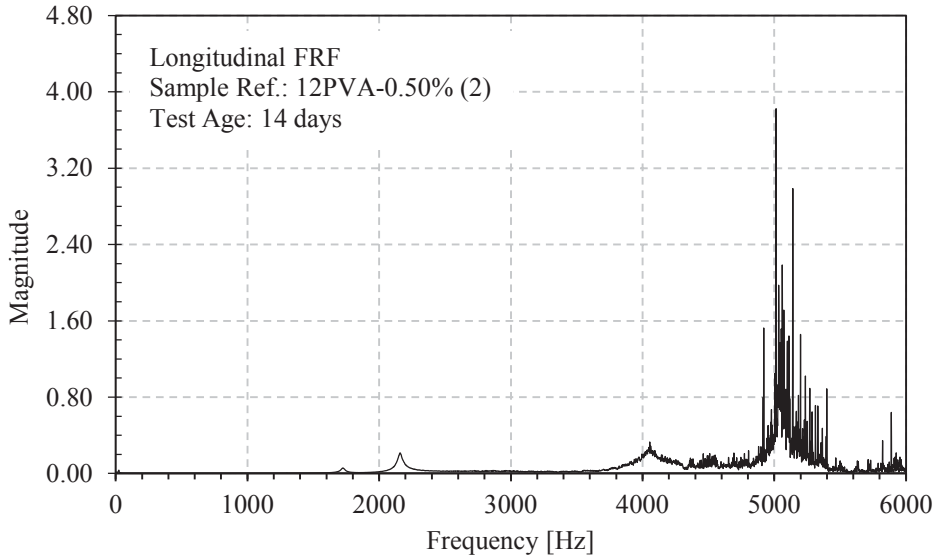
Longitudinal FRF
Sample Ref.: 12PVA-0.50% (2)
Test Age: 14 days
Magnitude
4.80
4.00
3.20
2.40
1.60
0.80
0.00
0
1000
2000
3000
4000
5000
6000
Frequency [Hz]

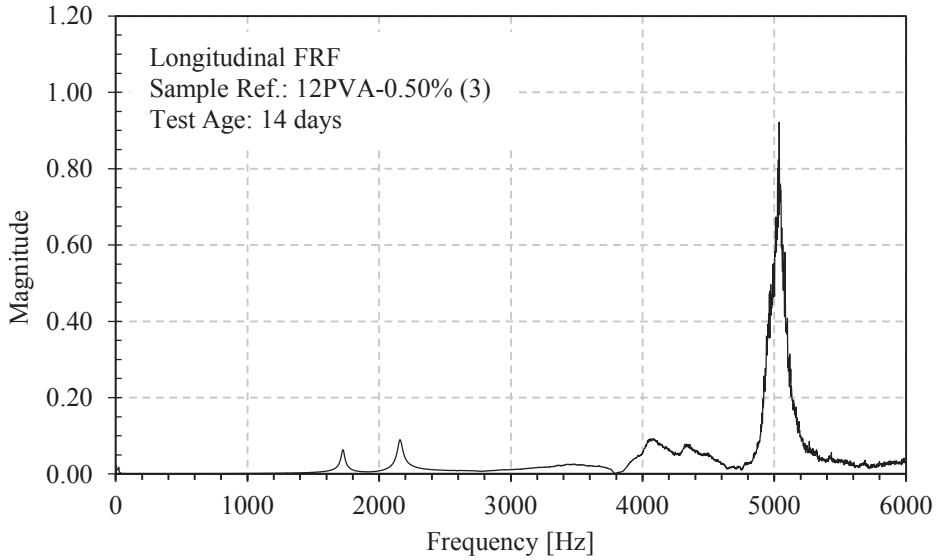
Longitudinal FRF
Sample Ref.: 12PVA-0.50% (3)
Test Age: 14 days
Magnitude
1.20
1.00
0.80
0.60
0.40
0.20
0.00
0
1000
2000
3000
4000
5000
6000
Frequency [Hz]

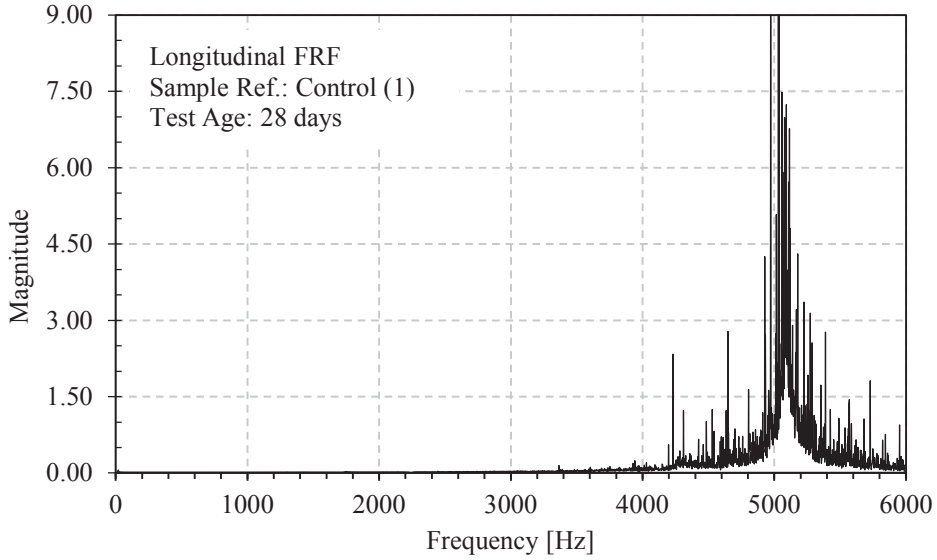
Longitudinal FRF
Sample Ref.: Control (1)
Test Age: 28 days
Magnitude
Frequency [Hz]
9.00
7.50
6.00
4.50
3.00
1.50
0.00
0
1000
2000
3000
4000
5000
6000

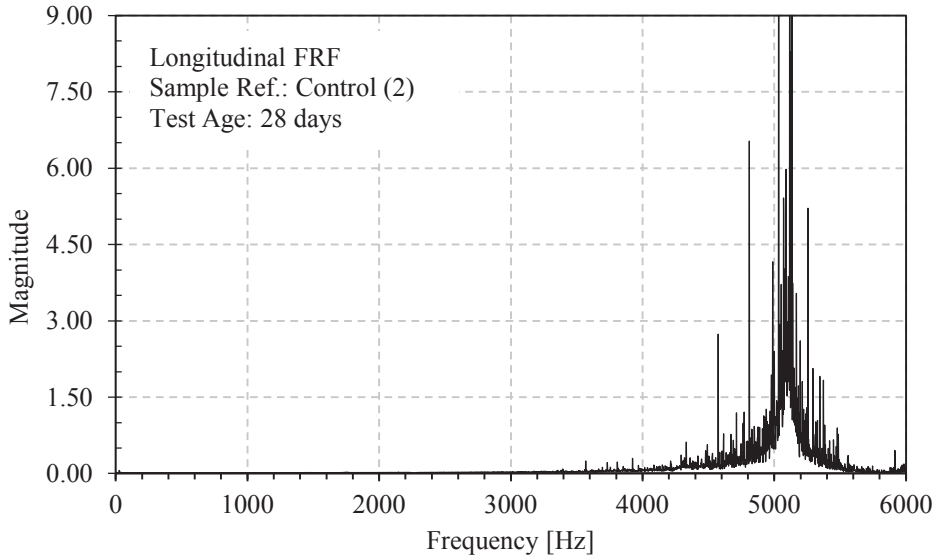
Longitudinal FRF
Sample Ref.: Control (2)
Test Age: 28 days
Magnitude
Frequency [Hz]
9.00
7.50
6.00
4.50
3.00
1.50
0.00
0
1000
2000
3000
4000
5000
6000

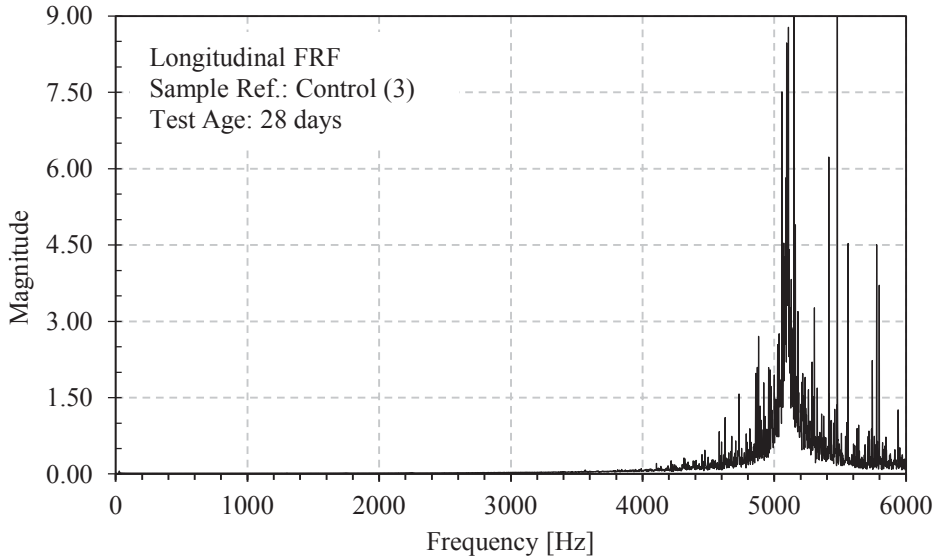
Longitudinal FRF
Sample Ref.: Control (3)
Test Age: 28 days
Magnitude
Frequency [Hz]
9.00
7.50
6.00
4.50
3.00
1.50
0.00
0
1000
2000
3000
4000
5000
6000

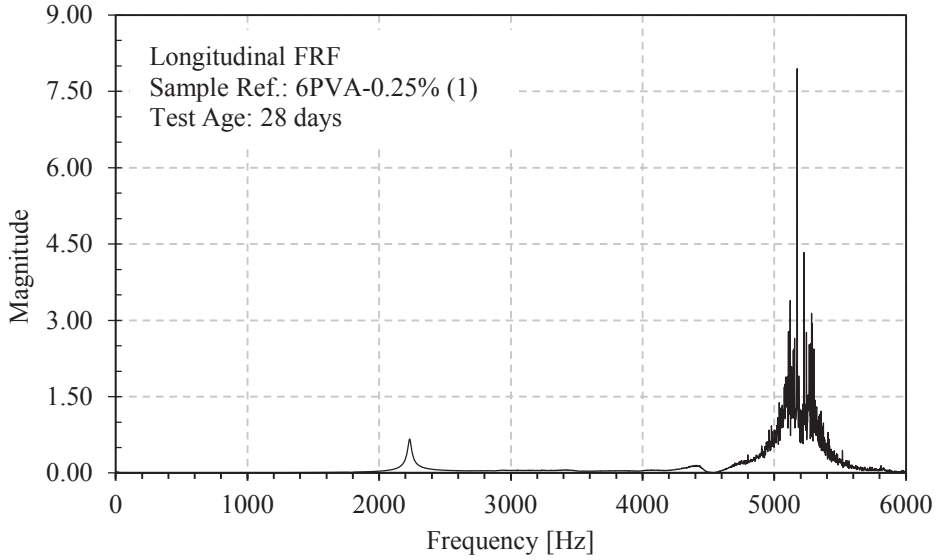
Longitudinal FRF
Sample Ref.: 6PVA-0.25% (1)
Test Age: 28 days
Magnitude
Frequency [Hz]
9.00
7.50
6.00
4.50
3.00
1.50
0.00
0
1000
2000
3000
4000
5000
6000

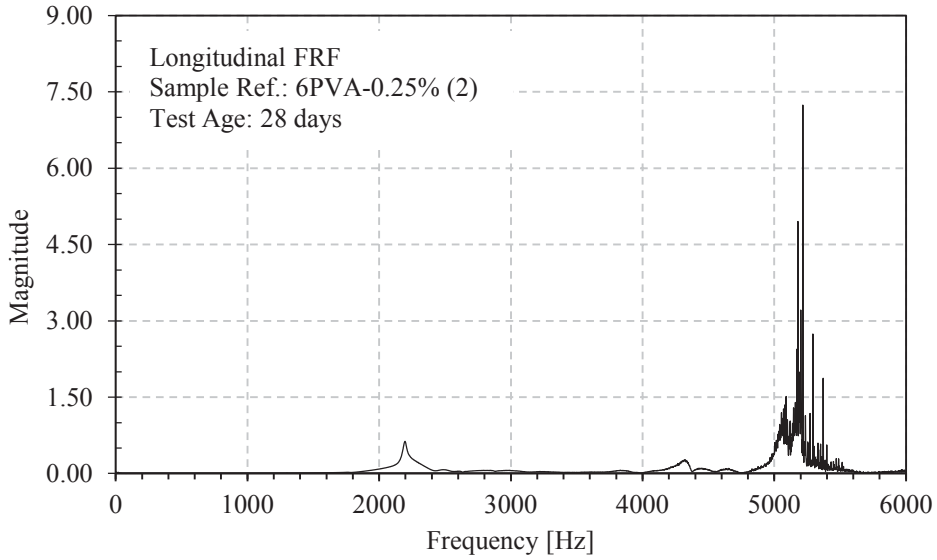
Longitudinal FRF
Sample Ref.: 6PVA-0.25% (2)
Test Age: 28 days
Magnitude
Frequency [Hz]
9.00
7.50
6.00
4.50
3.00
1.50
0.00
0
1000
2000
3000
4000
5000
6000

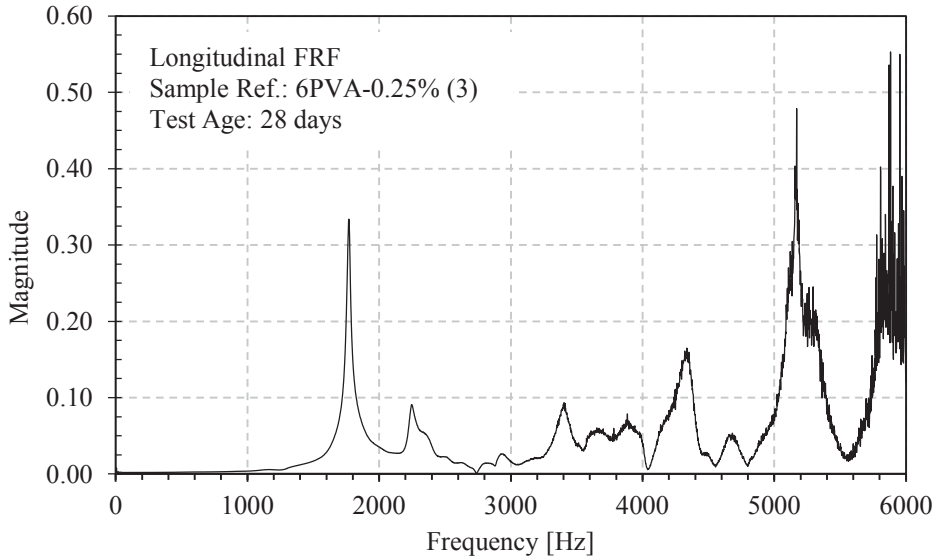
Longitudinal FRF
Sample Ref.: 6PVA-0.25% (3)
Test Age: 28 days
Magnitude
Frequency [Hz]
0.60
0.50
0.40
0.30
0.20
0.10
0.00
0
1000
2000
3000
4000
5000
6000

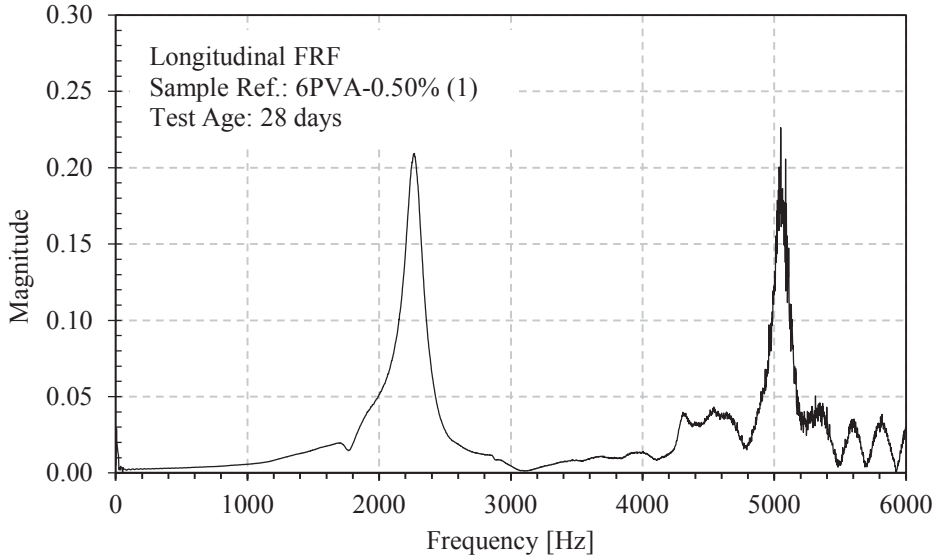
Longitudinal FRF
Sample Ref.: 6PVA-0.50% (1)
Test Age: 28 days
Magnitude
Frequency [Hz]
0.30
0.25
0.20
0.15
0.10
0.05
0.00
0
1000
2000
3000
4000
5000
6000

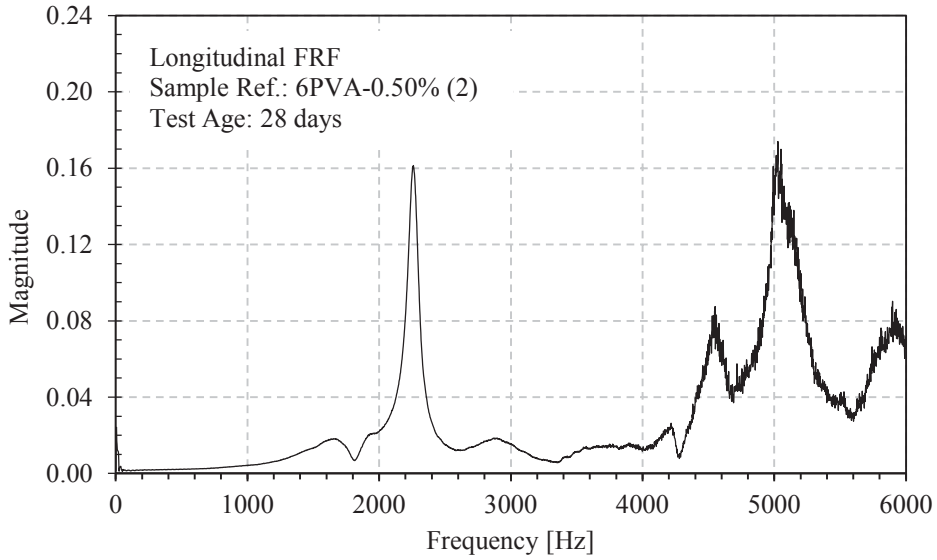
Longitudinal FRF
Sample Ref.: 6PVA-0.50% (2)
Test Age: 28 days
Magnitude
Frequency [Hz]
0.24
0.20
0.16
0.12
0.08
0.04
0.00
0
1000
2000
3000
4000
5000
6000

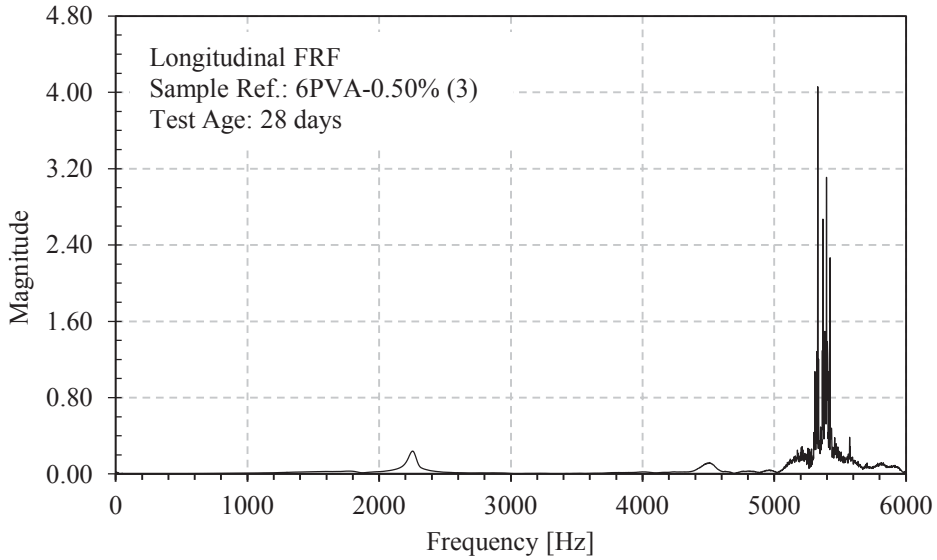
Longitudinal FRF
Sample Ref.: 6PVA-0.50% (3)
Test Age: 28 days
Magnitude
Frequency [Hz]
4.80
4.00
3.20
2.40
1.60
0.80
0.00
0
1000
2000
3000
4000
5000
6000

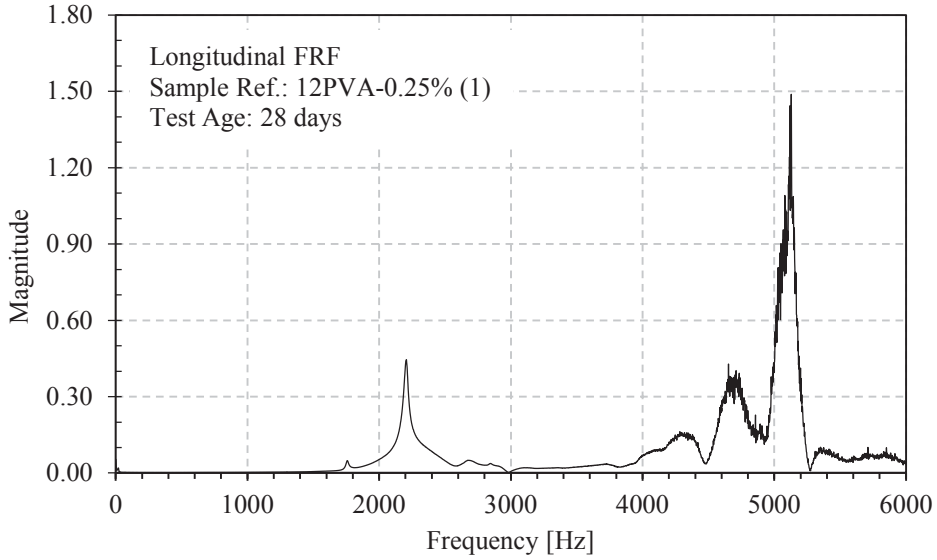
Longitudinal FRF
Sample Ref.: 12PVA-0.25% (1)
Test Age: 28 days
Magnitude
Frequency [Hz]
1.80
1.50
1.20
0.90
0.60
0.30
0.00
0
1000
2000
3000
4000
5000
6000

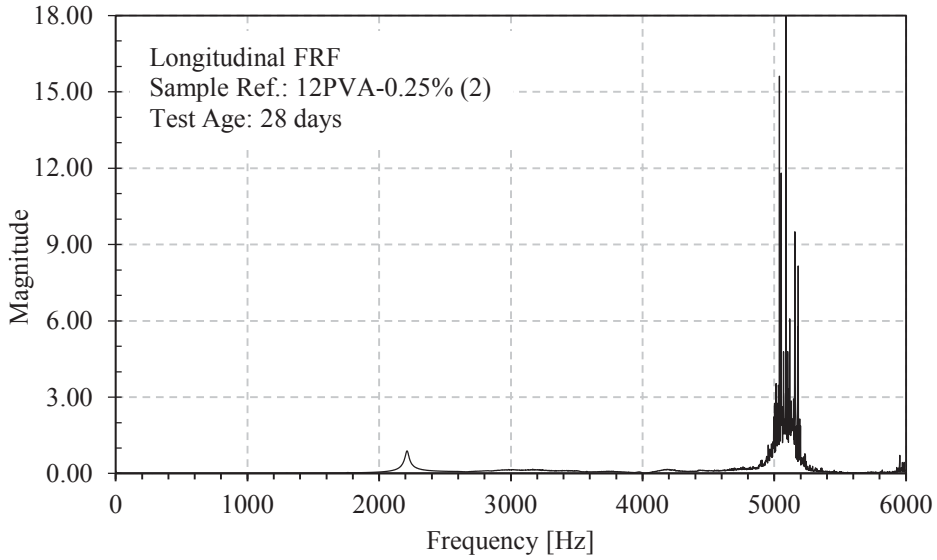
Longitudinal FRF
Sample Ref.: 12PVA-0.25% (2)
Test Age: 28 days
Magnitude
Frequency [Hz]
18.00
15.00
12.00
9.00
6.00
3.00
0.00
0
1000
2000
3000
4000
5000
6000

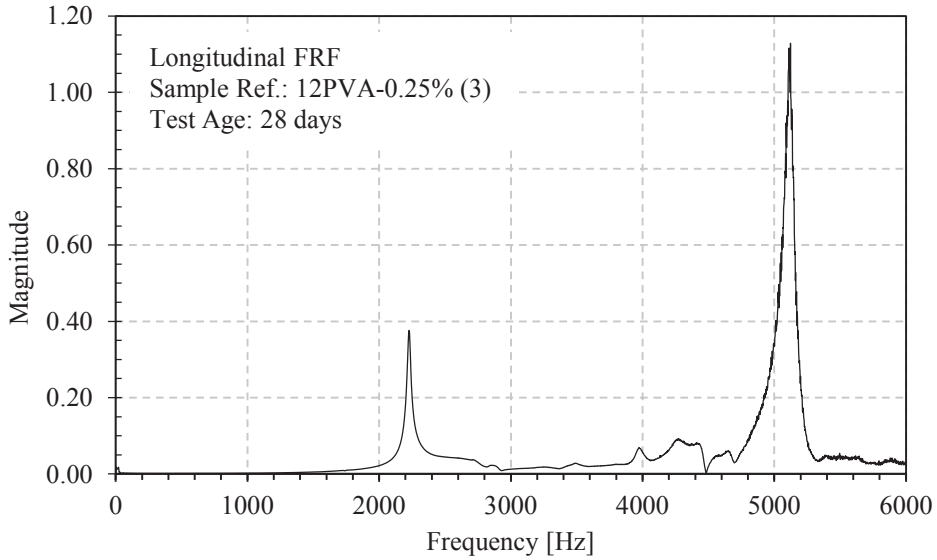
Longitudinal FRF
Sample Ref.: 12PVA-0.25% (3)
Test Age: 28 days
Magnitude
Frequency [Hz]
1.20
1.00
0.80
0.60
0.40
0.20
0.00
0
1000
2000
3000
4000
5000
6000

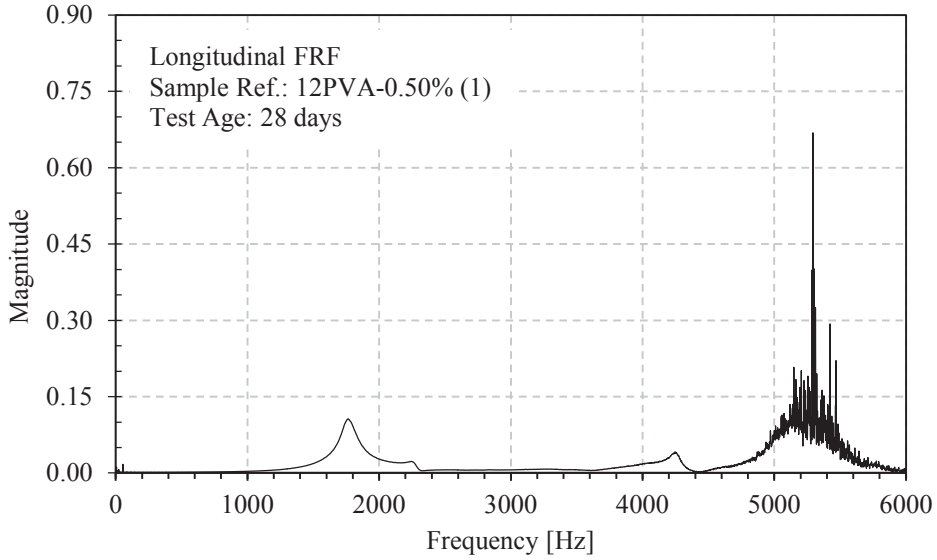
Longitudinal FRF
Sample Ref.: 12PVA-0.50% (1)
Test Age: 28 days
Magnitude
Frequency [Hz]
0.90
0.75
0.60
0.45
0.30
0.15
0.00
0
1000
2000
3000
4000
5000
6000

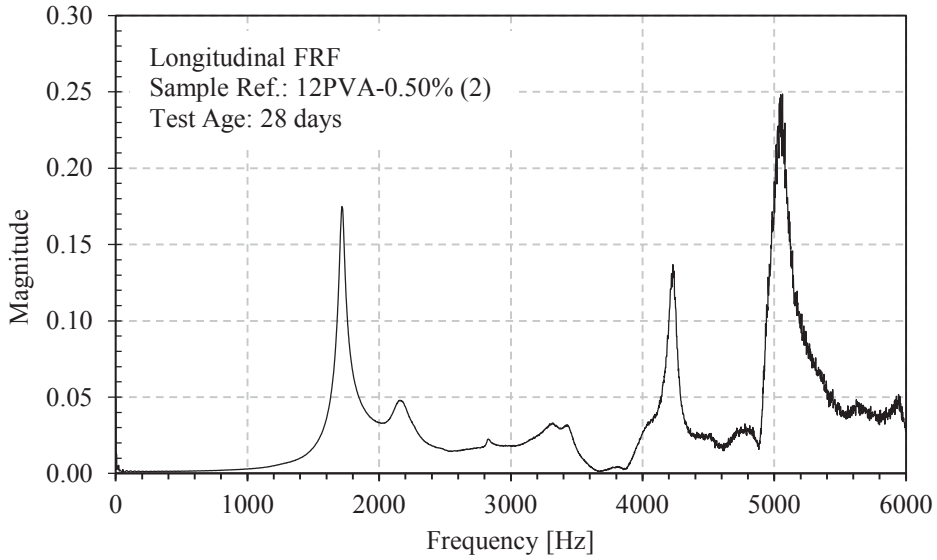
Longitudinal FRF
Sample Ref.: 12PVA-0.50% (2)
Test Age: 28 days
Magnitude
Frequency [Hz]
0.30
0.25
0.20
0.15
0.10
0.05
0.00
0
1000
2000
3000
4000
5000
6000

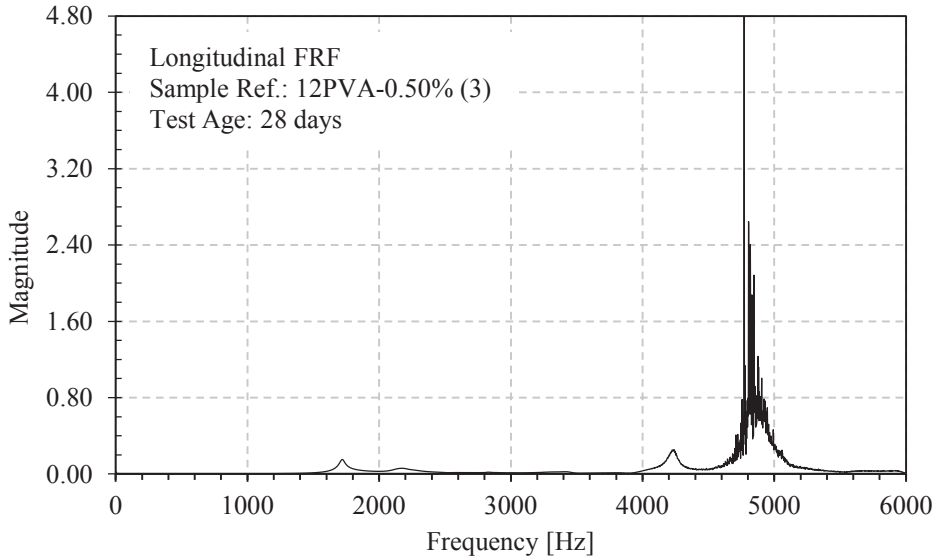
Longitudinal FRF
Sample Ref.: 12PVA-0.50% (3)
Test Age: 28 days
Magnitude
Frequency [Hz]
4.80
4.00
3.20
2.40
1.60
0.80
0.00
0
1000
2000
3000
4000
5000
6000

APPENDIX B

The load-deflection curves of concrete beams of series A and B under 3-point cyclic tests are presented in this appendix. Each graph is representing one loading cycle following the loading regimes previously described in section 3.6.12.

B.1 Load-deflection curves for beam Control (A)

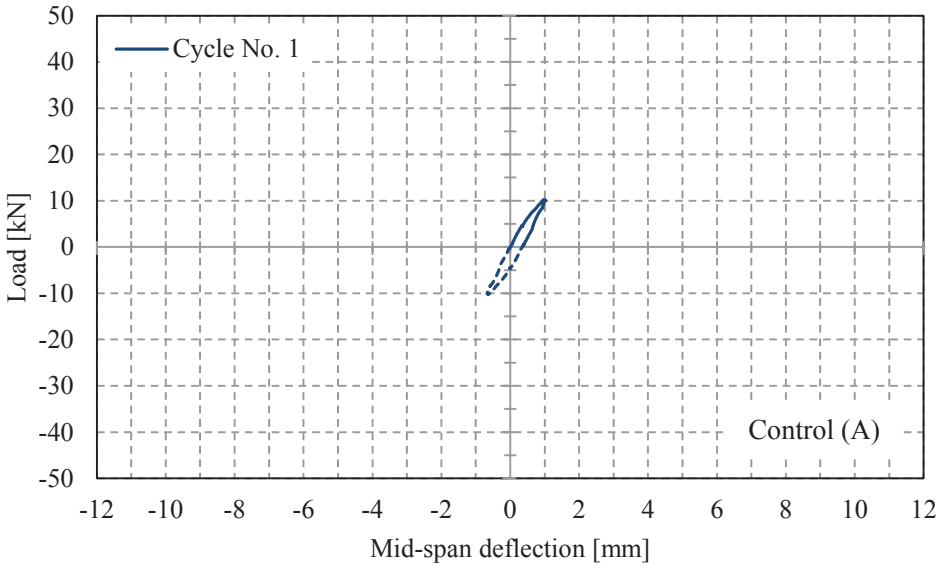

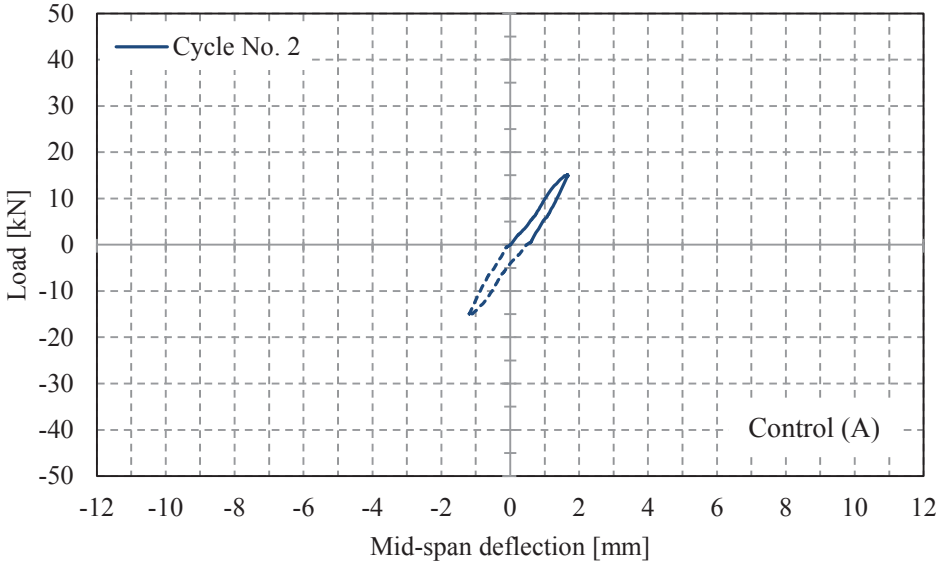

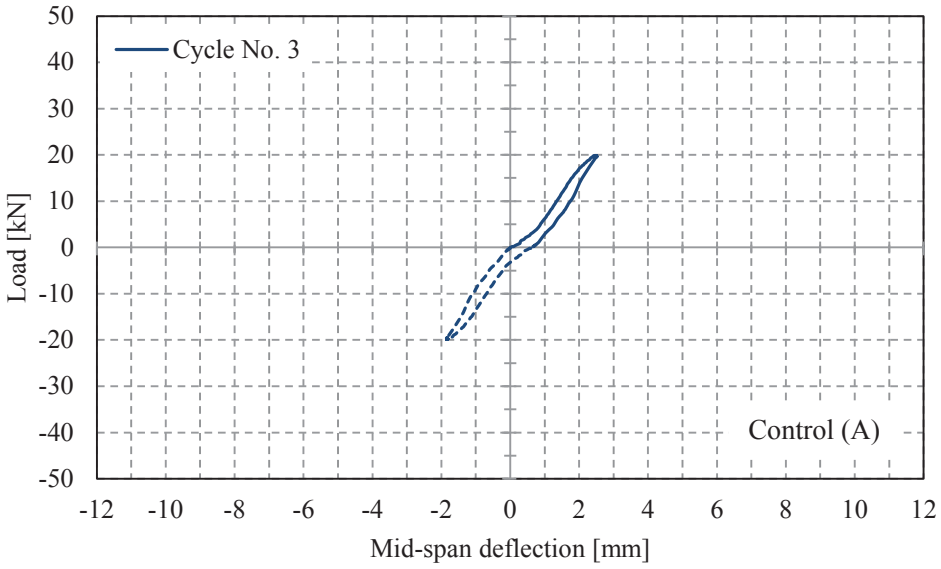
Cycle No. 3
Load [kN]
Mid-span deflection [mm]
Control (A)

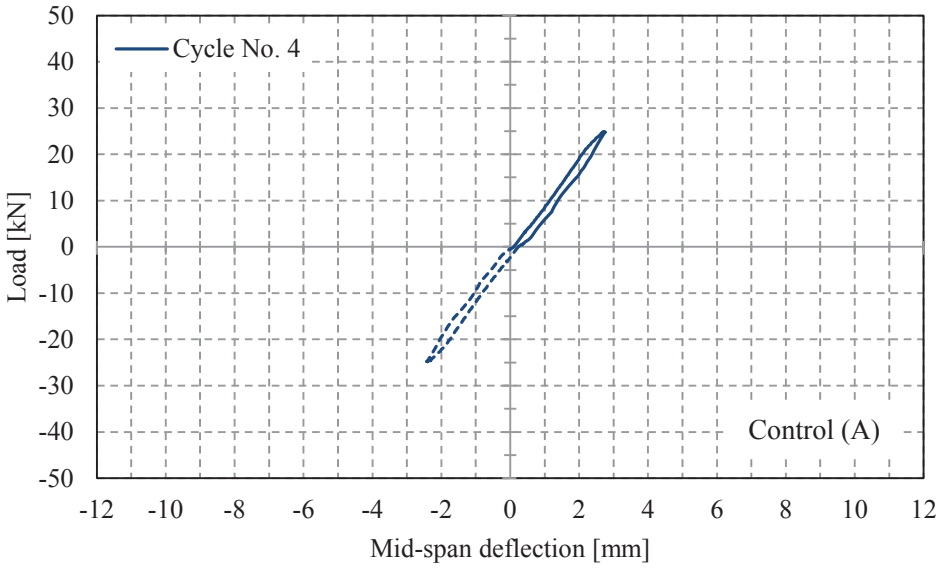
Cycle No. 4
Load [kN]
Mid-span deflection [mm]
Control (A)

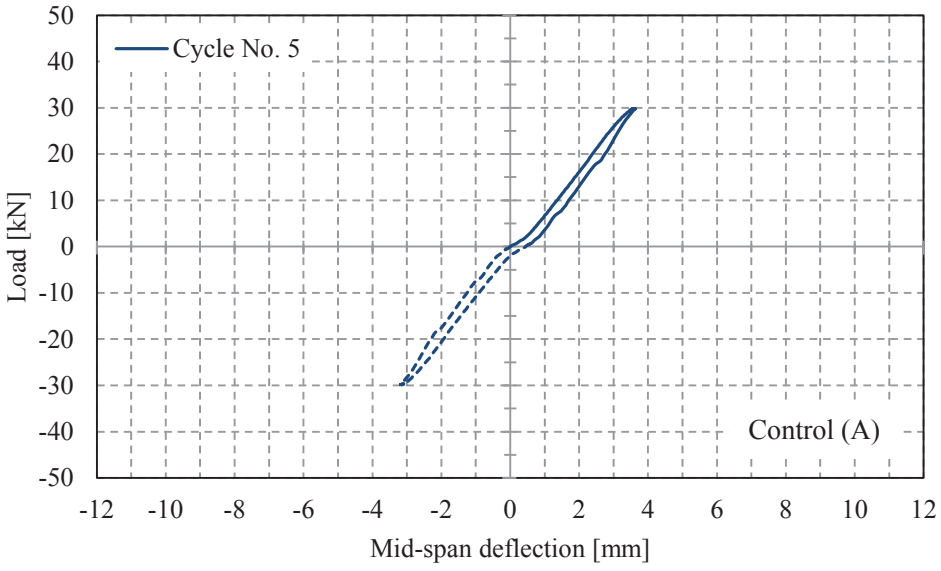
Cycle No. 5
Load [kN]
Mid-span deflection [mm]
Control (A)

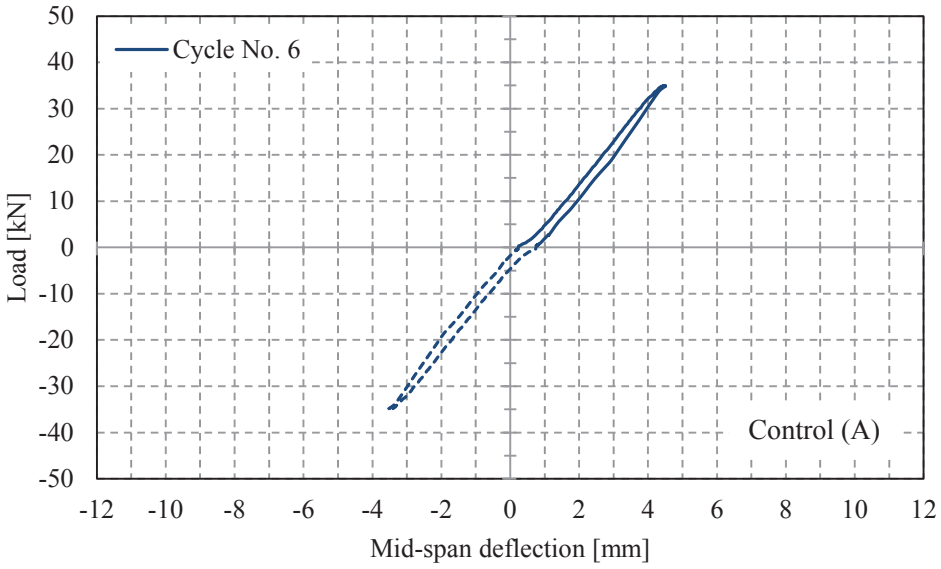
Cycle No. 6
Load [kN]
Mid-span deflection [mm]
Control (A)

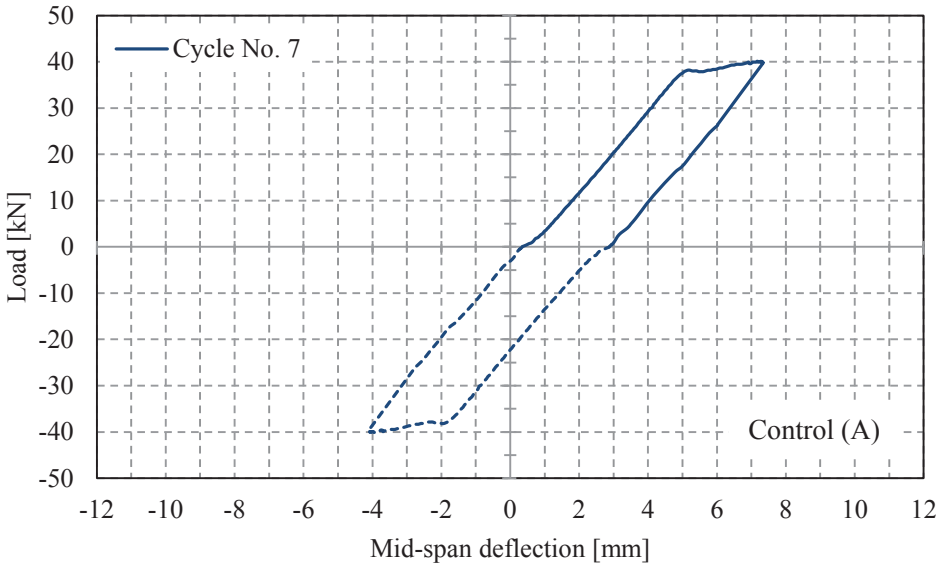
Cycle No. 7
Load [kN]
Mid-span deflection [mm]
Control (A)

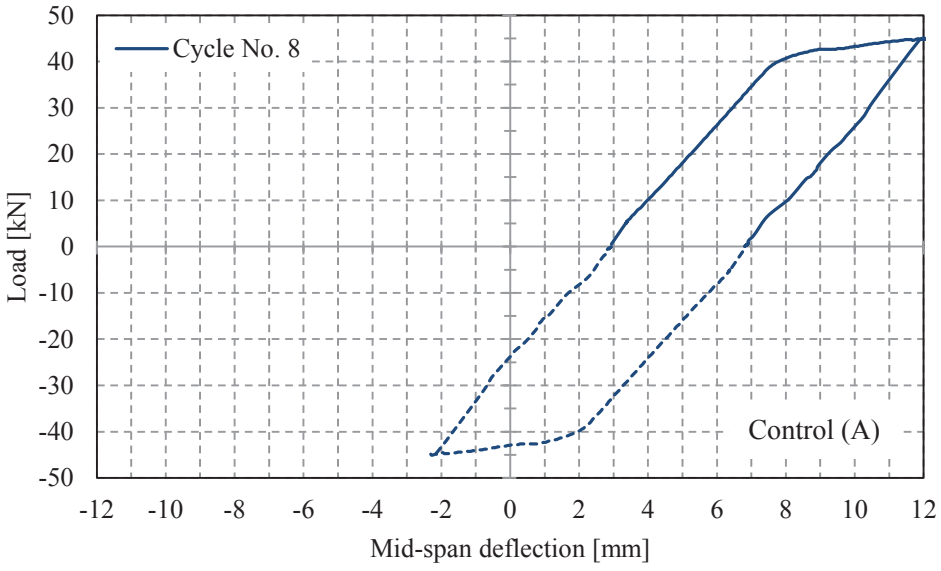
Cycle No. 8
Load [kN]
Mid-span deflection [mm]
Control (A)

B.2 Load-deflection curves for beam 6PVA0.25% (A)

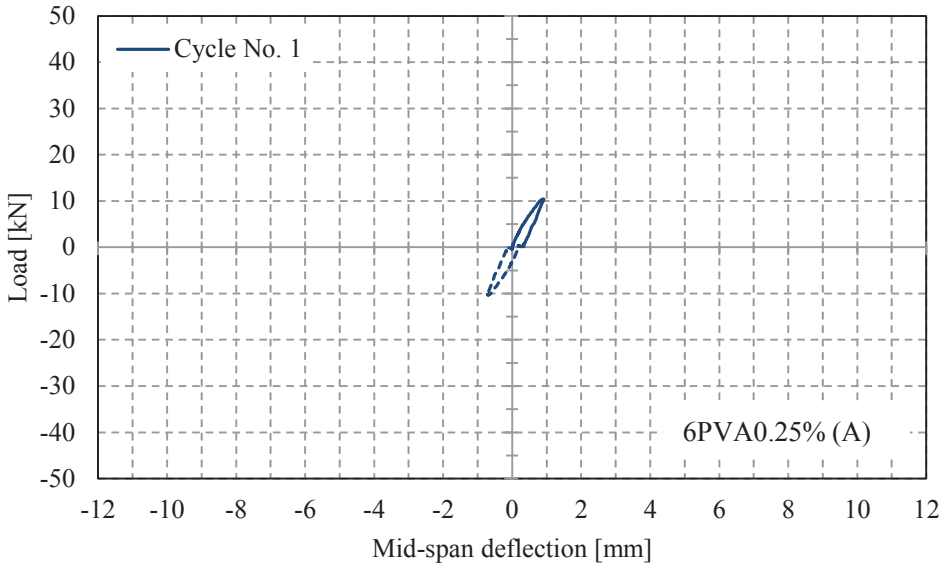

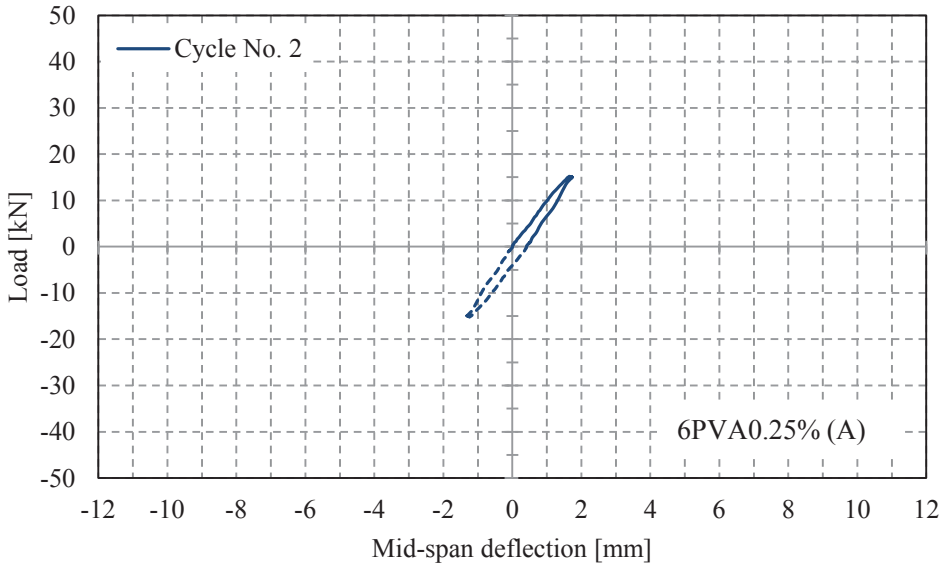

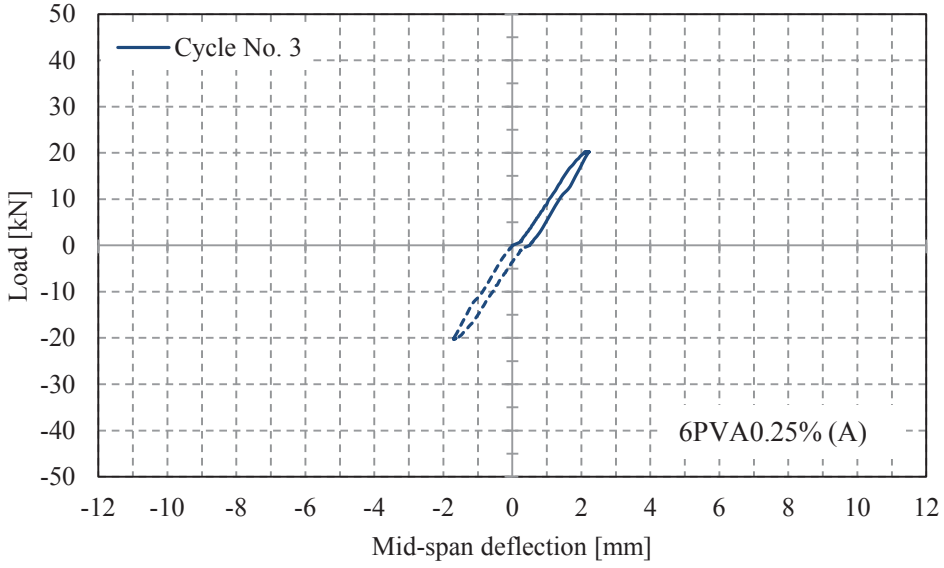

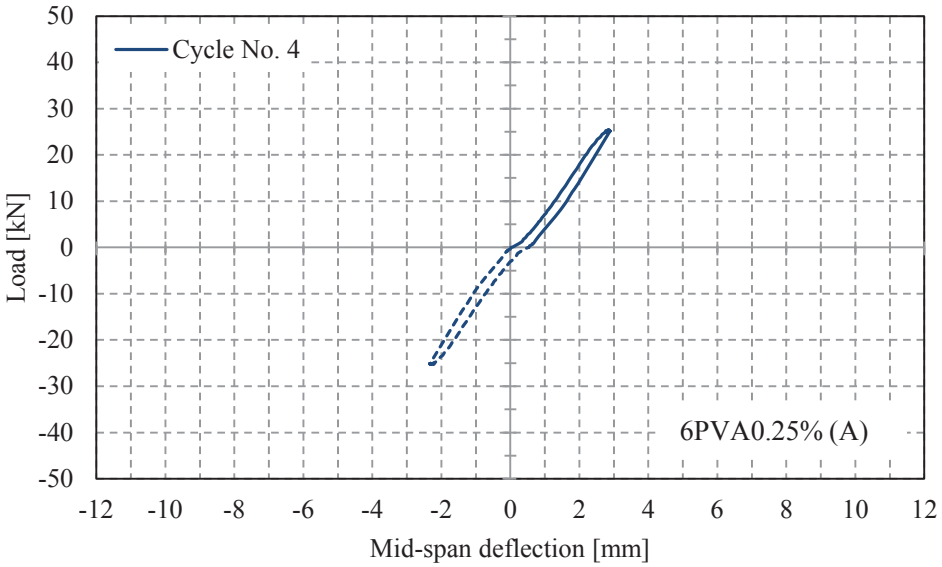
Cycle No. 4
Load [kN]
Mid-span deflection [mm]
6PVA0.25% (A)

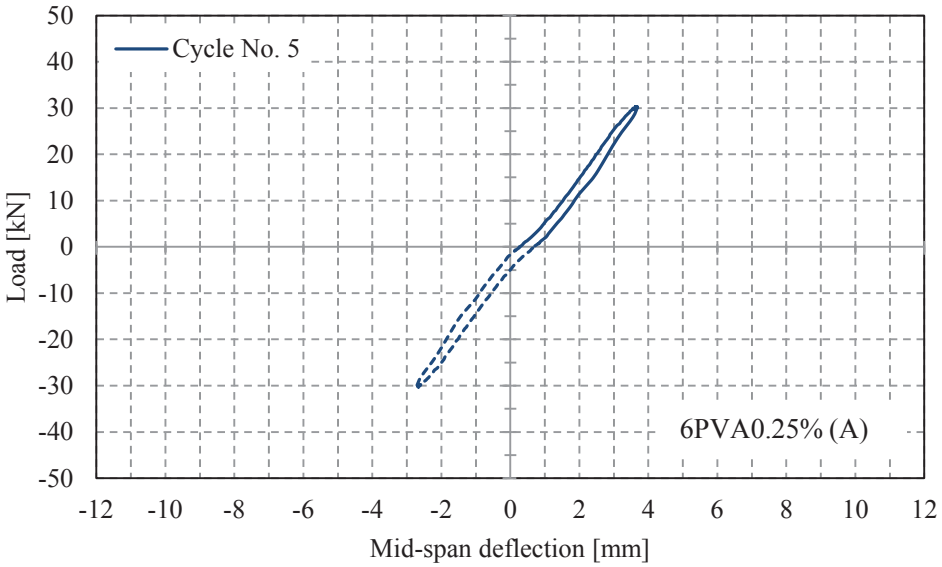
Cycle No. 5
Load [kN]
Mid-span deflection [mm]
6PVA0.25% (A)

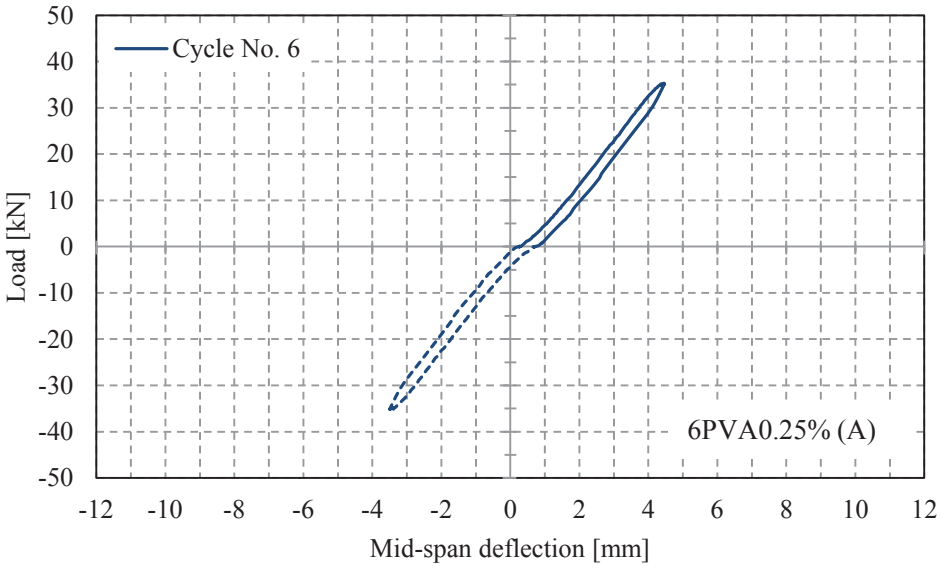
Cycle No. 6
Load [kN]
Mid-span deflection [mm]
6PVA0.25% (A)

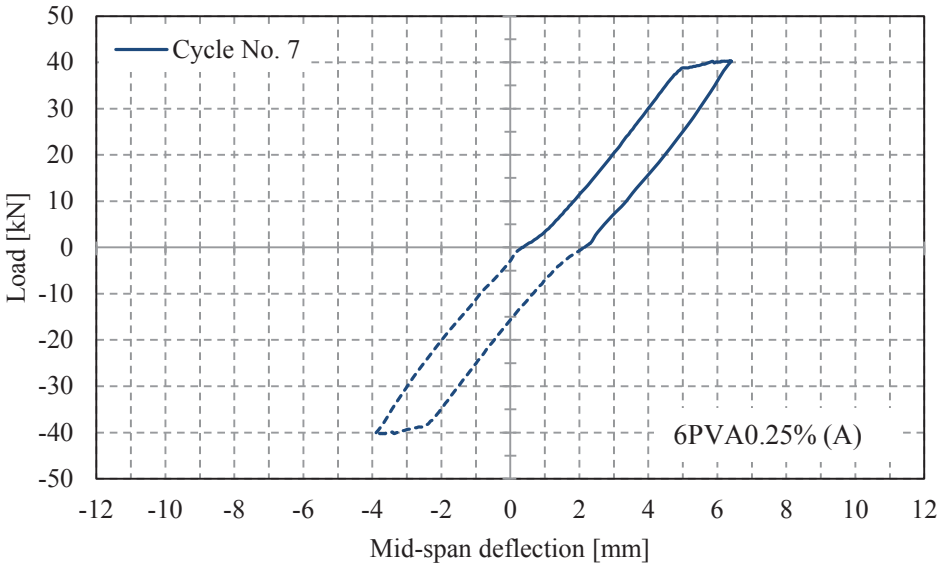
Cycle No. 7
Load [kN]
Mid-span deflection [mm]
6PVA0.25% (A)
50
40
30
20
10
0
-10
-20
-30
-40
-50
-12
-10
-8
-6
-4
-2
0
2
4
6
8
10
12

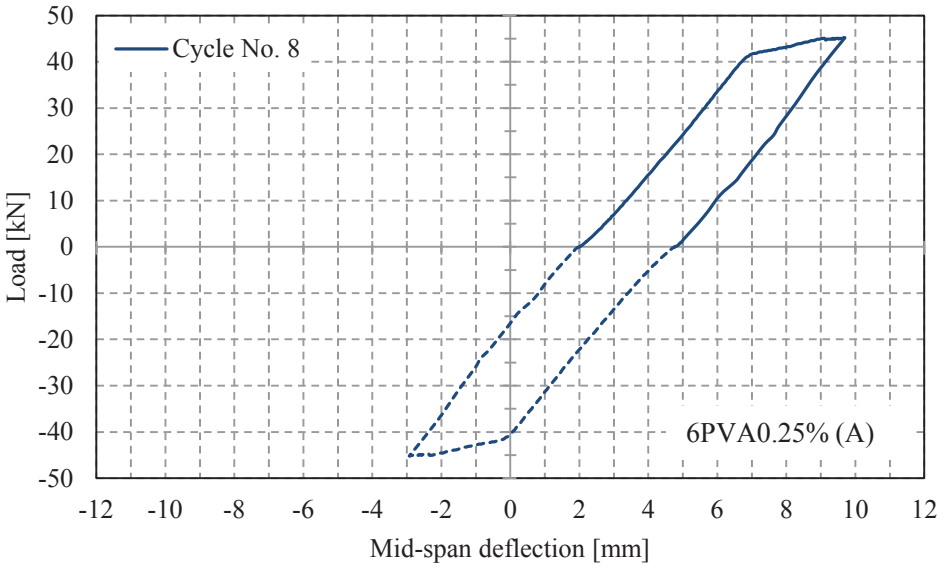
Cycle No. 8
Load [kN]
Mid-span deflection [mm]
6PVA0.25% (A)
50
40
30
20
10
0
-10
-20
-30
-40
-50
-12
-10
-8
-6
-4
-2
0
2
4
6
8
10
12

B.3 Load-deflection curves for beam 12PVA0.50% (A)

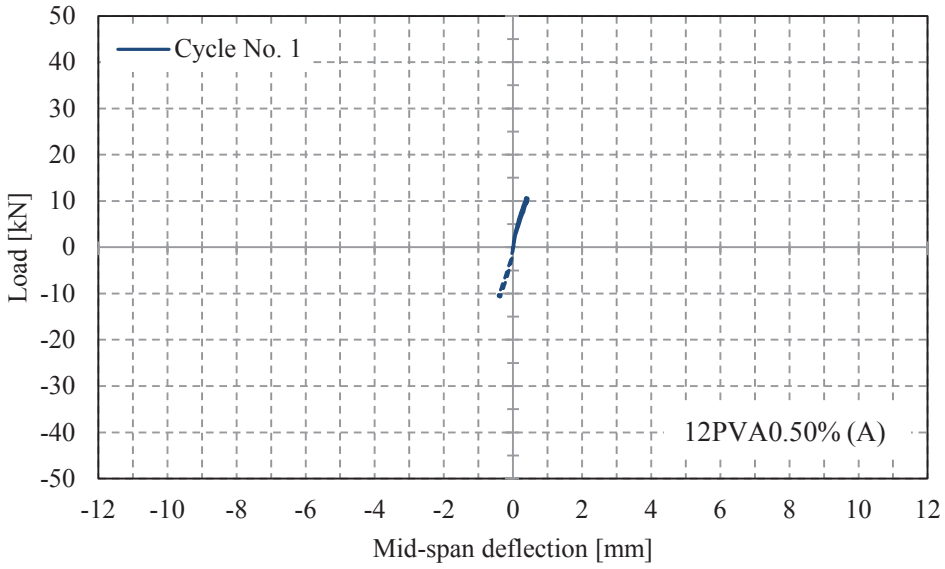

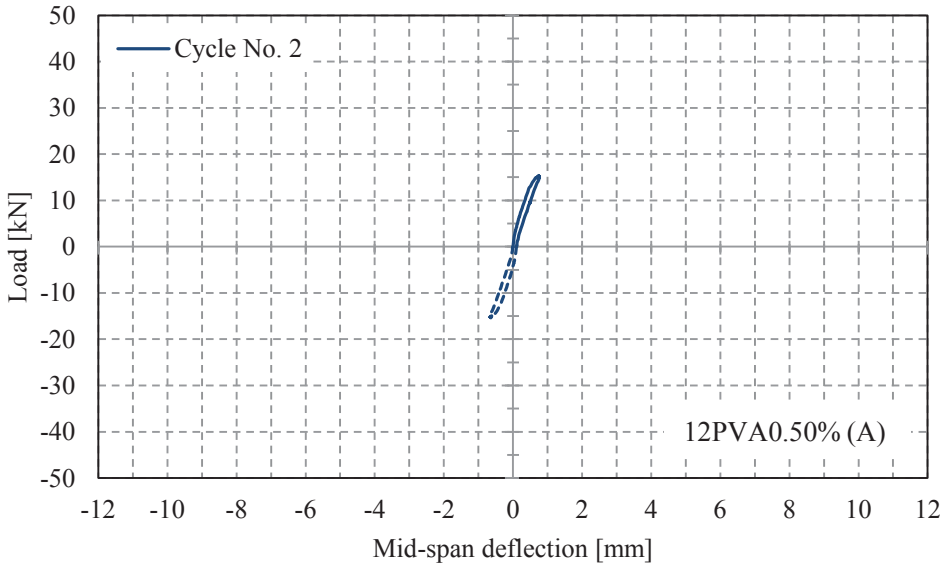

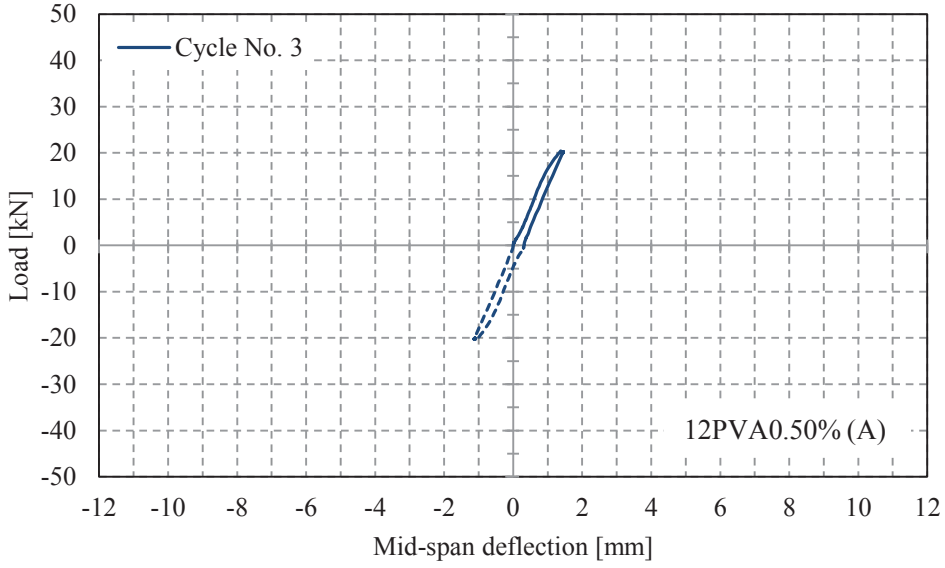

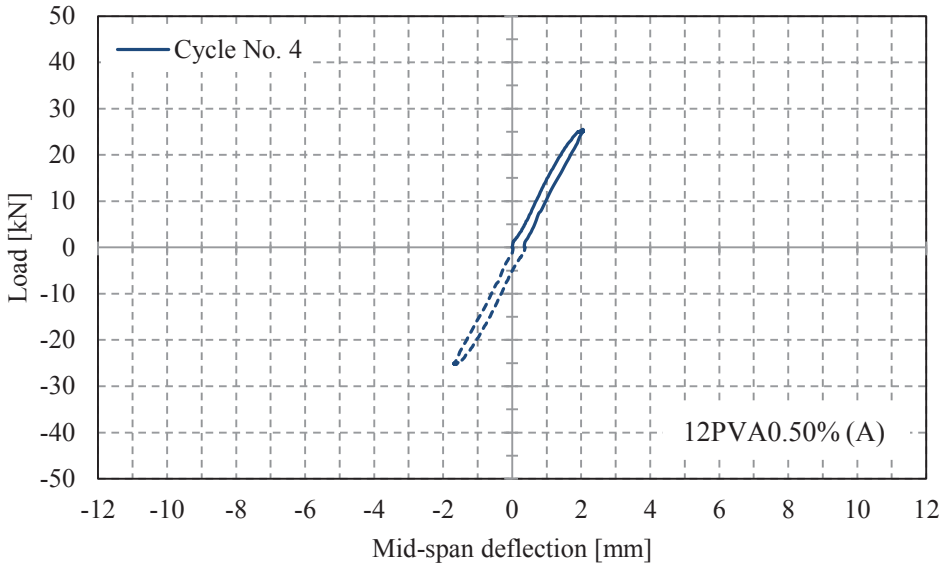
Cycle No. 4
Load [kN]
Mid-span deflection [mm]
12PVA0.50% (A)

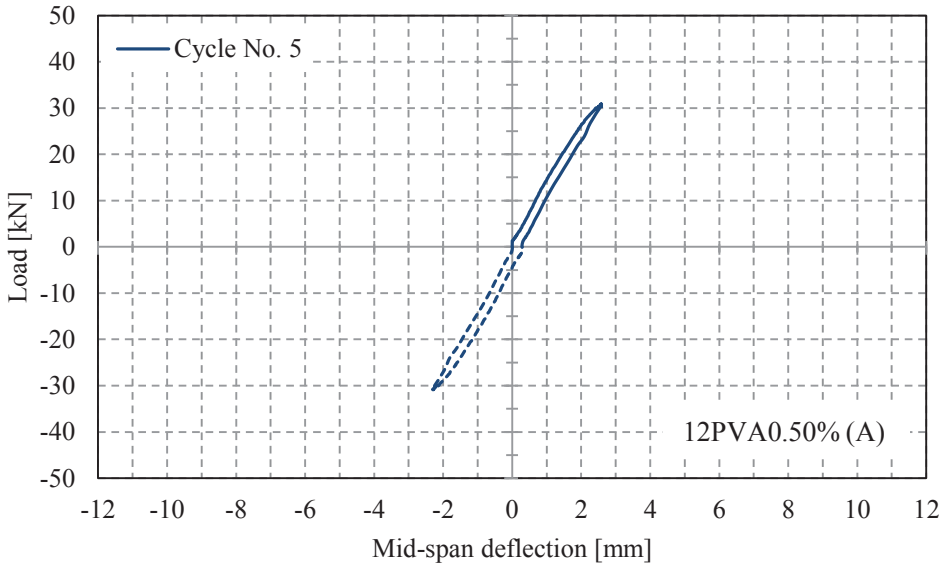
Cycle No. 5
Load [kN]
Mid-span deflection [mm]
12PVA0.50% (A)

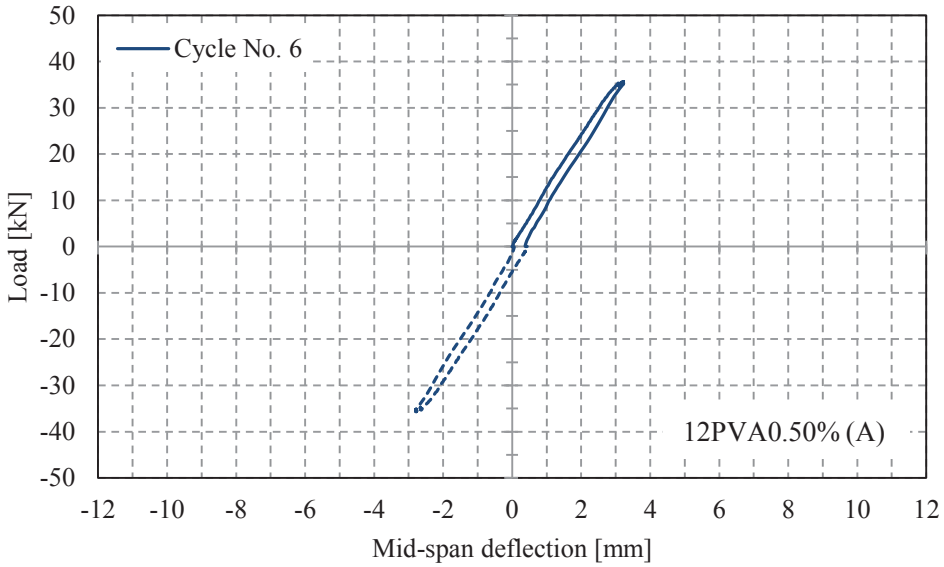
Cycle No. 6
Load [kN]
Mid-span deflection [mm]
12PVA0.50% (A)

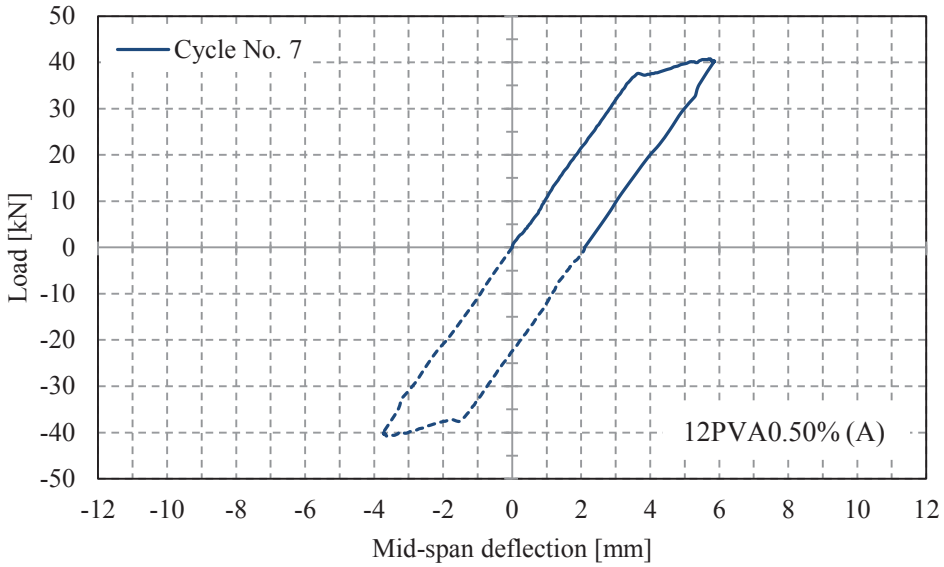
Cycle No. 7
Load [kN]
Mid-span deflection [mm]
12PVA0.50% (A)
50
40
30
20
10
0
-10
-20
-30
-40
-50
-12
-10
-8
-6
-4
-2
0
2
4
6
8
10
12

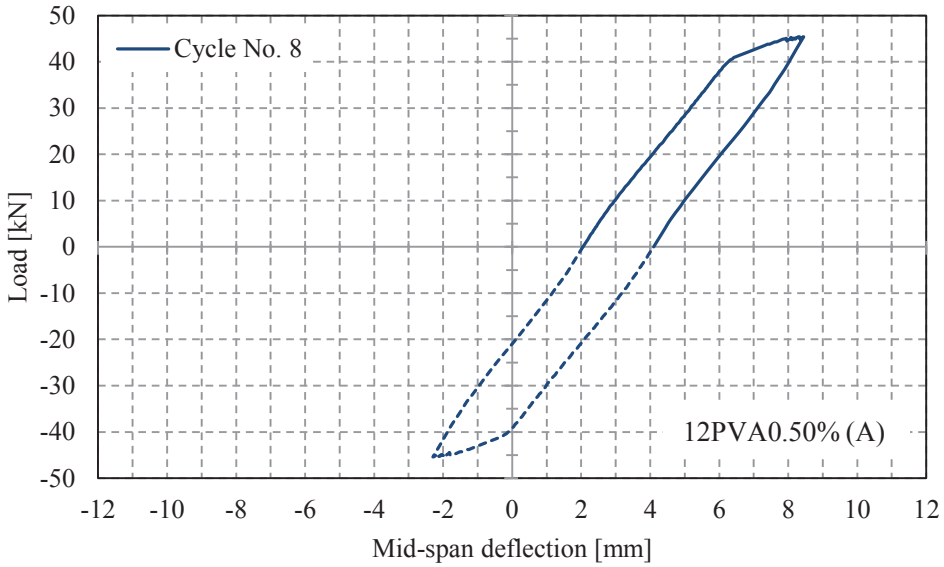
Cycle No. 8
Load [kN]
Mid-span deflection [mm]
12PVA0.50% (A)
50
40
30
20
10
0
-10
-20
-30
-40
-50
-12
-10
-8
-6
-4
-2
0
2
4
6
8
10
12

B.4 Load-deflection curves for beam Control (B)

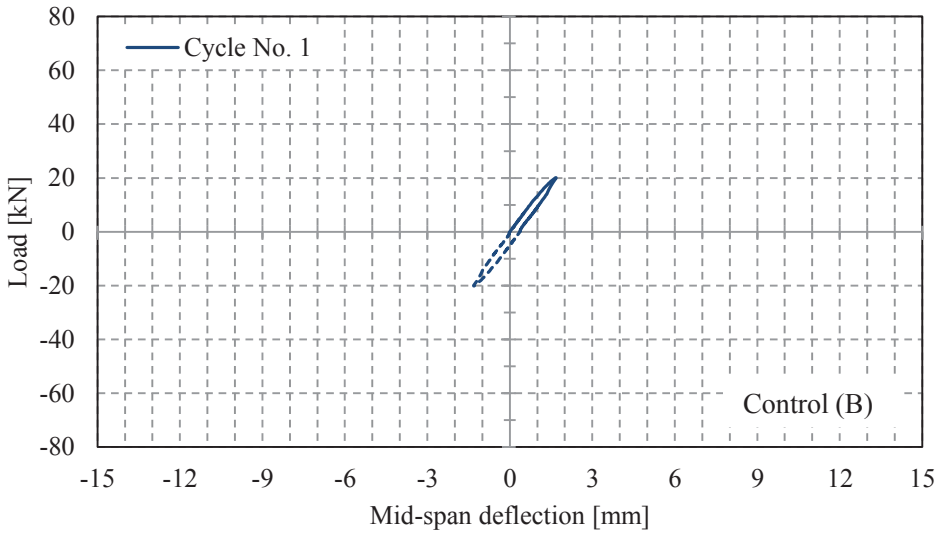

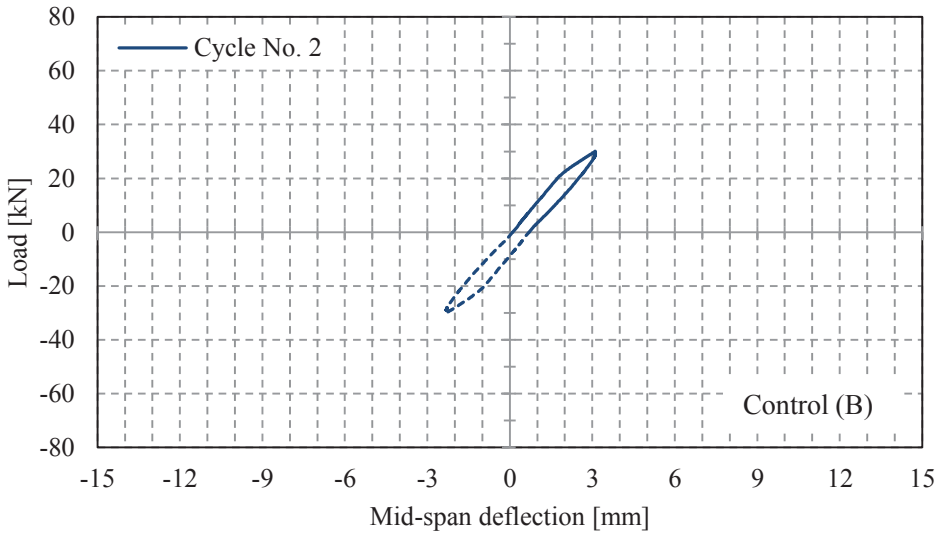

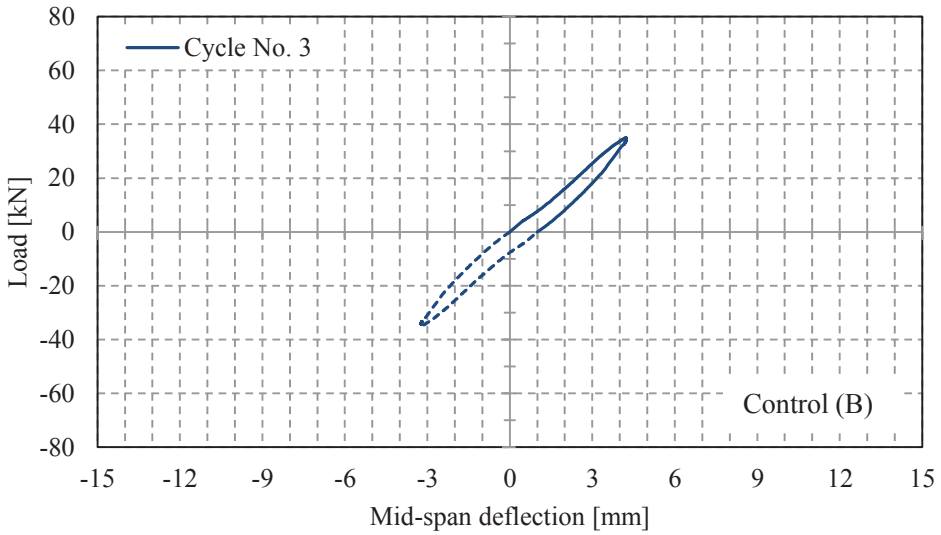

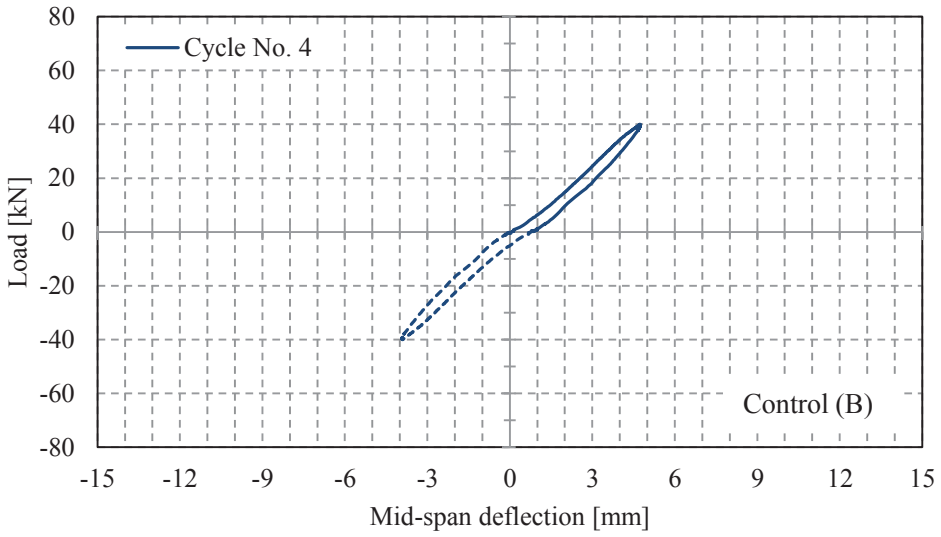
Cycle No. 4
Load [kN]
80
60
40
20
0
-20
-40
-60
-80
-15
-12
-9
-6
-3
0
3
6
9
12
15
Mid-span deflection [mm]
Control (B)

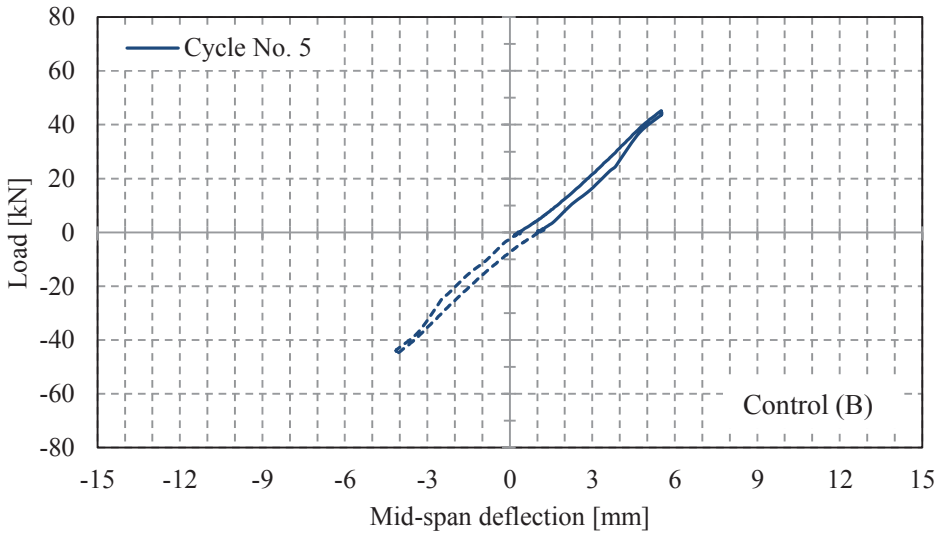
Cycle No. 5
Load [kN]
80
60
40
20
0
-20
-40
-60
-80
-15
-12
-9
-6
-3
0
3
6
9
12
15
Mid-span deflection [mm]
Control (B)

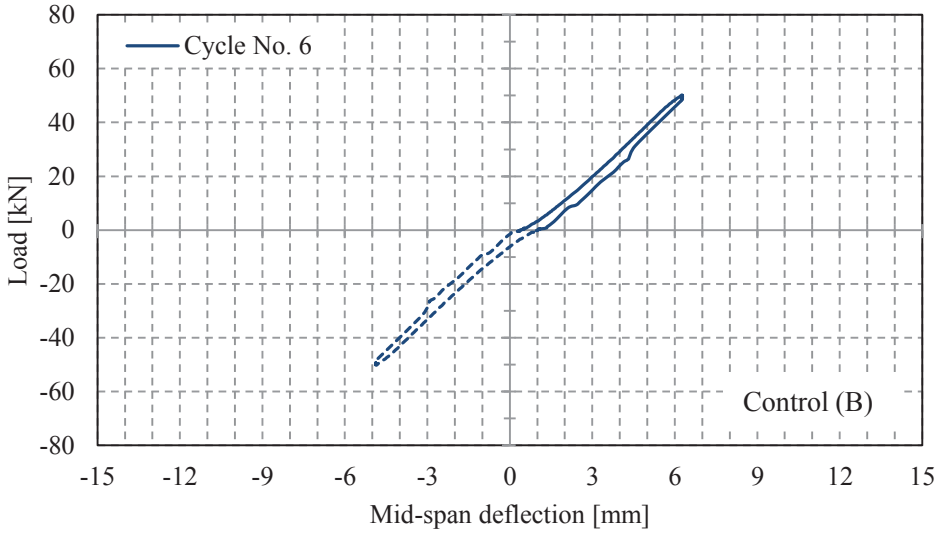
Cycle No. 6
Load [kN]
80
60
40
20
0
-20
-40
-60
-80
-15
-12
-9
-6
-3
0
3
6
9
12
15
Mid-span deflection [mm]
Control (B)

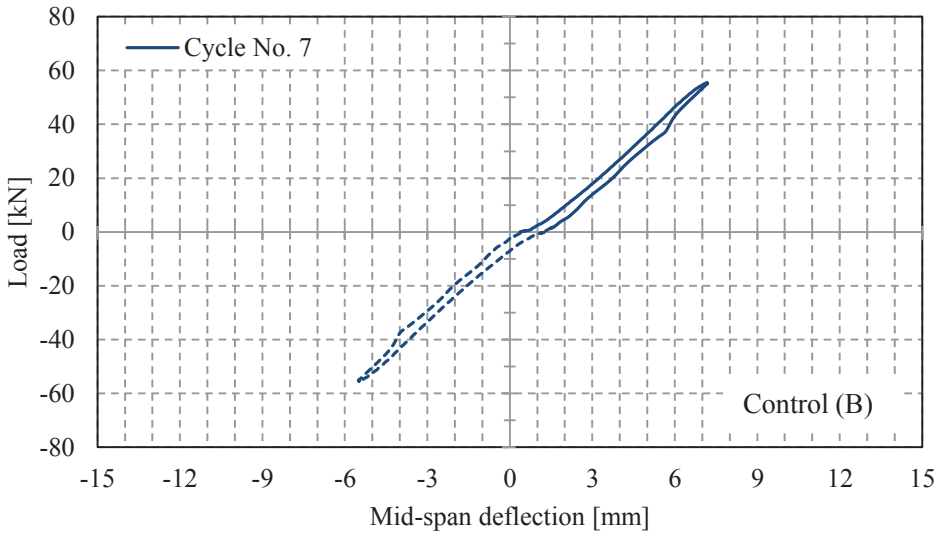
Cycle No. 7
Load [kN]
80
60
40
20
0
-20
-40
-60
-80
-15
-12
-9
-6
-3
0
3
6
9
12
15
Mid-span deflection [mm]
Control (B)

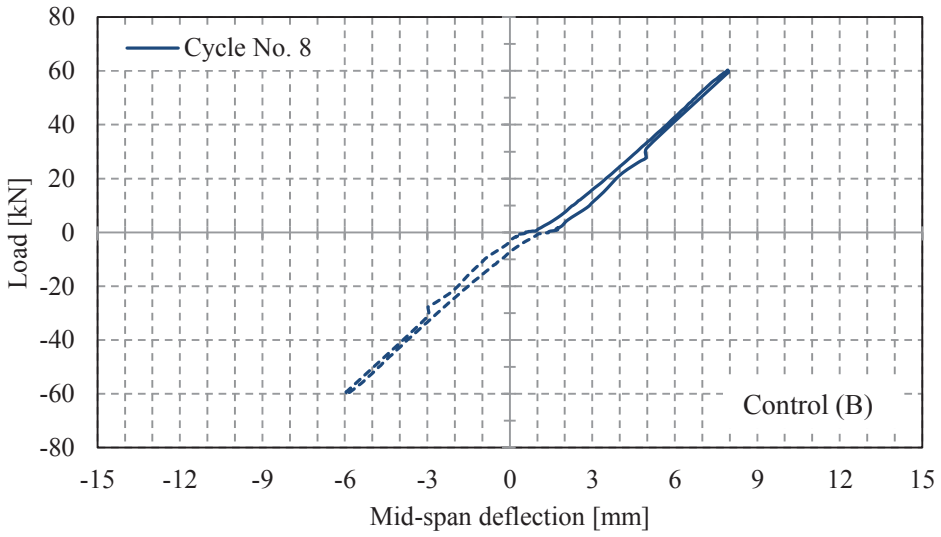
Cycle No. 8
Load [kN]
80
60
40
20
0
-20
-40
-60
-80
-15
-12
-9
-6
-3
0
3
6
9
12
15
Mid-span deflection [mm]
Control (B)

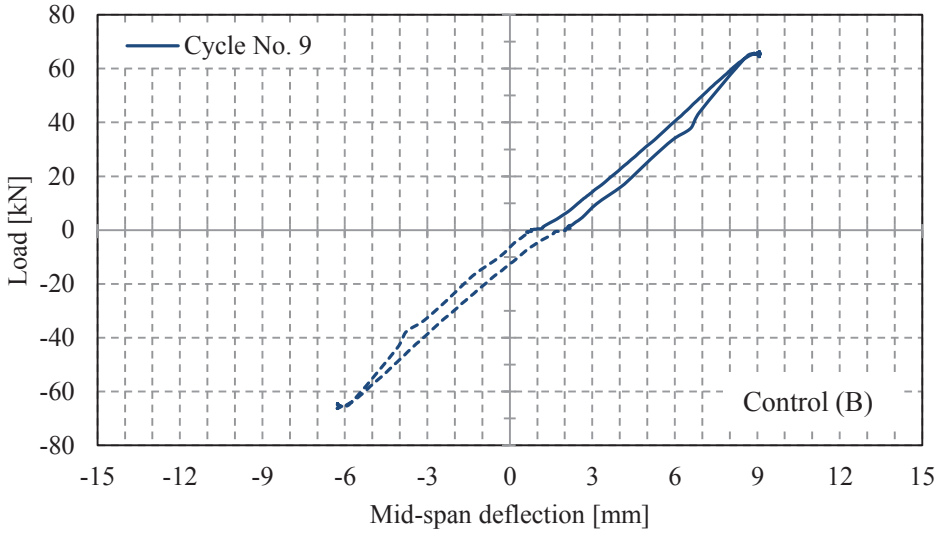
Cycle No. 9
Load [kN]
80
60
40
20
0
-20
-40
-60
-80
-15
-12
-9
-6
-3
0
3
6
9
12
15
Mid-span deflection [mm]
Control (B)

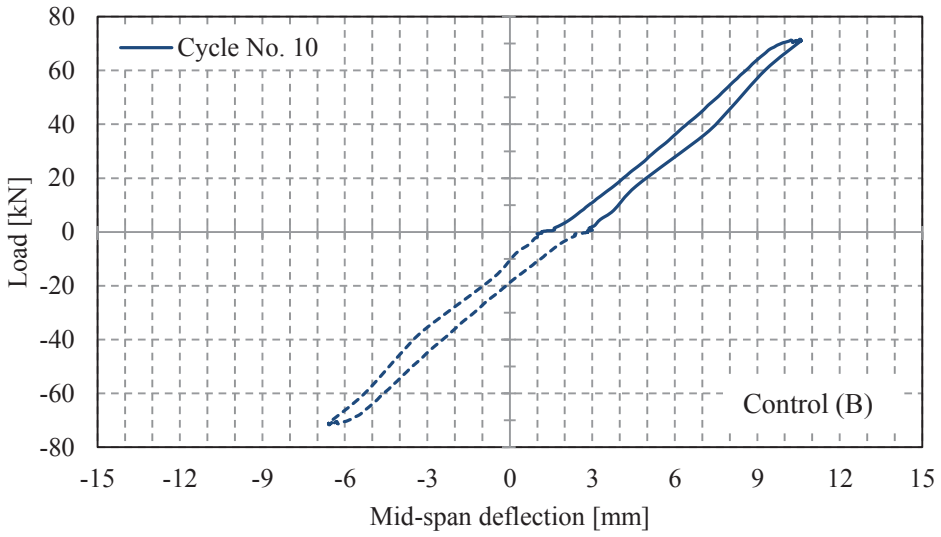
Cycle No. 10
Load [kN]
80
60
40
20
0
-20
-40
-60
-80
-15
-12
-9
-6
-3
0
3
6
9
12
15
Mid-span deflection [mm]
Control (B)

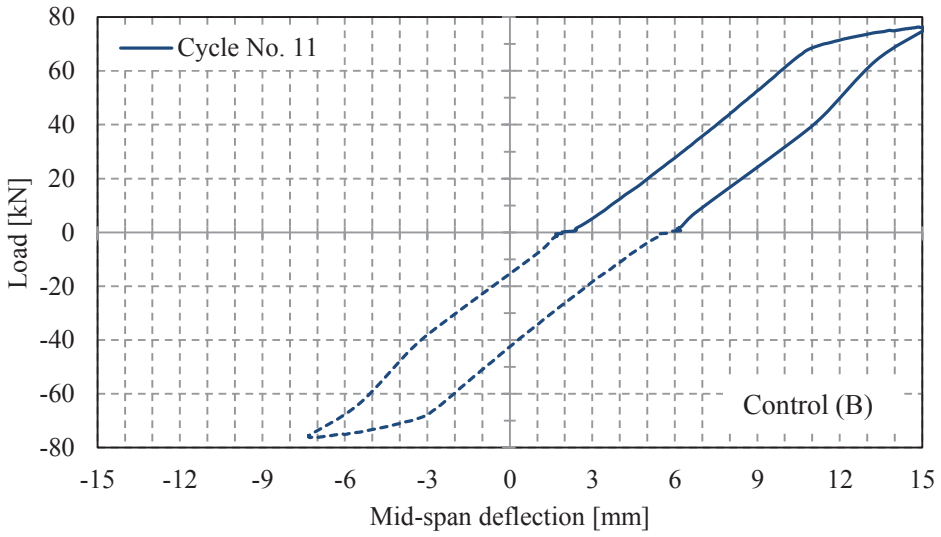
Cycle No. 11
Load [kN]
80
60
40
20
0
-20
-40
-60
-80
-15
-12
-9
-6
-3
0
3
6
9
12
15
Mid-span deflection [mm]
Control (B)

B.5 Load-deflection curves for beam 12PVA0.50% (B)

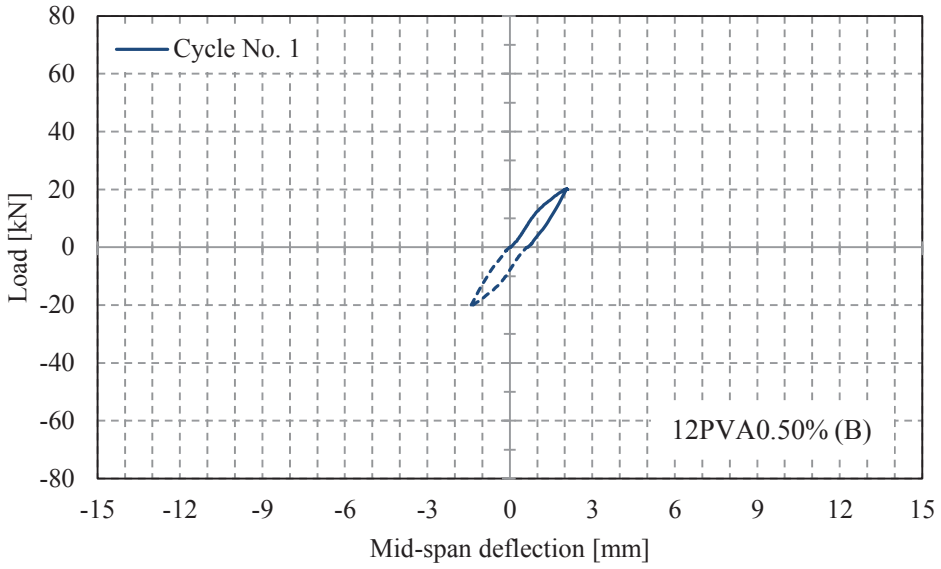

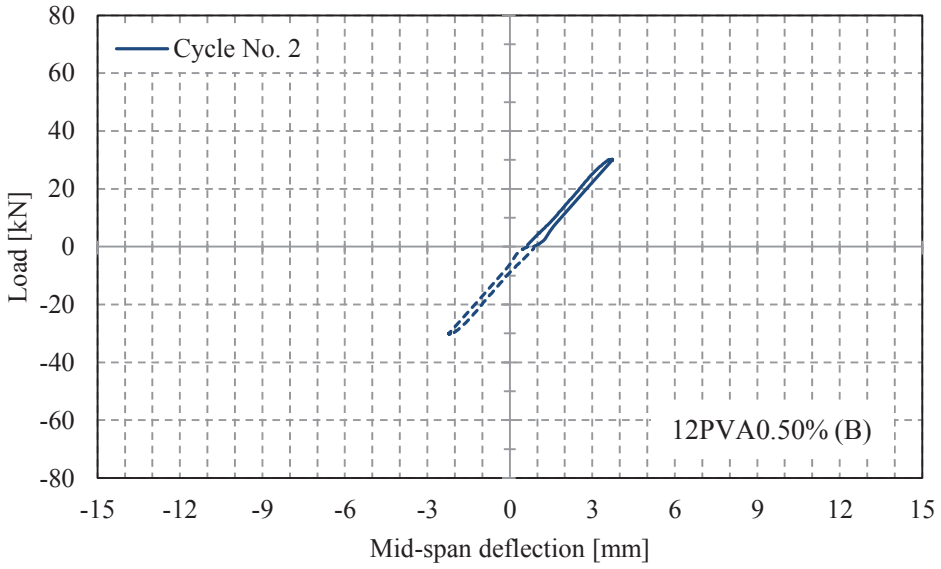

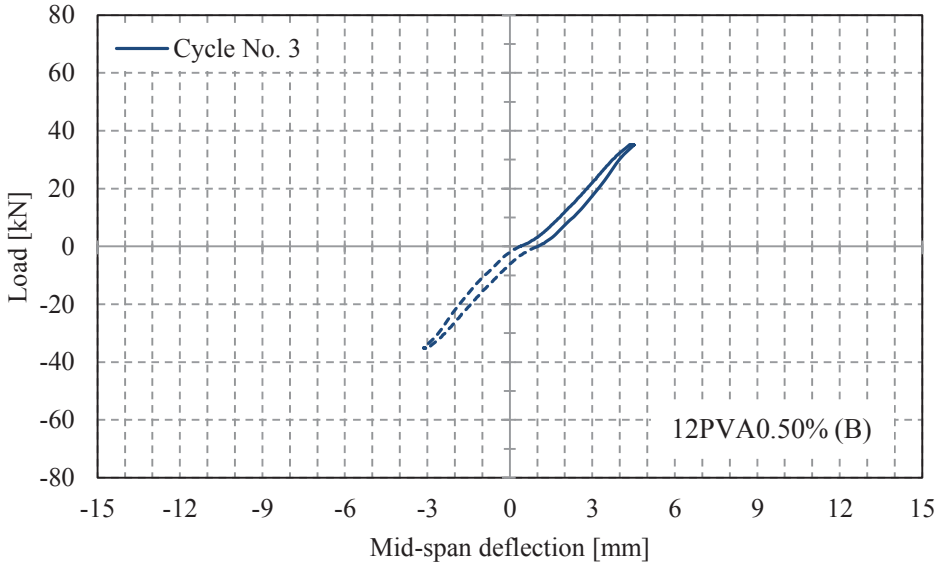

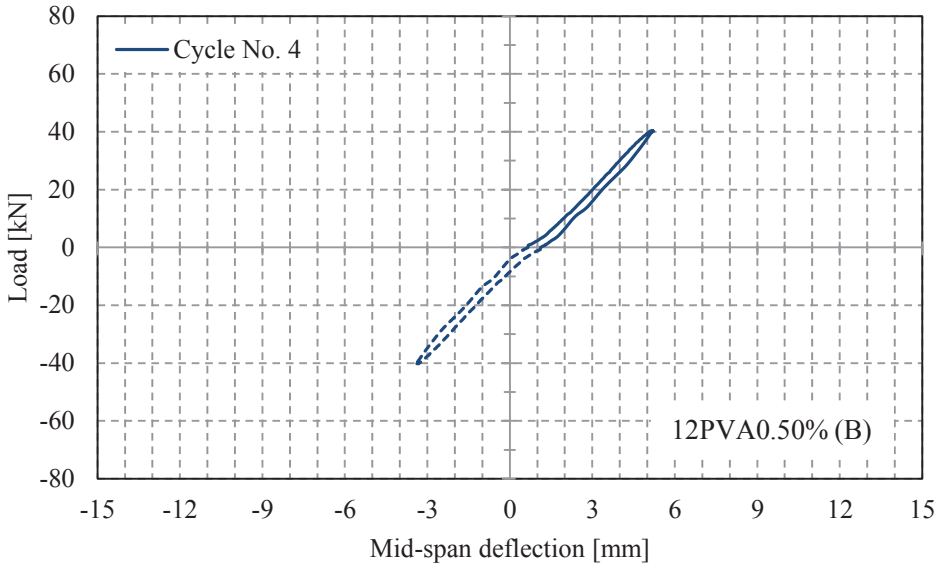
Cycle No. 4
Load [kN]
Mid-span deflection [mm]
12PVA0.50% (B)
80
60
40
20
0
-20
-40
-60
-80
-15
-12
-9
-6
-3
0
3
6
9
12
15

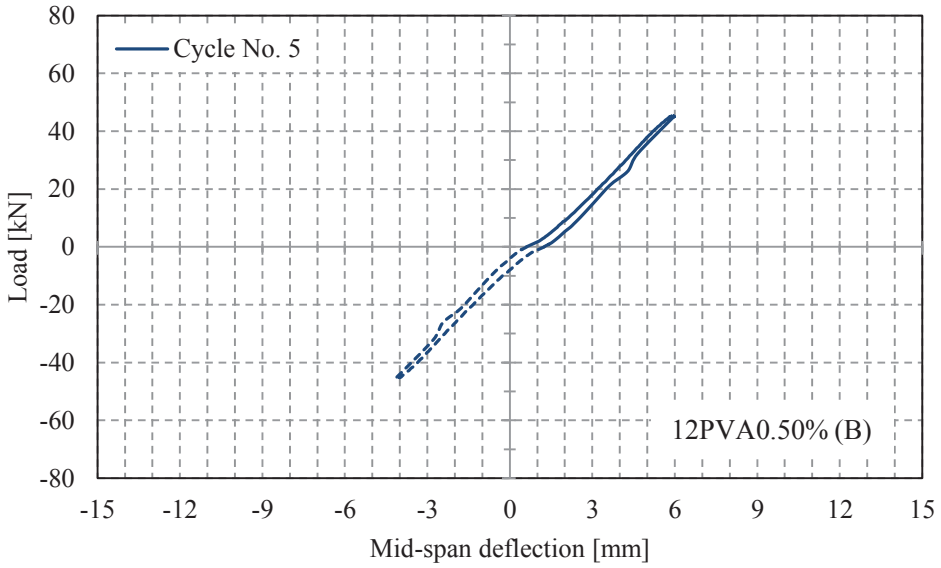
Cycle No. 5
Load [kN]
Mid-span deflection [mm]
12PVA0.50% (B)
80
60
40
20
0
-20
-40
-60
-80
-15
-12
-9
-6
-3
0
3
6
9
12
15

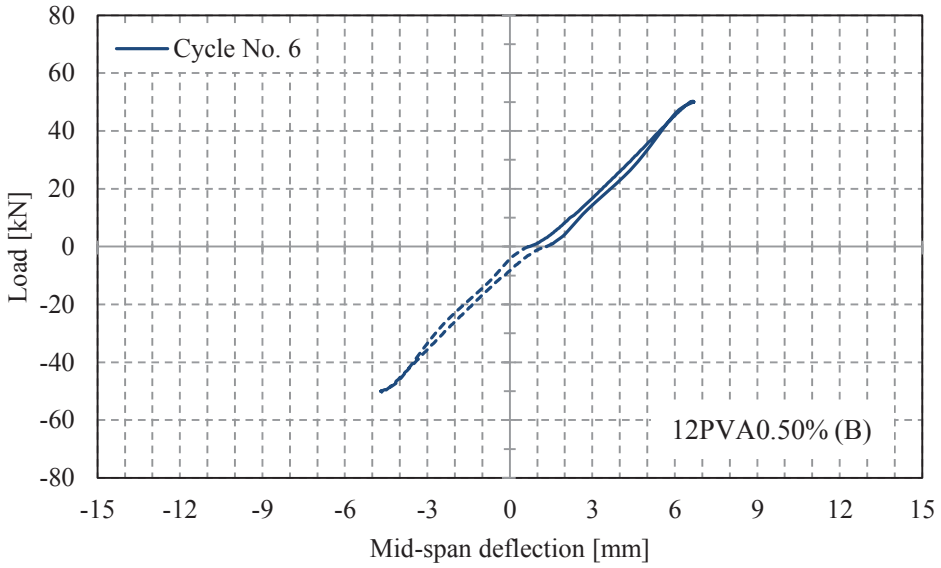
Cycle No. 6
Load [kN]
Mid-span deflection [mm]
12PVA0.50% (B)
80
60
40
20
0
-20
-40
-60
-80
-15
-12
-9
-6
-3
0
3
6
9
12
15

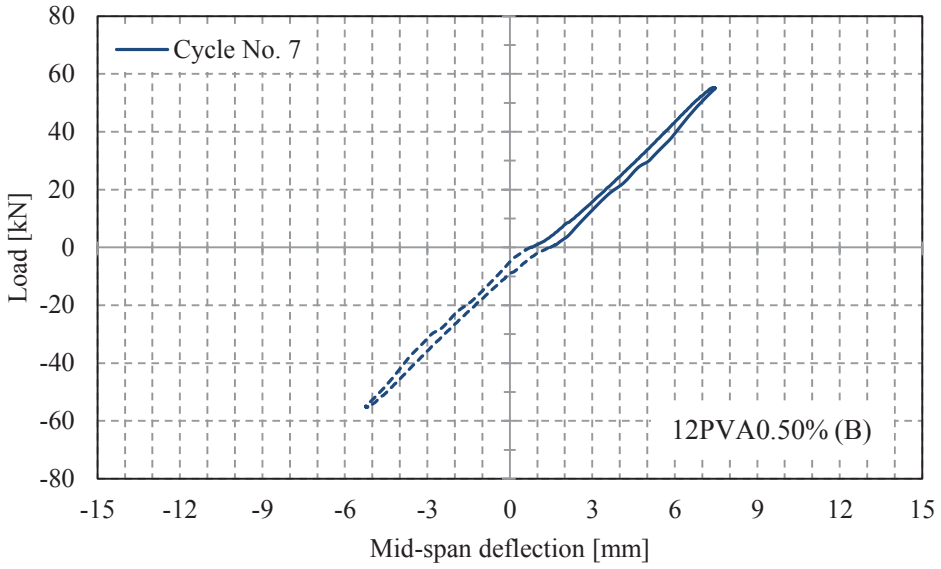
Cycle No. 7
Load [kN]
Mid-span deflection [mm]
12PVA0.50% (B)
80
60
40
20
0
-20
-40
-60
-80
-15
-12
-9
-6
-3
0
3
6
9
12
15

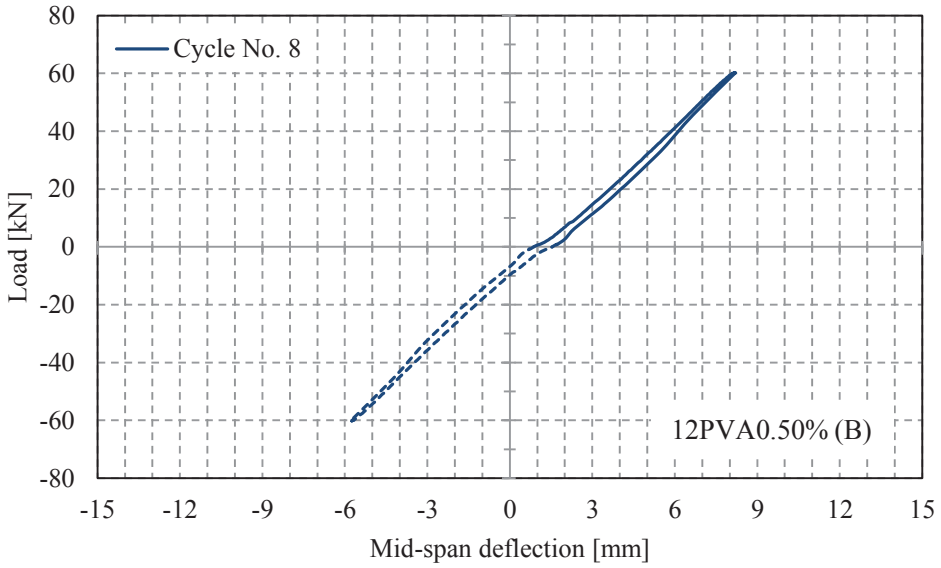
Cycle No. 8
Load [kN]
Mid-span deflection [mm]
12PVA0.50% (B)
80
60
40
20
0
-20
-40
-60
-80
-15
-12
-9
-6
-3
0
3
6
9
12
15

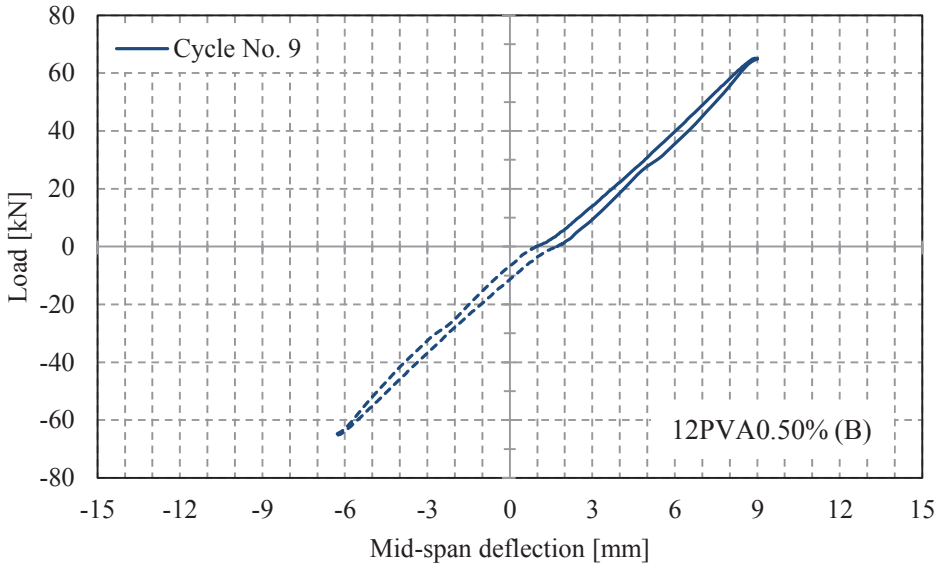
Cycle No. 9
Load [kN]
Mid-span deflection [mm]
12PVA0.50% (B)
80
60
40
20
0
-20
-40
-60
-80
-15
-12
-9
-6
-3
0
3
6
9
12
15

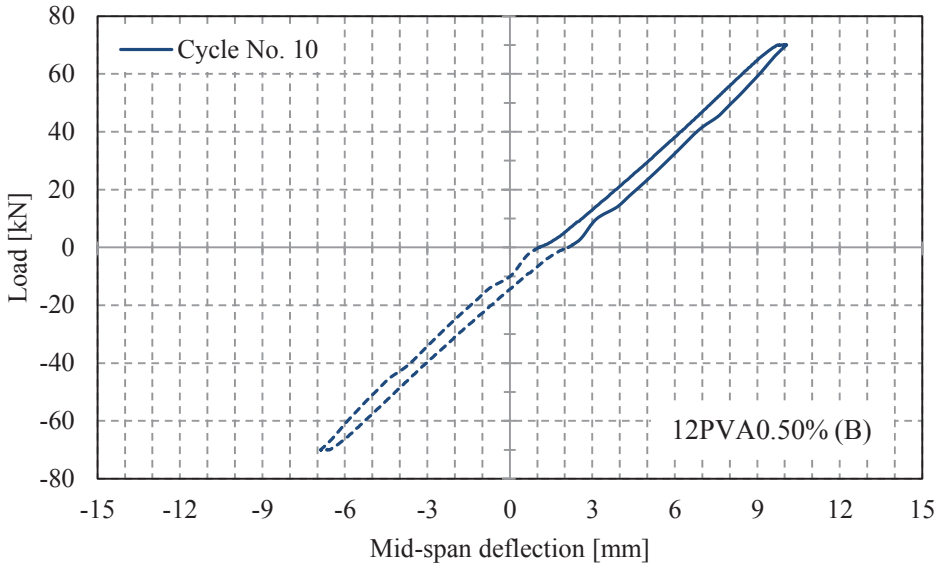
Cycle No. 10
Load [kN]
Mid-span deflection [mm]
12PVA0.50% (B)
80
60
40
20
0
-20
-40
-60
-80
-15
-12
-9
-6
-3
0
3
6
9
12
15

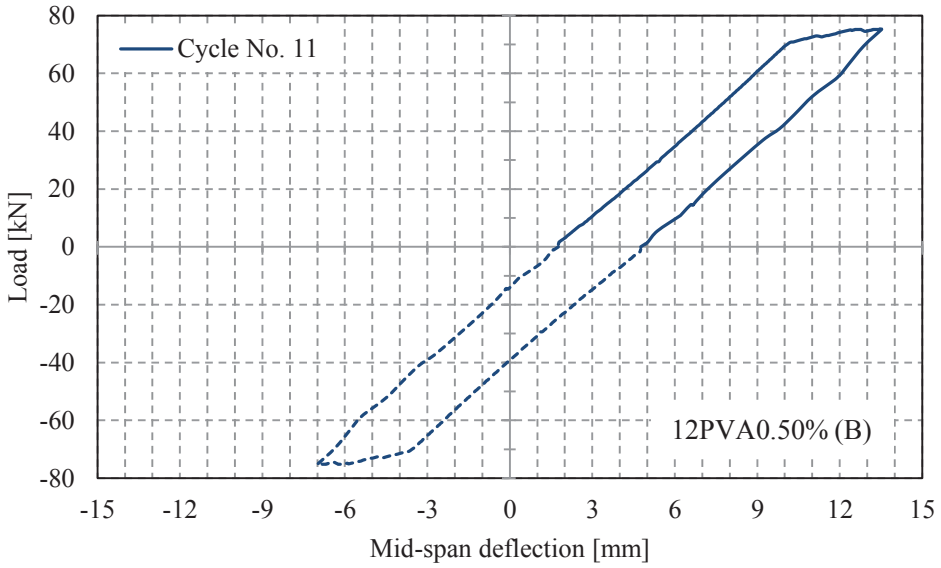
Cycle No. 11
Load [kN]
Mid-span deflection [mm]
12PVA0.50% (B)
80
60
40
20
0
-20
-40
-60
-80
-15
-12
-9
-6
-3
0
3
6
9
12
15

APPENDIX C

In this section, a comparison between the results of the current study with those of another research work (Ghosni 2012) conducted on Polypropylene (PP) fibres are presented. The research on PP fibre has been carried out in the same research group of this study in Centre for Built Infrastructure Research (CBIR) at University of Technology Sydney.

All the materials used in both studies have the same properties as explained previously in section 3.2 excluding the PP fibres. Two very popular types of PP fibres (monofilament and fibrillated) with properties presented in Table 55 have been used with volume fractions of 0.25% and 0.50%.

Table 55. Properties of PP fibres (provided by manufacturer - Sika Australia)

Type	Density [g/cm^3]	Length (L_f) [mm]	Diameter (d_f) [mm]	Young's Modulus (E_f) [GPa]	Elongation [%]
Monofilament (M)	0.91	18	0.022	3.5	63
Fibrillated (F)	0.91	19	0.055	3.5	17

Figure 154. 18 mm monofilament PP fibres (left) and 19 mm fibrillated PP fibres (right)

Table 56 shows compressive strength, modulus of rupture and modulus of elasticity of PVA and PP fibre reinforced concretes.

Table 56. Mechanical properties of PVA and PP fibre reinforced concretes

Mix reference	Fibre length [mm]	V_f [%]	$f_{c,7}$ [MPa]	$f_{c,28}$ [MPa]	$f_{c,56}$ [MPa]	$f_{ct,f,28}$ [MPa]	$E_{c,28}$ [GPa]
Control	N.A	N.A	46.0	60.0	72.5	5.6	39.3
6PVA-0.25%	6	0.25	48.0	67.0	82.5	6.8	40.1
6PVA-0.50%	6	0.50	40.5	61.5	70.0	6.3	38.8
12PVA-0.25%	12	0.25	43.5	64.5	73.0	6.7	39.2
12PVA-0.50%	12	0.50	39.5	58.5	64.0	6.2	33.2
18M-PP-0.25%	18	0.25	45.0	55.0	75.5	5.8	40.6
18M-PP-0.50%	18	0.50	37.0	47.0	54.0	5.5	34.5
19F-PP-0.25%	19	0.25	43.0	58.5	75.5	6.0	42.8
19F-PP-0.50%	19	0.50	38.5	51.0	55.0	5.3	40.5

A comparison between PVA-FRC and PP-FRC can be made using Figure 155 to Figure 159.

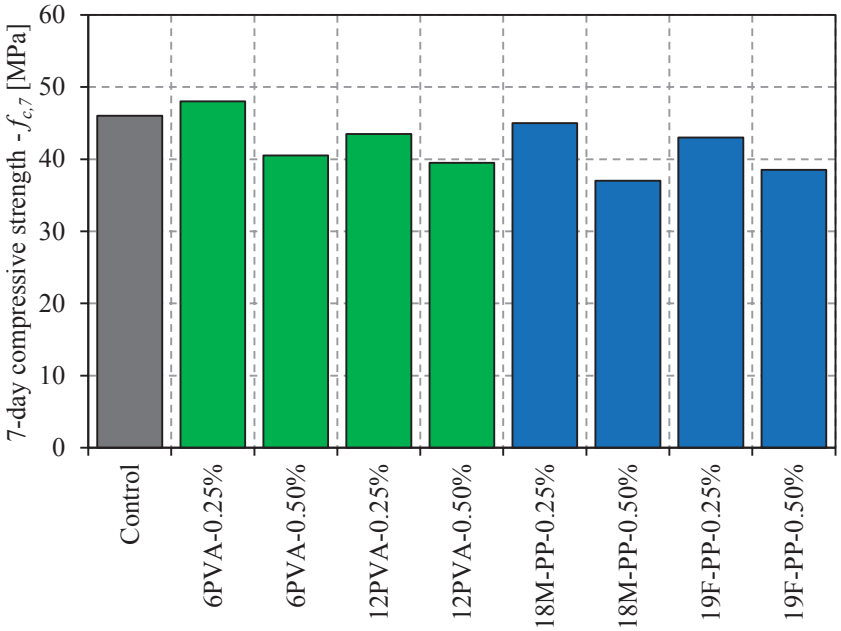

Figure 155. 7-day compressive strength of PVA and PP-FRCs

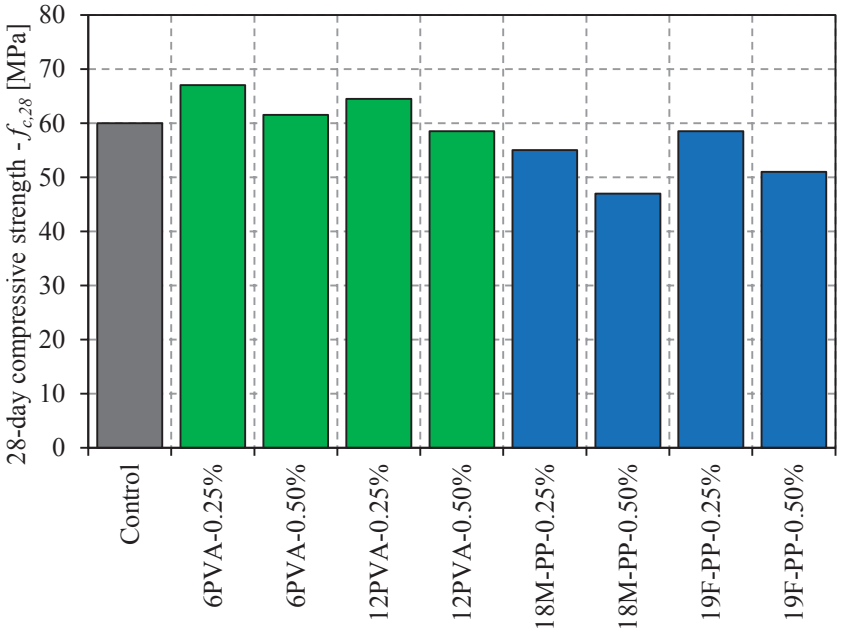

Figure 156. 28-day compressive strength of PVA and PP-FRCs

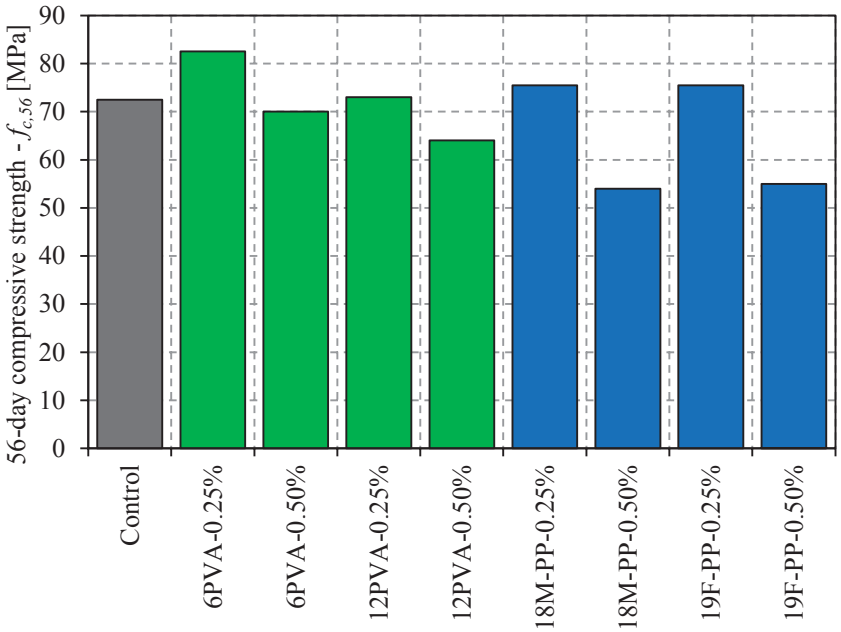

Figure 157. 56-day compressive strength of PVA and PP-FRCs

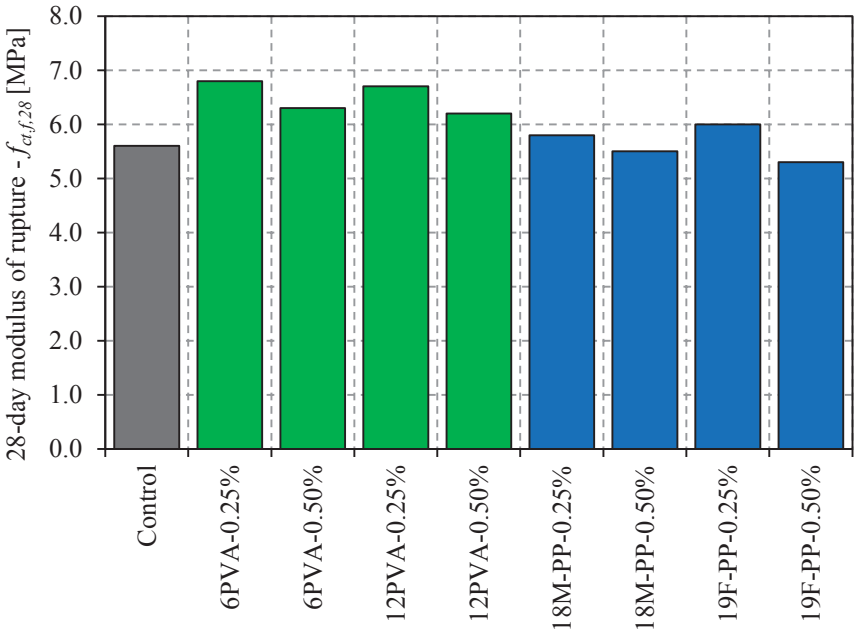

Figure 158. 28-day modulus of rupture of PVA and PP-FRCs

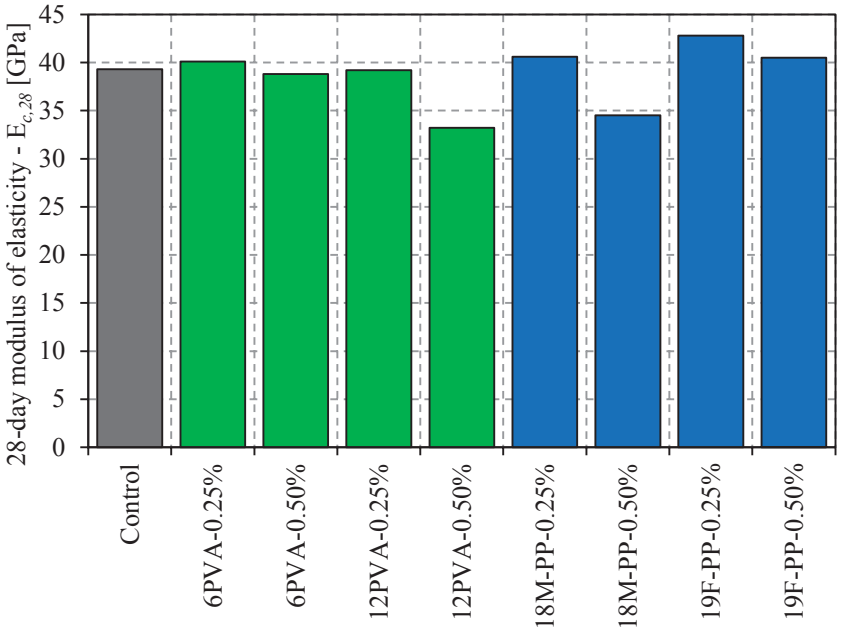

Figure 159. 28-day modulus of elasticity of PVA and PP-FRCs

APPENDIX D

The displacements and stress contour plots of the FE analysed beam elements at failure are presented in this section. The failure point (in model) is defined as where the maximum load is reached in experimental samples as shown in Figure 160.

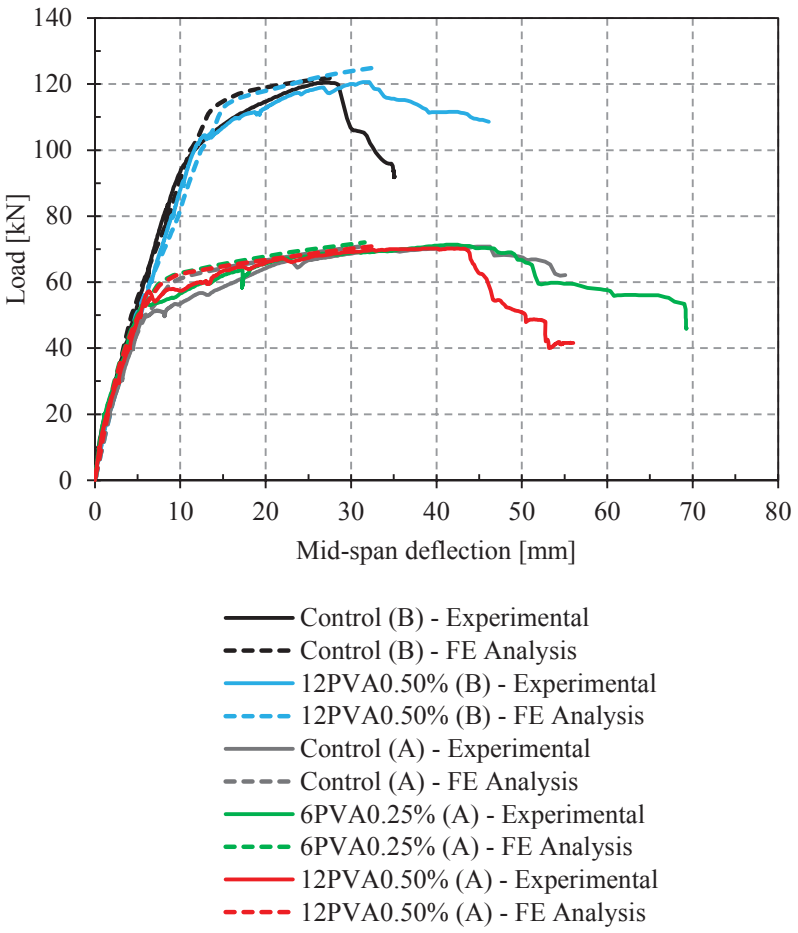

Figure 160. FE modelling results of beam element

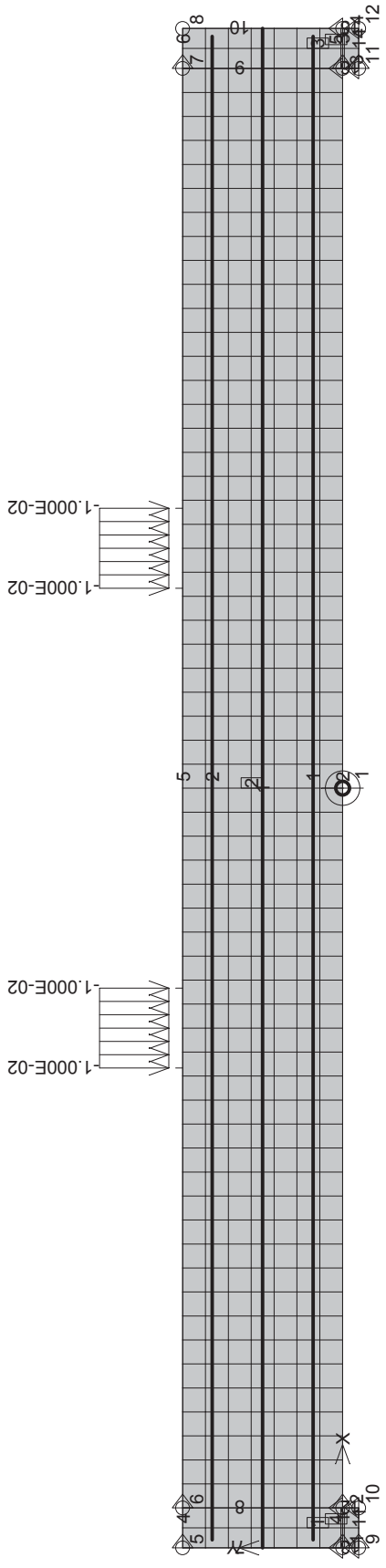

Scalars:iso-areas, Basic material, in nodes, Displacements, x(2), <-2.589E-02;1.623E-03>[m]

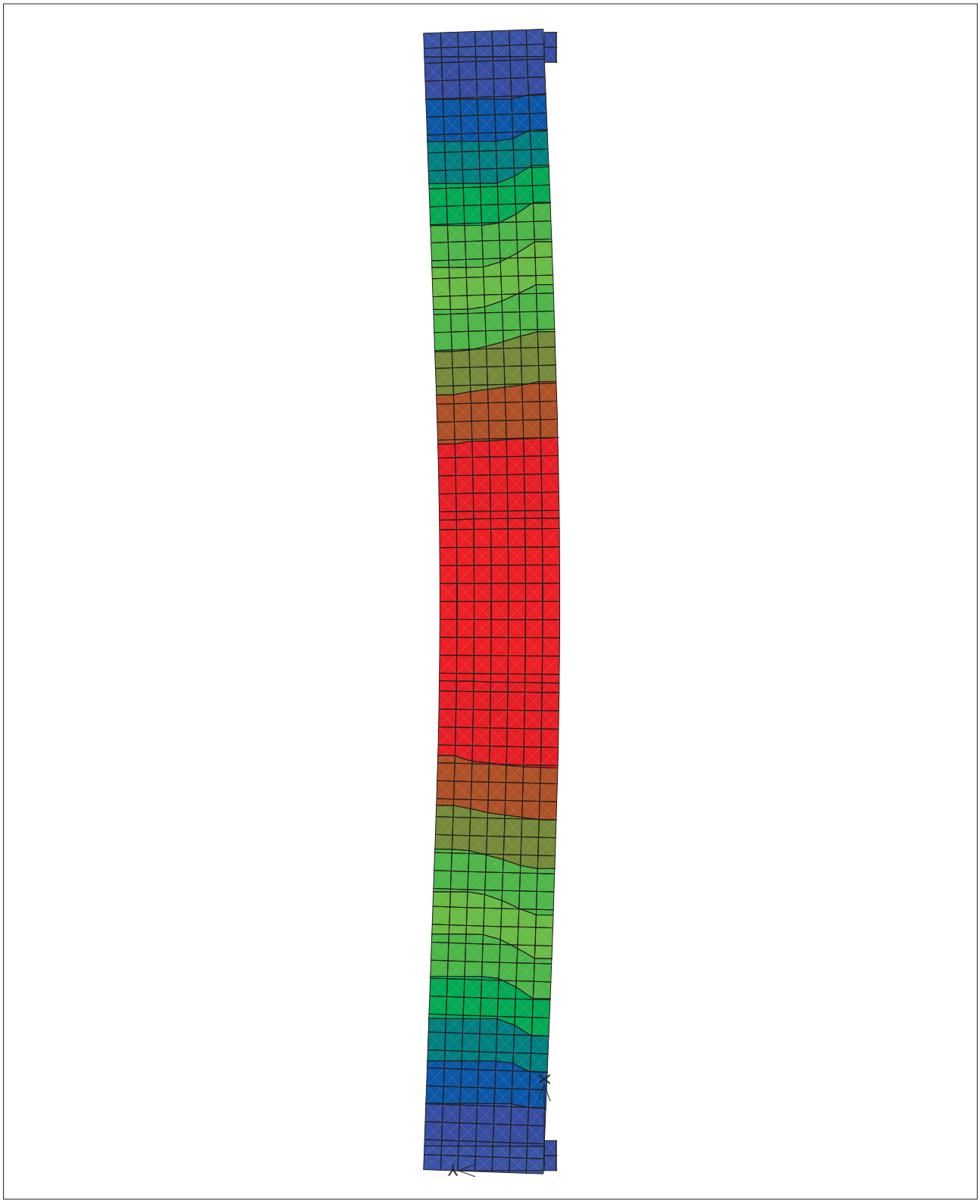

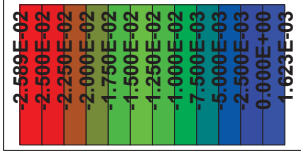

Scalars:iso-areas, Basic material, in nodes, Displacements, x(2), <-2.551E-02;1.581E-03>[m]

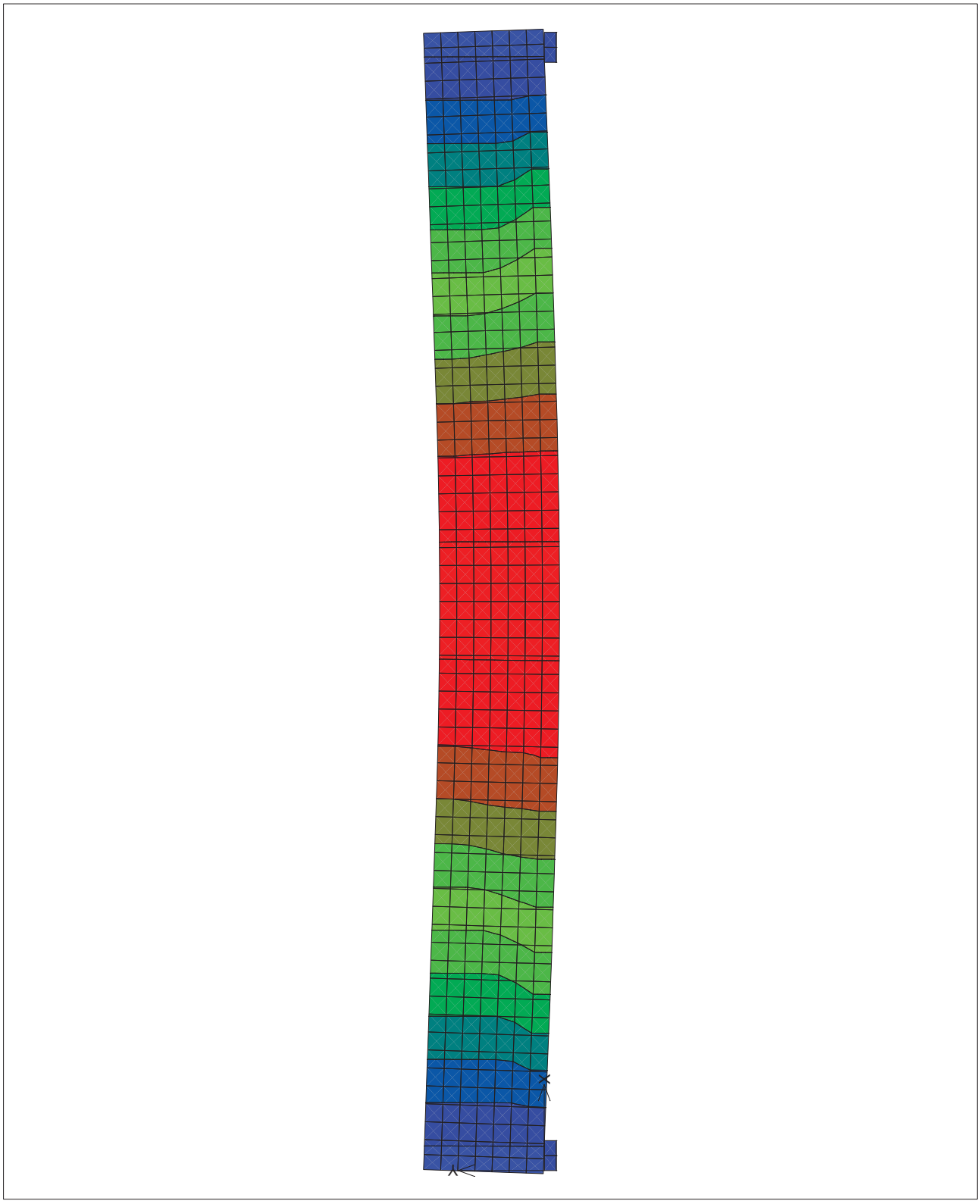

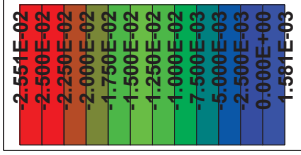

Scalars:iso-areas, Basic material, in nodes, Displacements, x(2), <-2.644E-02;1.641E-03>[m]

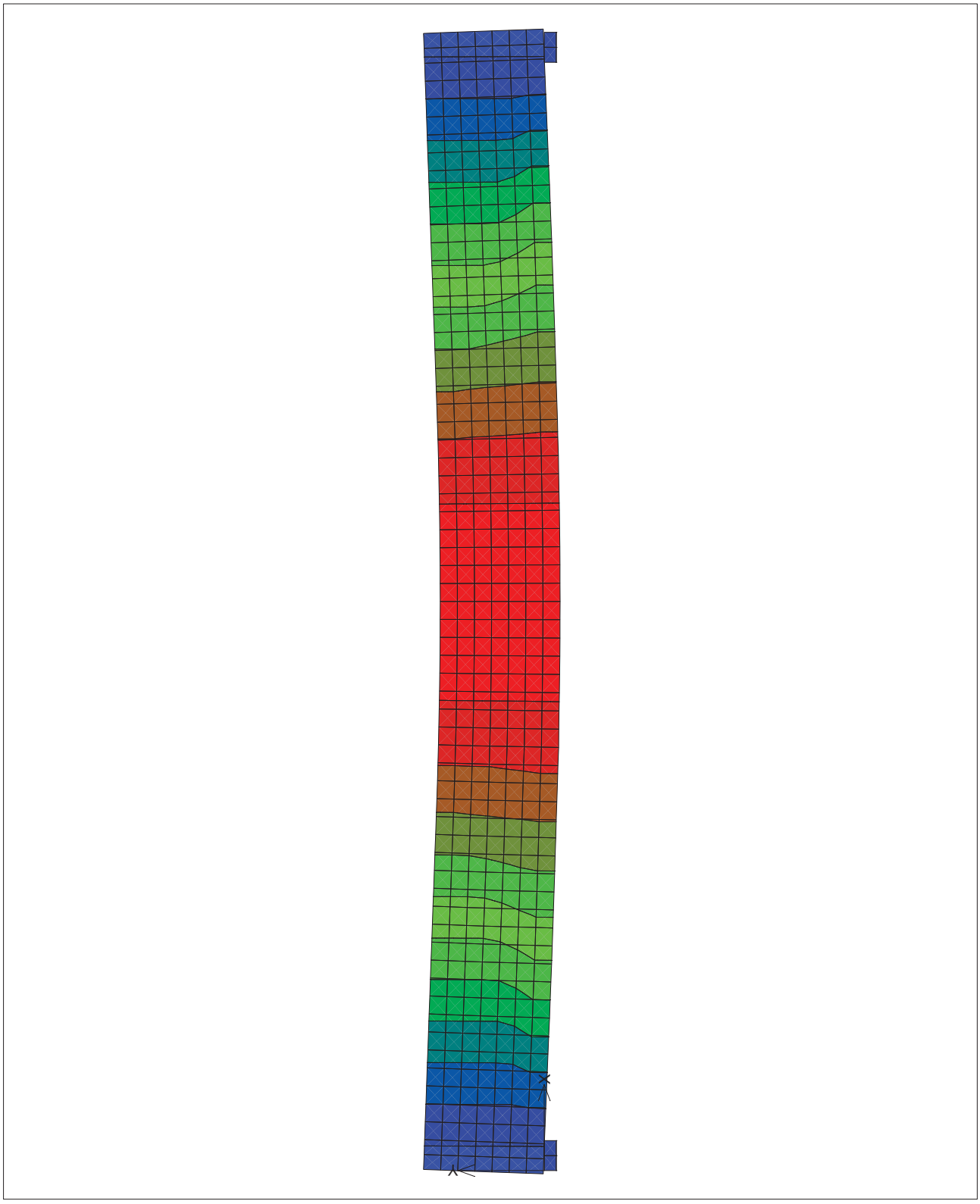

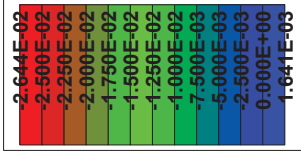

Scalars:iso-areas, Basic material, in nodes, Displacements, x(2), <-2.226E-02;1.389E-03>[m]

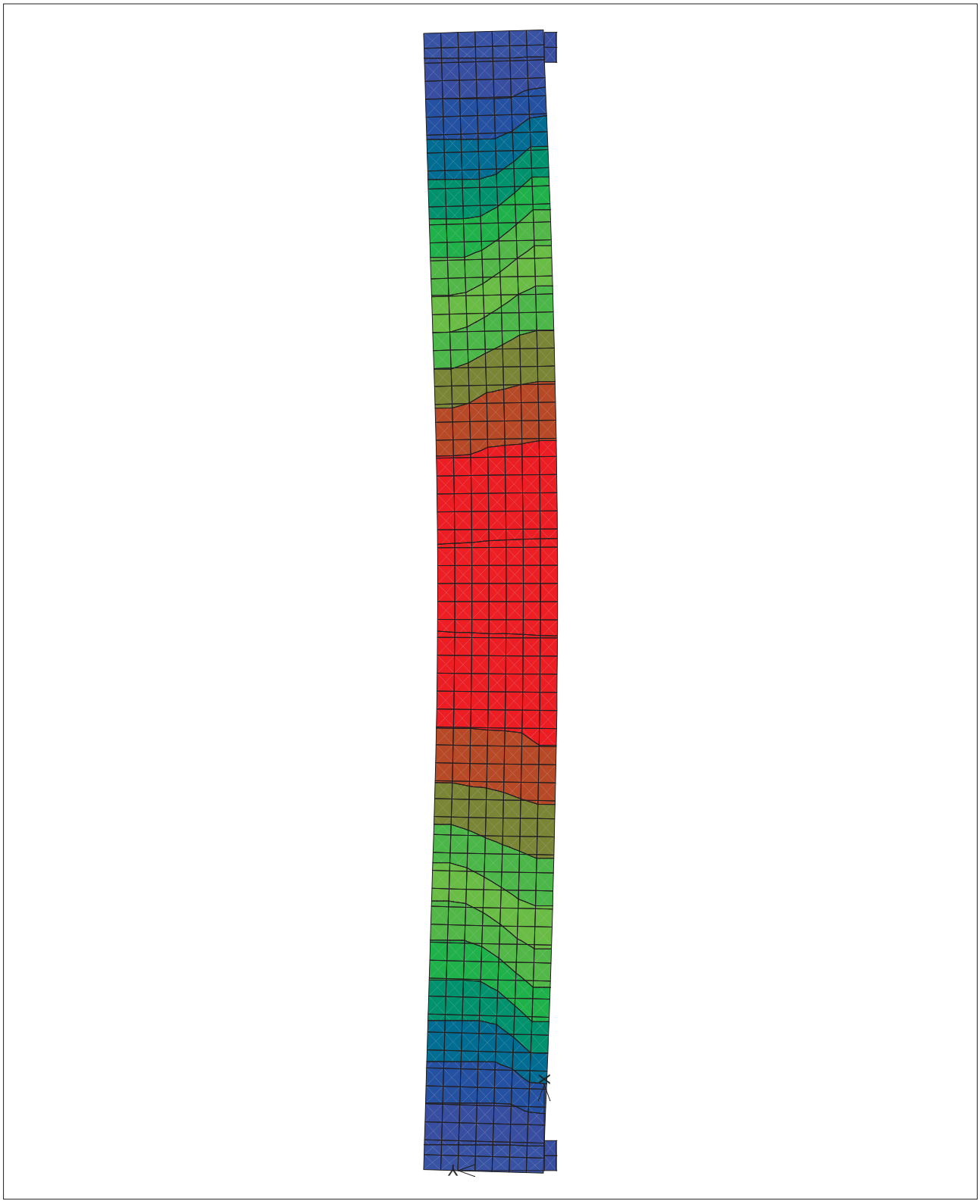

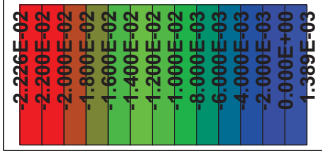

Scalars:iso-areas, Basic material, in nodes, Displacements, x(2), <-2.797E-02;1.740E-03>[m]

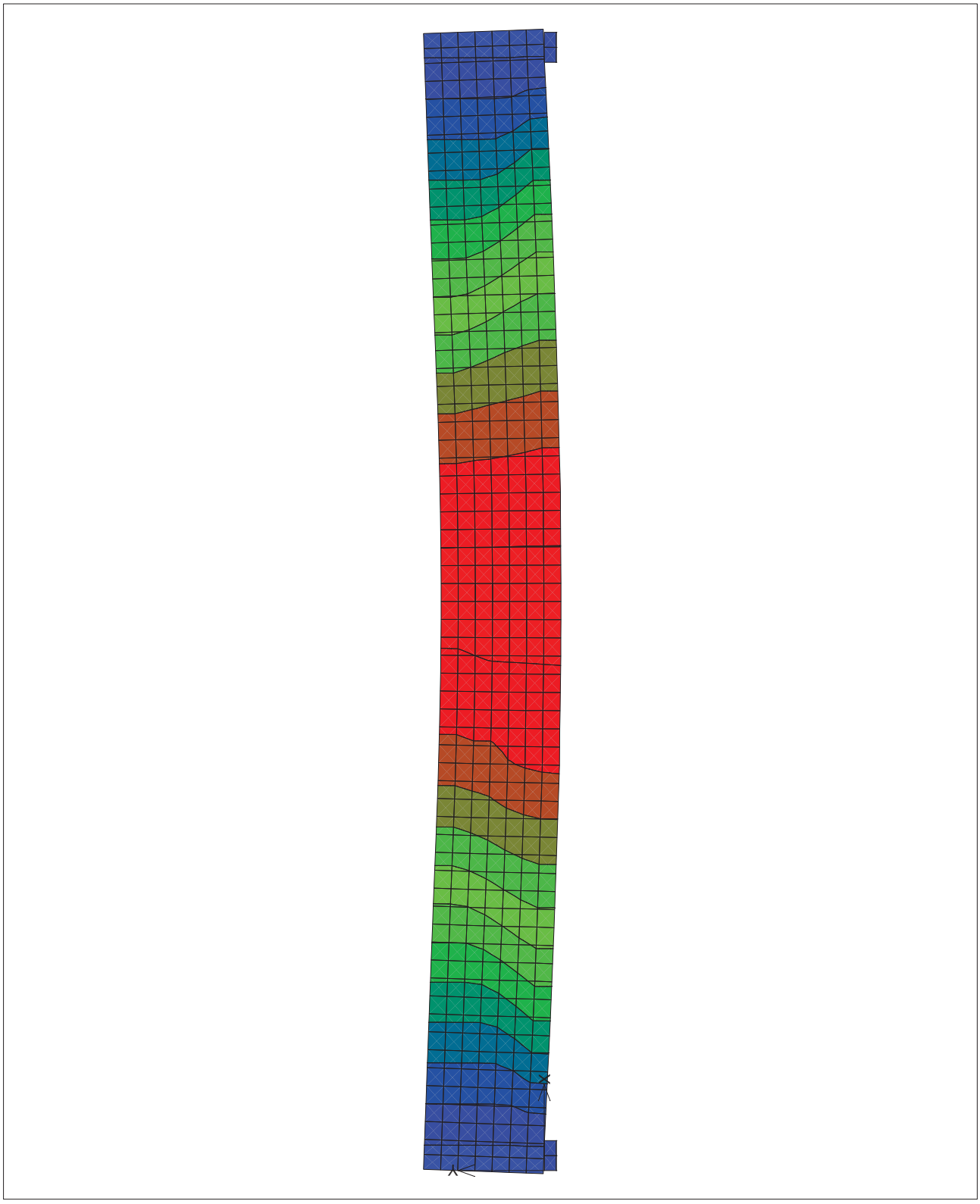

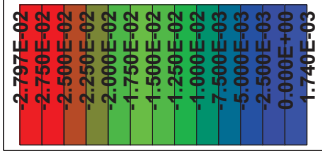

Scalars:iso-areas, Basic material, in nodes, Stress, Sigma xx, <-3.707E+01;1.548E+00>[MPa]

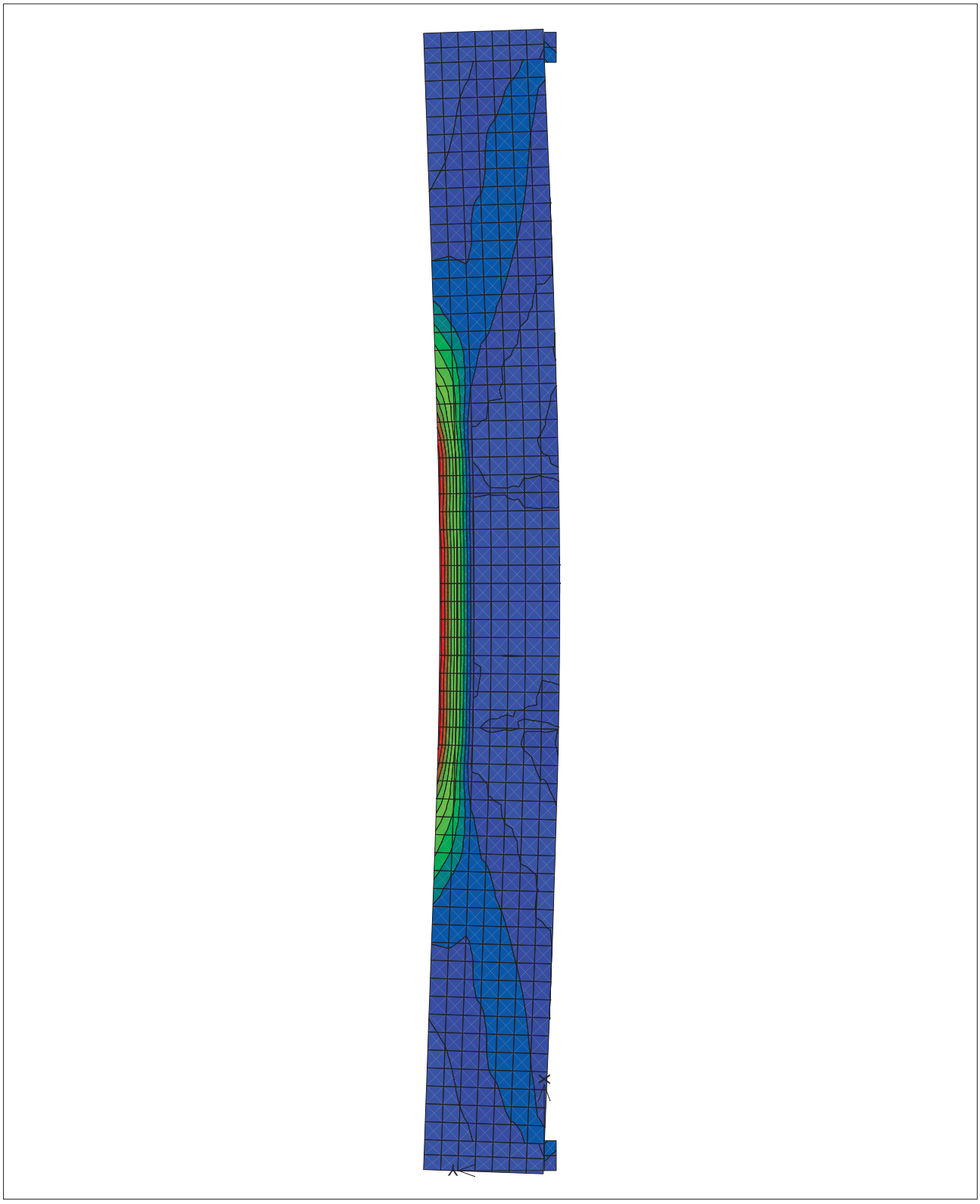

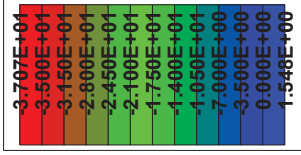

Scalars:iso-areas, Basic material, in nodes, Stress, Sigma xx, <-3.823E+01;1.471E+00>[MPa]

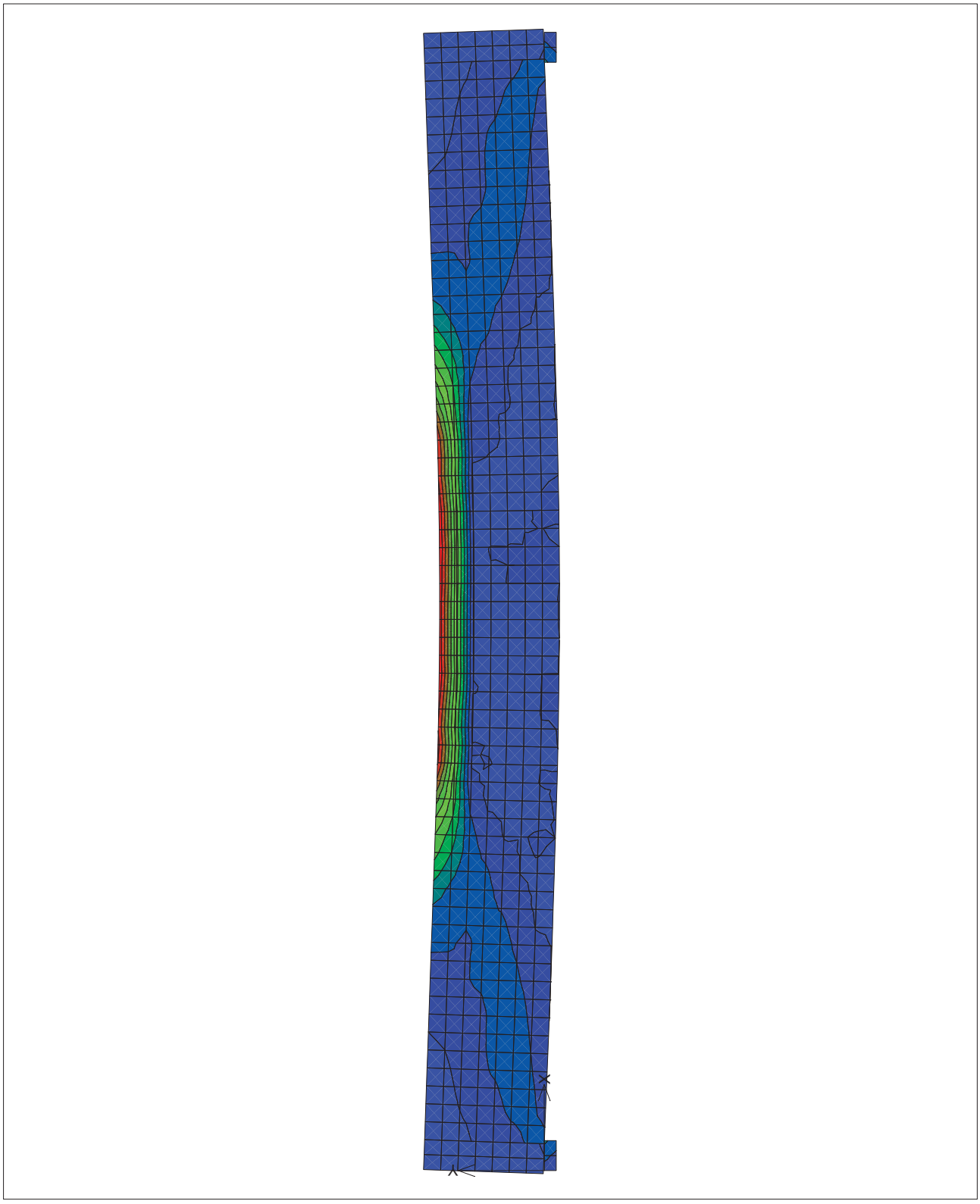

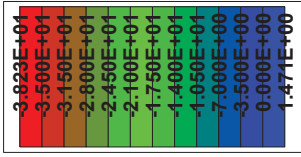

Scalars:iso-areas, Basic material, in nodes, Stress, Sigma xx, <-3.926E+01;1.502E+00>[MPa]

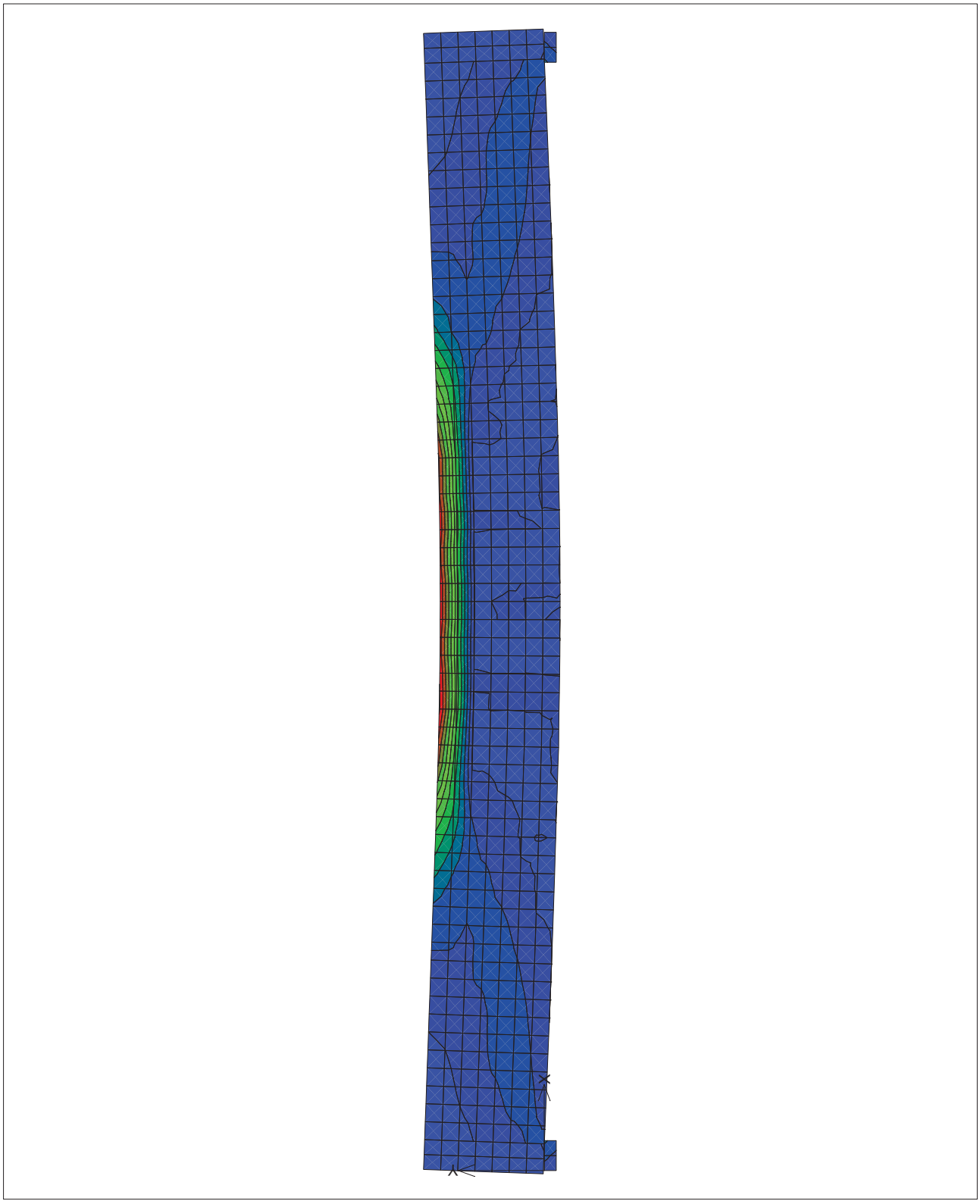

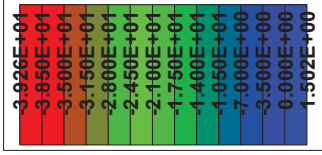

Scalars:iso-areas, Basic material, in nodes, Stress, Sigma xx, <-5.566E+01;2.921E+00>[MPa]

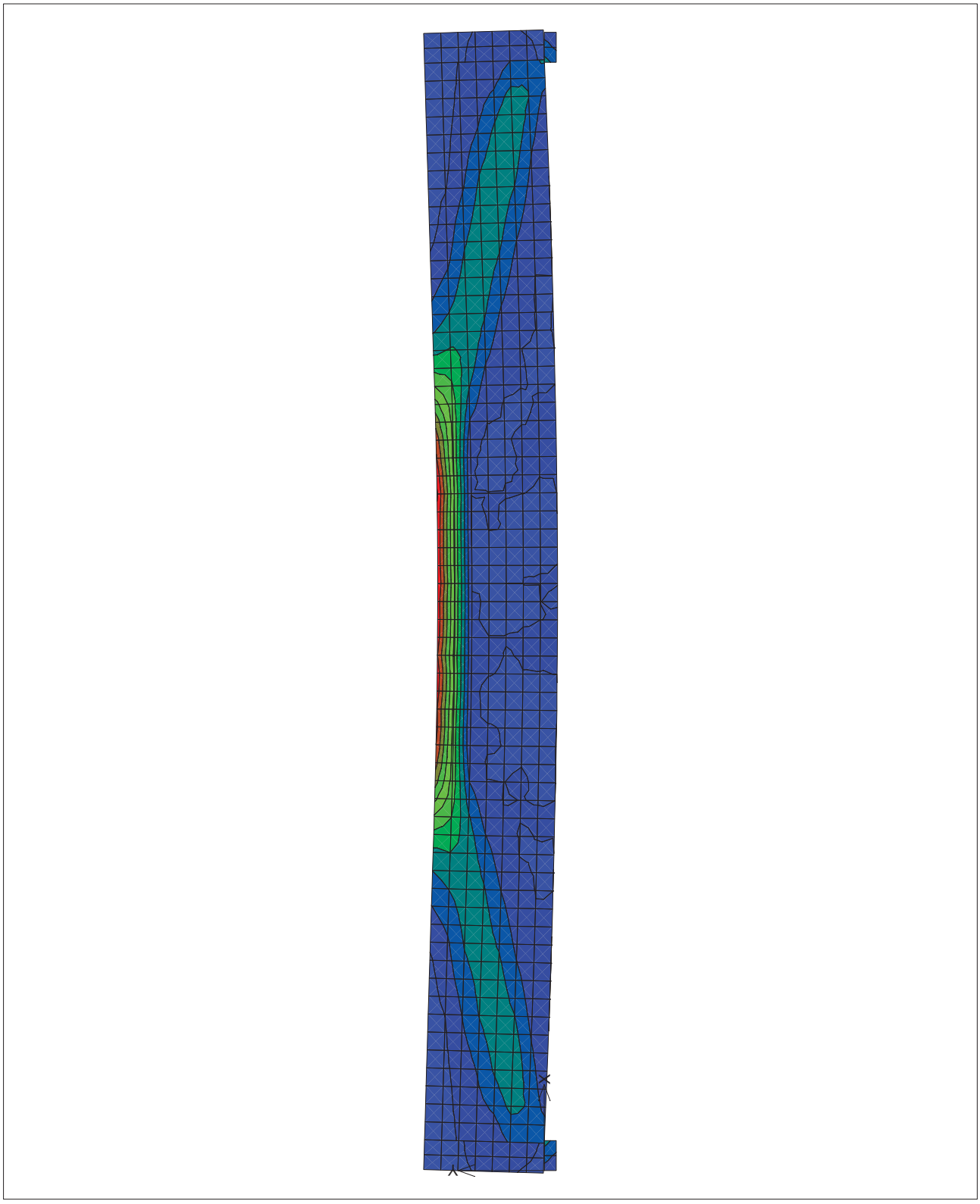

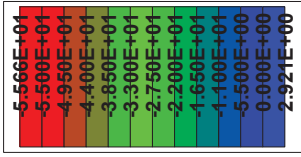

Scalars:iso-areas, Basic material, in nodes, Stress, Sigma xx, <-6.153E+01;2.773E+00>[MPa]